Synthesis and Characterization of Some Zn(II) and Zr(IV) Metal-Organic Frameworks and Their Applications in Fluorescence Sensing and Catalysis

A Dissertation Submitted to the
Indian Institute of Technology Guwahati
as Partial Fulfillment for the Degree of
DOCTOR of PHILOSOPHY
by

Chiranjib Gogoi

DEPARTMENT OF CHEMISTRY
INDIAN INSTITUTE OF TECHNOLOGY GUWAHATI
GUWAHATI-781039
INDIA

March 2021

Synthesis and Characterization of Some Zn(II) and Zr(IV) Metal-Organic Frameworks and Their Applications in Fluorescence Sensing and Catalysis

A Dissertation Submitted to the

Indian Institute of Technology Guwahati

as Partial Fulfillment for the Degree of

DOCTOR of PHILOSOPHY

in

CHEMISTRY

by

Chiranjib Gogoi

Roll No. 166122011

DEPARTMENT OF CHEMISTRY

INDIAN INSTITUTE OF TECHNOLOGY GUWAHATI

GUWAHATI-781039

INDIA

March 2021

Candidate's Declaration

I hereby declare that the submitted thesis titled as "**Synthesis and Characterization of Some Zn(II) and Zr(IV) Metal-Organic Frameworks and Their Applications in Fluorescence Sensing and Catalysis**" is the output of entire investigations carried out by me in the Department of Chemistry, Indian Institute of Technology Guwahati, under the proper guidance of Dr. Shyam P. Biswas. In keeping with the general practice of reporting scientific observations, due acknowledgements have been made wherever the work described is based on the findings of other investigators.

On following the scientific tradition all information provided in this thesis are correct to the best of my knowledge.

IIT Guwahati — Chiranjib Gogoi

March 2021 — Candidate

Dr. Shyam P. Biswas
Associate Professor
Department of Chemistry
Indian Institute of Technology Guwahati
Guwahati – 781039, India
Tel: +91 – 361 – 258 3309
Email: sbiswas@iitg.ernet.in

Certificate

This is to certify that Mr. **Chiranjib Gogoi** has been working under my supervision since July 2016 as a regular registered Ph. D. student. I am forwarding his thesis entitled "**Synthesis and Characterization of Some Zn(II) and Zr(IV) Metal-Organic Frameworks and Their Applications in Fluorescence Sensing and Catalysis**" being submitted to the Indian Institute of Technology Guwahati for the Ph. D. (Science) Degree. I certify that he has fulfilled all the requirements according to the rules of this institute regarding the investigations embodied in his thesis and this work has not been submitted elsewhere for a degree.

IIT Guwahati
March 2021

Dr. Shyam P. Biswas
Thesis supervisor
Department of Chemistry
Indian Institute of Technology Guwahati
Guwahati – 781039, Assam, India

Dedicated to My Parents and Sister

ACKNOWLEDGEMENT

First and foremost, I would like to express my deepest sense of gratitude to my thesis supervisor, Dr. Shyam Prosad Biswas whose timely help during the crucial phase of my career has made it possible to achieve this target. His valuable guidance, encouragement, inspiration and creative scientific ideas helped to raise my knowledge in research career. I am fortunate enough to have his guidance to cultivate scientific thought. My everlasting gratitude goes towards him.

I would like to acknowledge my sincere gratitude to my doctoral committee members Prof. Gopal Das, Prof. A. S. Achalkumar and Dr. Dipankar Srimani for their valuable time, advices and suggestions throughout my Ph. D. journey. Beside them, I extend my sincere thanks to all faculty members of Department of Chemistry of IIT Guwahati.

I take this opportunity to show my deep gratitude to our collaborators Dr. Helge Reinsch, Dr. Amarajothi Dhakshinamoorthy, Dr. Muhammed Yousufuddin, Dr. Dirk Volkmer and Nagarathinam Nagarjun for their invaluable contribution to my research work.

I express my sincere gratitude and acknowledgement to IIT Guwahati for the fellowship. I am also thankful to IIT Guwahati, Department of Chemistry and Central Instruments Facilities (CIF) for providing research and instrumental facilities. I would like to thank all scientific staffs of CIF and Department of Chemistry.

I thank my past and present lab mates Dr. Rana Dalapati, Dr. Mostakim SK, Dr. Anniruddha Das, Dr. Soutick Nandi, Dr. Kaustav Banerjee, Masud, Subhrajyoti and Abhijeet for their invaluable co-operation, their timely help and support and for creating a pleasant atmosphere in the lab. I thankful to our past project fellows, Aswini, Ankita, Shubasis and Ena.

I would like express my love and thanks to my friends Bikash, Tushar, Adit, Shilpa, Arup, Anuj, Senjuti, Paran, Niraj, Dipanjan, Srimanta and other research scholars of chemistry department who have shared their thoughts and views with me and all the joyful moments we shared at IIT Guwahati. I wish to show my love and thanks to my brothers Jun da, Bhai da, dodo, Kishor da, Santanu da, Uday da, Kuldip da, Madhurjya da, Nayan da, Saurav da, Nilutpal da, Dhurva da, Arun da, Ayushman da, Arup da, dibakar da, Puku, Raj, Monu, Pallav, Manas, Arindom, Rabu and my sisters Minakhi ba, Shivani ba, Rajashree ba, Emily ba, Amrita ba, Bidisha ba, Devipriya ba, Chandana ba, Madhu, Priyanka for their constant unfailing support, encouragement and all the help they bestowed whenever required.

Finally, my Ph. D. endeavor could not have been completed without the endless love, endless support, tolerance and blessings from my family. I wish to express my sincere gratitude to my parents (Nripen Gogoi and Swarnali Gogoi) and sister (Pronita Gogoi). They are the main soul and inspiration for each and every step in my life.

Chiranjib Gogoi

Thesis Title:	**Synthesis and Characterization of Some Zn(II) and Zr(IV) Metal-Organic Frameworks and Their Applications in Fluorescence Sensing and Catalysis**
Name of the Candidate:	Chiranjib Gogoi
Roll No.:	166122011
Thesis Supervisor:	Dr. Shyam P. Biswas
Department:	Chemistry
Institute:	Indian Institute of Technology Guwahati, Assam, India

Thesis Overview:

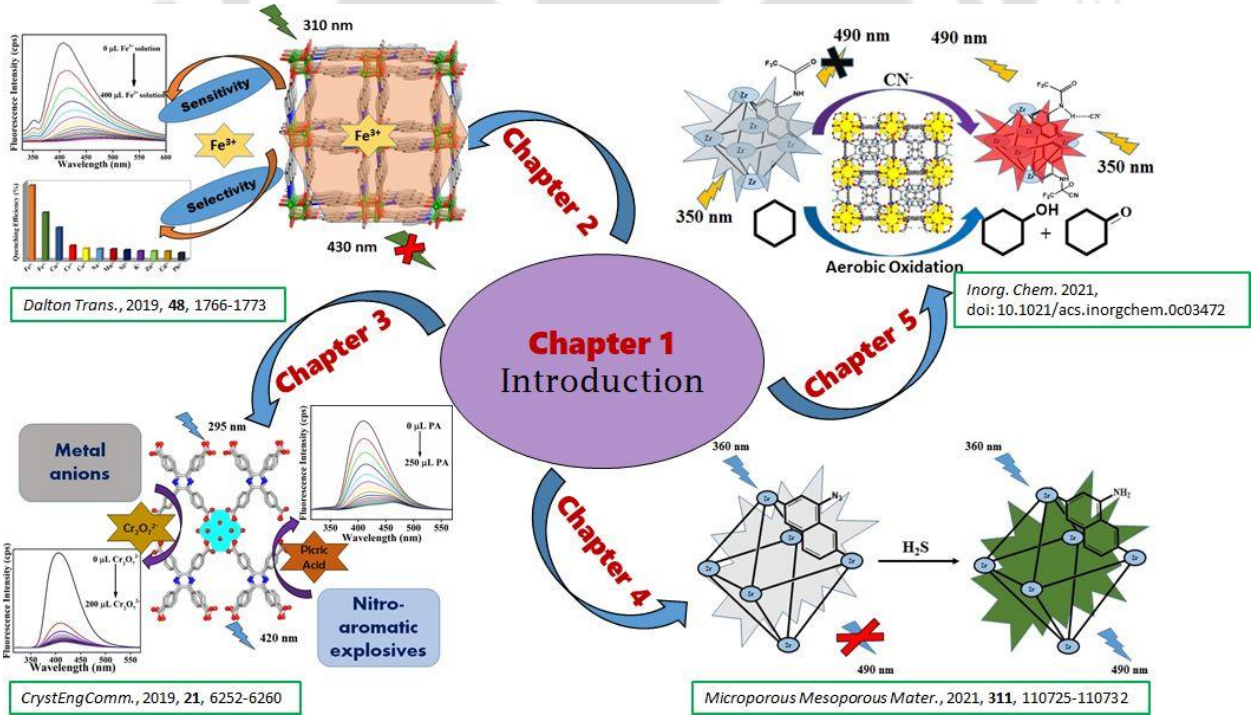

Chapter 1: Introduction

Metal-organic frameworks (MOFs) represent a class of porous materials which are formed by strong bonds between metal ions and organic linkers. They have some outstanding properties like very high surface area, high porosities, high thermal and chemical stability, various pore size and shape etc. Because of their excellent chemical and physical properties, this remarkable class of porous materials has a wide range of application like catalysis, gas storage, separation, polymerization, sensing, proton conductivity, drug delivery, bioimaging etc. MOFs have a high degree of customizability because they can be tailored by selecting different linkers and metal ions. Because of the tunable nature, MOFs can be tailored with precisely controlled pore size, shape and functionality for the specific application. In many areas, MOFs have shown excellent advantages over traditional materials and potential values for commercialization. Generally, MOFs are made up of secondary building units (SBUs). These are of two general types: (a) metal-containing units which may have single metal atom to infinite groups (rods and layers) and (b) polytopic organic linkers that may incorporate metal atoms (as in a porphyrin). Once the synthesis of the SBU is established, it could be used to direct the assembly of an ordered framework with rigid organic linkers. During the synthesis of MOFs, we should be more concerned about the stability of the framework. The unsatisfactory chemical stability of most of the MOFs hinders some of the fundamental studies and also hinders the implementation of MOFs for practical applications. One of the most well-studied MOFs, MOF-5 is not stable even in water vapor. The instability in water has considerably restricted further application of these MOFs under moisture-rich conditions. Water stability is a crucial property for any kind of material to be applicable in the real world. Hence, water-stable MOFs have been in great demand among the scientific community. In the last few decades, a great deal of effort has been devoted to explore the feasibility of luminescent MOFs (LMOFs) for sensing applications. MOF-based sensors have been directly used for the detection of gases, vapors, small molecules, metal ions, nitroaromatics, nerve agents and pesticides. In catalysis, MOFs are promising heterogeneous catalysts due to the presence of unsaturated coordinated metal sites and/or special functional groups of linkers. The unsaturated coordinated metal sites can be prepared by some special treatment like heating at high temperature and linker-exchange which in turn activate the metal nodes by removing weak-coordinated linkers from the nodes. The activated catalytic sites can also be made by introducing specific modification of linker such as bipyridine, porphyrin etc.

In view of the above context, the current thesis explores the synthesis strategy of water-stable MOFs and uses the luminescence property of MOFs for selective and sensitive detection of toxic ions like Fe^{3+}, $Cr_2O_7^{2-}$, CN^- and nitroaromatic explosives. The thesis also explores the use of the hydrophobic cavity of a MOF for the catalysis reaction.

Chapter 2: A new 3D luminescent Zn(II)-organic framework containing quinoline-2,6-dicarboxylate linker for the highly selective sensing of Fe(III) ions.

Chapter 2 describes the synthesis of a new 3D zinc-organic framework [Zn(QDA)]·0.7DMF·0.5H_2O (**1**, H_2QDA = quinoline-2,6-dicarboxylic acid, DMF = *N*,*N*-dimethylformamide) under solvothermal conditions. The single-crystal X-ray diffraction analysis reveals that **1** crystallizes in a tetragonal crystal system and exhibits $I4_1/a$ space group ($a = b$ = 19.9088(3) Å, c = 12.1905(3) Å). The asymmetric unit contains one unit of QDA linker with full occupancy and one unit of Zn^{2+} ion with half occupancy (Figure 1a). Within the crystal lattice, the central Zn^{2+} ion attains a distorted square pyramidal geometry with ZnO_4N configuration (Figure 1b). The overall framework has PtS topology (Figure 1d), where Zn^{2+} center acts as a 5-connected node and QDA linker as a spacer. The phase purity of the bulk sample was characterized by X-ray powder diffraction (XRPD), thermogravimetric analysis (TGA) and Fourier transform infrared (FT-IR) spectroscopy. The as-synthesized sample (**1**) was activated by stirring with acetone for 24 h, followed by heating under vacuum for 24 h at 120 °C. The TGA experiment indicated that both **1** and its activated form (**1'**) are stable up to 440 °C. The crystalline structure of the compound was retained after immersion in water, 1(M) HCl, acetic acid and NaOH (at pH = 10) solutions. Compound **1'** exhibited a very quick fluorescence quenching response after the addition of Fe^{3+} solution. It was clearly observed that after the addition of 400 µL of 10 mM Fe^{3+} solution to the methanolic suspension of **1'**, almost 97% fluorescence quenching occurred (Figure 2). For all the other competitive cations, the fluorescence quenching efficiencies were lower as compared to the Fe^{3+} ion (Figure 3). The selectivity for Fe^{3+} sensing was also examined in the presence of other metal cations. The experimental resulted showed that the quenching efficiency was not affected by the presence of competitive metal cations (Figure 4). A very low detection limit of 9.2 ppb was observed for Fe^{3+} ion, which is among the lowest values documented in the literature for MOF based fluorescence probes. Both fluorescence resonance energy transfer (FRET), as well as photo-induced electron transfer (PET), processes play major roles in the selective detection of Fe^{3+}

ions. The recyclability experiment suggested that **1'** can be used for the long-term detection of Fe^{3+} ion.

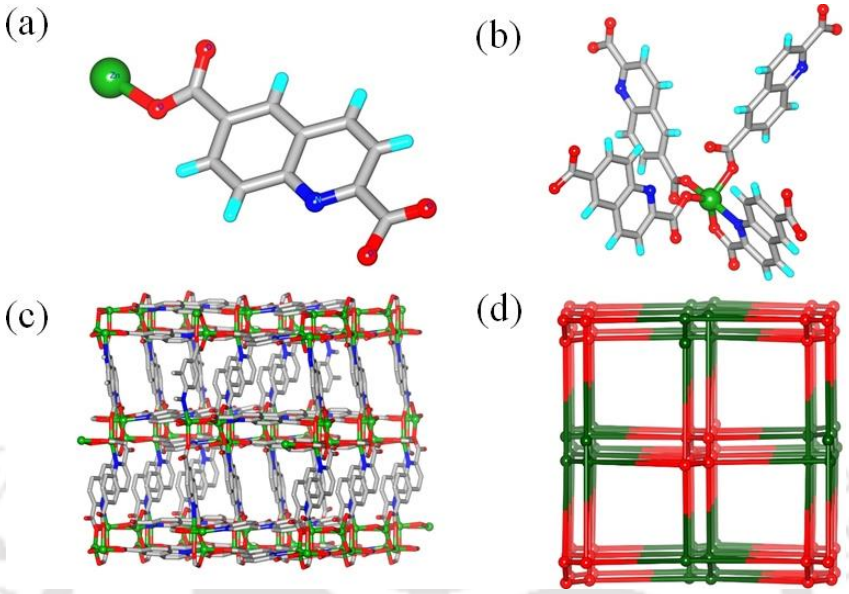

Figure 1. Illustrations for the crystal structure of **1**: (a) asymmetric unit, (b) coordination environment around Zn^{2+} ion, (c) side view of the overall 3D framework, and (d) PtS topology of the overall 3D framework. Color codes: Zn, green; C, grey; O, red; N, navy blue; H, sky blue.

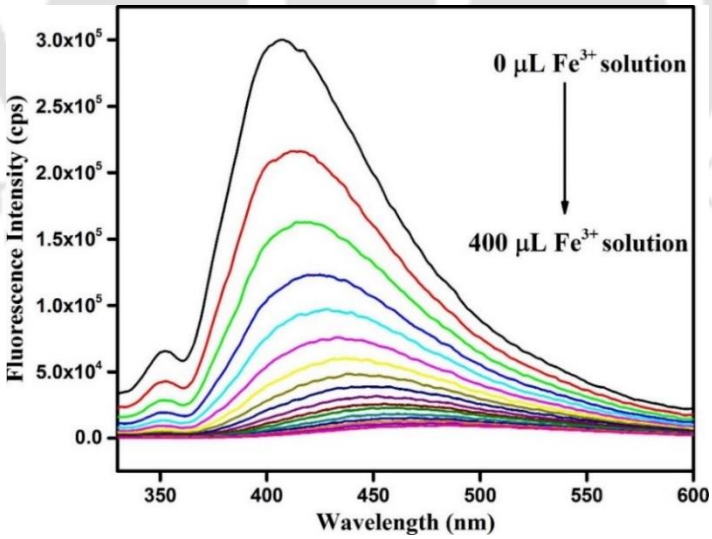

Figure 2. Quenching of the fluorescence intensity of the methanolic dispersion of **1'** after incremental addition of 10 mM Fe^{3+} solution.

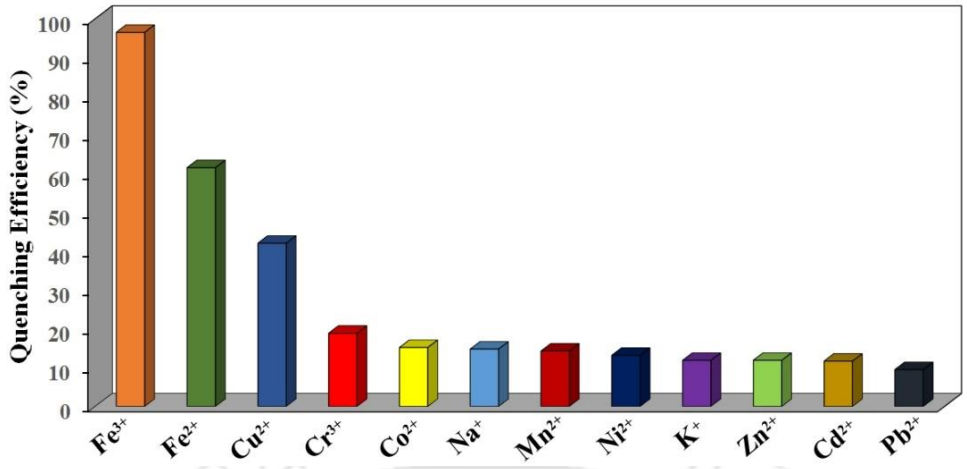

Figure 3. The effect of the other metal cations on the quenching efficiency of Fe^{3+}.

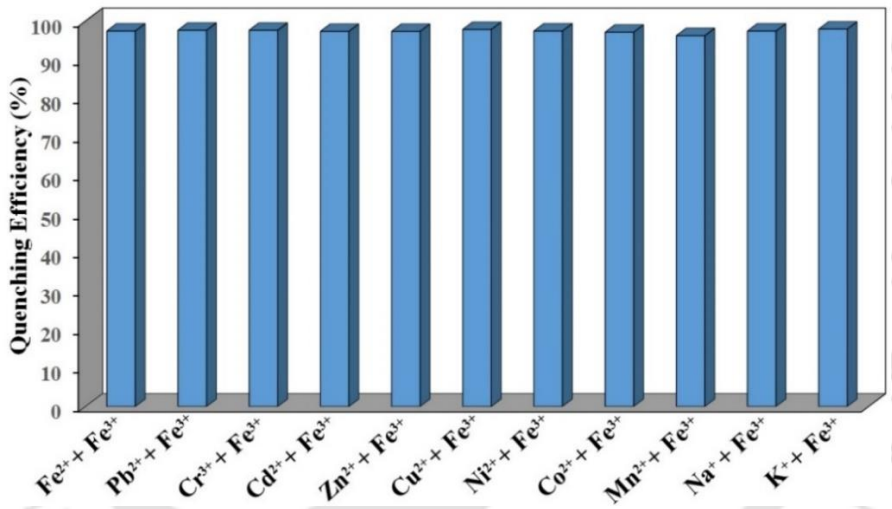

Figure 4. The effect of other metal cations on the quenching efficiency of Fe^{3+}.

Chapter 3: A pyrazine core-based luminescent Zr(IV)-organic framework for specific sensing of picric acid and $Cr_2O_7^{2-}$

Chapter 3 describes the synthesis of a MOF containing Zr(IV) ion and 2,3,5,6-tetrakis(4-carboxyphenyl)pyrazine (H_4**L**) linker by solvothermal method. $ZrOCl_2 \cdot 8H_2O$ was employed as the metal source along with H_4**L** linker and benzoic acid (modulator) in *N*,*N*-dimethylformamide (DMF) to synthesize the compound. The as-synthesized compound has the formula $[Zr_6(\mu_3\text{-}O)_4(\mu_3\text{-}OH)_4(OH)_4(H_2O)_4(\mathbf{L})_2] \cdot 3H_2O \cdot 2DMF$ (**2**). We indexed the XRPD pattern of **2** in an orthorhombic crystal system with space group *Cmmm* with a = 19.375(12) Å, b = 33.376(21) Å, c

= 12.712(12) Å. The results of Pawley refinement confirmed that the simulated and experimental XRPD data are in good agreement with each other for **2.** The refinement data also point out that **2** is isostructural with the Zr-CAU-24 MOF, which has been reported previously. The activation of **2** was carried out by using methanol-exchange and subsequent heating under a high vacuum at 130 °C. Both **2** and its activated form (**2'**) were characterized by XRPD, FT-IR and TGA. They displayed high chemical stability and thermal stability. Both **2** and **2'** are stable up to 440 °C. Compound **2'** has a very high BET surface area (1419 m^2/g) and CO_2 adsorption capacity (4.4 mmol/g at 1.4 bar and 0 °C). Being highly water-stable, luminescent **2'** can selectively recognize dichromate ($Cr_2O_7^{2-}$) (Figure 5) in water and picric acid (PA) (Figure 6) in dimethyl sulfoxide (DMSO), by fluorescence quenching mechanism. The detection limits were found to be 13.08 and 8.58 ppb for PA and $Cr_2O_7^{2-}$, respectively. These data are among the lowest limit of detection values exhibited by previously reported MOFs for the detection of PA and $Cr_2O_7^{2-}$. Moreover, the mechanisms behind this selective detection of analytes were also investigated. In both these cases, the compound showed reusability up to five cycles without any loss of sensing efficacy. These experimental data vividly depict that **2'** can be considered as a promising sensing material for PA and $Cr_2O_7^{2-}$.

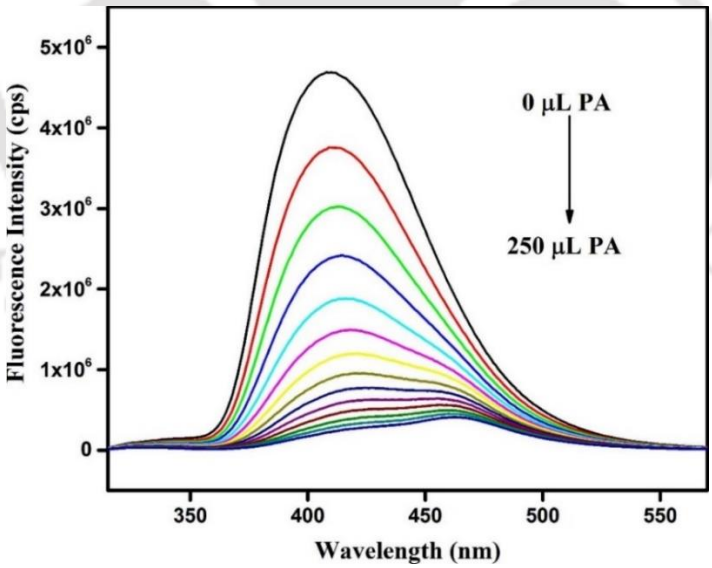

Figure 5. Fluorescence reduction for **2'** dispersed in water upon gradual addition of 3 mM PA solution prepared in DMSO.

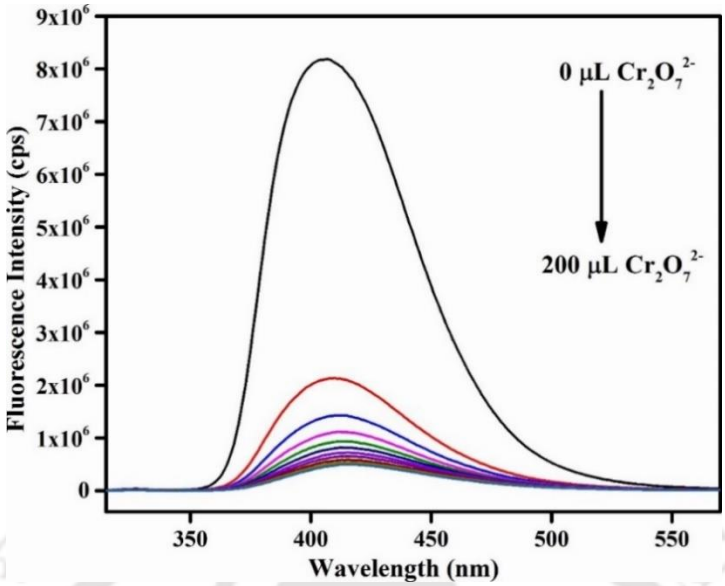

Figure 6. Fluorescence reduction for **2'** dispersed in water upon gradual addition of 3 mM $Cr_2O_7^{2-}$ solution prepared in water.

Chapter 4: Specific fluorescence sensing of hydrogen sulphide by an azide functionalized Zr(IV) MOF with DUT-52 structure.

Chapter 4 describes the synthesis and characterization of an azide functional group containing Zr(IV) based MOF with DUT-52 (DUT = Dresden University of Technology) structure *via a* solvothermal process. Acetic acid was used as a modulator to increase the crystallinity. The similarity between the XRPD pattern of the azide functionalized DUT-52 (DUT-52-N_3, **3**) material with the un-functionalized DUT-52 compound revealed that **3** has a similar structure as the parent DUT-52 MOF. The simulated cubic three-dimensional structural framework of **3** is shown in Figure 7. The cubic framework of **3** has hexanuclear $[Zr_6O_4(OH)_4]^{12+}$ building units. The three-dimensional cubic framework is formed by interconnecting these building units through the carboxylate groups of twelve NDC-N_3 linkers. The as-synthesized compound (**3**) was activated by exchanging occluded molecules with methanol and heating at 80 °C for 5 h. Both **3** and **3'** are thermally stable up to 320 °C and chemically stable in solvents like methanol, 1 (M) HCl and water. The BET surface area of **3'** was found to be 505 $m^2\ g^{-1}$. The CO_2 adsorption experiments revealed that the CO_2 uptakes of **3'** were 2.65 and 1.62 mmol/g at 0 and 25 °C, respectively. The data from fluorescence experiments suggested that **3'** exhibits sensitive and selective detection of H_2S in an aqueous medium (Figure 8). The response time of **3'** is very short (2 min) towards H_2S

(Figure 9). As shown in Figure 10, the other selected competitive analytes have negligible effects on the emission intensity of **3'** as compared to Na_2S. The fluorescence intensity increased by only 1-3 folds after the addition of other interfering analytes. In contrast, a remarkable luminescence increment up to 33 folds was observed for **3'** after the addition of Na_2S. The limit of detection (LOD) value was found to 0.50 µM. This value lies in the lowest range of H_2S detection by known MOFs. Moreover, the possible mechanism behind the enhancement of fluorescence intensity after the addition of Na_2S in **3'** was also examined. By using mass spectrometry, FT-IR and ^1H NMR spectroscopy, the mechanism for the reduction of azide into an amine group was established.

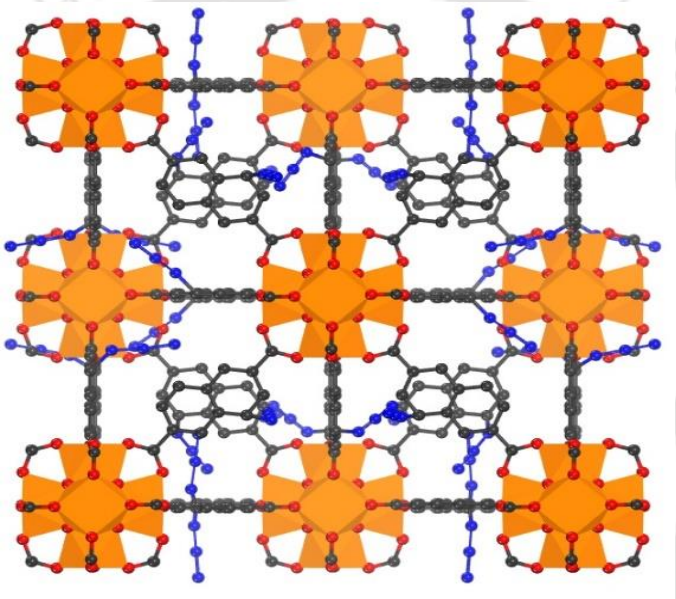

Figure 7. Perspective view of the simulated three-dimensional cubic framework of **3**. Color codes: Zr, orange polyhedra; C, grey; O, red; N, navy blue.

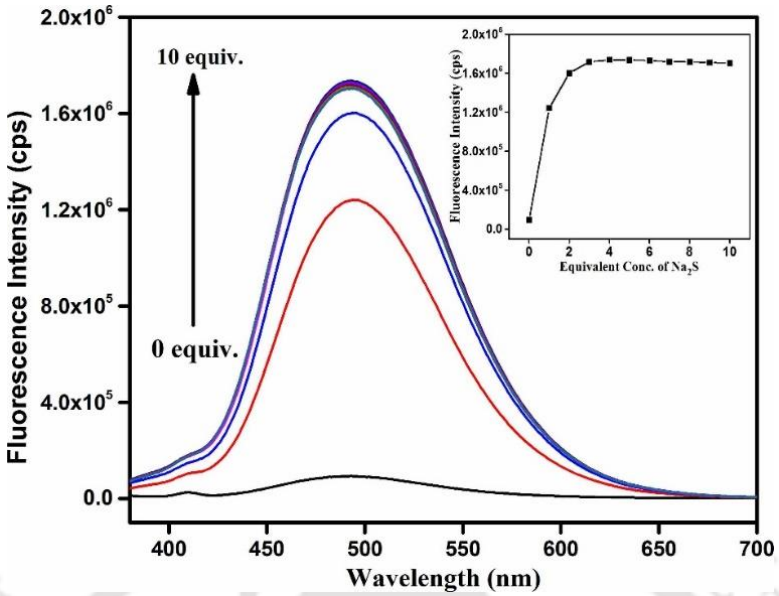

Figure 8. Fluorescence rise of **3'** in water with increasing concentration of Na_2S. Inset: fluorescence intensity is plotted against the concentration of Na_2S.

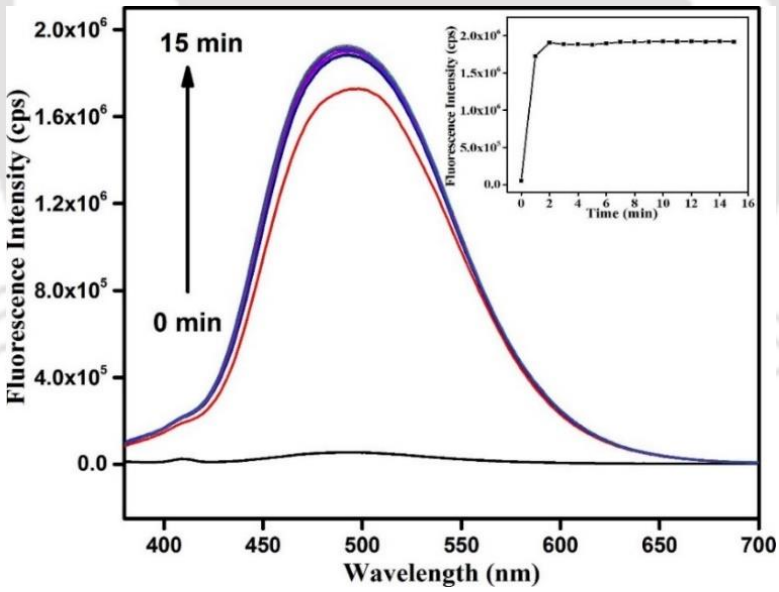

Figure 9. Fluorescence variation of **3'** after gradual addition of Na_2S (3 equiv. per azide group) with a time interval of 1 min up to 15 min. Insert: plot of fluorescence intensity versus time.

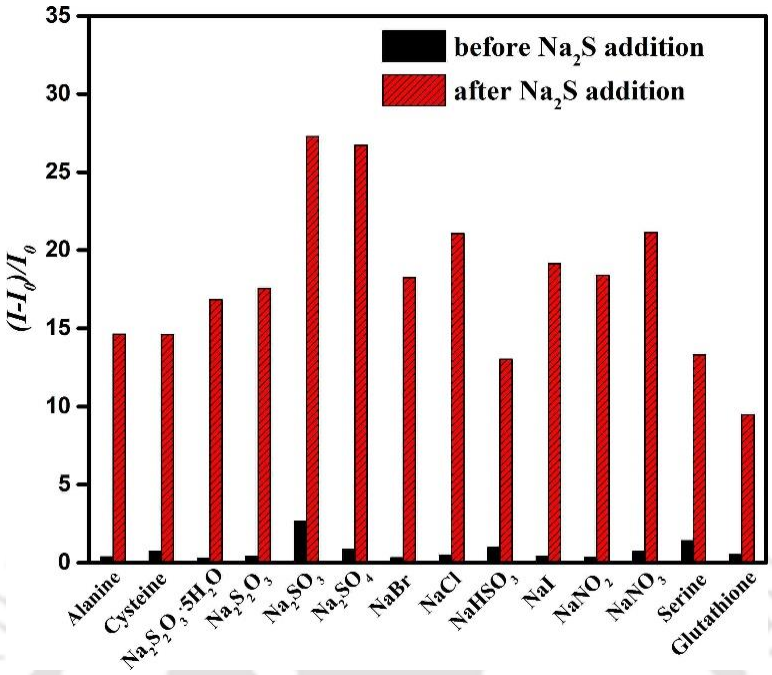

Figure 10. Fluorescence enhancement properties of **3'** in water upon the addition of different analytes (black) and further addition of H_2S into the same mixture (red).

Chapter 5: A Zr-based metal-organic framework with DUT-52 structure containing a trifluoroacetamido functionalized linker for aqueous-phase fluorescence sensing of cyanide ion and aerobic oxidation of cyclohexane.

Chapter 5 describes the synthesis and systematic characterization of a zirconium (Zr) metal-organic framework having DUT-52 structure with face-centred cubic (fcu) topology and bearing the rigid 1-(2,2,2-trifluoroacetamido) naphthalene-3,7-dicarboxylic acid (H_2NDC-NHCOCF$_3$) linker. In order to get the solvent-free compound (**4'**), **4** was stirred with methanol for overnight and subsequently heated at 100 °C for overnight under vacuum. As-synthesized (**4**) and activated (**4'**) compounds are thermally stable up to 300 °C. The BET surface area of **4'** was found to be 1105 $m^2 g^{-1}$. The emission band of compound **4'** upon excitation at 350 nm was found at 427 nm. Fluorescence titration experiments showed that after the addition of cyanide solution to **4'**, the emission intensity increased as well as a significant bathochromic shift of 63 nm was observed (Figure 11). This emission band at 490 nm indicated that the nucleophilic addition at trifluoroacetamide group took place by cyanide anion. Moreover, a very short response time (2 min) was shown by **4'** for CN^- detection (Figure 12). As shown in Figure 13, the increase in fluorescence intensity was negligible (0.7-0.9 fold) for all other competitive anions. The LOD was

found to be 0.23 µM. Compound **4'** can also be effectively used for CN^- detection in real water samples. The mechanism for the selective detection of CN^- was investigated systematically. Furthermore, the aerobic oxidation catalysis was performed with **4'** under mild reaction conditions, observing higher activity than analogous DUT-52 solid under identical conditions. These experimental results clearly indicate the benefits of the hydrophobic cavities of **4'** in achieving higher conversion and selectivity. The catalytic data of cyclohexane conversion and the selectivity of cyclohexanol and cyclohexanone are presented in Table 1. Catalyst stability is often checked by reusing the recovered solid in repeated cycles under the optimized reaction conditions. In this context, the stability of **4'** was tested by reusing the solid in subsequent runs and the observed results are shown in Table 1. These catalytic results clearly indicate that the catalyst retains its activity mostly and the minor decrease in its activity may be due to the loss in the recovery step.

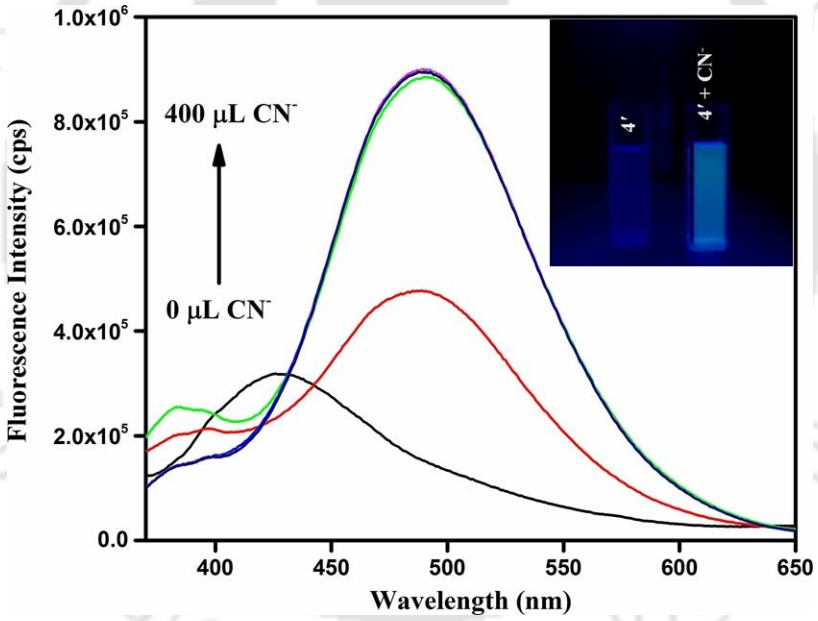

Figure 11. Fluorescence emission spectra of **4'** (in water) after incremental addition of aqueous CN^- solution (10 mM). Insert: digital images of cuvettes containing **4'** dispersion with and without CN^- solution under a UV lamp.

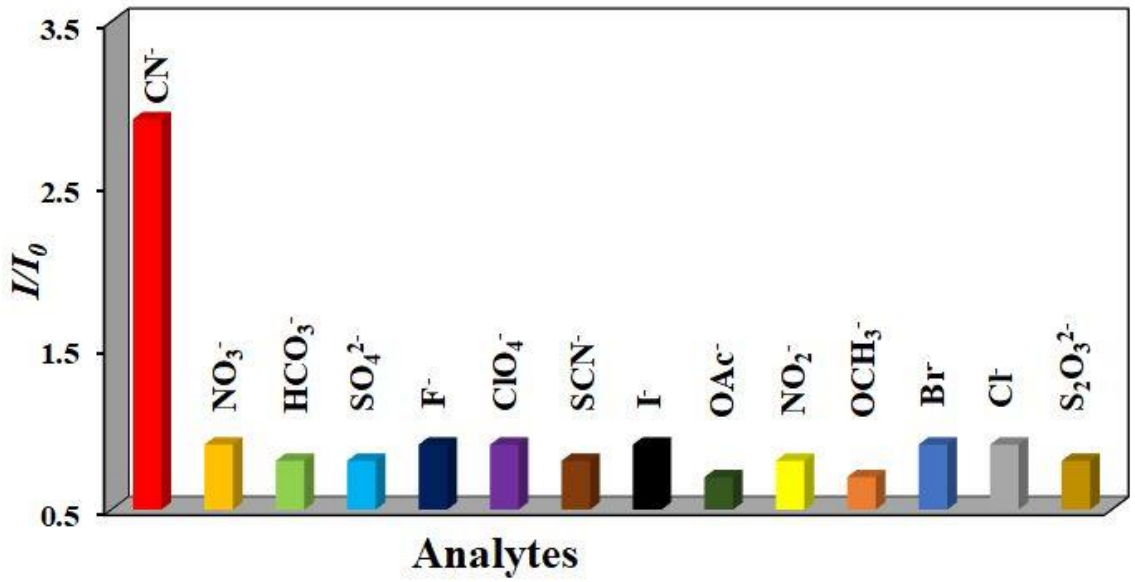

Figure 12. Fluorescence turn-on response of **4'** dispersion towards different anions (200 µL of 10 mM in water).

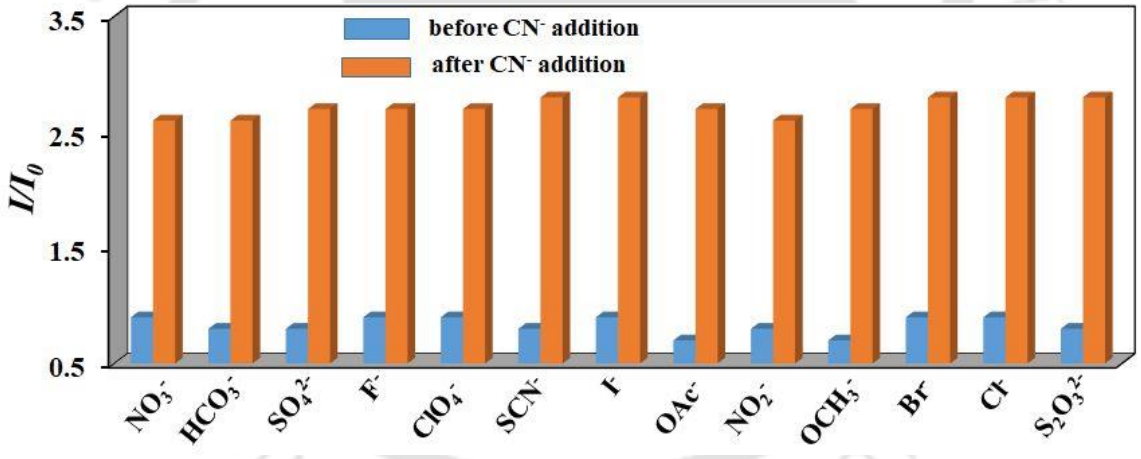

Figure 13. Comparison of fluorescence turn-on response of **4'** dispersion towards CN^- (200 µL of 10 mM solution in water) in presence of other potentially competitive anions (200 µL of 10 mM solutions in water).

Table 1. Aerobic oxidation of cyclohexane using **4'** and analogous catalysts.[a]

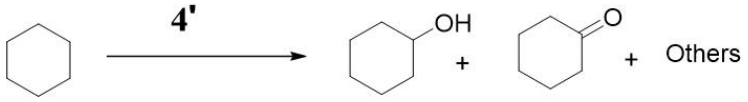

Entry	Catalyst	TBHP (µL)	Conversion[b] (%)	Selectivity[b] (%)	
				ol	one
1	**4'**	0	1	-	-
2	**4'**	8	21, 19,[c] 17[d]	29, 32,[c] 33[d]	55,51,[c] 47[d]
3	**4'**	20	42	33	48
4[e]	**4'**	8	-	-	-
5	DUT-52	8	6	32	48
6[f]	$ZrOCl_2 \cdot 8H_2O$	8	5	34	49
7[g]	$H_2NDC\text{-}NHCOCF_3$	8	3.5	36	46
8[h]	**4'**	8	11	36	47
9[i]	**4'**	8	15	25	51
10[j]	**4'**	8	11	28	47

[a] Reaction conditions: cyclohexane (1 mmol), catalyst (20 mg), CH_3CN (2.5 mL), $AgBF_4$ (26 mg), O_2 Purging, 60 °C, 24 h.
[b] Conversion and selectivity were determined by GC. Selectivity corresponds to the mixture of cyclohexanol and cyclohexanone. Other products are 2-hydroxycyclohexanone and adipic acid.
[c] First reuse.
[d] Second reuse.
[e] Pyridine (50 µL).
[f] 14 mg of $ZrOCl_2 \cdot 8H_2O$.
[g] 15 mg of $H_2NDC\text{-}NHCOCF_3$.
[h] Without $AgBF_4$.
[i] Cycloheptane as a substrate.
[j] Cyclooctane as a substrate.

Summary

The present thesis disseminates some of the strategies to synthesis water-stable MOFs and applies them for fluorescence sensing and catalytic application. The strategy behind the synthesis of MOFs for different applications is growing area of research within the MOF community. The inclusion of different functional sites within a single system expands the utility of MOF materials. The presence of hydrophobic cavity and also missing linker defects in metal clusters helps the researchers to explore the catalytic property of MOFs. The unique properties like high density of catalytically active sites contained within the confined nanospace allow MOFs to act as heterogeneous catalysts for many catalytic organic reactions with high efficiency and selectivity. The investigations in the present thesis disclose various aspects of research work on MOFs, which could be extended for future study. It is believed that our study will help the upcoming researchers to develop new MOF-related sensor compounds and also help to design new MOFs for catalytic study.

CHAPTER 1

Metal-organic frameworks (MOFs): synthesis, properties and applications

In the late 1990s, the discovery of a new type of highly crystalline porous materials has appealed great attention due to the potential of these materials in different applications such as catalysis, gas storage, drug delivery, luminescence, carbon dioxide capture, etc. These materials, termed metal-organic frameworks (MOFs), result from the combination of organic linker and metal ions/cluster, which form open frameworks. The major benefit of MOF instead of using other porous materials such as zeolites is that MOFs can be designed according to our purpose by selectively choosing the metal ion and organic linker. In this chapter, we mainly discuss brief history of MOFs along with different synthesis procedures and different applications of MOFs.

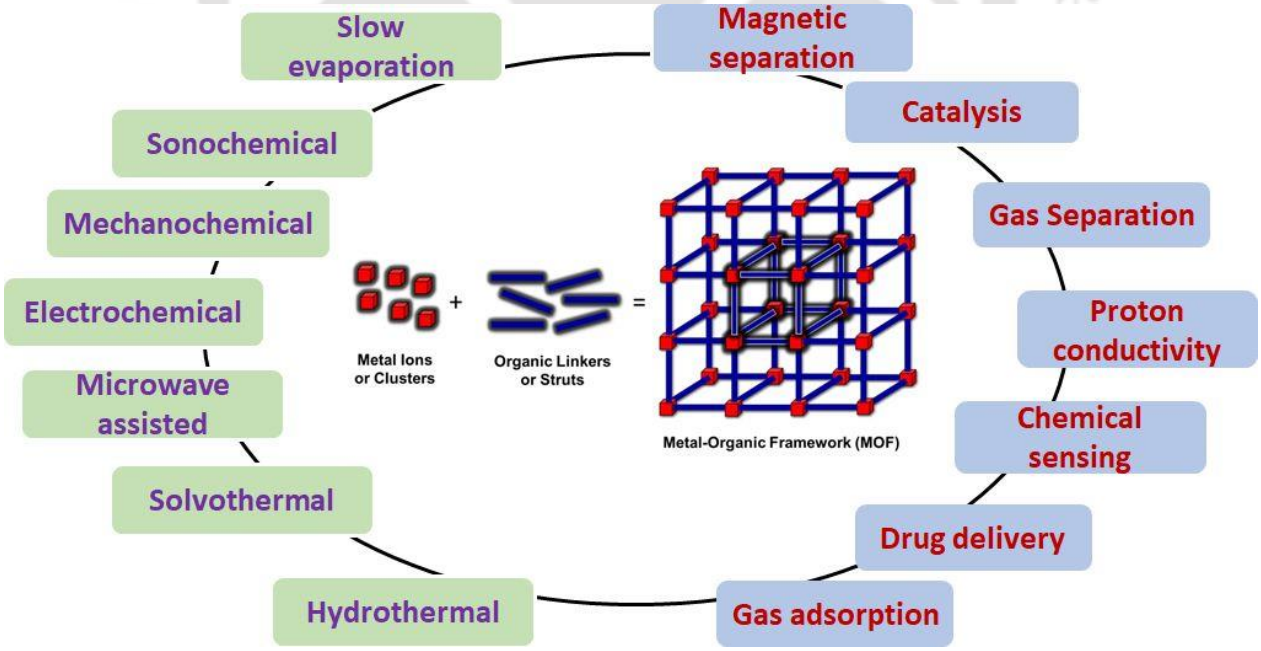

1.1 Introduction

Extensive research is carried out now-a-days on coordination polymers (CPs), which are a class of rapidly emerging crystalline porous materials.[1-3] In the past decade, there has been rapid growth for the development of organic polymer materials. CPs are highly crystalline than organic polymers. The term CP is used to define a compound, which has metal-organic units linked together at least in one dimension to form an infinite array through extended covalent or coordinate interactions or any other weak chemical interactions.[4-5] The metal ions and organic bridging linkers are mainly diversified in coordination behavior and geometry. It was first defined by J. C. Bailar in 1964.[6] The CPs have different forms like one-dimensional (1D) extended chains, two-dimensional (2D) sheets or three-dimensional (3D) frameworks. The different forms of CPs are recognized as two sub-classes: one is "coordination networks", which includes 1D, 2D, 3D or crosslinked CPs and another is "metal-organic framework" (MOFs) or "metal-organic coordination networks" (MOCNs) or "porous coordination polymers" (PCPs), which have coordination networks that contain potential voids.[1] So, we can say that MOFs are a subclass of CPs. As compare to CPs, MOFs usually exhibit higher thermal stability, permanent porosity and structural robustness.[7-8] Wikipedia defines MOF as a crystalline compound consisting of metal ions or clusters coordinated to often rigid organic molecules to form one-, two-, or three-dimensional structures that can be porous.[9] Yaghi et al. defined MOF as a porous structure constructed from the coordinative bonding between metal ions and organic linkers or bridging ligands (Figure 1.1).[10] During the past few decades, research on the synthesis and application of MOFs has experienced significant growth. The flexibility with which the constituent's geometry, size and functionality can be varied has led to thousands of compounds being prepared, characterized and studied each year. MOFs are renowned for their ability to impart functionality using a selective selection of linkers and metal nodes. There are many synthetic strategies by which we can tune the stability, particle size, surface area, hydrophobicity and flexibility of the frameworks.[11-12] The ability to tune such properties is a defining strength of MOFs as it provides strategic control over host-guest chemistry. Researchers performed further functionalization of MOFs using a number of strategies such as post-synthetic modification (PSM) of organic linkers or inorganic clusters, constructing frameworks using different pre-functionalized organic linkers etc. Due to unique chemical and physical properties like very large surface areas, ultrahigh porosity, various pore sizes and shapes and high thermal and mechanical stabilities, MOFs have many potential

applications like gas storage and separation,[13-15] catalysis,[16-19] bioimaging,[20-22] drug delivery,[23-26] chemical sensing[27-29] and so on.[30-35]

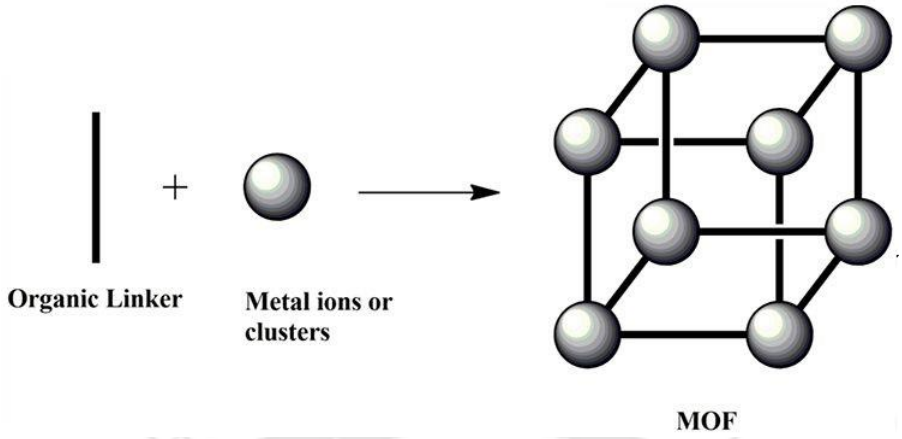

Figure 1.1 Structure of MOF.

Detecting environmental contaminants through simple and effective methods has been a long-term goal for researchers. Environmental contaminants are any physical, chemical, biological or radiological substance that has an adverse effect on air, water, soil or any living organism.[36-37] So, finding a chemical sensor to detect the contaminants selectively is uttermost important. Exploring the performances of MOFs as a chemical sensor is attracting intense interest among researchers, especially in the field of chemistry. Many investigators have begun exploring the potential of MOFs as chemical sensors. The ideal sensor materials are those which can show some characteristic properties like fast response time, highly sensitive and selective sensing towards particular contaminants, reusability, high stability in different conditions and most importantly low in cost. MOFs offer a unique platform to act as an ideal sensor as they have a degree of structural predictability as they contain both organic and inorganic components, coupled with high surface areas, high catalytic ability and structural flexibility.[38]

Solid materials with accurately controllable nanometer-scale porosity act as smart materials to be used in heterogeneous catalysis over their liquid analogs.[39] In this context, MOFs are often used as they has become one of the most attractive classes of solid supports currently in this field.[40] Because of their abundant unsaturated metal sites, high porosity and unprecedented degree of tunability, MOFs are considered ideal candidates for the heterogeneous catalysis.[41] Being highly crystalline materials, MOFs allow us to investigate the distribution of active sites within the framework and evaluate the influence of the framework on catalytic activity. The metal nodes and the functional organic linkers of the MOFs can be

fine-tuned either by utilizing different functional groups like -NH_2, -NO_2, -N_3 etc, or by the post-synthetic modification of parent MOFs. The modification of the linker by a suitable functional group can help significantly on activity, stability and catalytic properties of the MOFs.[42-45]

1.2 Overview of history

Traditionally, some of the highly porous solids have been produced by discovery-based synthetic chemistry. The robust porous materials can be constructed like "molecular scaffolds" by connecting rod like organic linkers with inflexible metal clusters which act as joints.[8] The applications of these materials highly depend on the functionality of the linker moieties. This strategy was used to develop coordination network between the organic linker and inorganic clusters. The term coordination polymer is undoubtedly the most nebulous, as it signifies the extended network between the metal and linker through coordination bonds. During the 90's, such network structures were still uncommon, even though the first use of the term coordination polymer can be traced back to 1916.[46] However, remarkable progress in this field has been made mainly from the 1990s when Robson and co-workers developed a framework of infinite molecules consisting of three-dimensionally linked rod-like segments.[47] The detailed study about the structures was carried out by Kitagawa and co-workers and Yaghi and co-workers. In 1995, Yaghi and co-workers coined the term metal-organic framework (MOF) and also demonstrated for the first time that it was possible to adapt the similar approach forwarded by Robson to make extensive families of compounds with specific structural topologies. In 1999, Yaghi and co-workers synthesized highly porous new materials namely MOF-5 ($Zn_4O(BDC)_3$, BDC = 1,4-benzendicarboxylate) using zinc(II) nitrate and 1,4-benzendicarboxylic acid in *N, N'*-dimethylformamide (DMF)/chlorobenzene mixture. In the same year, Williams and his group successfully synthesized a copper-containing MOF, namely HKUST-1 ($Cu_3(BTC)_2$, BTC = 1,3,5-benzenetricarboxylate). These two findings made a huge impact on the MOF chemistry. After that many scientists namely Ferey et al., Kitagawa et al., Stock et al., and many more started their research to find more about MOF chemistry. In the early stag,e due to the lack of a generally accepted definition, several research groups used a different name for this new type of hybrid materials. Among them, porous coordination polymer (PCP)[1], porous coordination network (PCN)[48], microporous coordination polymer (MCP),[49] bio-MOF,[50] zeolite-like metal-organic framework (ZMOF)[51] and zeolitic imidazolate framework (ZIF)[52] are most common. The scientists have published some literatures to elucidate the definitions of the terms.[4, 53] In 2012, the International Union of Pure and Applied Chemistry (IUPAC) has

revealed a provisional definition of MOF as "Metal-Organic Framework (MOF) is a Coordination Polymer (or alternatively Coordination Network) with an open framework containing potential voids."[9]

Among porous solid materials, inorganic and carbon-based materials are mainly known and used until the mid-1990. In 1990, Robson and co-workers synthesized three-dimensional porous coordination polymers which displayed ion-exchange properties.[47] The first robust and highly porous material, MOF-5 by Yaghi and co-workers made revolution in the field of porous solid materials (Figure 1.2).

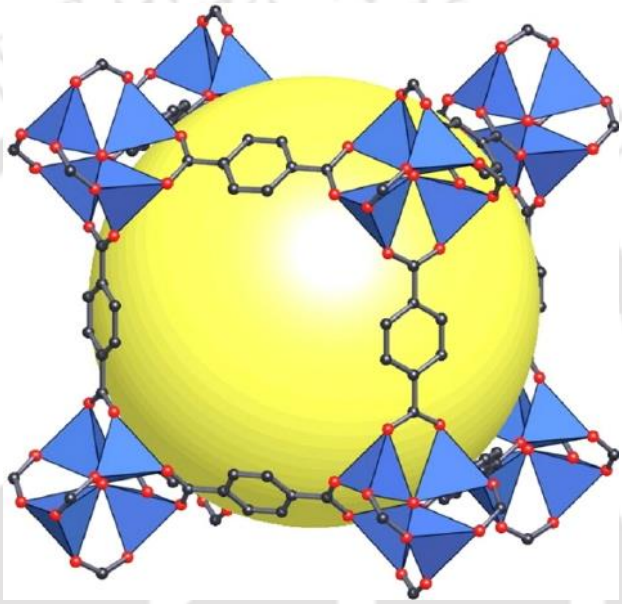

Figure 1.2 The MOF-5 structure shown as ZnO_4 tetrahedra (blue polyhedral) joined by benzene dicarboxylate linkers (O, red and C, black) to give an extended 3D cubic framework with interconnected pores of 8 Å aperture width and 12 Å pore (yellow sphere) diameter. Reproduced with permission from ref. 76. Copyright 2003 Nature.

The name MOF-5 has been coined in reminiscence of the popular zeolite ZSM-5.[54] This revolutionary compound is more porous than zeolite and activated carbon.[55-56] It is composed of BDC linkers and Zn_4O units which have been applied in various fields, particularly in gas storage, separation and catalytic conversion of CO_2. Interestingly, this compound is highly stable up to 300 °C. So, MOF-5 is the first example of MOF material with permanent porosity and high thermal stability. Since then, MOFs have become one of the hottest research areas in materials chemistry. In the last 20 years, the Cambridge Crystallographic Database Centre (CCDC) has recorded more than 90,000 MOF structures. As more researchers worked on it, MOF-5 can be adapted as a modular structure from which several other isorecticular

frameworks can be synthesized by merely changing the functionality and length of its organic linker.[56] After the discovery of MOF-5, many highly porous MOF materials wee reported in the literature. In 1997, a three-dimensional MOF was reported by Kondo et al. that exhibited gas sorption properties at room temperature.[57] Ferey et al. reported non-flexible as well as flexible MOFs namely MIL-47[58] and MIL-53[59], respectively in 2002. Since then, tremendous effort has been devoted to develope microporous MOFs such as MOF-177,[60] MIL-101 (Cr/Fe/Al),[61-63] ZIF-7,[64] UiO-66 (Zr/Hf/Ce),[65-66] MIL-53 (Al/Fe/Cr),[67-69] MIL-100 (Fe/Cr/Al),[70-71] PCN-224,[72] PCN-14,[73] DUT-52,[74] HKUST-1[75], etc.

1.3 Basic design and synthesis strategies of MOFs

The design of MOF material is one of the most important as well as a critical stage. Very well-prepared strategies for proper choice of metal centers and linker connectivity are required for the generation of a particular crystal structure or framework topology.[11, 76] Generally speaking, MOFs are self-assembled from organic linkers and metal ions through coordination bonds. The final three-dimensional structures of MOFs are formed by strong bonds between metal ions and organic secondary building units (SBU).[77] As far as the porous character is concerned, organic linkers with multiple bonds must be preferred to ensure rigid topologies with an open framework. The name MOF itself says that there are two types of components: inorganic connectors and organic linkers. The inorganic connectors are either isolated metal centers or clusters. This metal centers act as “nodes” of the framework, which are characterized by the number and direction of their connecting positions.[76] Transition metal ions are commonly used because of the fact that transition metal ions are well-known to prefer different coordination numbers and geometries such as linear, tetrahedral, square planar, square-pyramidal, trigonal-bipyramidal and octahedral geometries. On the other hand, organic linkers act as the “spacer” of the framework. The linkers are also characterized by their connectivity. The longer the organic linker is used in the synthesis process, the greater number of adsorption sites within the prepared materials are provided. Due to the infinite numbers of combinations of the metal cluster with linkers, there is an infinite number of possible network structures. Even the number of possible net topologies is infinite due to many topologically different vertices and the infinite ways of linkage of the vertices.[78] In Figure 1.3, for example, each metal center gives a different metal cluster according to the availability of their connectivity with terephthalic acid linker (linear rod-like connector).

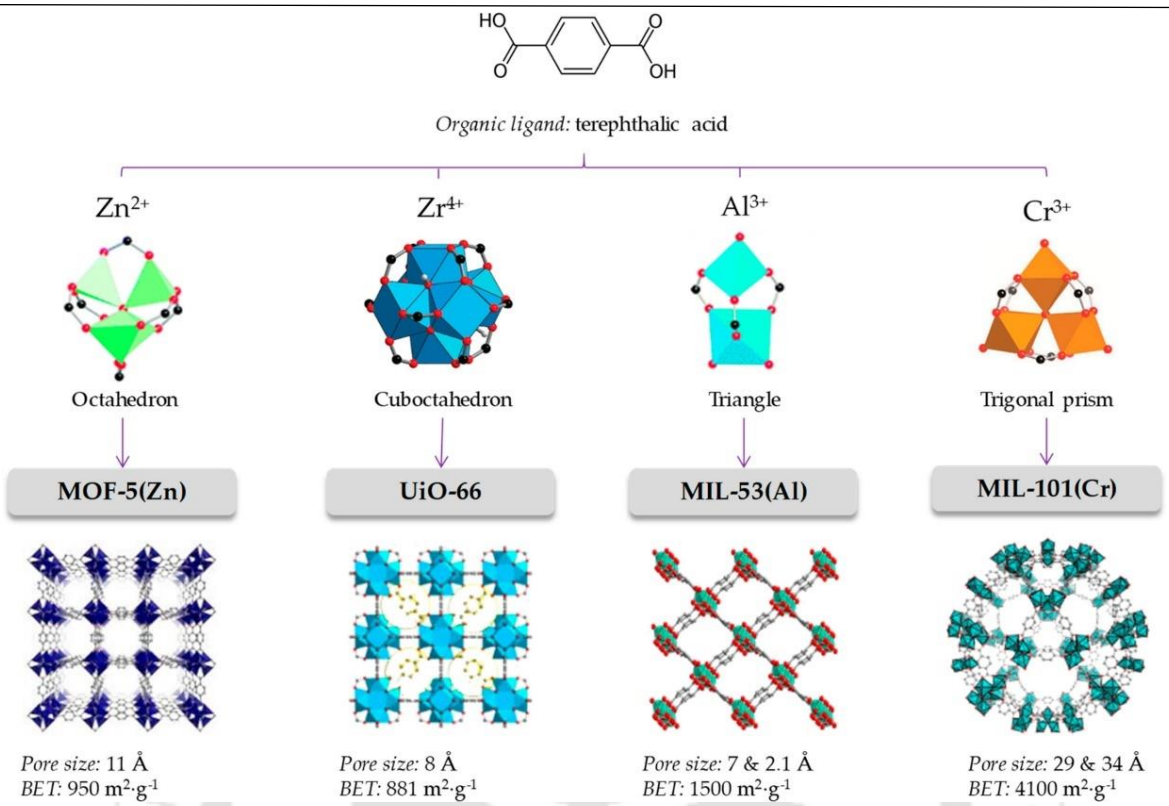

Figure 1.3 The node and connector approach to prepare MOFs. The adequate selection of the organic linker (linear in the case of terephthalic acid) and connection geometry of the metal cluster leads to the desired topology. Each framework topology has its characteristic pore size and available surface area. Reproduced with permission from ref. 76. Copyright 2019 MDPI.

When considering the structures of MOFs, it is important to recognize the SBUs, which dictate the final topology of a framework. The metal-cluster based SBUs are most commonly finite units with points of extension which form well-defined geometrical shape.[77] These shapes are joined by polytopic linkers into periodic frameworks. In the metal SBU, the group of metal atoms joined to one or more other metal atoms in the same SBU either by M-X-M links (X = N or O or any non-metal) or through a common point of extension such as M-O-C-O-M carboxylate. Figures 1.4a and 1.4b show SBU with a trigonal and a square planar arrangement of the metal atoms, respectively. Figure 1.4c shows a tetrahedron of metal atoms surrounding a central oxo anion and a dimetal paddlewheel SBU is shown in Figure 1.4d. In each case, the edges between two metal ions are bridged by the coordinating atoms of the linker and result in control of the orientation of the linker.[79] The geometry of the SBU, not only depends upon linker and metal but also metal to linker ratio, solvents and the source of anions to balance the charge of the metal ion.[80]

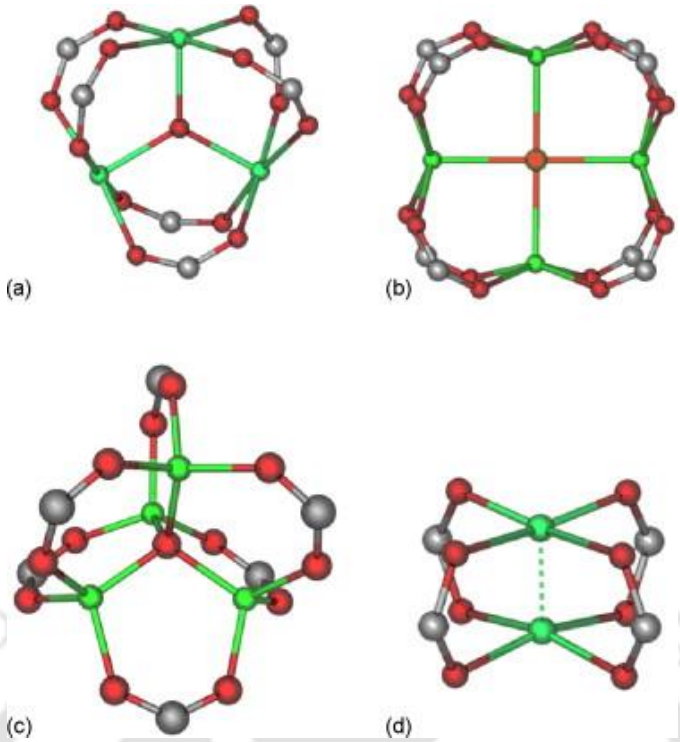

Figure 1.4 Structural representations of some SBUs, including (a) trigonal planar, (b) square planar, (c) tetrahedral, and (d) tetragonal paddlewheel. Reproduced with permission from ref. 79. Copyright 2009 Elsevier.

Once the synthesis of the SBU is established, it can be used to direct the assembly of ordered frameworks with rigid organic linkers; thus, it is easy to predict the chemistry of the resulting crystalline materials. Yaghi and his co-workers named this approach as "reticular synthesis".[81] They defined these terms as the process of assembling judiciously designed rigid molecular building blocks into predetermined ordered structures (networks), which are held together by strong bonding.[81] Overall, it is the combination of both SBUs (as connectors) and organic ligands (as linkers) that determines the final framework topology (Figures 1.5).[82] Reticular synthesis has been successfully applied to many MOF systems, including pillared paddlewheel MOFs, UiO-n, HKUST-1 and others.[83] As shown in Figure 1.5, a diamondoid net can be constructed from 4-connected tetrahedral clusters and ditopic linkers. On the other hand, a cubic net can be formed from 6-connected octahedral clusters and ditopic linear linkers.

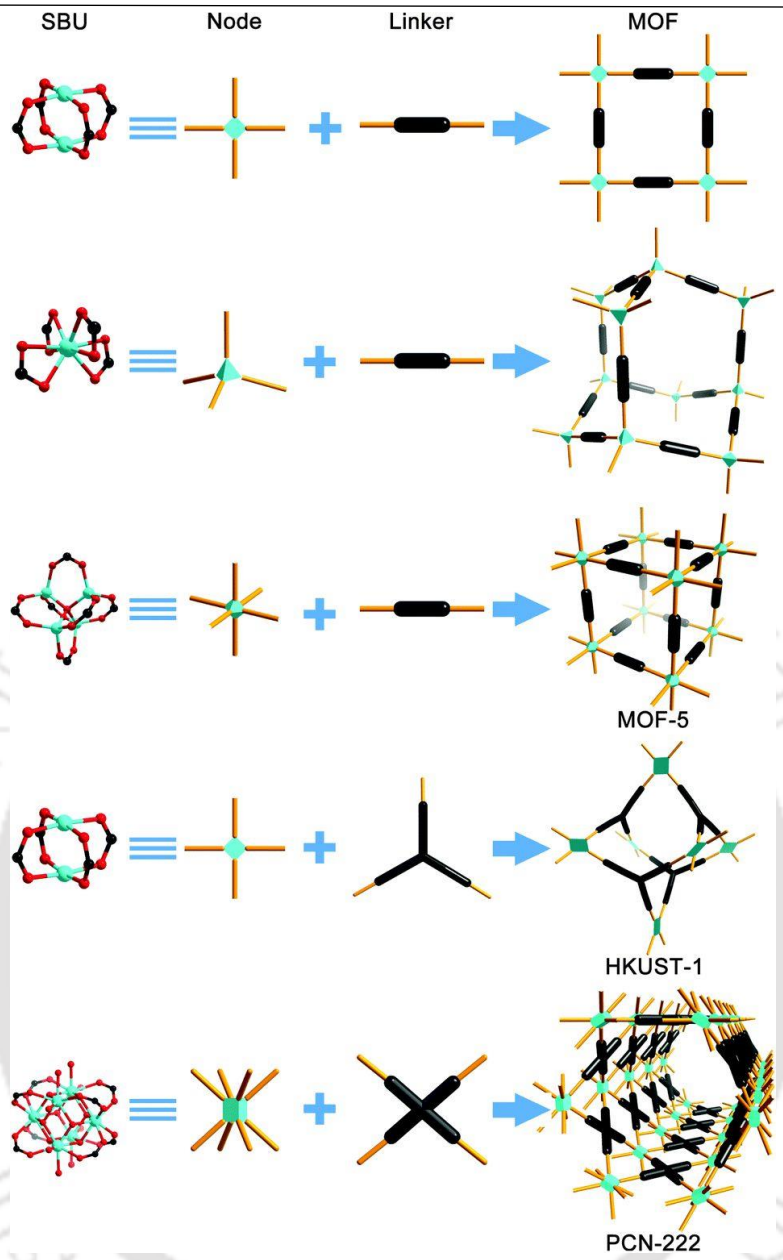

Figure 1.5 Graphical illustration of the construction of some representative coordination polymers/MOFs from SBUs and rigid linkers. Reproduced with permission from ref. 82. Copyright 2014 Royal Society of Chemistry.

1.4 Stability and rigidity of MOFs

At the early stage, MOFs made from divalent metals (Zn^{2+} or Cu^{2+}) exhibited exceptional porosity as well as showed a wide variety of applications but ultimately proved unsuitable for use under harsh conditions because of stability issues.[84] For the practical applications, the frameworks of MOFs should maintain their structural integrity. The lack of stability of the framework was mainly attributed to its large cavity and/or the solvent-

framework intermolecular forces. Metal-linker (M-L) coordination bond strength plays a key role in determining the stability of the MOF framework. Usually, metal carboxylate frameworks consist of high-valance metal ions with high charge density that could form a strong coordination bond towards the linkers. A high valence metal cluster with a higher coordination number leads to rigidity in the framework. The concept of the hard/soft acid-base principle is used for the basic design of MOFs. High-valance metal ions, such as Fe^{3+}, Cr^{3+}, Zr^{4+} have been exploited to synthesis stable carboxylate MOFs. For example, MIL-n, UiO-n, and PCN-n series of MOFs are highly stable in acidic and alkaline media.[85] The soft acidic metal cations such as Zn^{2+}, Co^{2+}, Ni^{2+} can also be used to coordinate with soft basic N-donor linkers, which form much stronger metal-N bonds. Soft basic linkers such as imidazolates, pyrazolates, triazolates are generally used to synthesize MOFs with soft divalent metal ions. Colombo et al. reported some microporous pyrazolate-based MOFs, $M_3(BTP)_2$ (M = Ni, Cu, Zn, Co) which exhibited great hydrothermal stability.[86] Another strategy to prepare stable MOFs is to use at least two different metal ions as nodes in the same framework. The incorporation of second or more metal ions i.e. mixed-metal organic frameworks (M-MOFs) provides structural/compositional diversity, multifunctionality as well as stability to the framework.[87] M-MOFs can be thermodynamically/kinetically controlled based on the nature and ratio of their different metal precursors and synthesis parameters.[88] Particularly in the field of heterogeneous catalysis, M-MOFs offer the possibility to have two centres of different catalytic activity in close spatial proximity. Sometimes, more than one linker (mixed linkers) is used to synthesize MOFs, which provide greater flexibility in terms of surface area and modifiable pore size.[89] Usually, one anionic linker and one neutral linker are used to synthesize a mixed-linker framework.

Water or moisture is usually present in most industrial processes. Unless a particular MOF is stable in water or moisture, it cannot be utilized. Hence, the structural stability of MOFs in aqueous media is one of the most important aspects to be considered for practical application. Water stability is also a crucial factor for the use of MOFs as a heterogeneous catalyst in an aqueous medium. In the case of luminescent sensing in biological media, the stability of MOFs in aqueous medium is crucial. It was observed that metal clusters present in MOFs are susceptible to the attack by nucleophilic water molecules, which in turn leads to linker displacement, phase change and even partial collapse of the framework. Hence, reducing the contact between a water molecule and host MOF framework was believed to be an effective strategy to enhance a MOF's stability. Introduction of the hydrophobic functionalized linker or

blocked metal ions can prevent water molecules to come close to the metal cluster.[90] It was observed that functional groups such as fluoro, alkoxy, alkyl, or aryl group can help the MOF structure to stabilize in the aqueous medium.[91] Moreover, polymers such as polydimethysiloxane (PDMS) can be used to cover the surface of MOF particles which in turn can help effectively to enhance the water resistance.[92] Power X-ray diffraction (XRPD) pattern of MOFs between post-exposure samples and pristine samples can provide an idea about the crystallinity of the MOF after treatment with water.[93] Gas sorption experiment, prior to and after exposure to water is another technique to determining the stability of the framework.[94] Over the last five years, significant research work has been conducted by researchers to improve the stability of the MOFs in an aqueous environment.[93, 95-97]

1.4.1 Linker design

MOFs can be designed with target specificity by the judicious selection of organic linkers. Different linkers have different binding abilities with the metal centers to give a hierarchy of MOF structures. The length, size and functional groups of linkers play an important role in determining the dimensionality, interpenetration and porosity of the frameworks. The organic linkers are carboxylates or other organic anions, such as phosphate, sulfonate and heterocyclic compounds (Figures 1.6-1.7). The most commonly reported linkers used to construct MOFs are carboxylic acids and heterocyclic compounds containing nitrogen donor atoms.[98] The main advantage to use a carboxylic acid linker is that it can adopt versatile coordination modes with a metal ion to produce a coordination network that displays high thermal stability.[99] Highly conjugated carboxylate linker can exhibit π-π stacking and hydrogen bonding interactions. Apart from aromatic carboxylic linkers, the heterocyclic carboxylic acid linkers are also used for the preparation of MOFs with various functionalities. Herein, the multiple sites such as proton donor and acceptor by nitrogen atom and carboxylate oxygen coordinated with metal ions form exact network structures with specific topologies.[100] The strength of nitrogen-transition metal bonds is greater than that of oxygen-transition metal bonds. N-heterocyclic linkers such as pyrazine, imidazole, have been extensively studied aiming to achieve more stable MOFs via nitrogen-metal coordination. All heterocyclic linkers contain several Lewis basic nitrogen atoms which act as both coordinating and guest-interactive sites.

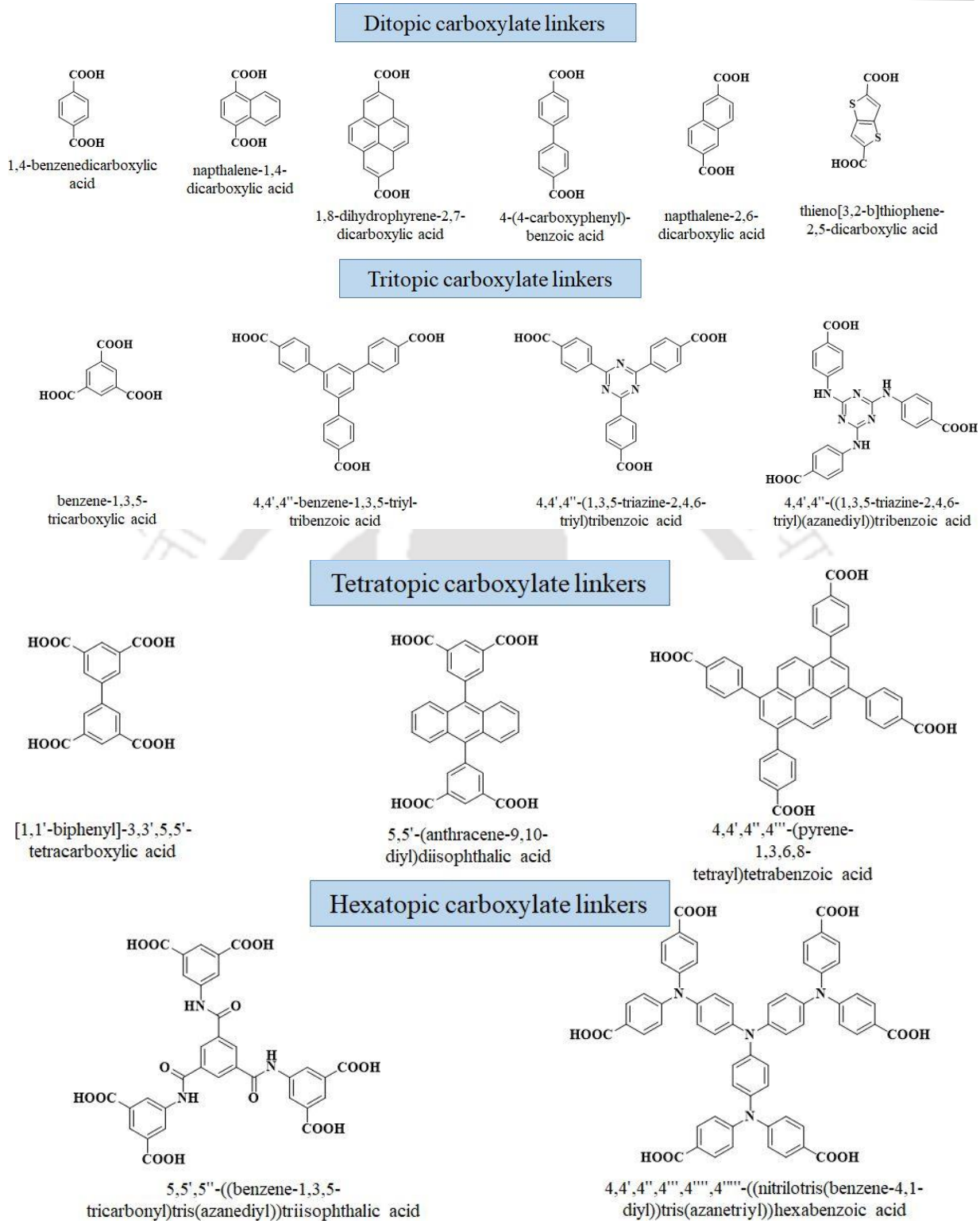

Figure 1.6 Examples of linkers based on carboxylic acid groups.

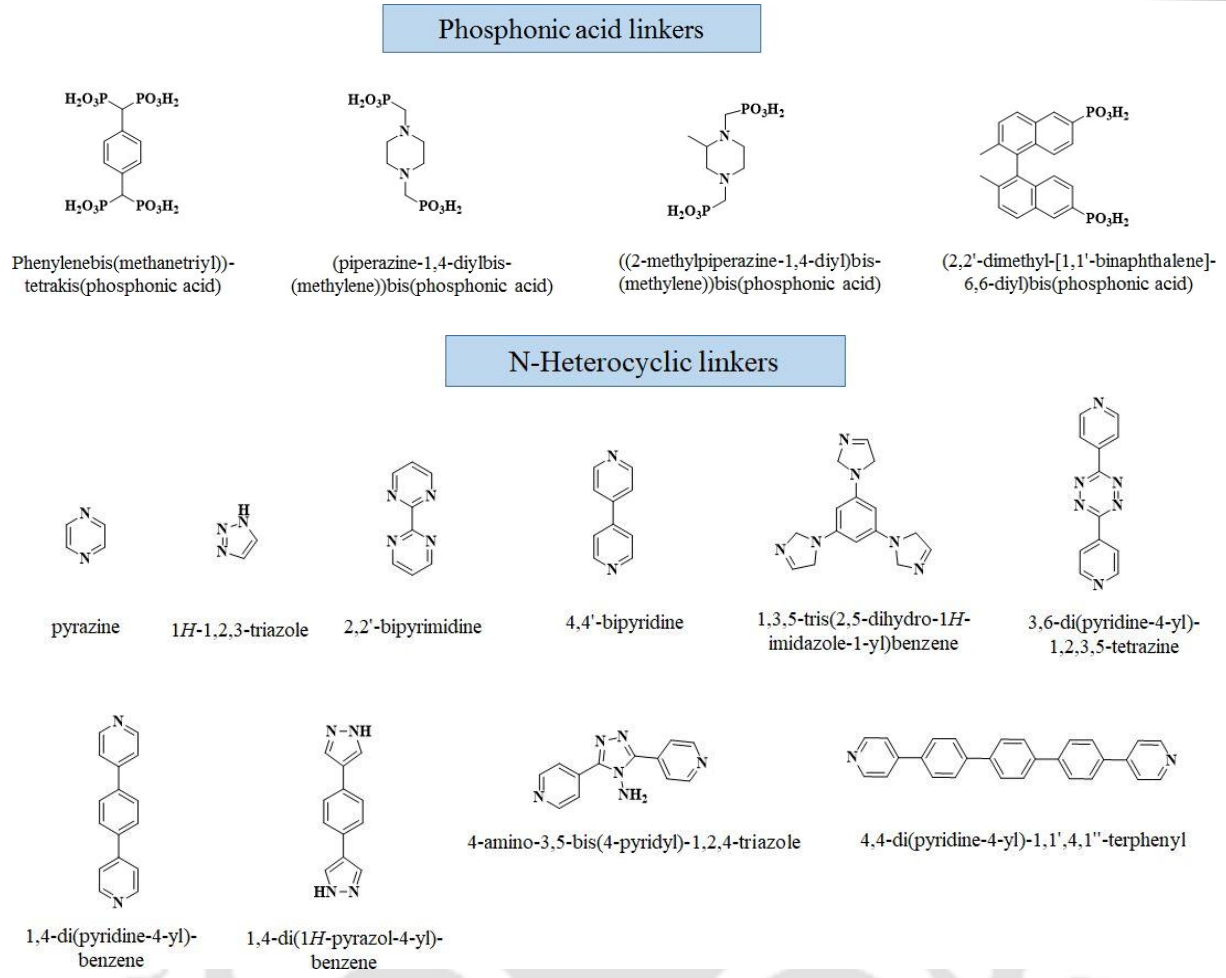

Figure 1.7 Examples of some phosphonic acid and N-heterocyclic linkers.

1.4.2 Functionalization of linker

One of the main reasons for the introduction of linker into MOF structure is to enrich the host-guest chemistry between MOFs as a host and other small molecules as a guest. With a selective functional group, MOF structure can be tuned which in turn shows improving property towards specific applications. The different functional groups of the linkers affect the structural properties of MOFs differently. Some properties such as crystallinity, porosity, flexibility and stability MOFs always depend on the type of functional group in the linkers.[101] Therefore, it is possible to synthesize functional MOFs with desired functionality, stability and porosity for specific application through pre-designing by functionalization using a chemically ideal organic functional group. The functional group can play different roles such as coordinating sites and guest-interactive sites. Some examples of functionalized linkers are shown in Figure 1.8.

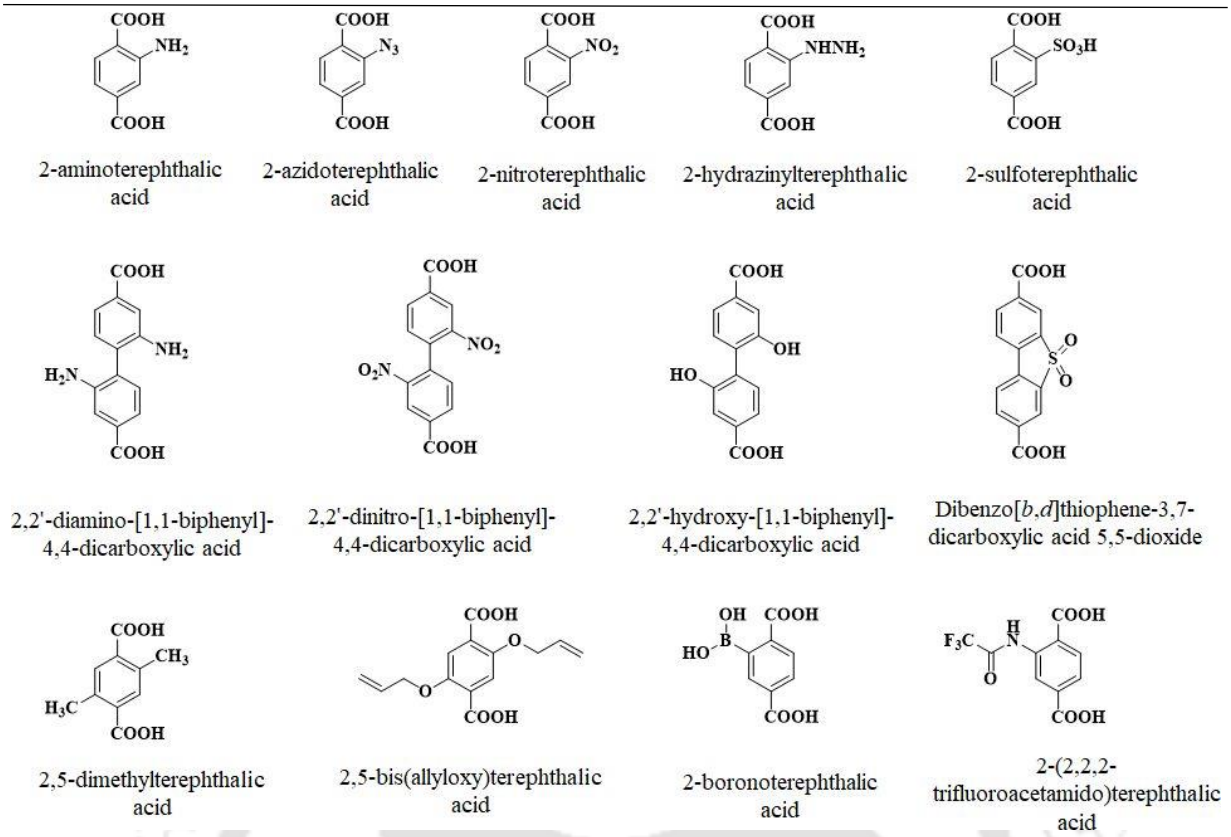

Figure 1.8 Examples of some pre-functionalized linkers based on carboxylic acid groups.

1.5 Synthetic protocols

Several types of methods were followed for the preparation of MOFs (Figure 1.9). It was observed that different synthesis methods can lead to different particle sizes, size distributions and morphologies which in turn leads to different applications.

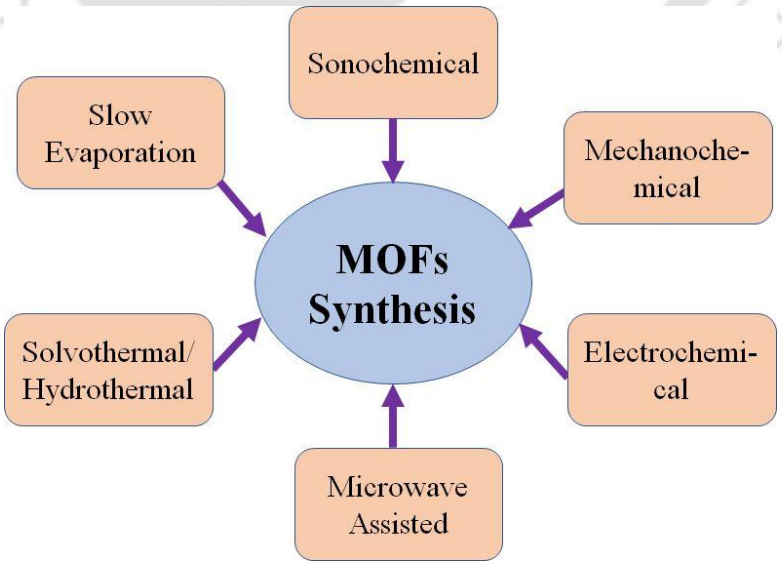

Figure 1.9 Common synthesis methods of MOFs.

1.5.1 Slow evaporation synthesis

This method of synthesis is most easy as no external energy supply is required. It is the commonly used conventional method to synthesize MOFs which requires more time compared with other well-known conventional methods. Here, the reactants i.e., metal salts and organic linkers are first mixed in the liquid phase with or without the aid of additional auxiliary molecules.[102] The resultant solution is concentrated by slow evaporation of the solvent at room temperature or any fixed temperature. Sometimes the process involves a mixture of solvents, which can increase the solubility of the reagents and can make the process faster by quicker evaporation of low-boiling solvents. Sometimes along with solvent (miscible the reactants), an immiscible solvent is used for layering. At the interface, crystal growth occurs due to the gradual diffusion of the two solvents. This method of synthesis is also known as the diffusion method.

1.5.2 Solvothermal/hydrothermal synthesis

In this liquid-phase synthesis method, organic linkers and metal salt are mixed together in high boiling solvent systems. These reactions are carried out in closed vessels under constant pressure (Figure 1.10).[103] The source of energy is mainly thermal energy between 353K-453K and reaction time is in between 48 to 96 h.[104] Usually Teflon-lined autoclaves or sealed Pyrex tubes are used in which reactants in high boiling organic, polar solvents such as dimethyl formamide (DMF), diethyl formamide (DEF), DMSO, water, acetonitrile, ethanol and methanol are taken.[1] When water is used as a solvent, then the synthesis method is called hydrothermal. The superheated solvents reduced the viscosity and enhance the diffusion of chemical species. The major advantage of this reaction is that it offers high solubility of the precursors and the formation of good quality MOF crystals suitable for structural characterization. This method usually requires long reaction times depending upon the factors such as solvent, temperature, reagent concentrations, pH etc. The schematic diagram for MOF synthesis by hydrothermal/solvothermal method is shown in Figure 1.10. Some examples of MOFs synthesized by this method are UiO-66,[65] DUT-52,[74] BUT-30,[105] NH_2-MIL-125,[106] etc.

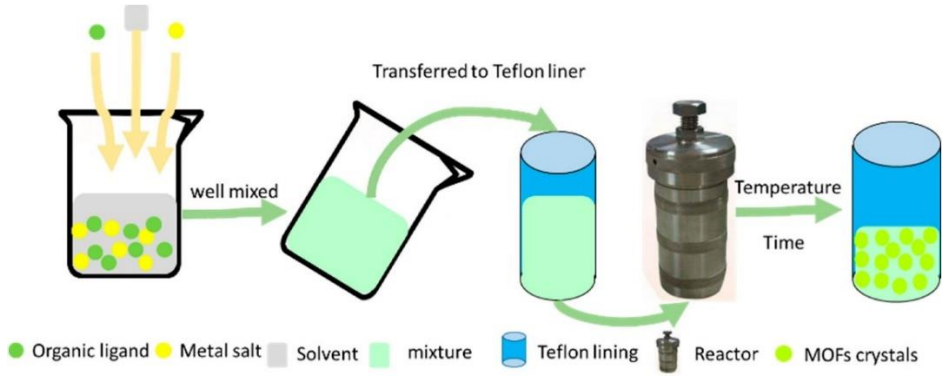

Figure 1.10 Schematic diagram for MOF synthesis by the hydrothermal method or the solvent heating method. Reproduced with permission from ref. 103. Copyright 2018 MDPI.

1.5.3 Microwave assisted synthesis

This synthesis method provides a very rapid method for the synthesis of MOFs. Here, microwave irradiation is used along with polar solvents like DMF, DEF, DMA, etc (Figure 1.11).[107] Beside rapid crystallization, this synthesis method also give very high phase selectivity and narrow particle size distribution. During this synthesis method, dipoles of the precursors in the reaction vessel rotate themselves and align with the electromagnetic energy. Consequently, the heat is generated due to the collision between reactant molecules. This synthesis method is also termed as "microwave-assisted solvothermal synthesis" as the quality of the crystals obtained here are generally the same as those produced by regular solvothermal processes, but the main advantage is that products are formed within a maximum of 1 h. Another advantage of microwave synthesis is that energy is generated directly throughout the bulk of the material instead of by conduction from the external surface. Cr-MIL-100 MOF,[108] Fe-MIL-53,[109] MOF-205,[110] and MOF-74 (Ni)[111] are some example of MOFs, which were synthesized using microwave-assisted synthesis method.

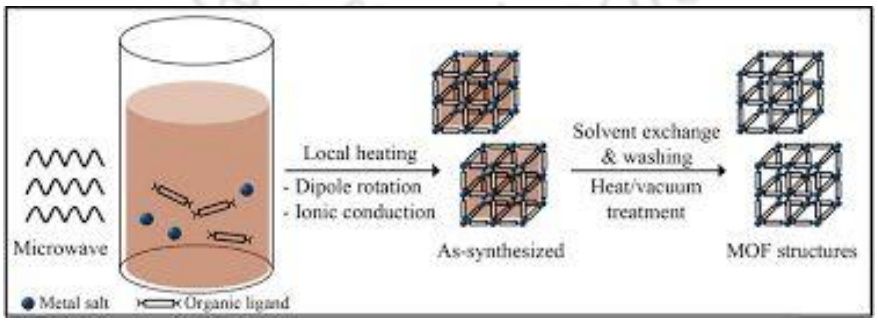

Figure 1.11 Microwave-assisted solvothermal synthesis of MOF structure. Reproduced with permission from ref. 107. Copyright 2013 Springer Nature.

1.5.4 Electrochemical synthesis

This synthesis method is mainly applied for the production of MOF samples on an industrial scale.[112] It requires two conducting electrodes and an ion source. It also necessitates an electrolyte and organic linkers for the synthesis of MOF materials. Metal deposition on the cathode is avoided by using protic solvents. Furthermore, compared to solvothermal methods, the electrochemical synthesis method possesses more parameters for fine-tuning due to the simple adjustment of the voltage or imposing particular signals. Mueller et al. first reported MOFs which were synthesized by electrochemical methods in large scale.[112] Li et al. reported a facial electrochemical plating method to prepare fluorescent MOF thin films ($Zn_3(BTC)_2$) (Figure 1.12).[113] Moreover, they also reported that the MOF thin films can be applied to distinguish nitro explosives by simply varying the solution concentration. Some other examples of MOFs synthesized by this method are Al-MIL-53,[114] MIL-100 (Fe),[115] ZIF-8,[115] etc.

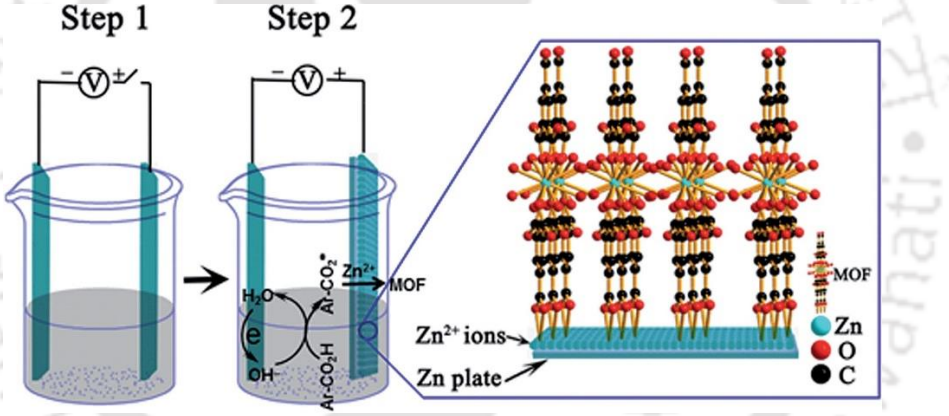

Figure 1.12 Electrochemical synthesis of fluorescent MOF film ($Zn_3(BTC)_2$). Reproduced with permission from ref. 113. Copyright 2013 Royal Society of Chemistry.

1.5.5 Mechanochemical synthesis

In the mechanochemical synthesis method, there is mechanical breakage of intramolecular bonds followed by a chemical transformation. It is a solvent-free synthesis method where mechanical force initiates the chemical reaction. The construction of bonds between the reactants through simple, fast, economical and environmentally friendly method is always advantageous in modern synthetic chemistry. Different types of mechanochemical techniques are used for MOFs synthesis such as dry grinding, liquid-assisted grinding, etc. Among all, dry grinding is considered as the easiest and simplest method. James et al. first reported MOFs which were synthesized by mechanochemical synthesis method. They

developed porous MOFs by simply grinding metallic Cu with linkers followed by ball milling for 10 min to yield porous MOFs with a 3D network. Some other examples of MOFs synthesized by this synthesis method are HKUST-1,[35, 116] ZIF-8,[117] MOF-74,[118] etc.

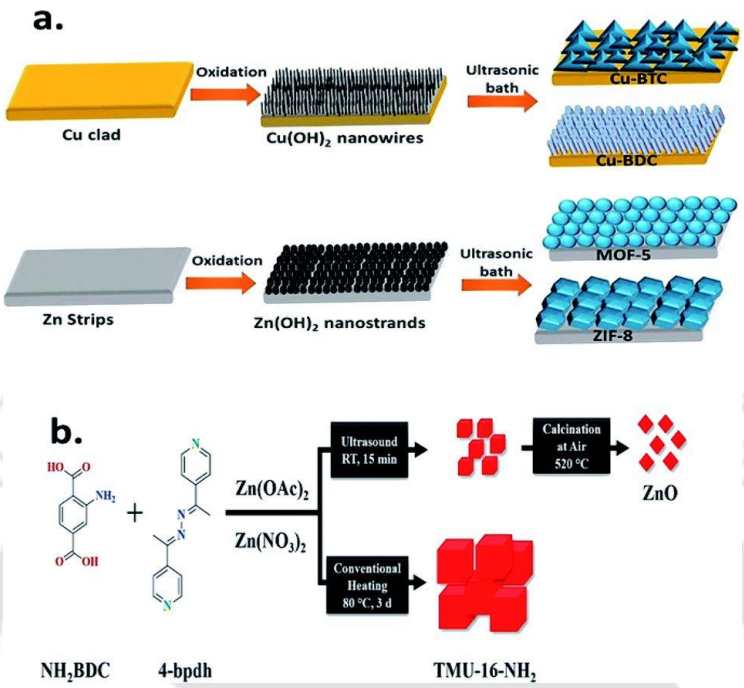

Figure 1.13 (a) Sonochemical fabrication of thin Cu–Zn-based MOF films and (b) schematic of particle size comparison between sonication and conventional heating processes for synthesising Zn-based MOFs. Reproduced with permission from ref. 121. Copyright 2018 Elsevier.

1.5.6 Sonochemical synthesis

In sonochemical synthesis, intensive ultrasound radiation between 20 kHz and 10 MHz is used to accelerate the nanostructure synthesis. The main principle of this synthesis method is to establish an energy-efficient, room-temperature and environmentally friendly methodology for MOF synthesis. This method can generate homogeneous nucleation centers and required less crystallization time as compared to conventional hydrothermal method and can lead to higher yield of MOFs. Qiu et al. reported the first MOFs which were synthesized by a sonochemical process.[119] It was observed that changing the reaction time and temperature can result in different sizes and morphologies of MOFs during sonochemical synthesis. In recent years, many other MOFs such as MOF-177,[56] HKUST-1[120] and MOF-5[56] have been synthesized using sonochemical synthesis methods. Abuzalat et al. demonstrated the growth of

MOFs on different substrates using this synthesis method (Figure 1.13).[121] Some factors like concentration, reaction time, pH also play an important role to get MOF growth rate.

1.6 Post-synthetic modification

Another alternative route to obtain MOFs having desired functionality is post-synthetic modification (PSM).[122] PSM is an excellent method to prepare MOFs which are topologically identical but functionally diverse with parent MOFs. The surface environment of the MOF can be modified to increase structural stability as well as introducing desired properties. It was observed that usually, the existing feature of a parent framework gets better in the resultant MOF after PSM.[123] Hence, it is becoming a key synthetic tool for advancing MOFs for a range of emerging applications, including selective gas sorption, catalysis and drug delivery. Various approaches of PSM include metal exchange, linker exchange, metal incorporation, linker installation, linker removal and guest incorporation inside the pores (Figure 1.14).[123]

In the meat exchange process, the breaking of coordinate bond and formation of new coordinate bond take place between the organic struts and metal ions. Different factors such as crystal field stabilization energy (CFSE) and ionic radius of the incoming metal ions influence the stability of the final framework. Post-synthetic metathesis and oxidation (PSMO) is another interesting and less explored pathway to obtain high-valence MOFs. This synthesis technique is useful to prepare single crystals of Cr(III)-based MOFs.[124] Here, the Mg(II) MOF (PCN-426-Mg) crystals were synthesized and the metal ions were exchanged with Cr(II). Then, the samples were oxidized in air to produce the corresponding Cr(III) MOF single crystals. The linker modification method is another important method to prepare MOFs from the parent framework. The linker can be modified with a new functional group, which can act as adsorption sites for various target molecules. Zhang et al. reported that a typical azide-alkyne click reaction can be employed to modify the azide functional group in UiO-66-N_3 with phenylacetylene (Figure 1.15).[125] The click-generated triazole unit can act as the metal-binding site to coordinate with Hg^{2+}, which exhibits selective and sensitive fluorescence responses towards Hg^{2+} over other metal ions.

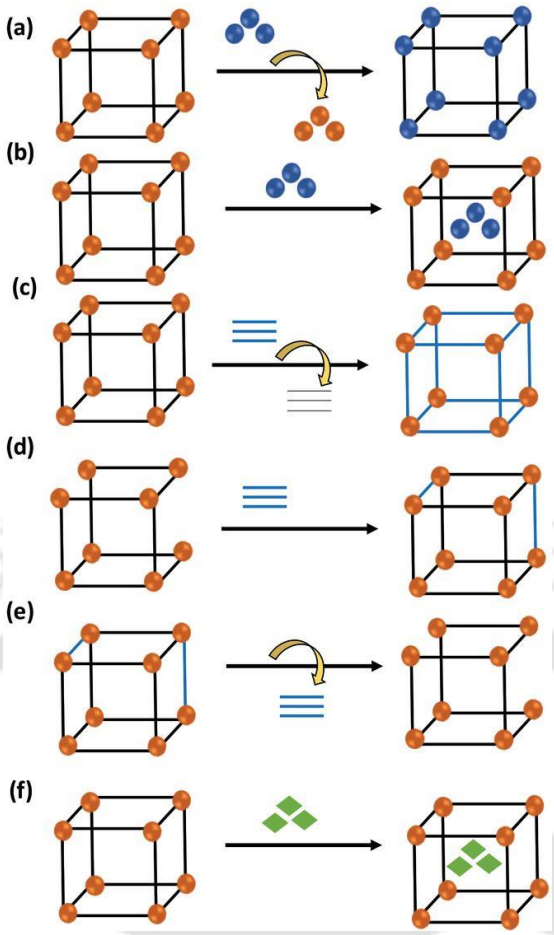

Figure 1.14 Possible pathways of PSM in MOFs: a) metal exchange, b) metal incorporation, c) linker exchange, d) linker installation, e) linker removal, and e) guest incorporation inside the pores. Reproduced with permission from ref. 123. Copyright 2020 John Wiley and Sons.

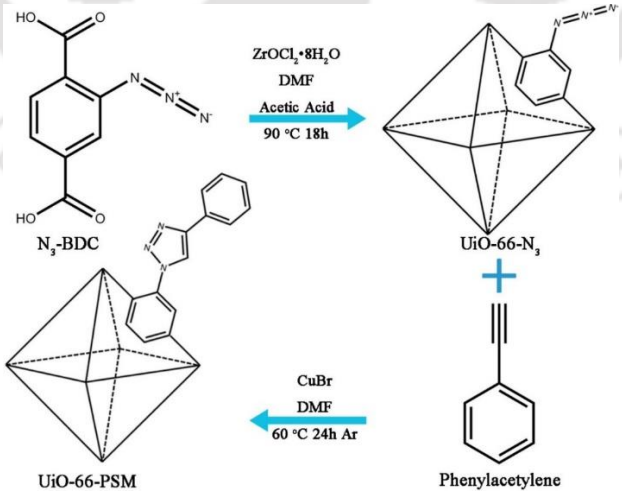

Figure 1.15 The synthesis procedure of UiO-66-N_3 and phenylacetylene functionalization of UiO-66-N_3 by click reaction. The topology is shown in a simplified form as an octahedral cage. Reproduced with permission from ref. 125. Copyright 2017 Elsevier.

1.7 Zirconium and zinc MOFs constructed from carboxylate linkers

1.7.1. Zirconium-carboxylate based MOFs

Generally, the MOFs constructed from group IV metal-based nodes such as zirconium and hafnium display exceptional thermal stability and chemical stability in acidic and neutral aqueous solutions.[97, 126] Especially, the outstanding property of Zr^{4+} ion is because of the high charge and strong oxophilicity of the ion. The strong coordination bond between the Zr^{4+} cation and the carboxylate linker makes Zr-MOFs an exceptional family.[127] The first reported Zr MOF is UiO-66 in the year 2008 (UiO stands for the University of Oslo) by using benzene-1,4-dicarboxylic acid (BDC) as the organic linker.[65] It was reported by Lillerud et al. and has formula $Zr_6(\mu_3\text{-}O)_4(\mu_3\text{-}OH)_4(BDC)_6$ with 12-coordinated $Zr_6(\mu_3\text{-}O)_4(\mu_3\text{-}OH)(CO_2)_{12}$ clusters. Six vertices of the octahedra are occupied by Zr^{4+} and eight triangular faces are alternatively capped by four μ_3-OH and four μ_3-O. The $Zr_6(\mu_3\text{-}O)_4(\mu_3\text{-}OH)_4$ core is further terminated by 12 carboxylates forming $Zr_6(\mu_3\text{-}O)_4(\mu_3\text{-}OH)(CO_2)_{12}$ clusters. Two types of micropores namely tetrahedral and octahedral cages are observed in the structure with BET surface area around 1200 $m^2\ g^{-1}$. The framework of UiO-66 exhibited very high stability among other reported MOFs at that time. Another two MOFs namely UiO-67 and UiO-68 were reported by using elongation of the linkers used in UiO-66 (Figure 1.16).[84] In 2011, Schaate et al. introduced the modulated synthetic strategy to prepare Zr-MOFs with controlled particle sizes.[128] They obtained a single crystal of UiO-68-NH_2. Its structure was solved by single-crystal X-ray diffraction analysis. First aliphatic Zr-MOFs were reported by De Vos and his group in 2015.[129] They used aliphatic linker adipic acid and $ZrOCl_2 \cdot 8H_2O$ as a metal salt to obtain a framework with bcu topology in aqueous conditions. Zhou et al. in 2012 reported a Zr-MOF namely PCN-22 with 8-connected $Zr_6(\mu_3\text{-}O)_4(\mu_3\text{-}OH)_4(OH)_4(H_2O)_4(COO)_8$ cluster in which four equatorial carboxylates were replaced by four pairs of the terminal $-OH^-/H_2O$ linkers.[130] It was observed that although the connection numbers are reduced but the stability of MOFs with 8-connected Zr-clusters is not compromised. Interestingly, PCN-222 and its analogous compounds are stable in conc. HCl and the presence of unsaturated Zr-cluster opens a platform for versatile applications.[131] The 6-connected $Zr_6(\mu_3\text{-}O)_4(\mu_3\text{-}OH)_4(OH)_6(H_2O)_6(COO)_6$ clusters were also reported which demonstrating the strong tolerance of Zr-clusters towards the elimination of linkers.[132]

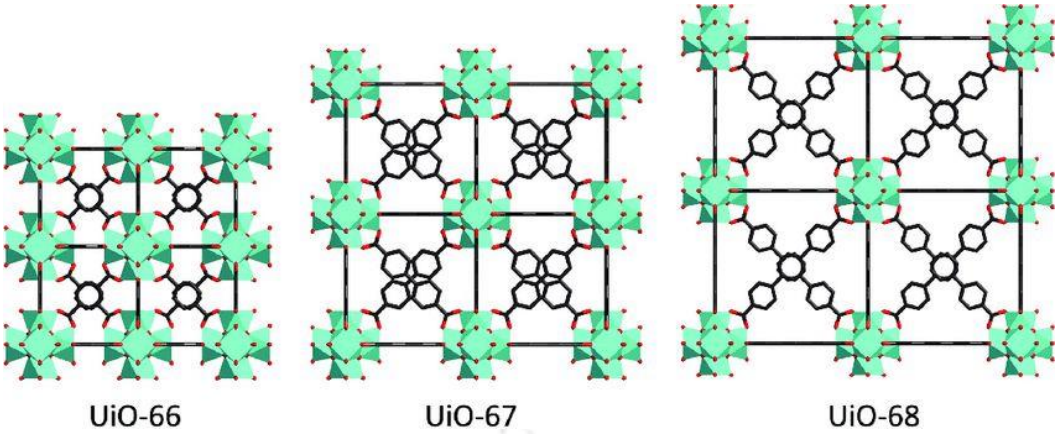

Figure 1.16 Structures of UiO-66, UiO-67, and UiO-68. Reproduced with permission from ref. 84. Copyright 2018 John Wiley and Sons.

There are many applications already reported for Zr-MOFs. The metal cluster composed of Zr^{4+} ion can be manipulated by dehydration or by the induction of defects in the structure to yield highly active Lewis acidic catalysts.[133] Vermoortele et al. revealed that coordinatively unsaturated metal sites in UiO-66 can be drastically increased by using specific modulators during the synthesis of MOFs.[133] The Zr-MOFs formed by terephthalate and 2-aminoterephthalate linker were used for the photocatalytic activity for hydrogen generation.[134] Zr-MOFs have been also investigated as electrocatalysts.[135] Farha and his co-workers have investigated the catalytic activity of several MOFs (including NU-1000) with Zr_6 node for the degradation of nerve agents and their simulants.[136] NU-1000 has a very wide mesoporous channel (31 Å) that helps for the diffusion of the substrate throughout the material which ultimately leads to superior catalytic activity.[136] Zr-MOFs were also used as fluorescent probes. In most cases, the fluorescence of Zr-MOFs originates from organic linkers. Considering the variable connection number as well as wide applications, numerous new members of the Zr-MOFs can be expected in the future. Some Zr-MOFs with their linker are summarized in Table 1.1.

Table 1.1 Summary of some reported Zr-MOFs.

Zr-MOF	Linker	Topology	Ref.
UiO-66	BDC	fcu, 12-connected	65
UiO-67	BPDC	fcu, 12-connected	65
UiO-68	TPDC	fcu, 12-connected	65

NU-1000	TBAPy	Csq, (4,8)-connected	137
MOF-801	FUM	fcu, 12-connected	95
MOF-802	PZDC	bct, 10-connected	95
MOF-808	BTC	spn, (3,6)-connected	95
MOF-812	MTB	ith, (4,12)-connected	95
MOF-841	MTB	flu, (4,8)-connected	95
MOF-525	TCPP	ftw, (4,12)-connected	138
MOF-545	TCPP	csq, (4,8)-connected	138
PCN-94	ETTC	ftw, (4,12)-connected	139
PCN-221	TCPP	ftw, (4,12)-connected	140
PCN-222	TCPP	csq, (4,8)-connected	141
PCN-777	TATB	spn, (3,6)-connected	142
DUT-51	DTTDC	reo, 8-connected	143
DUT-52	2,6-NDC	fcu, 12-connected	74
DUT-84	2,6-NDC	(4,4)llb, 6-connected	74
DUT-67	TDC	reo, 8-connected	144
BUT-10	FDCA	fcu, 12-connected	145
BUT-30	EDDB	fcu, 12-connected	105
Zr-TTMC	TTMC	fcu, 12-connected	146
Zr-BTB	BTB	kgd, (3,6)-connected	147
Zr-AP-2	AP	dia, 4-connected	148
Zr-BTBA	BTBA	ftw, (4,12)-connected	149

Linkers are abbreviated as: BDC = terephthalic acid, BPDC = biphenyl-4,4′-dicarboxylic acid, TPDC = [1,1′:4′,1″-terphenyl]-4,4′-dicarboxalic acid, TBAPy = 1,3,6,8-tetrakis(p-benzoate)pyrene, FUM = fumaric acid, PZDC = 1-H-pyrazole-3,5-dicarboxyalic acid, BTC = benzene-1,3,5-tricarboxylic acid, MTB= 4′,4″,4‴,4⁗-methanetetrayltetrabiphyl, TCPP = meso-tetrakis(4-carboxylatephenyl)porphyrin, TATB = 4,4′,4″-s-triazine-2,4,6-triyl-tribenzoic acid, DTTDC = dithieno[3,2-b;2′,3′-d]-thiophene-2,6-dicarboxylic acid, 2,6-NDC =

naphthalene-2,6-dicarboxilc acid, TDC = 2,5-thophenedicarboxlic acid, FDCA = 9-fluorenone-2,7-dicarboxylic acid, EDDB = 4,4′-(ethyne-1,2-diyl)dibenzoic acid, TTMC = (2E, 4E)-hexa-2,4-dienedioate, BTB = 5′-(4-carboxyphenyl)[1,1′:3′,1″-terphenyl]-4,4″-dicarboxylic acid, AP = adipic acid, BTBA = 4,4′,4″,4‴-([1,1′-biphenyl]-3,3′,5,5′-tetrayltetrakis(ethyne-2,1-diyl))tetrabenzoic acid.

1.7.2. Zinc-carboxylate based MOFs

According to the HSAB principle, some stable MOFs can be formed by soft divalent metal ions (Zn^{2+}, Cd^{2+}) and soft azolate-based linkers. Examples of some azolate-based linkers are imidazole, pyrazole, triazole, etc. Similar to carboxylic acids, the azoles are usually deprotonated in order to coordinate with the metal cations. The metal ions especially having d^{10} electronic configuration generally show high complexation affinity to carboxylate and do not interfere with luminescence properties because they can display varied coordination numbers and geometries, and exhibit outstanding luminescent properties. As a result, this type of material is promising candidates for potential photoactive materials. In 1999, Yaghi et al. first developed a zinc containing MOF namely MOF-5 which contains clusters of Zn_4O located at the corners of the structure that are connected orthogonally to six units of terephthalate. Zinc-based MOFs have been studied as hydrogen storing materials like MOF-5,[8, 150] MOF-177,[151] IRMOF-6, IRMOF-20,[152] etc. Among all the MOFs with a reasonable hydrogen storing capability, MOF-5 and MOF-177 are the most interesting members of the family. Both MOF-5 and MOF-177 can be synthesized with a similar metal source (zinc nitrate hexahydrate), same organic solvents (DMF or DEF) and different organic linkers. Benzene dicarboxylic acid and 1,3,5-benzene tribenzoic acid are the organic linkers for MOF-5 and MOF-177, respectively.[153] Garcia and his co-workers examined the semiconductor behaviour of MOF-5.[154] In 2014, Karmakar et al. synthesized three Zn-MOFs under hydrothermal conditions, which were used as efficient catalysts for diastereoselective Henry reaction and transesterification.[155] Qiu et al. reported a fluorescent Zn-MOF (HNU-50) for effective detection and extraction of U(VI).[156] Ma et al. designed and prepared a fluorescent Zn-MOF for nitroaromatic sensing.[157] Recently, Sun and his group reported stable Zn-MOFs constructed by fluorenone carboxylate linker for multifunction detection and photocatalysis property.[158] Some Zn-MOFs with their linkers are summarized in Table 1.2.

Table 1.2 Summary of some reported Zn-MOFs.

Zn-MOF	Linker	Topology	Ref.
MOF-5	BDC	pcu	81
UMCM-1-NH_2	BTB	-	159
$[Zn_2(L)_2(bpe)_2(H_2O)_2]$	PMBD	-	160
NNU-1	HFIPBB	bcu, (4,6)-connected	93
GDMU-3	DCPP	lvt, (4,8)-connected	161
GDMU-4	TPTC	-	162
Zn-MOF	DPCBIC	flu, (3,6)-connected	163
HPU-1	DPTMIA	-	164
BIPT-1	BIPF	-	165
[Zn(L)]·2.7DMF	BTTA	$CdSO_4$ net	166
Zn-MGO	BDC	-	167
ZIF-90	ICA	SOD	168
$[NH_4]_2[ZnL]\cdot 6H_2O$	BTC	PtS	169
Zn-MOF	BDC, BPCDA	-	170
MOF1	BSPT	-	171
NJMU-001	BTC	Lcy	157
$[Zn_2(TBIB)_2(HTCPB)_2]$	TBIB	Sql	172
HNU-50	NPYC, PMA	-	156
MOF-205	NDC, BTB	ith-d	110
Zn-MOF-74	DHTA	-	118

Linkers are abbreviated as: BTB =1,3,5-tris(4-carboxyphenyl)benzene, PMBD = 4,4′-((1,2-phenylenebis(methylene))bis(oxy))dibenzoic acid, TTC-1 = (1,1′:4′,1″-terphenyl)-2′,3,3″,5′-tetracarboxylic acid, TTC-2 = (1,1′:4′,1″-terphenyl)-2′,4,4″,5′-tetracarboxylic acid, HFIPBB = 4,4′-(hexafluoroisopropylidene)bis(benzoic acid, DCPP = 2,5-di(3′,5′-dicarboxylphenyl)pyridine, TPTC = [1,1′,3′,1″-terphenyl]-3,3″,5,5″-tetracarboxylic acid, DPCBIC = *N*-(3,5-dicarboxylphenyl)-*N*′-(4-carboxylbenzyl)imidazoliumchloride, DPTMIA = (5-(3,5-di-pyridin-4-yl-[1,2,4]triazol-1-ylmethyl)-isophthalic acid), BIPF = bis-(3-carboxy-phenyl)furan-2,5-dicarboxamide, BTTA = 1,4-bis(triazol-1-yl)terephthalic acid, BDC = 1,4-

benzenedicarboxylate, ICA = imidazolate-2-carboxyaldehyde, BTC = 1,2,4,5-benzenetetracarboxylate), BPCDA = *N*,*N*-bis(pyridin-3-ylmethylene)-cyclohexane-1,4-diamine, BSPT = 2,5-bis-(3,5-dicarboxyphenyl)thiopheneamide, BTC = 1,3,5-benzenetricarboxylic acid, TBIB = 1,3,5-tri(1H-benzo[d]imidazol-1-yl)benzene. NPYC = *N*,*N*-pyridin-4-ylpyridine-4-carboxamide, PMA = pyromellitic acid, DHTA = 2,5-dihydroxyterephthalic acid.

1.8 Applications of MOFs

MOF-based materials are reasonably considered as the ideal candidates for various applications because of their unique chemical and physical properties as well as their unique structural assets (Figure 1.17). Now-a-days, MOF-based materials are preferred over zeolites and activated carbons because of their large surface area and well-defined pore properties which make them more useful for volume-specific applications like separation, purification and adsorption processes. This intriguing class of ultraporous materials has been explored for diverse industrial and technological applications in different areas, including proton-conductivity[35], magnetic separation,[173] nanofluids,[174] gas separation,[13-15] catalysis,[16-19] bioimaging,[20-22] drug delivery,[23-26] chemical sensing,[27-29] etc. This thesis is mainly focused on the fluorescence sensing and catalysis applications of MOFs.

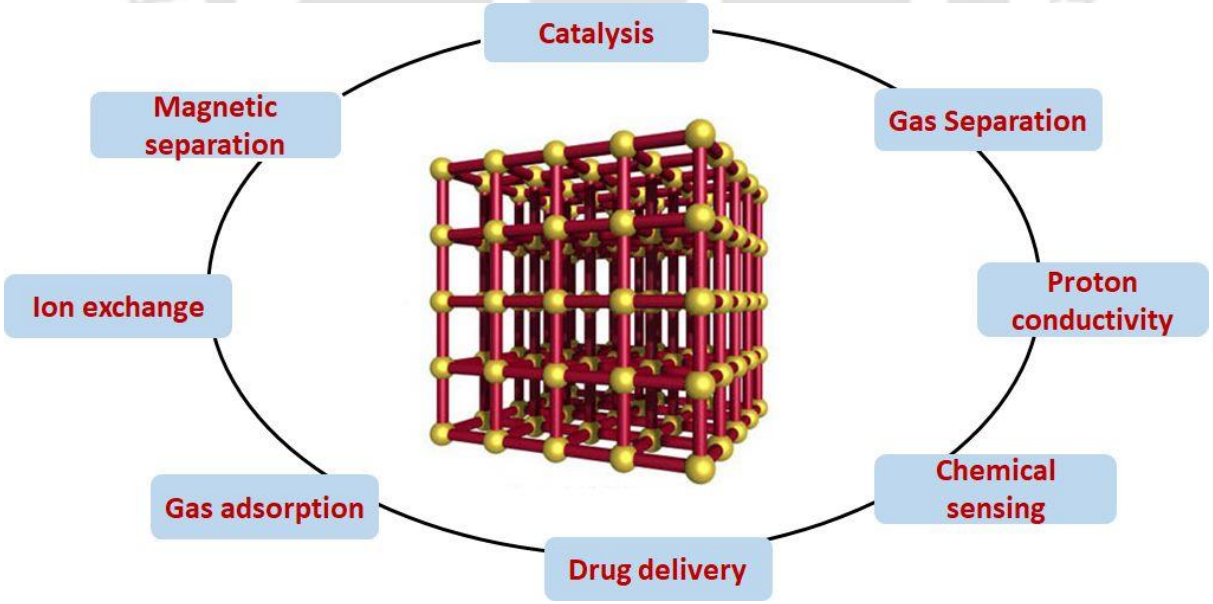

Figure 1.17 Wide ranging applications of MOFs.

1.8.1 Fluorescence sensing

The development of fluorescence-based sensors for the detection of toxic species has aroused tremendous interest among researchers since fluorescence techniques are highly sensitive and easy to operate. MOFs can be used as a fluorescence-based sensor not only because of their inherent luminescent properties but also because of their low framework density, open metal sites for interaction, customizable pore size, quick response with high sensitivity and selectivity as well as real-time monitoring.[175] The term luminescence is used to describe a process where spontaneous emission of light occurs after the absorption of energy by the material.[20] Luminescence consists of two fundamental forms: fluorescence and phosphorescence, depending on multiple spin states during the radiative relaxation process. The various photophysical processes are schematically summarized in the Jablonski diagram (Figure 1.18a). Fluorescence is a spin-allowed transition occurring from the lowest singlet excited electronic state (S_1) to the ground state (S_0) that normally lasts no longer than 10 ns whereas phosphorescence is an emission of light occurring from triplet electronic state (T_1) to ground singlet state (S_0) with different spin multiplicity that takes longer time, up to microseconds to seconds.[20, 176] In MOFs, luminescence can arise directly from organic linkers (especially from the highly conjugated linkers), metal-centered emission (particularly for lanthanide MOFs), charge-transfer such as linker-to-metal charge transfer (LMCT), metal-to linker charge transfer (MLCT) and linker-to linker charge transfer (LLCT) and guest induced luminescence (Figure 1.18b).[20, 37, 176] Luminescent MOFs have been employed in the wide number of possible applications such as lighting, optical communications, biomedical devices and chemical sensing.[176]

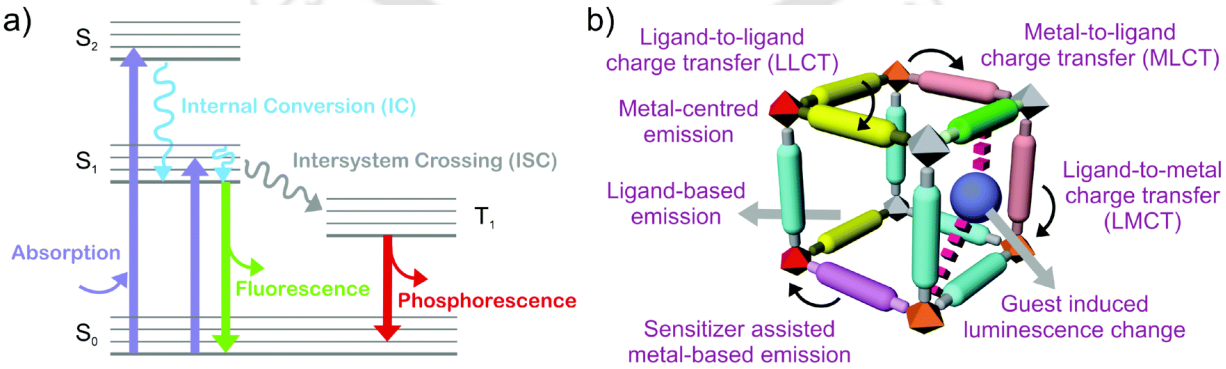

Figure 1.18 (a) Schematic illustration of the various photophysical process, (b) schematic representation of the various possibilities contributing to the emission of MOFs. Reproduced with permission from ref. 37. Copyright 2017 Royal Society Chemistry.

1.8.1.1 Sensing of toxic compounds

In the past decades, environmental pollution has become a serious problem for the ecosystem as well as human health with increasing population boom and industrial development. Many types of pollutants such as toxic organic compounds, heavy metals, nitro-aromatic explosives and some metal ions are associated with health risks. Therefore, fast and highly selective sensing of trace amounts of a toxic compound has become one of the most urgent issues now-a-days.

Iron is one of the most abundant transition metal in the human body and plays a crucial role in many biological processes.[177] It plays important role in brain function and synthesis of DNA and RNA.[178] A definite concentration of Fe^{3+} is needed for the formation of muscle and haemoglobin. An excess or deficiency of Fe^{3+} in an organism can induce various disorders including health hazards, such as anemia, skin ailments, insomnia, Alzheimer's disease, Parkinson's disease, pathological disorders, depression, etc.[179-180] Therefore, it is very necessary to develop a rapid and selective sensor for the recognition of Fe^{3+}. The fluorescence chemosensors have been one of the promising probe materials for metal ion sensing through the change of fluorescence.[181] In the last decades, porous MOFs have attracted much attention for the detection of Fe^{3+} owing to their large surface areas, tunable structures and strong fluorescence emission ability. Fe^{3+} is an efficient quencher credited to its d^5- paramagnetic configuration as reported previously.[182] MOF-based chemosensors have selectively detected Fe^{3+} by several mechanisms such as cation exchange,[164] framework collapse, fluorescence resonance energy transfer (FRET),[29] photo-induced electron transfer (PET),[183] interaction between Fe^{3+} and organic linker,[184] etc. In this study, luminescence MOF is used for the selective detection of Fe^{3+} with a very good detection limit.

Sensitive and selective detection of toxic anions like SeO_3^{2-}, AsO_4^{3-} and $Cr_2O_7^{2-}$ from our environment is of uttermost importance now-a-days. Among these toxic anions, $Cr_2O_7^{2-}$ is widely used in the field of glassmaking, modern agriculture, stainless steel formation, making of chromite, oxidative dyeing, wood preservation, paint manufacturing industry, etc.[185-186] The excessive use of $Cr_2O_7^{2-}$ in the industry has brought severe environmental pollution. Toxic $Cr_2O_7^{2-}$ is a strong oxidizing agent, which can be accumulated in living organisms. This accumulation can cause water-borne diseases and adverse visceral damage.[187] Carcinogenic $Cr_2O_7^{2-}$ can damage the DNA (deoxyribonucleic acid) and also disrupt the protein and enzyme system of the human body, even at very low concentrations.[188] Due to the highly toxic and carcinogenic as well as the mutagenic nature of $Cr_2O_7^{2-}$, the International Agency for Research

on Cancer (IARC) classified $Cr_2O_7^{2-}$ as one of the first types of carcinogens.[189] Because of these reasons, the detection of $Cr_2O_7^{2-}$ is very much important, especially in an aqueous medium. In this thesis work, MOF based fluorescence sensor was developed to detect trace amount of $Cr_2O_7^{2-}$.

Cyanide ion (CN^-) is one of the most toxic and lethal pollutants of the environment as listed by the Environment Protection Agency (EPA) and the World Health Organization (WHO).[190] According to WHO, the maximum permissive level of cyanide in drinking water is 1.9 µM (90.05 mg/L).[190] It is widely used in the petrochemical industry, gold mining, synthetic fibers, electroplating and metallurgy industries.[191] It has a dreadful impact on living beings.[192] It strongly binds to the active site of cytochrome-c and prevents the electron transport process which ultimately leads to decreased oxidative metabolism and oxygen utilization.[193] There is therefore a strong need for CN^- selective receptors for selective and sensitive determination of CN^- by simple assay. Ghosh et al. first developed a post -synthetically modified ZIF-90 MOF having dicyanovinyl functionalization for sensitive and selective aqueous-phase detection of CN^-. The limit of detection value was calculated to be 2 µM. As compared to CN^-, a very little quenching was observed in the case of other competing anions like F^-, Cl^-, Br^-, SCN^-, NO_3^-, NO_2^- and N_3. Biswas group has developed some MOFs namely carbazole-functionalized Zr(IV) MOF,[194] CAU-10-N_2H_3 MOF[195] and Hf(IV) based UiO-66 MOF[196] having detection capability of cyanide in pure aqueous medium with detection limit values of 0.14, 0.48 and 0.35 µM, respectively. Chen and his co-worker synthesized MOFs from luminescent Tb(III), adenosine diphosphate (ADP) and biphridyl (Bipy) (Figure 1.19).[197] Tb-ADP-Bipy MOF-based assay showed excellent selectivity and high sensitivity with a detection limit as low as 30 nM. It can satisfactorily detect cyanide in saliva samples, which probably provides an alternative mean for the forensic investigation of cyanide.

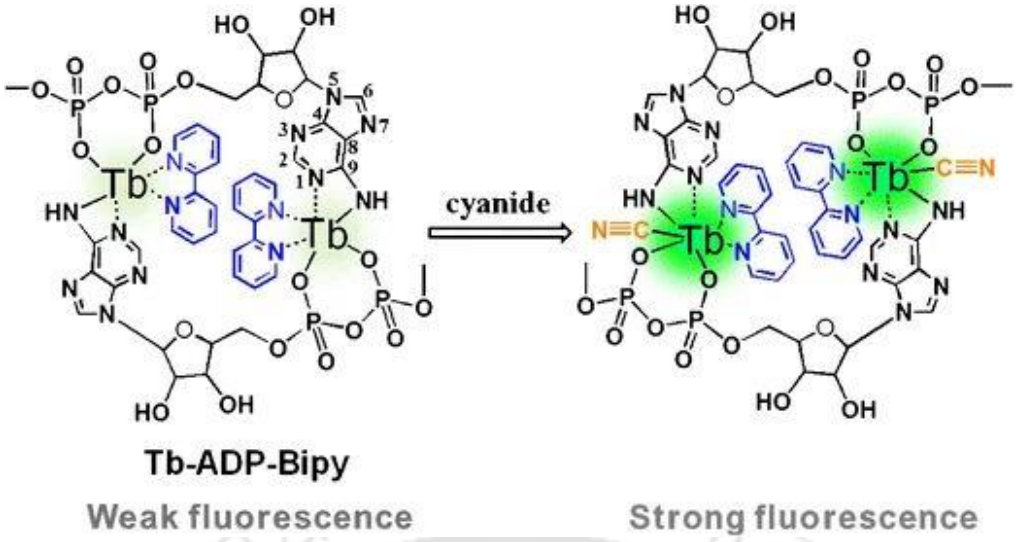

Figure 1.19 Schematic diagram of the detection of cyanide using Tb-ADP-Bipy MOF via extended π-conjugation-induced fluorescence enhancement. Reproduced with permission from ref. 197. Copyright 2017 Springer Nature.

Considering human health and environmental protection, researchers have devoted a lot of efforts to contribute rapid and selective detection of nitroaromatic compounds (NACs).[198-200] Some commonly used nitro explosives are 2,4,6-trinitrophenol (TNP or picric acid), 2,6-dinitrotoluene (2,6-DNT), 2,4-dinitrotoluene (2,4-DNT), 2,4,6-trinitrotoluene (TNT) and nitrobenzene (NB). Among all, picric acid is an extremely hazardous and strong explosive that can cause serious environmental pollution by contaminating soil and aquatic systems.[201] It can also cause serious health problems such as anaemia, abnormal liver function and male infertility.[202-203] It is also difficult for the biodegradation of PA via electrophilic attack because of its high electron-deficient character, giving it a xenobiotic character.[204] Hence, there is a requirement for fast, sensitive and selective detection of picric acid in presence of other NACs. MOFs having various functionalized linkers and different metal ions were used for the selective detection of picric acid. Ghosh et al. reviewed the developments in aqueous phase picric acid sensing, showing that very few water-stable MOFs have been reported for detection of picric acid in an aqueous medium.[205] Biswas and his group synthesized water-stable amide-functionalized cadmium tetrazolate framework[206] and thiadiazole-functionalized Zr(IV)-based framework[207] for selective detection of picric acid. Mobin and his co-worker reported Dy(III)-based framework, which can selectively detect picric acid in an aqueous medium with an impressive detection limit of 0.71 μM with quenching constant 8.55×10^4 M^{-1}.[208] Yang and his co-workers reported an Eu(III) based nano-flake MOF film for efficient fluorescent sensing of picric acid.[209]

Hydrogen sulfide (H_2S), the smallest sulfhydryl compound, is a colourless, highly flammable, corrosive, explosive gas with a characteristic smell of rotten eggs.[210-211] H_2S, which is also known as achemical asphyxiation gas, can react rapidly with haemoglobin in the blood.[212] Exposure to very lower concentrations of H_2S can lead to eye irritation, sore throat and cough, nausea, shortness of breath and fluid in the lungs.[211] Traditionally, H_2S was simply considered to be an environmentally toxic species. However, it has recently emerged as the third gasotransmitter gas after nitric oxide (NO) and carbon monoxide (CO).[213-214] The abnormal levels of H_2S in cells are known to be related to Alzheimer's disease, diabetes, Down's syndrome, Parkinson's disease and cancer.[215-217] In the light of associated potential hazards of H_2S on living beings and the environment, it is highly significant to develop a smart and effective probe for the detection of H_2S. Although there are numerous reports on the detection of H_2S using various techniques and approaches, there still exists a gap in terms of the limit of detection and feasibility. The H_2S-sensitive fluorescence probes were designed by some approaches like the reduction of azide and nitro groups to amines,[218] substitution reactions,[219] nucleophilic reactions,[220] high adsorption of S^{2-} to Cu^{2+},[221] reactions with the unsaturated double bond,[222] etc. Qian and his co-workers reported a highly water stable, robust and nano UIO-66-CH=CH_2 MOF for successful detection of H_2S under physiological conditions (HEPES buffer, pH = 7.4).[223] The same group also reported a MOF in which azide group was reduced to amine for the detection of H_2S (Figure 1.20).[122] They first synthesized amine functional group containing MOF (IRMOF-3). Then, post-synthetic modification was applied to convert amine moiety to azide via diazotization route, which in turn was applied for turn-on response after addition of NaSH at physiological pH.[122]

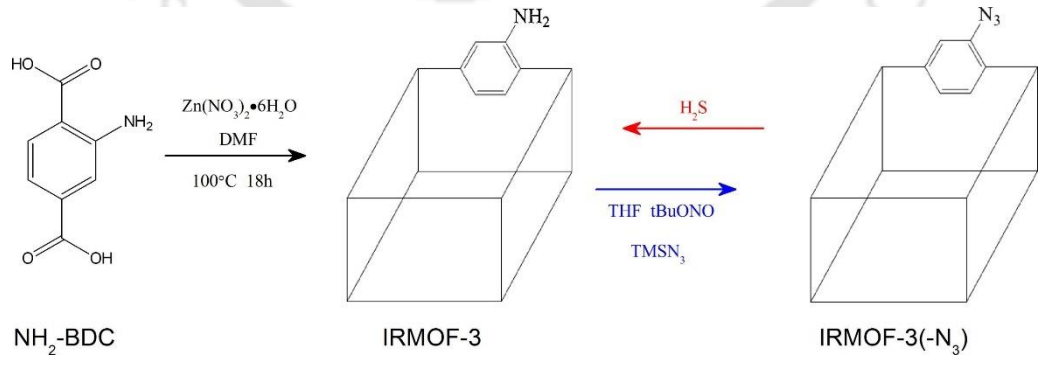

Figure 1.20 Schematic illustration of design of MOF-based selective turn-on probe for H_2S. Post-synthetic chemical modification of IRMOF-3 to IRMOF-3(–N_3) via diazotizationroute. Reduction of IRMOF-3(–N_3) to IRMOF-3 upon addition of NaHS at physiological pH giving

rise to fluorescence turn-on response (H_2S mediated reduction). Reproduced with permission from ref. 122. Copyright 2015 Elsevier.

1.8.2 Heterogeneous catalysis

Heterogeneous catalysis streamlines industrial processes due to high stability in different environments and easy separation. It is one of the vital solutions to the overall development of society since many chemical processes can be carried out cost-effectively using heterogeneous catalysis. The synthetic versatility and structural variability have made MOFs as attractive scaffolds for catalytic application in recent years.[18, 224] In 1994, MOFs was first explored as heterogeneous catalysis.[225] For better catalytic applications, active sites are definitely indispensable and their origin is of great importance. As shown in Figure 1.21, the single-site heterogeneous catalysts within MOFs are present at the nodes, linkers and pores.[226] The most important property responsible for their catalytic activity is the lack of non-accessible volume. The high porosity and high surface area help the adsorption and enrichment of substrates, which in turn helps the contact and interaction between catalytic sites and reactants and helps to improve the overall catalytic efficiency.[227] MOFs display better catalytic properties than the traditional porous materials such as zeolites, clays or mesoporous silica. Some of the advantages are: 1) the structural diversity and tunability properties of MOF components (nodes, linker and pores) makes it feasible to develop MOF-based catalysts by immobilizing various catalytic sites into a single MOF; 2) researchers can understand the mechanism of the reaction at the molecular level because of the well-defined structures of MOFs; 3) the recognition and transportation of substrates and products can be favored by the mutable pore environments (hydrophilic and hydrophobic); 4) the synergistic catalysis can be demonstrated via the various catalytic sites and collaborative microenvironment. Till now, MOFs were widely used as catalysts and catalyst supports for a diversity of organic transformations including Friedel-Crafts reactions,[228-229] Knoevenagel condensation,[230-231] aldol condensation,[232-233] oxidation,[130, 234] Suzuki-Miyaura cross coupling,[235-236] cyano silylation,[231, 237] carbon dioxide fixation,[238-239] etc.[234, 240-242] Table 1.3 shows some examples of MOF used as heterogeneous catalysts which have been utilized for different organic reactions.

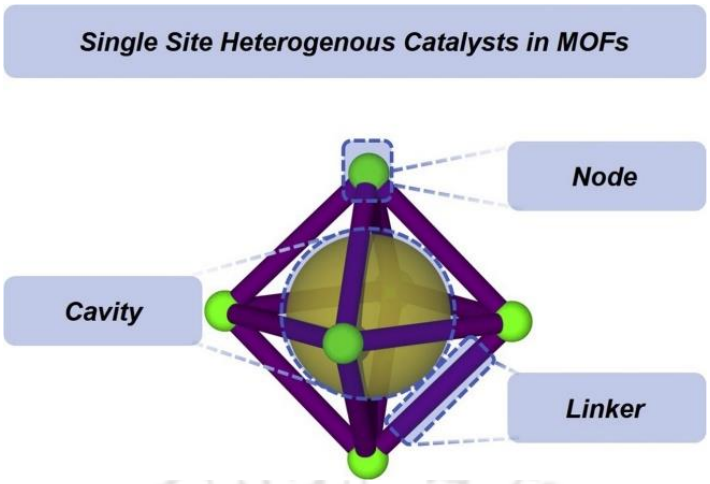

Figure 1.21 Single-site heterogeneous catalysts on MOFs are accessible through modifying the node, linker and content of the cavity. Reproduced with permission from ref. 226. Copyright 2019 Elsevier.

Table 1.3 Summary of some reported MOFs utilized as a heterogeneous catalysts for different organic reactions.

MOF	Catalysis reaction	Active Center (Metal/Linker)	Ref
Pd@MIL-101(Cr)-NH_2	Suzuki-Miyaura cross coupling	Pd	235
NU-1000(Zr)	Dimerization	Ni	243
Hf-NU-1000	CO_2 cycloaddition	Hf	242
PCN-124	Knoevenagel condensation	Cu, pyridine, amide	230
Ce_{53}/Zr-CAU-24	Reduction of NO	Ce	244
Ce-BTC	Hydroboration and hydrophosphination	Ce	245
MOF-808	Hydrolysis of dipeptides	Metal cluster	246
MIL-101(Cr)-NH_2	Cycloaddition of CO_2 and epoxides	Cr metal, linker	247
UiO-66-NH_2	Hydrolysis of dipeptides	Metal cluster	248
Ti_3-BPDC-CoH	Cascade reduction of N-heteroarenes	Ti, Co	249
$Cu_3(btc)_2$	Beckmann rearrangement	Cu	250
UiO—68(Zr)	Amination	CoCl/FeBr	251

Cu-MOF-75	Friedel-craft acylation	Metal cluster	229
$Cu_3(btc)_2$	Friedel-craft alkylation	Metal cluster	252
NH_2-UiO-66(Zr)	Photocatalytic CO_2 reduction	Zr, linker	240
VUiO-66	Gas-phase oxidative dehydrogenation of cyclohexene	V	241
NU-1000(Zr)	Oxidation	Co-Al complex	234
CuNPs@NU-1000	Semihydrogenation of acetylene	Cu	253
PCN-222(Fe)	Oxidation	linker	130
bpy-UiO	C-H borylation of arenes	Ir-/Pd-functinalized linker	254
Fe4SP@HKUST-1	Selectively Encapsulated Heme	Fe4SP	255
Mn-salen@MIL-101(Al)	Enantioselective epoxidation	Mn-salen	256

1.9 Motivation and aim of the thesis work

As described in this chapter, MOFs possess diverse and interesting properties, including luminescence, unique aesthetically pleasing structures, extraordinarily large surface areas, functionality of linker, which make them great candidates in numerous applications like gas adsorption, catalysis, gas separation, drug delivery, chemical sensing, etc. Among them, chemical sensing based on MOF materials has become a particularly promising application because of the presence of numerous active sites in MOFs for accelerating surface host-guest reactions. Due to the crystalline nature of MOFs, the pores of MOFs are well arranged. The size and shape of the pores can be tuned by an appropriate selection of organic linker and their connectivity with metal nodes. Due to their porous nature, MOFs are found to be highly useful in catalysis. The most important characteristic responsible for their catalytic ability is the lack of non-accessible volume. The defect in the framework of the MOFs also helps to increase the catalytic performance.

Hence, this thesis work mainly focused on the design, synthesis and characterization of Zn(II) and Zr(IV) based water-stable MOFs for selective and sensitive detection of toxic ions such as Fe^{3+}, $Cr_2O_7^{2-}$, CN^- and as well as nitroaromatic explosives. The thesis also explored the

application of the hydrophobic cavity of MOF for the heterogeneous catalysis reaction. This work mainly used carboxylic acid linkers to design MOFs since carboxylates can chelate with metal clusters and lock them into a rigid structure. Keeping the focus on selective detection of specific analytes, a proper functional group has been introduced in the linkers to synthesize MOFs.

1.10 References

1. Kitagawa, S.; Kitaura, R.; Noro, S.-i. Functional porous coordination polymers. *Angew. Chem. Int. Ed.* **2004,** *43*, 2334-2375.
2. Dzhardimalievaa, G. I.; Uflyand, I. E. Design and synthesis of coordination polymers with chelated units and their application in nanomaterials science. *RSC Adv.* **2017,** *7*, 42242-42299.
3. Jiao, S.; Zhang, Y.; Zhang, X.; Liu, K.; Ma, D.; Yang, B.; Li, S.; Wang, L. Construction, structure diversity, luminescent and dye absorption propertiesof coordination polymers comprising semi-rigid6-(carboxymethoxy)-2-naphthoic acid. *J. Solid State Chem.* **2021,** *293*, 121773.
4. Janiaka, C. Engineering coordination polymers towards applications. *Dalton Trans.* **2003**, 2781-2804.
5. Fromm, K. M.; Sague, J. L.; Mirolo, L. Coordination polymer networks: an alternative to classical polymers? *Macromol. Symp.* **2010,** *75*, 291-292.
6. J. C. Bailar; Jr., *Prep. Inorg. React.* **1964,** *1*, 1-57.
7. Silva, P.; Vilela, S. M. F.; Tome, J. P. C.; Paz, F. A. A. Multifunctional metal-organic frameworks: from academia to industrial applications. *Chem. Soc. Rev.* **2015,** *44*, 6774-6803.
8. Rowsell, J. L. C.; Yaghi, O. M. Metal–organic frameworks: a new class of porous materials. *Microporous Mesoporous Mater.* **2004,** *73*, 3-14.
9. Biradha, K.; Ramanan, A.; Vittal, J. J. Coordination polymers versus metal-organic frameworks. *Cryst. Growth Des.* **2009,** *9*, 2969-2970.
10. Jamesa, S. L. Metal-organic frameworks. *Chem. Soc. Rev.* **2003,** *32*, 276-288.
11. Furukawa, H.; Cordova, K. E.; O'Keeffe, M.; Yaghi, O. M. The chemistry and applications of metal-organic frameworks. *Science* **2013**, 1230444–1230444.
12. Baumann, A. E.; Burns, D. A.; Liu, B.; Tho, V. S. Metal-organic framework functionalization and design strategies for advanced electrochemical energy storage devices. *Commun. Chem.* **2019,** *2*, 86.

13. Suh, M. P.; Park, H. J.; Prasad, T. K.; Lim, D.-W. Hydrogen storage in metal organic frameworks. *Chem. Rev.* **2012,** *112*, 782-835.

14. Wang, R.; Zhong, Y.; Bi, L.; Yang, M.; Xu, D. Accelerating discovery of metal-organic frameworks for methane adsorption with hierarchical screening and deep learning. *ACS Appl. Mater. Interfaces* **2020,** *12*, 52797-52807.

15. Li, J.-R.; Sculley, J.; Zhou, H.-C. Metal organic frameworks for separations. *Chem. Rev.* **2012,** *112*, 869-932.

16. Zeng, L.; Guo, X.; He, C.; Duan, C. Metal-organic frameworks: versatile materials for heterogeneous photocatalysis. *ACS Catal.* **2016,** *6*, 7935-7947.

17. Farrusseng, D.; Aguado, S.; Pinel, C. Metal-organic frameworks: opportunities for catalysis. *Angew. Chem., Int. Ed.* **2009,** *48*, 7502-7513.

18. Lee, J.; Farha, O. K.; Roberts, J.; Scheidt, K. A.; Nguyen, S. T.; Hupp, J. T. Metal-organic framework materials as catalysts. *Chem. Soc. Rev.* **2009,** *38*, 1450-1459.

19. Wang, Z.; Huang, J.; Mao, J.; Guo, Q.; Chen, Z.; Lai, Y. Metal-organic frameworks and their derivatives with graphene composites: preparation and applications in electrocatalysis and photocatalysis. *J. Mater. Chem. A* **2020,** *8*, 2934-2961.

20. Cui, Y.; Yue, Y.; Qian, G.; Chen, B. Luminescent functional metal-organic frameworks. *Chem. Rev.* **2012,** *112*, 1126-1162.

21. Liu, D.; Lu, K.; Poon, C.; Lin, W. Metal-organic frameworks as sensory materials and imaging agents. *Inorg. Chem.* **2014,** *53*, 1916-1924.

22. Rieter, W. J.; Taylor, K. M. L.; An, H.; Lin, W.; Lin, W. Nanoscale metal-organic frameworks as potential multimodal contrast enhancing agents. *J. Am. Chem. Soc.* **2006,** *128*, 9024-9025.

23. Lázaro, I. A.; Lázaroa, S. A.; Forgan, R. S. Enhancing anticancer cytotoxicity through bimodal drug delivery from ultrasmall Zr MOF nanoparticles. *Chem. Commun.* **2018,** *54*, 2792-2795.

24. Lázaro, I. A.; Wells, C. J. R.; Forgan, R. S. Multivariate modulationofthe Zr MOF UiO-66 for defect-controlled combination anticancer drug delivery. *Angew. Chem. Int. Ed.* **2020,** *59*, 5211-5217.

25. Schnabel, J.; Ettlinger, R.; Bunzen, H. Zn-MOF-74 as pH-responsive drug-delivery system of arsenic trioxide. *ChemNanoMat* **2020,** *6*, 1229-1236.

26. Wu, M.-X.; Yang, Y.-W. Metal-organic framework (MOF)-based drug/cargo delivery and cancer therapy. *Adv. Mater.* **2017,** *29*, 1606134-1606154.

27. Kreno, L. E.; Leong, K.; Farha, O. K.; Allendorf, M.; Duyne, R. P. V.; Hupp, J. T. Metal-organic framework materials as chemical sensors. *Chem. Rev.* **2012,** *112*, 1105-1125.

28. Lan, A.; Li, K.; Wu, H.; Olson, D. H.; Emge, T. J.; Ki, W.; Hong, M.; Li, J. A luminescent microporous metal-organic framework for the fastand reversible detection of high explosives. *Angew. Chem. Int. Ed.* **2009,** *48*, 2334-2338.

29. Gogoi, C.; Biswas, S. A new quinoline based luminescent Zr(IV) metal–organic framework for the ultrasensitive recognition of 4-nitrophenol and Fe(iii) ions. *Dalton Trans.* **2018,** *47*, 14696-14705.

30. Meng, H.; Zhao, C.; Li, Y.; Nie, M.; Wang, C.; Wang, T. An implanted paramagnetic metallofullerene probe within a metal-organic framework. *Nanoscale* **2018,** *10*, 3291-3298.

31. Li, H.-Y.; Zhao, S.-N.; Zang, S.-Q.; Li, J. Functional metal-organic frameworks as effective sensors of gases and volatile compounds. *Chem. Soc. Rev.* **2020,** *49*, 6364-6401.

32. Ma, T.; Li, H.; Ma, J.-G.; Cheng, P. Application of MOF-based materials in electrochemical sensing. *Dalton Trans.* **2020,** *49*, 17121-17129.

33. Li, B.; Chrzanowski, M.; Zhang, Y.; Ma, S. Applications of metal-organic frameworks featuring multi-functionalsites. *Coord. Chem. Rev* **2016,** *307*, 106-129.

34. Ni, K.; Lan, G.; Lin, W. Nanoscale metal-organic frameworks generate reactive oxygen species for cancer therapy. *ACS Cent. Sci.* **2020**, 861-868.

35. Jeong, N. C.; Samanta, B.; Lee, C. Y.; Farha, O. K.; Hupp, J. T. Coordination-chemistry control of proton conductivity in the iconic metal-organic framework material HKUST-1. *J. Am. Chem. Soc.* **2011,** *134*, 51-54.

36. D'Surney, S. J.; Smith, M. D. Chemicals of environmental concern. *Encyclopedia of Toxicology* **2005**, 526-530.

37. Lustig, W. P.; Mukherjee, S.; Rudd, N. D.; Desai, A. V.; Li, J.; Ghosh, S. K. Metal–organic frameworks: functional luminescent and photonic materials for sensing applications. *Chem. Soc. Rev.* **2017,** *46*, 3242-3285.

38. Fang, X.; Zong, B.; Mao, S. Metal-organic framework-based sensors for environmental contaminant sensing. *Nano-Micro Lett.* **2018,** *10*, 64-82.

39. Zhu, L.; Liu, X.-Q.; Jiang, H.-L.; Sun, L.-B. Metal-organic frameworks for heterogeneous basic catalysis. *Chem. Rev.* **2017,** *117*, 8129-8176.

40. Pascanu, V.; Miera, G. G.; Inge, A. K.; Martín-Matute, B. Metal-organic frameworks as catalysts for organic synthesis: A critical perspective. *J. Am. Chem. Soc.* **2019,** *141*, 7223-7234.

41. Dhakshinamoorthy, A.; Asiri, A. M.; García, H. Metal-organic frameworks as multifunctional solid catalysts. *Trends Analyt. Chem.* **2020,** *2*, 454-466.

42. Chen, L.; Xu, Q. Metal-organic framework composites for catalysis. *Matter* **2019,** *1*, 57-89.

43. Vellingiri, K.; Philip, L.; Kim, K.-H. Metal–organic frameworks as media for the catalytic degradation of chemical warfare agents. *Coord. Chem. Rev.* **2017,** *353* 159-179.

44. Sun, W.-J.; Gao, E.-Q. Sulfonic-functionalized MIL-101 as bifunctional catalyst for cyclohexene oxidation. *Mol. Catal.* **2020,** *482*, 110746-110753.

45. Rostamnia, S.; Mohsenzad, F. Nanoarchitecturing of open metal site Cr-MOFs for oxodiperoxomolybdenum complexes [MoO(O2)2@En/MIL-100(Cr)] as promisingand bifunctional catalyst for selective thioether oxidation. *Mol. Catal.* **2018,** *445*, 12-20.

46. Shibata, Y. CAN 11:5339. *J. College Sci. Imperial Univ. Tokyo* **1916,** *37*, 1-17.

47. Hoskins, B. F.; Robson, R. Design and construction of a new class of scaffolding-like materials comprising infinite polymeric frameworks of 3-D-linked molecular rods. . *J. Am. Chem. Soc.* **1990,** *112*, 1546-1554.

48. Ma, S.; Zhou, H.-C. A metal-organic framework with entatic metal centers exhibiting high gas adsorption affinity. *J. Am. Chem. Soc.* **2006,** *128*, 11734-11735.

49. Cychosz, K. A.; W.-Foy, A. G.; Matzger, A. J. Liquid phase adsorption by microporous coordination polymers: removal of organosulfur compounds. *J. Am. Chem. Soc.* **2008,** *130*, 6938-6939.

50. Imaz, I.; R.-Martínez, M.; An, J.; S.-Font, I.; Rosi, N. L.; Maspoch, D. Metal-biomolecule frameworks (MBioFs). *Chem. Commun.* **2011,** *47*, 7287-7302.

51. Liu, Y.; Kravtsov, V. C.; Larsen, R.; Eddaoudi, M. Molecular building blocks approach to the assembly of zeolite-like metal-organic frameworks (ZMOFs) with extra-large cavities. *Chem. Commun., 2006, 1488-1490* **2006**.

52. Park, K. S.; Ni, Z.; Cote, A. P.; Choi, J. Y.; Huang, R. D.; UribeRomo, F. J.; Chae, H. K.; O'Keeffe, M.; Yaghi, O. M. Exceptional chemical and thermal stability of zeolitic imidazolate frameworks. *Proc. Natl. Acad. Sci. U.S.A.* **2006,** *103*, 10186.

53. Férey, G. Microporous solids: from organically templated inorganic skeletons to hybrid frameworks...ecumenism in chemistry. *Chem. Mater.* **2001,** *13*, 3084-3098.

54. Eddaoudi, M.; Kim, J.; Rosi, N. Systematic design of pore size and functionality in isorecticular MOFs and their application in methane storage. *Science* **2002,** *295*, 469-472.

55. Chae, H. K.; Siberio-Perez, D. Y.; Kim, J.; Go, Y. B.; Eddaoudi, M.; Matzger, A. J.; O'Keeffe, M.; Yaghi, O. M. A route to high surface area, porosity and inclusion of large molecules in crystals. *Nature* **2004,** *427*, 523-527.

56. Tranchemontagne, D. J.; Hunt, J. R.; Yaghi, O. M. Room temperature synthesis of metal-organic frameworks: MOF-5, MOF-74,MOF-177, MOF-199, and IRMOF-0. *Tetrahedron* **2008,** *64*, 8553-8557.

57. Kondo, M.; Yoshitomi, T.; Seki, K.; Matsuzaka, H.; Kitagawa, S. Three-dimensional framework with channeling cavities for small molecules: $\{[M_2(4,4'\text{-bpy})_3(NO_3)_4]\cdot xH_2O\}_n$ (M=Co, Ni, Zn). *Angew. Chem., Int. Ed. Engl.* **1997,** *36*, 1725.

58. Barthelet, K.; Marrot, J.; Riou, D.; Ferey, G. A breathing hybrid organic–inorganic solid with very large pores and high magnetic characteristics. *Angew. Chem., Int. Ed.* **2002,** *41*, 281.

59. Serre, C.; Millange, F.; Thouvenot, C.; Nogues, M.; Marsolier, G.; Louër, D.; Ferey, G. Very large breathing effect in the first nanoporous chromium(III)-based solids: MIL-53 or Cr(III)(OH)x[O(2)C-C(6)H(4)-CO(2)]x[HO(2)C-C(6)H(4)-CO(2)H](x)xH(2)O(y). *J. Am. Chem. Soc.* **2002,** *124*, 13519.

60. Li, X.; Cheng, F.; Zhang, S.; Chen, J. Shape-controlled synthesis and lithium-storage study of metal-organic frameworks Zn_4O(1,3,5-benzenetribenzoate)$_2$. *J. Power Sources* **2006,** *160*, 542-547.

61. Férey, G.; Serre, C.; M.-Draznieks, C.; Millange, F.; Surblé, S.; Dutour, J.; Margiolaki, I. A hybrid solid with giant pores prepared by a combination of targeted chemistry, simulation, and powder diffraction. *Angew. Chem. Int. Ed.* **2004,** *43*, 6296-6301.

62. Bauer, S.; Serre, C.; Devic, T.; Horcajada, P.; Marrot, J.; Férey, G.; Stock, N. High-throughput assisted rationalization of the formation of metal organic frameworks in the iron(III) aminoterephthalate solvothermal system. *Inorg. Chem.* **2008,** *47*, 7568-7576.

63. S.-Crespo, P.; R.-Fernandez, E. V.; Gascon, J.; Kapteijn, F. Synthesis and characterization of an amino functionalized MIL-101(Al): Separation and catalytic properties. *Chem. Mate.* **2011,** *23*, 2565-2572.

64. Li, Y. S.; Liang, F. Y.; Bux, H.; Feldhoff, A.; Yang, W. S.; Caro, J. Molecular sieve membrane: Supported metal-organic framework with high hydrogen selectivity. *Angew. Chem.* **2010,** *122*, 558-561.

65. Cavka, J. H.; Jakobsen, S.; Olsbye, U.; Guillou, N.; Lamberti, C.; Bordiga, S.; Lillerud, K. P. A new zirconium inorganic building brick forming metal organic frameworks with exceptional stability. *J. Am. Chem. Soc.* **2008,** *130*, 13850-13851.

66. Lammert, M.; Wharmby, M. T.; Smolders, S.; Bueken, B.; Lieb, A.; Lomachenko, K. A.; Vos, D. D.; Stock, N. Cerium-based metal organic frameworks with UiO-66 architecture: synthesis, properties and redox catalytic activity. *Chem. Commun.* **2015,** *51*, 12578-12581.

67. Loiseau, T.; Serre, C.; Huguenard, C.; Fink, G.; Taulelle, F.; Henry, M.; Bataille, T.; Férey, G. A rationale for the large breathing of the porous aluminum terephthalate (MIL-53) upon hydration. *Chem. Eur. J.* **2004,** *10*, 1373-1382.

68. Whitfield, T. R.; Wang, X.; Liu, L.; Jacobson, A. J. Metal-organic frameworks based on iron oxide octahedral chains connected by benzenedicarboxylate dianions. *Solid State Sci.* **2005,** *7*, 1096-1103.

69. Loiseau, T.; Serre, C.; Huguenard, C.; Fink, G.; Taulelle, F.; Henry, M.; Bataille, T.; Fÿrey, G. A rationale for the large breathing of the porous aluminum terephthalate(MIL-53) upon hydration. *Chem. Eur. J.* **2004,** *10*, 1373-1382.

70. Mahmoodi, N. M.; Abdi, J.; Oveisi, M.; Asli, M. A.; Vossoughi, M. Metal-organic framework (MIL-100 (Fe)): Synthesis, detailed photocatalyticdye degradation ability in colored textile wastewater and recycling. *Mater. Res. Bull.* **2018,** *100*, 357-366.

71. Zhong, G.; Liu, D.; Zhang, J. Applications of Porous Metal–Organic Framework MIL-100(M) (M = Cr, Fe, Sc, Al, V). *Cryst. Growth Des.* **2018,** *18*, 7730-7744.

72. Park, J.; Jiang, Q.; Feng, D.; Mao, L.; Zhou, H. Size-controlled synthesis of porphyrinic metal-organic framework and functionalization for targeted photodynamic therapy. *J. Am. Chem. Soc.* **2016,** *138*, 3518-3525.

73. Ma, S.; Sun, D.; Simmons, J. M.; Collier, C. D.; Yuan, D.; Zhou, H.-C. Metal-organic framework from an anthracene derivative containing nanoscopic cages exhibiting high methane uptake. *J. Am. Chem. Soc.* **2008,** *130*, 1012-1016.

74. Bon, V.; Senkovska, I.; Weiss, M. S.; Kaskel, S. Tailoring of network dimensionality and porosity adjustment in Zr- and Hf-based MOFs. *CrystEngComm.* **2013,** *15*, 9572-9577.

75. Lin, K.-S.; Adhikari, A. K.; Ku, C.-N.; Chiang, C.-L.; Kuo, H. Synthesis and characterization of porous HKUST-1 metal organic frameworks for hydrogen storage. *Int. J. Hydrogen Energy* **2012,** *37*, 13865-13871.

76. R.-Bautista, P.; T.-Mancera, I.; Pasán, J.; Pino, V. Metal-organic frameworks in green analytical chemistry. *Separations 2019* **2019,** *6*, 33.

77. Férey, G. Hybrid porous solids: past, present, future. *Chem. Soc. Rev.* **2008,** *37*, 191-214.

78. Kim, D.; Liu, X.; Lah, M. S. Topology analysis of metal-organic frameworks based on metal-organic polyhedra as secondary or tertiary building units. *Inorg. Chem. Front.* **2015,** *2*, 336-360.

79. Kuppler, R. J.; Timmons, D. J.; Fang, Q.-R.; Li, J.-R.; Makal, T. A.; Young, M. D.; Yuan, D.; Zhao, D.; Zhuang, W.; Zhou, H.-C. Potential applications of metal-organic frameworks. *Coord. Chem. Rev* **2009,** *253*, 3042-3066.

80. Collins, C. S.; Sun, D.; Liu, W.; Zuo, J.-L.; Zhou, H.-C. Reaction-condition-controlled formation of secondary-building-units in threecadmium metal-organic frameworks with an orthogonal tetrakis(tetrazolate) ligand. *J. Mol. Struct.* **2008,** *890*, 163-169.

81. Yaghi, O. M.; O'Keeffe, M.; Ockwig, N. W.; Chae, H. K.; Eddaoudi, M.; Kim, J. Reticular synthesis and the design of new materials. *Nature* **2003,** *423*, 705-714.

82. Lu, W.; Wei, Z.; Gu, Z.-Y.; Liu, T.-F.; Park, J.; Park, J.; Tian, J.; Zhang, M.; Zhang, Q.; III, T. G.; Boscha, M.; Zhou, H.-C. Tuning the structure and function of metal-organic frameworks via linker design. *Chem. Soc. Rev.* **2014,** *43*, 5561-5593.

83. Dau, P. V.; Tanabe, K. K.; Cohen, S. M. Functional group effects on metal–organic framework topology. *Chem. Commun.* **2012,** *48*, 9370-9372.

84. Yuan, S.; Feng, L.; Wang, K.; Pang, J.; Bosch, M.; Lollar, C.; Sun, Y.; Qin, J.; Yang, X.; Zhang, P.; Wang, Q.; Zou, L.; Zhang, Y.; Zhang, L.; Fang, Y.; Li, J.; Zhou, H.-C. Stable metal-organic Frameworks: Design, Synthesis, and Applications. *Adv. Mater.* **2018,** *30*, 1704303.

85. Leus, K.; Bogaerts, T.; Decker, J. D.; Depauw, H.; Hendrickx, K.; Vrielinck, H.; Speybroeck, V. V.; Voort, P. V. D. Systematic study of the chemical and hydrothermal stability of selected "stable" metal organic frameworks. *microporous mesoporous mater.* **2016,** *226*, 110-116.

86. Colombo, V.; Galli, S.; Choi, H. J.; Han, G. D.; Maspero, A.; Palmisano, G.; Masciocchi, N.; Long, J. R. High thermal and chemical stability in pyrazolate-bridged metal–organic frameworks with exposed metal sites. *Chem. Sci.* **2011,** *2*, 1311-1319.

87. Abednatanzi, S.; Derakhshandeh, P. G.; Depauw, H.; Coudert, F.-X.; Vrielinck, H.; Voort, P. V. D.; Leus, K. Mixed-metal metal-organic frameworks. *Chem. Soc. Rev.* **2019,** *48*, 2535-2565.

88. Rajak, R.; Kumar, R.; Ansari, S. N.; Saraf, M.; Mobin, S. M. Recent highlights and future prospects on mixed-metal MOFs as emerging supercapacitor candidates. *Dalton Trans.* **2020,** *49*, 11792-11818.

89. Haldar, R.; Maji, T. K. Metal–organic frameworks (MOFs) based on mixed linker systems: structural diversities towards functional materials. *CrystEngComm* **2013,** *15*, 9276-9295.

90. Lv, X.-L.; Yuan, S.; Xie, L.-H.; Darke, H. F.; Chen, Y.; He, T.; Dong, C.; Wang, B.; Zhang, Y.-Z.; Li, J.-R.; Zhou, H.-C. Ligand rigidification for enhancing the stability of metal-organic frameworks. *J. Am. Chem. Soc.* **2019,** *141*, 10283-10293.

91. Yang, C.; Kaipa, U.; Mather, Q. Z.; Wang, X.; Nesterov, V.; Venero, A. F.; Omary, M. A. Fluorous metal-organic frameworks with superior adsorption and hydrophobic properties toward oil spill cleanup and hydrocarbon storage. *J. Am. Chem. Soc.* **2011,** *133*, 18094-18097.

92. Zhang, W.; Hu, Y.; Ge, J.; Jiang, H.-L.; Yu, S.-H. A facile and general coating approach to moisture/water-resistant metal-organic frameworks with intact porosity. *J. Am. Chem. Soc.* **2014,** *136*, 16978-16981.

93. Hou, B.-L.; Tian, D.; Liu, J.; Dong, L.-Z.; Li, S.-L.; Li, D.-S.; Lan, Y.-Q. A water-stable metal-organic framework for highly sensitive and selective sensing of Fe^{3+} ion. *Inorg. Chem.* **2016,** *55*, 10580-10586.

94. Gelfand, B. S.; Shimizu, G. K. H. Parameterizing and grading hydrolytic stability in metal-organic frameworks. *Dalton Trans.* **2016,** *45*, 3668-3678.

95. Furukawa, H.; Gándara, F.; Zhang, Y.-B.; Jiang, J.; Queen, W. L.; Hudson, M. R.; Yaghi, O. M. Water adsorption in porous metal-organic frameworks and related materials. *J. Am. Chem. Soc.* **2014,** *136*, 4369-4381.

96. Burtch, N. C.; Jasuja, H.; Walton, K. S. Water stability and adsorption in metal-organic frameworks. *Chem. Rev.* **2014,** *114*, 10575.

97. Howarth, A. J.; Liu, Y.; Li, P.; Li, Z.; Wang, T. C.; Hupp, J. T.; Farha, O. K. Chemical, thermal and mechanical stabilities of metal-organic frameworks. *Nat. Rev. Mater.* **2016,** *1*, 15018.

98. Paz, F. A. A.; Klinowski, J.; Vilela, S. M. F.; Tomé, J. P. C.; Cavaleiro, J. A. S.; Rocha, J. Ligand design for functional metal-organic frameworks. *Chem. Soc. Rev.* **2012,** *41*, 1088-1110.

99. Lin, X.; Blake, A. J.; Wilson, C.; Sun, X. Z.; Champness, N. R.; George, M. W.; Hubberstey, P.; Mokaya, R.; Schröder, M. A porous framework polymer based on a zinc(II) 4,4'-bipyridine-2,6,2',6'-tetracarboxylate: synthesis, structure, and "zeolite-like" behaviors. *J. Am. Chem. Soc.* **2006,** *128*, 10745-10753.

100. Liu, R.; Yu, T.; Shi, Z.; Wang, Z. The preparation of metal–organic frameworks and their biomedical application. *Int. J. Nanomedicine* **2016,** *11*, 1187-1200.

101. Razavi, S. A. A.; Morsali, A. Linker functionalized metal-organic frameworks. *Coord. Chem. Rev.* **2019,** *399*, 2130233.

102. Seetharaj, R.; Vandana, P. V.; Arya, P.; Mathew, S. Dependence of solvents, pH, molar ratio and temperature in tuning metal organic framework architecture. *Arabian J. Chem.* **2019,** *12*, 295-315.

103. Bian, Y.; Xiong, N.; Zhu, G. Technology for the remediation of water pollution: A review on the fabrication of metal organic frameworks. *Processes* **2018,** *6*, 122.

104. Augustus, E. N.; Nimibofa, A.; Kesiye, I. A.; Donbebe, W. Metal-organic frameworks as novel adsorbents: A preview. *Am. J. Environ. Prot.* **2017,** *5*, 61-67.

105. Lv, X.-L.; Tong, M.; Huang, H.; Wang, B.; Gan, L.; Yang, Q.; Zhong, C.; Li, J.-R. A high surface area Zr(IV)-based metal–organic framework showing stepwise gas adsorption and selective dye uptake. *Solid State Chem.* **2015,** *223*, 104-108.

106. Fu, Y.; Sun, D.; Chen, Y.; Huang, R.; Ding, Z.; Fu, X.; Z. Li , A. C. An amine-functionalized titanium metal-organic framework photocatalyst with visible-light-induced activity for CO_2 reduction. **2012,** *124*, 3420-3423.

107. Lee, Y. R.; Kim, J.; Ahn, W. S. Synthesis of metal-organic frameworks: A mini review. *Korean J. Chem. Eng.* **2013,** *30*, 1667-1680.

108. Jhung, S. H.; Lee, J. H.; Chang, J. S. Microwave synthesis of a nanoporous hybrid material, chromium trimesate. *Bull. Korean Chem. Soc.* **2005,** *26*, 880.

109. Taylor-Pashow, K. M. L.; Rocca, J. D.; Xie, Z.; Tran, S.; Lin, W. Postsynthetic modifications of iron-carboxylate nanoscale metal-organic frameworks for imaging and drug delivery. *J. Am. Chem. Soc.* **2009,** *131*, 14261.

110. Babu, R.; Kuruppathparambil, R. R.; Kathalikkattil, A. C.; Kim, D. W.; Park, D. W. Rapid, microwave-assisted synthesis of cubic, three-dimensional, highly porous MOF-205 for room temperature CO_2 fixation via cyclic carbonate synthesis. *ACS Appl. Mater. Interfaces* **2016,** *8*, 33723-33731.

111. Albuquerque, H.; Herman, G. S. Chemically modulated microwave-assisted synthesis of MOF-74(Ni) and preparation of metal-organic framework-matrix based membranes for removal of metal ions from aqueous media. *Cryst. Growth Des.* **2017,** *17*, 156-162.

112. Mueller, U.; Schubert, M.; Teich, F.; Puetter, H.; Schierle-Arndt, K.; Pastre, J. Metal-organic frameworks-prospective industrial applications. *J. Mater. Chem.* **2006,** *16*, 626-636.

113. Li, W.-J.; Lü, J.; Gao, S.-Y.; Li, Q.-H.; Cao, R. Electrochemical preparation of metal–organic framework films for fast detection of nitro explosives. *J. Mater. Chem. A* **2014,** *2*, 19473-19478.

114. Joaristi, A. M.; J.-Alcañiz, J.; S.-Crespo, P.; Kapteijn, F.; Gascon, J. Electrochemical synthesis of some archetypical Zn^{2+}, Cu^{2+}, and Al^{3+} metal organic frameworks. *Cryst. Growth Des.* **2012,** *12*, 3489-3498.

115. Al-Kutubi, H.; Gascon, J.; Sudhçlter, E. J. R.; L. Rassaei Electrosynthesis of metal-organic frameworks: Challenges and opportunities. *ChemElectroChem.* **2015,** *2*, 462-474.

116. Pichon, A.; James, S. L. An array-based study of reactivity under solvent-free mechanochemical conditions-insights and trends. *CrystEngComm* **2008,** *10*, 1839-1847.

117. Beldon, P. J.; Fbin, L.; Stein, R. S.; Thirumurugan, A.; Cheetham, A. K.; Friscic, T. Rapid room-temperature synthesis of zeolitic imidazolate frameworks by using mechanochemistry. *Angew. Chem., Int. Ed.* **2010,** *49*, 9640-9643.

118. Julien, P. A.; Užarevi, K.; Katsenis, A. D.; Kimber, S. A. J.; Wang, T. C.; Farha, O. K.; Zhang, Y.; Casaban, J.; Germann, L.; Etter, M.; Dinnebier, R. E.; James, S. L.; Halasz, I.; Friscic, T. In situ monitoring and mechanism of the mechanochemical formation of a microporous MOF-74 framework. *J. Am. Chem. Soc.* **2016,** *138*, 2929-2932.

119. Qiu, L.-G.; Li, Z.-Q.; Wu, Y.; Wang, W.; Xua, T.; Jiang, X. Facile synthesis of nanocrystals of a microporous metal–organic framework by an ultrasonic method and selective sensing of organoamines. *Chem. Commun.* **2008**, 3642-3644.

120. Schlesinger, M.; Schulze, S.; Hietschold, M.; Mehring, M. Evaluation of synthetic methods for microporous metal-organic frameworks exemplified by the competitive formation of $[Cu_2(btc)_3(H_2O)_3]$ and $[Cu_2(btc)(OH)(H_2O)]$. *Microporous Mesoporous Mater.* **2010,** *132*, 121-127.

121. Abuzalat, O.; Wong, D.; Elsayed, M.; Park, S.; Kim, S. Sonochemical fabrication of Cu(II) and Zn(II) metal-organic framework films on metal substrates. *Ultrason Sonochem.* **2018,** *45*, 180-188.

122. Zhang, X.; Zhang, J.; Hu, Q.; Cui, Y.; Yang, Y.; Qian, G. Postsynthetic modification of metal-organic framework for hydrogensulfide detection. *Appl. Surf. Sci.* **2015,** *355*, 814-819.

123. Mandal, S.; Natarajan, S.; Mani, P.; Pankajakshan, A. Post-synthetic modification of metal-organic frameworks toward applications. *Adv. Funct. Mater.* **2021,** *31*, 2006291.

124. Liu, T.-F.; Zou, L.; Feng, D.; Chen, Y.-P.; Fordham, S.; Wang, X.; Liu, Y.; Zhou, H.-C. Stepwise synthesis of robust metal-organic frameworks via postsynthetic metathesis and oxidation of metal nodes in a single-crystal to single-crystal transformation. *J. Am. Chem. Soc.* **2014,** *136*, 7813-7816.

125. Zhang, X.; Xia, T.; Jiang, K.; Cui, Y.; Yang, Y.; Qian, G. Highly sensitive and selective detection of mercury (II) based on a zirconium metal-organic framework in aqueous media. *J. Solid State Chem.* **2017,** *253*, 277-281.

126. Kandiah, M.; Nilsen, M. H.; Usseglio, S.; Jakobsen, S.; Olsbye, U.; Tilset, M.; Larabi, C.; Quadrelli, E. A.; Bonino, F.; Lillerud, K. P. Synthesis and stability of tagged UiO-66 Zr-MOFs. *Chem. Mater.* **2010,** *22*, 6632-6640.

127. Wang, C.; Liu, X.; Demir, N. K.; Chen, J. P.; Li, K. Applications of water stable metal-organic frameworks. *Chem. Soc. Rev.* **2016,** *45*, 5107-5134.

128. Schaate, A.; Roy, P.; Godt, A.; Lippke, J.; Waltz, F.; Wiebcke, M.; Behrens, P. Modulated synthesis of Zr-based metal-organic frameworks: From nano to single crystals. *Chem. Eur. J.* **2011,** *17*, 6643-6651.

129. Reinsch, H.; Stassen, I.; Bueken, B.; Lieb, A.; Ameloot, R.; Vos, D. D. First examples of aliphatic zirconium MOFs and the influence of inorganic anions on their crystal structures. *CrystEngComm* **2015,** *17*, 331-337.

130. Feng, D.; Gu, Z. Y.; Li, J. R.; Jiang, H. L.; Wei, Z.; Zhou, H. C. Zirconium-metalloporphyrin PCN-222: Mesoporous metal-organic frameworks with ultrahigh stability as biomimetic catalysts. *Angew. Chem.* **2012,** *51*, 10307-10310.

131. Deria, P.; Bury, W.; Hupp, J. T.; Farha, O. K. Versatile functionalization of the NU-1000 platform by solvent-assisted ligand incorporation. *Chem. Commun.* **2014,** *50*, 1965-1968.

132. Feng, D.; Chung, W.-C.; Wei, Z.; Gu, Z.-Y.; Jiang, H.-L.; Chen, Y.-P.; Darensbourg, D. J.; Zhou, H.-C. Construction of ultrastable porphyrin Zr metal-organic frameworks through linker elimination. *J. Am. Chem. Soc.* **2013,** *135*, 17105-17110.

133. Vermoortele, F.; Bueken, B.; Bars, G. L.; Voorde, B. V. d.; Vandichel, M.; Houthoofd, K.; Vimont, A.; Daturi, M.; Waroquier, M.; Speybroeck, V. V.; Kirschhock, C.; Vos, D. D. Synthesis modulation as a tool to increase the catalytic activity of metal-organic frameworks: The unique case of UiO-66(Zr). *J. Am. Chem. Soc.* **2013,** *135*, 11465-11468.

134. Silva, C. G.; Luz, I.; Xamena, F. X. L.; Corma, A.; Garcia, H. Water stable Zr-benzenedicarboxylate metal-organic frameworks as photocatalysts for hydrogen generation. *Chem. Eur. J.* **2010,** *16*, 11133-11138.

135. Lin, Q.; Bu, X.; Kong, A.; Mao, C.; Zhao, X.; Bu, F.; Feng, P. New heterometallic zirconium metalloporphyrin frameworks and their heteroatom-activated high-surface-area carbon derivatives. *J. Am. Chem. Soc.* **2015,** *137*, 2235-2238.

136. Mondloch, J. E.; Katz, M. J.; III, W. C. I.; Ghosh, P.; Liao, P.; Bury, W.; Wagner, G. W.; Hall, M. G.; DeCoste, J. B.; Peterson, G. W. Destruction of chemical warfare agents using metal-organic frameworks. *Nat. Mater.* **2015,** *14*, 512-516.

137. Deria, P.; Mondloch, J. E.; Tylianakis, E.; Ghosh, P.; Bury, W.; Snurr, R. Q.; Hupp, J. T.; Farha, O. K. Perfluoroalkane functionalization of NU-1000 via solvent-assisted ligand incorporation: Synthesis and CO_2 adsorption studies. *J. Am. Chem. Soc.* **2013,** *135*, 16801-16804.

138. Morris, W.; Volosskiy, B.; Demir, S.; Ga´ndara, F.; McGrier, P. L.; Furukawa, H.; Cascio, D.; Stoddart, J. F.; Yaghi, O. M. Synthesis, structure, and metalation of two new highly porous zirconium metal-organic frameworks. *Inorg. Chem.* **2012,** *51*, 6443-6445.

139. Wei, Z.; Gu, Z.-Y.; Arvapally, R. K.; Chen, Y.-P.; McDougald, R. N.; Ivy, J. F.; Yakovenko, A. A.; Feng, D.; Omary, M. A.; Zhou, H.-C. Rigidifying fluorescent linkers by metal-organic framework formation for fluorescence blue shift and quantum yield enhancement. *J. Am. Chem. Soc.* **2014,** *136*, 8269-8276.

140. Feng, D.; Jiang, H.-L.; Chen, Y.-P.; Gu, Z.-Y.; Wei, Z.; Zhou, H.-C. Metal-organic frameworks based on previously unknown Zr8/Hf8 cubic clusters. *Inorg. Chem.* **2013,** *52*, 12661-12667.

141. Feng, D.; Gu, Z.-Y.; Li, J.-R.; Jiang, H.-L.; Wei, Z.; Zhou, H.-C. Zirconium-metalloporphyrin PCN-222: Mesoporous metal-organic frameworks with ultrahigh stability as biomimetic catalysts. *Angew. Chem., Int. Ed.* **2012,** *51*, 10307-10310.

142. Feng, D.; Wang, K.; Su, J.; Liu, T.-F.; Park, J.; Wei, Z.; Bosch, M.; Yakovenko, A.; Zou, X.; Zhou, H.-C. A highly stable zeotype mesoporous zirconium metal-organic framework with ultralarge pores. *Angew. Chem., Int. Ed.* **2015,** *54*, 149-154.

143. Bon, V.; Senkovskyy, V.; Senkovska, I.; Kaskel, S. Zr(iv) and Hf(iv) based metal–organic frameworks with reo-topology. *Chem. Commun.* **2012,** *48*, 8407-8409.

144. Bon, V.; Senkovska, I.; Baburin, I. A.; Kaskel, S. Zr- and Hf-based metal-organic frameworks: Tracking down the polymorphism. *Cryst. Growth Des.* **2013,** *13*, 1231-1237.

145. Wang, B.; Huang, H.; Lv, X.-L.; Xie, Y.; Li, M.; Li, J.-R. Tuning CO_2 Selective Adsorption over N_2 and CH_4 in UiO-67 Analogues through ligand functionalization. *Inorg. Chem.* **2014,** *53*, 9254-9259.

146. Guillerm, V.; Gross, S.; Serre, C.; Devic, T.; Bauer, M.; Fe´rey, G. A zirconium methacrylate oxocluster as precursor for the low-temperature synthesis of porous zirconium(iv) dicarboxylates. *Chem. Commun.* **2010,** *46*, 767-769.

147. Wang, R.; Wang, Z.; Xu, Y.; Dai, F.; Zhang, L.; Sun, D. Porous zirconium metal-organic framework constructed from 2D → 3D interpenetration based on a 3,6-connected kgd net. *Inorg. Chem.* **2014,** *53*, 7086-7088.

148. Reinsch, H.; Stassen, I.; Bueken, B.; Lieb, A.; Ameloot, R.; Vos, D. D. First examples of aliphatic zirconium MOFs and the influence of inorganic anions on their crystal structures. *CrystEngComm.* **2015,** *17*, 331-337.

149. Kalidindi, S. B.; Nayak, S.; Briggs, M. E.; Jansat, S.; Katsoulidis, A. P.; Miller, G. J.; Warren, J. E.; Antypov, D.; Cora`, F.; Slater, B.; Prestly, M. R.; M.-Gastaldo, C.; Rosseinsky, M. J. Chemical and structural stability of zirconium-based metal-organic frameworks with large three-dimensional pores by linker engineering. *Angew. Chem., Int. Ed.* **2015,** *54*, 221-226.

150. Saha, D.; Wei, J.; Deng, S. Hydrogen adsorption equilibrium and kinetics metal–organic framework (MOF-5) synthesized with DEF approach. *Sep Purif Technol* **2009,** *64*, 280-287.

151. Furukawa, H.; Miller, M. A.; Yaghi, M. Independent verification of the saturation hydrogen uptake in MOF-177 and establishment of a benchmark for hydrogen adsorption in metal-organic frameworks. *J Mater Chem* **2007,** *17*, 3197-3204.

152. Rowsell, J. L. C.; Yaghi, O. M. Strategies for hydrogen storage in metal organic frameworks. *Angew Chem Int Ed* **2005,** *44*, 4670-4679.

153. Saha, D.; Deng, S. Synthesis, characterization and hydrogen adsorption in mixed crystals of MOF-5 and MOF-177. *Int. J. Hydrogen Energy* **2009,** *34*, 2670-2678.

154. Alvaro, M.; Carbonell, E.; Ferrer, B.; Xamena, F. X. L.; Garcia, H. Semiconductor behavior of a metal-organic framework (MOF). *Chem. Eur. J.* **2007,** *13*, 5106-5112.

155. Karmakar, A.; Fátima, M.; Silva, C. G. d.; Pombeiro, A. J. L. Zinc metal-organic frameworks: efficient catalysts for the diastereoselective Henry reaction and transesterification. *Dalton Trans.* **2014,** *43*, 7795-7810.

156. Qin, X.; Yang, W.; Yang, Y.; Gu, D.; Guo, D.; Pan, Q. A zinc metal-organic framework for concurrent adsorption and detection of uranium. *Inorg. Chem.* **2020,** *59*, 9857-9865.

157. Ma, Y.; Xu, G.; Wei, F.; Cen, Y.; Song, Y.; Shi, M.; Xu, X.; Sohail, M.; Hu, Q. Fluorescent zinc(ii)-based metal-organic frameworks for nitroaromatics sensing. *New J. Chem.* **2018,** *42*, 5162-5167.

158. Cheng, J.; Hu, T.; Li, W.; Chang, Z.; Sun, C. Stable zinc metal-organic framework materials constructed by fluorenone carboxylate ligand: Multifunction detection and photocatalysis property. *J. Solid State Chem.* **2020,** *282*, 121125.

159. Xiang, Z.; Fang, C.; Lenga, S.; Cao, D. An amino group functionalized metal-organic framework as a luminescent probe for highly selective sensing of Fe^{3+} ions. *J. Mater. Chem. A* **2014,** *2*, 7662-7665.

160. Hu, F.-l.; Shi, Y.-X.; Chena, H.-H.; Lang, J.-P. A Zn(ii) coordination polymer and its photocycloaddition product: syntheses, structures, selective luminescence sensing of iron(iii) ions and selective absorption of dyes. *Dalton Trans.* **2015,** *44*, 18795-18803.

161. Liu, J.-Q.; Wu, J.; Li, F.-M.; Liu, W.-C.; Li, B.-H.; Wang, J.; Li, Q.-L.; Yadave, R.; Kumar, A. Luminescent sensing from a new Zn(II) metal-organic framework. *RSC Adv.* **2016,** *6*, 31161-31166.

162. Li, B.-H.; Wu, J.; Liu, J.-Q.; Gu, C.-Y.; Xu, J.-W.; Luo, M.-M.; Yadav, R.; Kumar, A.; Batten, S. R. A luminescent zinc(II) metal-organic framework for selective detection of nitroaromatics, Fe^{3+} and CrO_4^{2-}: A versatile threefold fluorescent sensor. *ChemPlusChem* **2016,** *81*, 885-892.

163. Wang, L.; Yao, Z.-Q.; Ren, G.-J.; Han, S.-D.; Hu, T.-L.; Bu, X.-H. A luminescent metal-organic framework for selective sensing of Fe^{3+} with excellent recyclability. *Inorg. Chem. Commun.* **2016,** *65*, 9-12.

164. Li, H.; He, Y.; Li, Q.; Li, S.; Yi, Z.; Xu, Z.; Wang, Y. Highly sensitive and selective fluorescent probe for Fe^{3+} and hazardous phenol compounds based on a water-stable Zn-based metal–organic framework in aqueous media. *RSC Adv.* **2017,** *7*, 50035-50039.

165. Qu, T.-G.; Hao, X.-M.; Wang, H.; Cui, X.-G.; Chen, F.; Wu, Y.-B.; Yang, D.; Zhang, M.; Guo, W.-L. A luminescent 2D zinc(II) metal–organic framework for selective sensingof Fe(III) ions and adsorption of organic dyes. *Polyhedron* **2018,** *156*, 208-217.

166. Jin, J.-C.; Wu, J.; Liu, W.-C.; Ma, A.-Q.; Liu, J.-Q.; Singh, A.; Kumar, A. A new Zn(ii) metal–organic framework having 3D CdSO4 topology as luminescent sensor and photocatalyst for degradation of organic dyes. *New J. Chem.* **2018,** *42*, 2767-2775.

167. Hao, L.; Song, H.; Su, Y.; Lv, Y. A cubic luminescent graphene oxide functionalized Zn-based metal-organic framework composite for fast and highly selective detection of Cu^{2+} ions in aqueous solution. *Analyst* **2014,** *139*, 764-770.

168. Liu, C.; Yan, B. Luminescent zinc metal-organic framework (ZIF-90) for sensing metal ions, anions and small molecules. *Photochem. Photobiol. Sci.* **2015,** *14*, 1644-1650.

169. Liu, S.; Li, J.; Luo, F. The first transition-metal metal-organic framework showing cation exchange for highly selectively sensing of aqueous Cu(II) ions. *Inorg. Chem. Commun* **2010,** *13*, 870-872.

170. Sohail, M.; Altaf, M.; Baig, N.; Jamil, R.; Sher, M.; Fazal, A. A new water stable zinc metal organic framework as an electrode material for hydrazine sensing. *New J. Chem.* **2018,** *42*, 12486-12491.

171. Wang, F.; Xu, K.; Jiang, Z.; Yan, T.; Wang, C.; Pu, Y.; Zhao, Y. A multifunctional zinc-based metal-organic framework for sensing and photocatalytic applications. *J. Lumin* **2018,** *194*, 22-28.

172. Agarwal, R. A.; Gupta, A. K.; De, D. Flexible Zn-MOF exhibiting selective CO_2 adsorption and efficient lewis acidic catalytic activity. *Cryst. Growth Des.* **2019,** *19*, 2010-2018.

173. Ricco, R.; Malfatti, L.; Takahashi, M.; Hill, A. J.; Falcaro, P. Applications of magnetic metal-organic framework composites. *J. Mater. Chem. A* **2013,** *1*, 13033-13045.

174. McGrail, B. P.; Thallapally, P. K.; Blanchard, J.; Nune, S. K.; Jenks, J.; Dang, L. X. Metal-organic heat carrier nanofluids. *Neno Energy* **2013,** *2*, 845-855.

175. Pamei, M.; Puzari, A. Luminescent transition metal-organic frameworks: An emerging sensor for detecting biologically essential metal ions. *Nano-Struct. Nano-Objects* **2019,** *19*, 100364.

176. Kanan, S. M.; Malkawi, A. Recent advances in nanocomposite luminescent metal-organic framework sensors for detecting metal ions. *Comments Inorg. Chem.* **2021,** *41*, 1-66.

177. Chen, C.-H.; Wang, X.-S.; Li, L.; Huang, Y.-B.; Cao, R. Highly selective sensing of Fe^{3+} by an anionic metal–organic framework containing uncoordinated nitrogen and carboxylate oxygen sites. *Dalton Trans.* **2018,** *47*, 3452-3458.

178. Aisen, P.; Wessling-Resnick, M.; Leibold, E. A. Iron metabolism. *Curr. Opin. Chem. Biol.* **1999,** *3*, 200-206.

179. Andrews, N. C. Disorders of iron metabolism. *N. Engl. J. Med* **1999,** *341*, 1986-1995.

180. B.-Bon, A.; Costero, A. M.; Gil, S.; Parra, M.; Soto, J.; Sancenón, R. M.-M. a. a. F. A new selective fluorogenic probe for trivalent cations. *Chem. Commun.* **2012,** *48*, 3000-3002.

181. Xu, H.; Cao, C.-S.; Zhao, B. A water-stable lanthanide-organic framework as a recyclable luminescent probe for detecting pollutant phosphorus anions. *Chem. Commun.* **2015,** *51*, 10280-10283.

182. Varnes, A. W.; Dodson, R. B.; Wehry, E. L. Interactions of transition-metal ions with photoexcited states of flavins. fluorescence quenching studies. *J. Am. Chem. Soc.* **1972,** *94*, 946-950.

183. Jin, L.; Liu, C.; An, N.; Zhang, Q.; Wang, J.; Zhao, L.; Lu, Y. Fluorescence turn-on detection of Fe^{3+} in pure water based on a cationic poly(perylene diimide) derivative. *RSC Adv.* **2016,** *6*, 58394-58400.

184. Li, X.; Tang, J.; Liu, H.; Gao, K.; Meng, X.; Wu, J.; Hou, H. A highly sensitive and recyclable Ln-MOF luminescent sensor for the efficient detection of Fe^{3+} and Cr^{VI} anions. *chem. asian j* **2019,** *14*, 3721-3727.

185. Lai, X.; Sun, D.; Hou, Y.; Zuo, Y.; Li, Y.; Zhang, L. Amino-functionalized multilayer core-shell mesoporous organosilica nanospheres for Cr(VI) removal. *Adv. Mater. Interfaces* **2018,** *5*, 1800630-1800640.

186. Kan, W.-Q.; Wen, S.-Z. A fluorescent coordination polymer for selective sensing of hazardousnitrobenzene and dichromate anion. *Dyes Pigm.* **2017,** *139*, 372-380.

187. Costa, M.; Klein, C. B. Toxicity and carcinogenicity of chromium compounds in humans. *Crit. Rev. Toxicol.* **2006,** *36*, 155-163.

188. Zhitkovich, A. Importance of chromium-DNA adducts in mutagenicity and toxicity of chromium(VI). *Chem. Res. Toxicol.* **2005,** *18*, 3-11.

189. Chen, Z.; Mi, X.; Wang, S.; Lu, J.; Li, Y.; Li, D.; Dou, J. Two novel penetrating coordination polymers based on flexible S-containing dicarboxylate acid with sensing properties towards Fe^{3+} and $Cr_2O_7^{2-}$ ions. *J. Solid State Chem.* **2018,** *261*, 75-85.

190. Guidelines for Drinking-Water Quality. *World Health Organization, Geneva, Switzerland* **1996**.

191. Dutra, A. J. B.; Rocha, G. P.; Pombo, F. R. Copper recovery and cyanide oxidation by electro winning from a spent copper-cyanide electroplating electrolyte. *J Hazard Mater* **2008,** *152*, 648-655.

192. Baud, F. J. Cyanide: critical issues in diagnosis and treatment. *Hum. Exp. Toxicol* **2007,** *26*, 191-201.

193. Shiraishi, Y.; Sumiya, S.; Manabe, K.; Hirai, T. Thermoresponsive copolymer containing a coumarin-spiropyran conjugate: Reusable fluorescent sensor for cyanide anion detection in water. *ACS Appl. Mater. Interfaces* **2011,** *3*, 4649-4656.

194. Das, A.; Biswas, S. A multi-responsive carbazole-functionalized Zr(IV)-based metal-organic framework for selective sensing of Fe(III), cyanide and p-nitrophenol. *Sens. Actuators, B.* **2017,** *250*, 121-131.

195. Dalapati, R.; Nandi, S.; Reinsch, H.; Bhunia, B. K.; Mandal, B. B.; Stock, N.; Biswas, S. Fluorogenic naked-eye sensing and live-cell imaging of cyanide by a hydrazine-functionalized CAU-10 metal-organic framework. *CrystEngComm* **2018,** *20*, 4194-4201.

196. Dalapati, R.; Nandi, S.; Biswas, S. Post-synthetic modification of a metal-organic framework with a chemodosimeter for the rapid detection of lethal cyanide via dual emission. *Dalton Trans.* **2020,** *49*, 8684-8692.

197. Wang, L.; Wang, S.; Chen, Y. Detection of cyanide via extended π-conjugation-induced fluorescence enhancement of a metal organic framework composed of terbium(III), bipyridyl and adenosine diphosphate. *Microchimica Acta* **2017,** *184*, 4597-4602.

198. Hu, Y.; Ding, M.; Liu, X.-Q.; Sun, L.-B.; Jiang, H.-L. Rational synthesis of an exceptionally stable Zn(ii) metal–organic framework for the highly selective and sensitive detection of picric acid. *Chem. Commun.* **2016,** *52*, 5734-5737.

199. Sun, L.; Xing, H.; Xu, J.; Liang, Z.; Yua, J.; Xu, R. A novel (3,3,6)-connected luminescent metal-organic framework for sensing of nitroaromatic explosives. *Dalton Trans.* **2013,** *42*, 5508-5513.

200. M.-Buschbaum, K.; Beuerle, F.; Feldmann, C. MOF based luminescence tuning and chemical/physical sensing. *Microporous and Mesoporous Mater.* **2015,** *216*, 171-199.

201. Nagarkar, S. S.; Joarder, B.; Chaudhari, A. K.; Mukherjee, S.; Ghosh, S. K. Highly selective detection of nitro explosives by a luminescent metal-organic framework. *Angew. Chem. Int. Ed.* **2013,** *52*, 2881-2885.

202. Wyman, J. F.; Serve, M. P.; Hobson, D. W.; Lee, L. H.; Uddin, D. E. Acute toxicity, distribution, and metabolism of 2,4,6-trinitrophenol (picric acid) in Fischer 344 rats. *J. Toxicol. Environ. Health* **1992,** *37*, 313-327.

203. Udhayakumari, D.; Velmathi, S.; Venkatesan, P.; Wu, S. P. A pyrene-linked thiourea as a chemosensor for cations and simple fluorescent sensor for picric acid. *Anal. Methods* **2015,** *7*, 1161-1166.

204. Shen, J.; Zhang, J.; Zuo, Y.; Wang, L.; Sun, X.; Li, J.; Han, W.; He, R. Biodegradation of 2, 4, 6-trinitrophenol by Rhodococcus sp. isolated from a picric acid-contaminated soil. *J Hazard Mater* **2009,** *163*, 1199-1206.

205. Nagarkar, S. S.; Desai, A. V.; Ghosh, S. K. Engineering metal–organic frameworks for aqueous phase 2,4,6-trinitrophenol (TNP) sensing. *CrystEngComm* **2016,** *18*, 2994-3007.

206. Buragohain, A.; Yousufuddin, M.; Sarma, M.; Biswas, S. 3D luminescent amide-functionalized cadmium tetrazolate framework for selective detection of 2,4,6-trinitrophenol. *Cryst. Growth Des.* **2016,** *16*, 842-851.

207. SK, M.; Biswas, S. A thiadiazole-functionalized Zr(iv)-based metal–organic framework as a highly fluorescent probe for the selective detection of picric acid. *CrystEngComm* **2016,** *18*, 3104-3113.

208. Rajak, R.; Saraf, M.; Verma, S. K.; Kumar, R.; Mobin, S. M. Dy(III)-based metal-organic framework as a fluorescent probe for highly selective detection of picric acid in aqueous medium. *Inorg. Chem.* **2019,** *58*, 16065-16074.

209. Zhang, F.; Zhang, G.; Yao, H.; Wang, Y.; Chu, T.; Yang, Y. A europium (III) based nano-flake MOF film for efficient fluorescent sensing of picric acid. *Microchimica Acta* **2017,** *184*, 1207-1213.

210. Hao, Y.; Chen, S.; Zhou, Y.; Zhang, Y.; Xu, M. Recent progress in metal-organic framework (MOF) based luminescent chemodosimeters. *Nanomaterials* **2019,** *9*, 974.

211. Yoo, K. S.; Han, S. D.; Moon, H. G.; Yoon, S.-J.; Kang, C.-Y. Highly sensitive H_2S sensor based on the metal-catalyzed SnO_2 nanocolumns fabricated by glancing angle deposition. *Sensors* **2015,** *15*, 15468-15477.

212. Surya, S. G.; Bhanoth, S.; Majhi, S. M.; More, Y. D.; Teja, V. M.; Chappand, K. N. A silver nanoparticle-anchored UiO-66(Zr) metal–organic framework (MOF)-based capacitive H_2S gas sensor. *CrystEngComm* **2019,** *21*, 7303-7312.

213. Szabo, C. Hydrogen sulphide and its therapeutic potential. *Nat. Rev. Drug Discov* **2007,** *6*, 917-935.

214. Bailey, T. S.; Pluth, M. D. Chemiluminescent detection of enzymatically produced hydrogen sulphide: substrate hydrogen bonding influences selectivity for H_2S over biological thiols. *J. Am. Chem. Soc.* **2013,** *135*, 16697-16704.

215. Kamoun, P.; Belardinelli, M.-C.; Chabli, A.; Lallouchi, K.; Chadefaux-Vekemans, B. Endogenous hydrogen sulphide overproduction in down syndrome. *Am. J. Med. Genet.* **2003,** *116A*, 310-311.

216. Eto, K.; Asada, T.; Arima, K.; Makifuchi, T.; Kimura, H. Brain hydrogen sulphide is severely decreased in Alzheimer's disease. *Bio-chem. Biophys. Res. Commun.* **2002,** *293*, 1485-1488.

217. Cao, Y.-Y.; Guo, X.-F.; Wang, H. High sensitive luminescence metal-organic framework sensor forhydrogen sulfide in aqueous solution: A trial of novel turn-onmechanism. *Sens. Actuators B* **2017,** *243*, 8-13.

218. Buragohain, A.; Biswas, S. Cerium based azide- and nitro-functionalized UiO-66 frameworks as turn-on fluorescent probes for the sensing of hydrogen sulphide. *CrystEngComm* **2016,** *18*, 4374-4381.

219. Men, J.; Yang, X.; Zhang, H.; Zhou, J. A near-infrared fluorescent probe based on nucleophilic substitution–cyclization for selective detection of hydrogen sulfide and bioimaging. *Dyes Pigments* **2018,** *153*, 206-212.

220. Liu, C.; Pan, J.; Li, S.; Zhao, Y.; Wu, L. Y.; C. E. Berkman; Whorton, A. R.; Xian, M. Capture and visualization of hydrogen sulfide by a fluorescent probe. *Angew. Chem. Int. Ed.* **2011,** *50*, 10327-10329.

221. Li, H. A regenerated "turn on" fluorescent probe for sulfide detection in live cells and read samples based on dihydroxyhemicyanine-Cu^{2+} dye. *anal. chim. acta* **2018,** *1010*, 69-75.

222. Li, H.; Feng, X.; Guo, Y.; Chen, D.; Li, R.; Ren, X.; Jiang, X.; Dong, Y.; Wang B. A malonitrile-functionalized metal-organic framework for hydrogen sulfide detection and selective amino acid molecular recognition. *Sci. Rep.* **2014,** *4*, 4366-4370.

223. Li, Y.; Zhang, X.; Zhang, L.; Jiang, K.; Cui, Y.; Yang, Y.; Qian, G. A nanoscale Zr-based fluorescent metal-organic framework for selective and sensitive detection of hydrogen sulfide. *J. Solid State Chem.* **2017,** *255*, 97-101.

224. Yang, D.; Gates, B. C. Catalysis by metal organic frameworks: perspective and suggestions for future research. *ACS Catal.* **2019,** *9*, 1779-1798.

225. Fujita, M.; Kwon, Y. J.; Washizu, S.; Ogura, K. Preparation, clathration ability, and catalysis of a two-dimensional square network material composed of cadmium(II) and 4,4'-bipyridine. *J. Am. Chem. Soc.* **1994,** *116*, 1151-1152.

226. Wasson, M. C.; Buru, C. T.; Chen, Z.; Islamoglu, T.; K.Farha, O. Metal-organic frameworks: A tunable platform to access single-site heterogeneous catalysts. *Appl. Catal, A* **2019,** *586*, 117214.

227. Li, D.; Xu, H.-Q.; Jiao, L.; Jiang, H.-L. Metal-organic frameworks for catalysis: State of the art, challenges, and opportunities. *EnergyChem* **2019,** *1*, 100005.

228. Zhu, C.; Mao, Q.; Li, D.; Li, C.; Zhou, Y.; Wu, X.; Luo, Y.; Li, Y. A readily available urea based MOF that act as a highly active heterogeneous catalyst for Friedel–Crafts reaction of indoles and nitrostryenes. *Catal. Commun.* **2018,** *104*, 123-127.

229. Calleja, G.; Sanz, R.; Orcajo, G.; Briones, D.; Leo, P.; Martínez, F. Copper-based MOF-74 material as effective acid catalyst in Friedel–Crafts acylation of anisole. *Catal. Today* **2014,** *227*, 130-137.

230. Park, J.; Li, J.-R.; Chen, Y.-P.; Yu, J.; Yakovenko, A. A.; Wang, Z. U.; Sun, L.-B.; Balbuena, P. B.; Zhou, H.-C. A versatile metal-organic framework for carbon dioxide capture and cooperative catalysis. *Chem. Commun.* **2012,** *48*, 9995-9997.

231. Neogi, S.; Sharma, M. K.; Bharadwaj, P. K. Knoevenagel condensation and cyanosilylation reactions catalyzed by a MOF containing coordinatively unsaturated Zn(II) centers. *J. Mol. Catal. A Chem* **2009,** *299*, 1-4.

232. Saha, D.; Maity, T.; Sen, R.; Koner, S. Heterogeneous catalysis over a barium carboxylate framework compound: synthesis, X-ray crystal structure and aldol condensation reaction. *Polyhedron* **2012,** *43*, 63-70.

233. Pathan, N. B.; Rahatgaonkar, A. M.; Chorghade, M. S. Metal-organic framework $Cu_3(BTC)_2(H_2O)_3$ catalyzed Aldol synthesis of pyrimidine-chalcone hybrids. *Catal. Commun.* **2011,** *12*, 1170-1176.

234. Thompson, A. B.; Pahls, D. R.; Bernales, V.; Gallington, L. C.; Malonzo, C. D.; Webber, T.; Tereniak, S. J.; Wang, T. C.; Desai, S. P.; Li, Z.; Ki, I. S.; Gagliardi, L.; Penn, R. L.; Chapman, K. W.; Stein, A.; Farha, O. K.; Hupp, J. T.; Martinson, A. B. F.; Lu, C. C. Installing heterobimetallic cobalt-aluminum single sites on a metal organic framework support. *Chem. Mater.* **2016,** *28*, 6753-6762.

235. Carson, F.; Pascanu, V.; Gómez, A. B.; Zhang, Y.; Prats, A. E. P.; Zou, X.; M.-Matute, B. Influence of the base on Pd@MIL-101–NH2(Cr) as a catalyst for the suzuki-miyaura cross-coupling reaction. *Chem. Eur. J.* **2015,** *21*, 10896-10902.

236. Chen, L.; Gao, Z.; Li, Y. Immobilization of Pd(II) on MOFs as a highly active heterogeneous catalyst for Suzuki–Miyaura and Ullmann-type coupling reactions. *Catal. Today* **2015,** *145*, 122-128.

237. Bhunia, A.; Dey, S.; Moreno, J. M.; Diaz, U.; Concepcion, P.; Hecke, K. V.; Janiak, C.; Voort, P. V. D. A homochiral vanadium-salen based cadmium bpdc MOF with permanent porosity as an asymmetric catalyst in solvent-free cyanosilylation. *Chem. Commun.* **2016,** *52*, 1401-1404.

238. Babu, R.; Roshan, R.; Gim, Y.; Jang, Y. H.; Kurisingal, J. F.; Kim, D. W.; Park, D. Inverse relationship of dimensionality and catalytic activity in CO2 transformation: a systematic investigation by comparing multidimensional metal–organic frameworks. *J. Mater. Chem. A* **2017,** *5*, 15961-15969.

239. Babu, R.; Roshan, R.; Kathalikkattil, A. C.; Kim, D. W.; Park, D. W. Rapid, microwave-assisted synthesis of cubic, three-dimensional, highly porous MOF-205 for room temperature CO_2 fixation via cyclic carbonate synthesis. *ACS Appl. Mater. Interfaces* **2016,** *8*, 33723-33231.

240. Fu, Y.; Wu, J.; Du, R.; Guo, K.; Ma, R.; Zhang, F.; Zhu, W.; Fan, M. Temperature modulation of defects in NH_2-UiO66(Zr) for photocatalytic CO_2 reduction. *RSC Adv.* **2019,** *9*, 37733-37738.

241. Nguyen, H. G. T.; Schweitzer, N. M.; Chang, C.-Y.; Drake, T. L.; So, M. C.; Stair, P. C.; Farha, O. K.; Hupp, J. T.; Nguyen, S. T. Vanadium-node-functionalized UiO-66: A

thermally stable MOF-supported catalyst for the gas-phase oxidative dehydrogenation of cyclohexene. *ACS Catal.* **2014,** *4*, 2496-2500.

242. Beyzavi, M. H.; Klet, R. C.; Tussupbayev, S.; Borycz, J.; Vermeulen, N. A.; Cramer, C. J.; Stoddart, J. F.; Hupp, J. T.; Farha, O. K. A hafnium-based metal-organic framework as an efficient and multifunctional catalyst for facile CO_2 fixation and regioselective and enantioretentive epoxide activation. *J. Am. Chem. Soc.* **2014,** *136*, 15861-15864.

243. Liu, J.; Ye, J.; Li, Z.; Otake, K.-i.; Liao, Y.; Peters, A. W.; Noh, H.; Truhlar, D. G.; Gagliardi, L.; Cramer, C. J.; Farha, O. K.; Hupp, J. T. Beyond the active site: Tuning the activity and selectivity of a metal-organic framework-supported Ni catalyst for ethylene dimerization. *J. Am. Chem. Soc.* **2018,** *140*, 11174-11178.

244. Smolders, S.; Jacobsen, J.; Stock, N.; Vos, D. D. Selective catalytic reduction of NO by cerium-based metal-organic frameworks. *Catal. Sci. Technol.* **2020,** *10*, 337-341.

245. Ji, P.; Sawano, T.; Lin, Z.; Urban, A.; Boures, D.; Lin, W. Cerium-hydride secondary building units in a porous metal-organic framework for catalytic hydroboration and hydrophosphination. *J. Am. Chem. Soc.* **2016,** *138*, 14860-14863.

246. Ly, H. G. T.; Fu, G.; Kondinski, A.; Bueken, B.; Vos, D. D.; P.-Vogt, T. N. Superactivity of MOF-808 toward peptide bond hydrolysis. *J. Am. Chem. Soc.* **2018,** *140*, 6325-6335.

247. Ma, D.; Li, B.; Liu, K.; Zhang, X.; Zou, W.; Yang, Y.; Li, G.; Shi, Z.; Feng, S. Bifunctional MOF heterogeneous catalysts based on the synergy of dual functional sites for efficient conversion of CO_2 under mild and co-catalyst free conditions. *J. Mater. Chem. A* **2015,** *3*, 23136-23142.

248. Ly, H. G. T.; Fu, G.; Azambuja, F. d.; Vos, D. D.; P.-Vogt, T. N. Nanozymatic activity of UiO-66 metal-organic frameworks: Tuning the nanopore environment enhances hydrolytic activity toward peptide bonds. *ACS Appl. Nano Mater.* **2020,** *3*, 8931-8938.

249. Feng, X.; Song, Y.; Chen, J. S.; Li, Z.; Chen, E. Y.; Kaufmann, M.; Wang, C.; Lin, W., Cobalt-bridged secondary building units in a titanium metal–organic framework catalyze cascade reduction of N-heteroarenes. *Chem. Sci.* **2019,** *10*, 2193-2198.

250. Opanasenko, M.; Shamzhy, M.; Lamač, M.; Čejka, J. The effect of substrate size in the Beckmann rearrangement: MOFs vs. zeolites. *Catal. Today* **2013,** *204*, 94-100.

251. Manna, K.; Ji, P.; Lin, Z.; Greene, F. X.; Urban, A.; Thacker, N. C.; Lin, W. Chemoselective single-site earth-abundant metal catalysts at metal-organic framework nodes. *Nat. Commun.* **2016,** *7*, 12610.

252. Anbu, N.; Dhakshinamoorthy, A. $Cu_3(BTC)_2$ as viable heterogeneous solid catalyst for Friedel-Craftsalkylation of indoles with nitroalkenes. *J. Colloid Interface Sci.* **2017,** *494*, 282-289.

253. Redfern, L. R.; Li, Z.; Zhang, X.; Farha, O. K. Highly selective acetylene semihydrogenation catalyzed by Cu nanoparticles supported in a metal-organic framework. *ACS Appl. Nano Mater.* **2018,** *1*, 4413-4417.

254. Manna, K.; Zhang, T.; Lin, W. Postsynthetic metalation of bipyridyl-containing metal–organic frameworks for highly efficient catalytic organic transformations. *J. Am. Chem. Soc.* **2014,** *136*, 6566-6569.

255. Larsen, R. W.; Wojtas, L.; Perman, J.; Musselman, R. L.; Zaworotko, M. J.; Vetromile, C. M. Mimicking heme enzymes in the solid state: metal-organic materials with selectively encapsulated heme. *J. Am. Chem. Soc.* **2011,** *133*, 10356-10359.

256. Bogaerts, T.; Deyne, A. V. Y.-D.; Liu, Y.-Y.; Lynen, F.; Speybroeck, V. V.; Voort, P. V. D. Mn-salen@MIL101(Al): a heterogeneous, enantioselective catalyst synthesized using a 'bottle around the ship' approach. *Chem. Commun.* **2013,** *49*, 8021-8023.

CHAPTER 2

A new 3D luminescent Zn(II)-organic framework containing quinoline-2,6-dicarboxylate linker for the highly selective sensing of Fe(III) ions

*This chapter represents synthesis and characterization of a new 3D zinc-organic framework under solvothermal conditions. The overall framework has PtS topology, where Zn^{2+} center acts as a 5-connected node and QDA (QDA = quinoline-2,6-dicarboxylate) linker as a spacer. The activated compound (**1'**) exhibited a very quick fluorescence quenching response after addition of Fe^{3+}. The selectivity for Fe^{3+} sensing was also examined in the presence of other metal cations. The experimental resulted showed that the quenching efficiency was not affected by the presence of competitive metal cations. A very low detection limit of 9.2 ppb was observed for Fe^{3+}, which is among the lowest values documented in the literature for MOF based fluorescence probes. Both fluorescence resonance energy transfer (FRET) as well as photo-induced electron transfer (PET), processes play major roles in the selective detection of Fe^{3+}.*

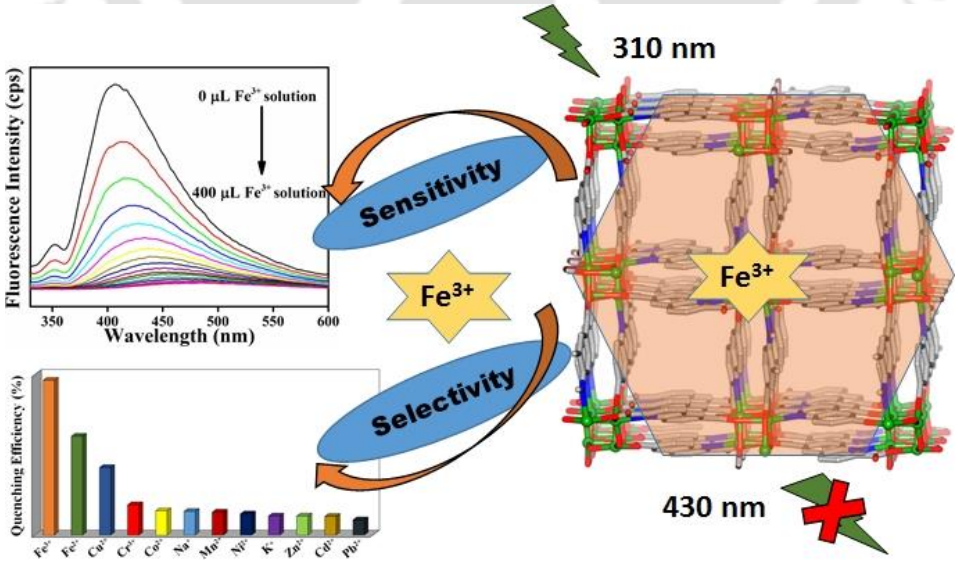

Dalton Transactions

C. Gogoi, M. Yousufuddin and S. Biswas, *Dalton Trans.* 2019, ***48***, 1766-1773.

2.1 Introduction

Metal-organic frameworks (MOFs) is a class of porous hybrid organic-inorganic solids[1-3] in which different metal ions are linked by polyfunctional organic linkers.[4] They have porous periodic networks with large surface areas and pore volumes. This remarkable class of porous materials has wide range of applications like catalysis,[5-6] gas storage,[7-8] separation,[9-10] polymerization,[11] sensing,[12-15] drug delivery,[16] electronic conductivity,[15] proton conductivity[17-18] and many more.[19-21] In many areas, MOFs have shown excellent advantages over traditional materials and potential values for commercialization.[22] By varying the metal ions as well as the organic linker molecules, we can introduce various pore sizes and functionalities into the MOF materials. These new porous materials display robustness because of strong bonding as well as geometrically well-defined structures. Still, there are some drawbacks of these materials over other types of porous materials (such as zeolites and activated carbons) like relatively lower thermal and chemical stability.[23] Many MOFs show thermal stability only up to 250 °C, beyond which the decomposition of framework starts.[24] Furthermore, some of them are susceptible to decomposition in presence of air or moisture.[25] Therefore, the design and synthesis of thermally and chemically more stable MOFs are still challenging for the chemists. Among different properties of MOFs, luminescence properties are very interesting because of their potential applications in sensing of guest molecules.[26] MOFs as chemical sensors have advantageous over other kinds of sensors.[26] MOFs exhibit highly size-selective detection of analytes because of the tuneable nature of their porosity (pore size and pore volume).[27-28] They display photoluminescence properties based on metal ion or linker molecule. Lanthanide and actinide-containing MOFs usually exhibit metal-based properties and transition metal-based MOFs show linker-based photoluminescence properties.[28]

Fe^{3+} is an essential metal cation for most of the living organisms. It plays many important roles in biological systems and has many functions like haemoglobin formation, brain function, synthesis of DNA and RNA, oxygen metabolism and many more.[29-31] The excess or deficiency of Fe^{3+} is so detrimental that it damages nucleic acids and proteins and also leads to a variety of health diseases such as anemia, Alzheimer's disease, depression, cardiac arrest, etc.[32-33] Therefore, the development of newer low-cost, selective, sensitive and accurate process for the detection of Fe^{3+} is highly necessary.

In this chapter, we have discussed the synthesis of a Zn(II) containing quinoline-based MOF by solvothermal process. The as-synthesized form of compound **1** having formula

[Zn(QDA)]·0.7DMF·0.5H_2O was activated to remove the guest solvent molecules from the pores. The activated compound (**1'**) was used for the selective detection of Fe^{3+} in methanol. Compound **1'** showed excellent recyclability and hence it can be used several times for Fe^{3+} sensing. The Fe^{3+} sensing ability was unaffected by the presence of other competitive metal cations including Fe^{2+}. These results disclose that **1'** can serve as a MOF-based fluorescence probe for the selective detection of Fe^{3+} in biological systems. Till date, according to best of our knowledge, this is the first quinoline-based Zn-MOF for the fluorimetric detection of Fe^{3+}.

2.2 Experimental section

2.2.1 Materials and instrumental techniques

The linker, H_2QDA (quinoline-2,6-dicarboxylic acid) was prepared using the earlier reported procedure.[34-35] It was characterized by using ^{1}H NMR spectroscopy and ESI-MS spectrometry. These data matched well with the earlier reported values. All chemical reagents and solvents were received from the chemical suppliers and the solvents were used without purification. The X-ray powder diffraction (XRPD) measurements were carried out using Bruker D2 Phaser X-ray diffractometer which was employed at 30 kV, 10 mA using Cu-*K*α (λ = 1.5406 Å) radiation. The Fourier transform infrared (FT-IR) spectra were recorded based on KBr pellets in the range of 4000−400 cm^{-1} with the help of Perkin Elmer Spectrum Two FT-IR spectrometer. In the FT-IR spectra, the peaks were characterized by using notations such as: very strong (vs), strong (s), weak (w), shoulder (sh), medium (m) and broad (br). Thermogravimetric analyses (TGA) of **1** and **1'** were performed from 25 to 600 °C at a heating rate of 10 °C min^{-1} under argon atmosphere by using a SDT Q600 V20.9 Build 20 thermogravimetric analyzer. Nitrogen sorption isotherms were recorded on a Quantachrome Autosorb iQMP volumetric gas adsorption equipment at -196 °C. Edinburgh Instrument Life-Spec II spectrometer was used for the fluorescence lifetime measurement. A pulsed diode laser was used for exciting the samples at 336 nm, maintaining the emission wavelength at 407 nm for metal ions. The energy dispersive X-ray (EDX) experiment was conducted by using a Hitachi S3400N SEM-EDX instrument.

2.2.2 Crystallographic study

A crystal of good shape and size was carefully chosen from the mother liquor and immersed in silicone oil. Then, it was mounted on the tip of a glass fibre and cemented using epoxy resin. The diffraction data of the crystal was collected at 293 K with Mo-*K*α radiation (λ = 0.71073 Å) with an Oxford SuperNova diffractometer equipped with a graphite

monochromator and an APEX CCD camera. With the help SMART software, data collection, indexing and determination of the unit cell parameters were carried out. SAINT[36] and XPREP softwares were used in data reduction and cell refinement. The final crystal structure was solved by direct methods and refined by full-matrix least-squares on F^2 with anisotropic displacement using SHELXTL9.[37] An empirical absorption correction was carried out by SADABS.[38] The hydrogen atoms of **1** was refined with isotropic thermal parameters. The guest solvent molecules were removed by the SQUEEZE[39] program implemented within PLATON[40] because they are highly disordered and cannot be precisely located using X-ray crystallography. All the other calculations were made by WinGX system.[41] The X-ray crystallographic coordinates for structures reported in this article have been deposited at the Cambridge Crystallographic Data Centre (CCDC), under deposition number CCDC 1870130. These data can be obtained free of charge from The Cambridge Crystallographic Data Centre via www.ccdc.cam.ac.uk/data_request/cif.

2.2.3 Synthesis of [Zn(QDA)]·0.7DMF·0.5H_2O (1)

A mixture of $Zn(ClO_4)_2 \cdot 6H_2O$ (34 mg, 0.09 mmol) and H_2QDA linker (10 mg, 0.05 mmol) in DMF (3 mL) was taken in a Pyrex tube. The suspension was sonicated for 20 min. Then, we added 150 µL of conc. HNO_3 to get a clear solution of the reaction mixture. After sonicating again for 1 h, the resulting solution was heated in a sealed Pyrex tube at 140 °C for 72 h using an oil bath to afford colorless block-shaped X-ray quality crystals. Yield: 64 mg (0.23 mmol), 64% based on metal salt. FT-IR (KBr pellet, cm^{-1}): 3429 (br), 2926 (w), 2850 (w), 1654 (sh), 1630 (s), 1504 (w), 1403 (w), 1168 (s), 1104 (w), 796 (s), 650 (s), 489 (s). Anal. Calcd. for $C_{11.9}H_{7.1}N_{1.3}O_{4.3}Zn$ in %: C, 47.25; H, 2.36; N, 6.02. Found: C, 47.13; H, 2.09; N 6.36.

2.2.4 Activation procedures of 1

The as-synthesized compound (100 mg) was stirred with acetone (15 mL) for 24 h at room temperature. Then, the compound was filtered and kept in an oven at 70 °C for 6 h. This compound was again heated under vacuum for 24 h at 120 °C.

2.2.5 Fluorescence sensing investigations

Firstly, luminescence behavior of **1'** was examined in different solvents by placing 3 mg of **1'** in a glass vial and adding different solvents (3 mL) to it. After that, the mixture was sonicated for 30 min and the suspension was kept undisturbed for 1 day. This stable dispersion

was used for the further fluorescence experiments. The titration measurement was performed with an excitation wavelength (λ_{ex}) of 310 nm. The emission spectra were measured from 330 nm to 600 nm. For the sensing of metal cations, we chose eleven metal nitrate salts and one sulphate salt (for Fe^{2+} ion). The solution (10 mM) of different metal cations (Fe^{3+}, Fe^{2+}, Pd^{2+}, Cr^{3+}, Cd^{2+}, Zn^{2+}, Cu^{2+}, Ni^{2+}, Co^{2+}, Mn^{2+}, Na^{+} and K^{+}) were prepared in methanol. Some metal salts like Pb^{2+} and K^{+} are moderately soluble in methanol. We used 200 µL of water to get clear solutions. In a quartz cuvette, 2800 µL of methanol was taken and then 200 µL of the suspension of **1'** in methanol was introduced. This resulting suspension (3 mL) was then employed for the fluorescence sensing experiment. At the time of fluorescence titration experiments, solutions of metal cations were added in a stepwise manner (50 µL in each step) to the suspension of **1'** in methanol. If the starting fluorescence intensity of **1'** is I_o and the fluorescence intensity after inclusion of the analyte is I, then the quenching efficiency was calculated as $(1\text{-}I/I_o) \times 100$ %.

2.3 Results and discussion

2.3.1 Synthesis and characterization of MOF

There were many possible ways to perform reactions in order to get optimized conditions for the synthesis of **1**. By varying different zinc salts like $ZnCl_2$, $Zn(ClO_4)_2{\cdot}6H_2O$, $Zn(CH_3COO)_2{\cdot}2H_2O$ and $Zn(NO_3)_2{\cdot}6H_2O$, reactions were performed in different solvents like DMF, *N*,*N*-diethyl formamide (DEF) and *N*,*N*-dimethylacetamide (DMA) at different temperatures (80 to 150 °C). To get clear solutions, we added 150 µL of conc. nitric acid (HNO_3) into the reaction mixtures before heating. Among all the reaction conditions, block-shaped single-crystals were obtained at 140 °C for 72 h, when $Zn(ClO_4)_2{\cdot}6H_2O$ was used as the metal salt and DMF as the solvent. Single-crystals of similar shape were also achieved with $Zn(NO_3)_2{\cdot}6H_2O$ using the same reaction conditions. However, the size of these crystals was insufficient for single-crystal X-ray analysis.

The as-synthesized crystals of **1** were filtered from the mother liquor and thoroughly washed with acetone to remove the physisorbed DMF molecules from the crystals. The activation of **1** was performed to remove the guest solvent molecules from the pores. This was performed by stirring **1** with low-boiling point solvent like acetone. The phase-purity of the bulk sample after the synthesis and activation was checked by XRPD analysis. The obtained XRPD patterns were compared with the simulated pattern based on the data obtained from the single-crystal X-ray diffraction experiment. The comparison plot is shown in Figure 2.1. The

diffraction pattern of the as-synthesized compound is in good agreement with the simulated data. The XRPD data of the activated compound is similar to the simulated data. Hence, both **1** and **1'** exhibit excellent phase-purity.

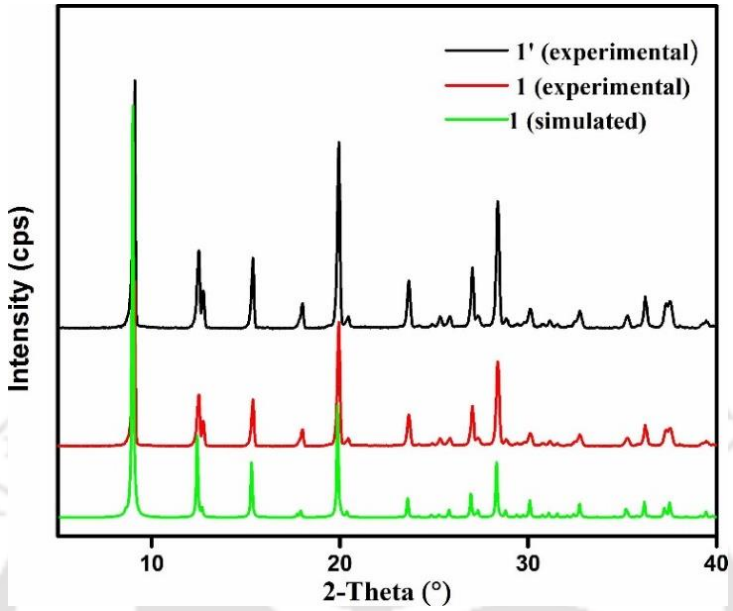

Figure 2.1 XRPD patterns of calculated **1**, as-synthesized **1** and thermally activated **1'**.

2.3.2 FT-IR spectroscopy

The FT-IR spectra of both **1** and **1'** consist of almost similar absorption bands, except the shoulder at around 1654 cm^{-1} which is additionally observed in the IR spectrum of **1** (Figure 2.2). For **1**, the absorption peak at around 1654 cm^{-1} is due to the stretching vibration of the carbonyl groups of the guest DMF molecules. This absorption peak disappeared after activation.[42-43] The absorption bands at around 1630 and 1410 cm^{-1} in both as-synthesized and activated samples correspond to the asymmetric and symmetric stretching vibrations of the carboxylate groups of the coordinated QDA linker molecules, respectively.

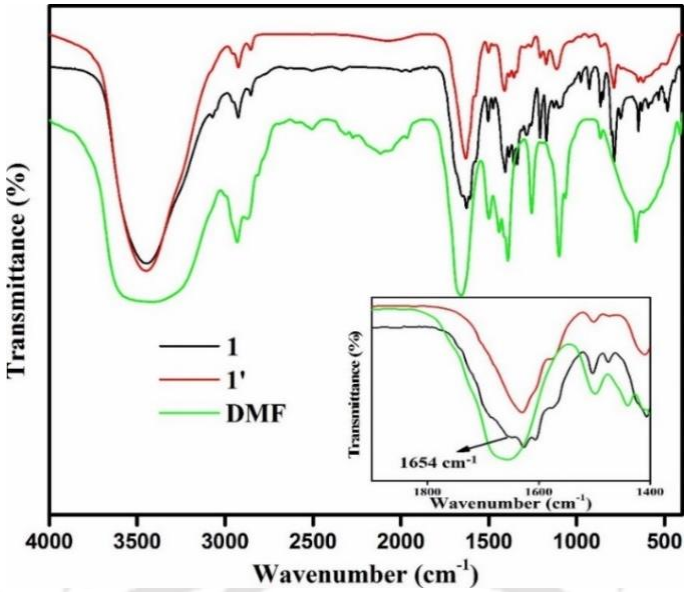

Figure 2.2 FT-IR spectra of compound **1** (black), **1'** (red) and DMF (green).

2.3.3 Structure description

Single-crystal X-ray diffraction study revealed that **1** crystallized in a tetragonal crystal system and exhibits $I4_1/a$ space group ($a = b = 19.9088(3)$ Å, $c = 12.1905(3)$ Å). The asymmetric unit of **1** is shown in Figure 2.3a. The asymmetric unit contains one unit of QDA linker with full occupancy and one unit of Zn^{2+} ion with half occupancy. Within the crystal lattice, the central Zn^{2+} ion attains a distorted square pyramidal geometry with ZnO_4N configuration. The basal plane of the square-pyramid is constituted by one N and three O atoms from three different QDA linkers whereas the other corner is coordinated to the O atom from an adjacent QDA linker. Such coordination around Zn^{2+} ion generates a ZnO_4N type of square pyramidal secondary building unit (SBU), which propagates along the crystallographic *c*-axis leading to a 1D zig-zag chain (Figure 2.3c). Two such adjacent 1D chains are further connected *via bis*-chelation from QDA linker generating an extended 2D layer propagating along the crystallographic *bc* plane (Figure 2.3d). The adjacent 2D layers are further connected via such chelating QDA linkers to give rise to an extended 3D framework (Figure 2.3e) with PtS topology,[44] where Zn^{2+} center acts as a 5-connected node and QDA linker as a spacer (Figure 2.3f). According to the program PLATON,[40, 45] the total potentially accessible void volume is 1297.10 $Å^3$, which is 26.8% of the total unit cell volume (4831.83 $Å^3$). These voids are occupied by the solvent molecules before activation. The crystallographic data and refinement parameters of **1** are listed in Table 2.1.

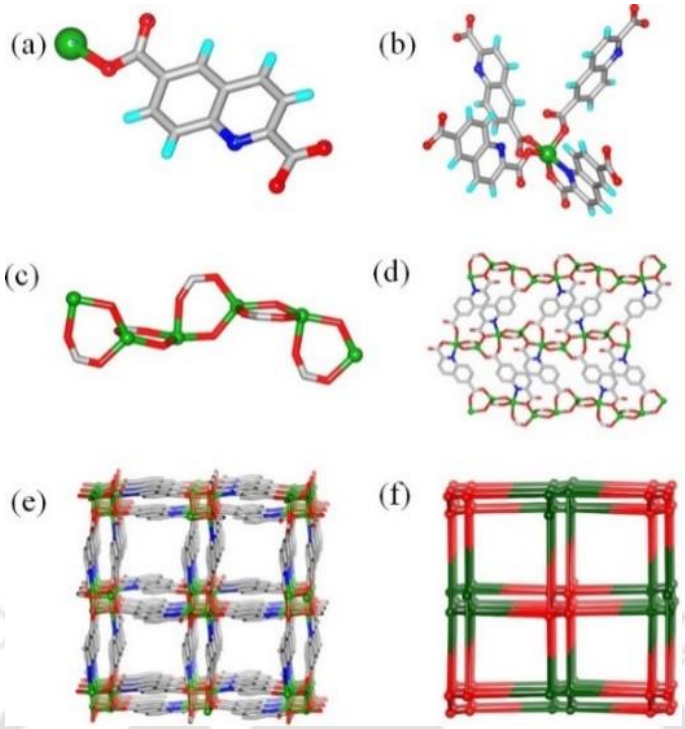

Figure 2.3 Illustrations for the crystal structure of **1**: (a) asymmetric unit, (b) coordination environment around Zn^{2+} ion, (c) 1D zigzag chain, (d) 2D layer constructed *via* linking adjacent chains, (e) extended 3D framework and (f) PtS topology of the overall 3D framework. Color codes: Zn, green; C, grey; O, red; N, navy blue; H, sky blue

Table 2.1 Single-crystal X-ray data and structure refinement parameters for compound **1**.

Formula	$C_{11}H_5NO_4Zn$
Formula Weight	280.53
Crystal System	Tetragonal
Space group	$I4_1/a$
a/Å	19.9088(3)
b/Å	19.9088(3)
c/Å	12.1905(3)
V/Å^3	4831.83(19)
Z	16
D_e/g cm^{-3}	1.543
μ Mo K_α/mm^{-1}	2.033
F000	2240.0
T/K	293(2)
Theta range	2.894 to 28.697°
Total no. of reflections	5395

Independent reflections	2747 [R(int) = 0.0174]
Observed reflections	1830
Parameters refined	154
Final R indices [I>2sigma(I)]	R_1 = 0.0274, wR_2 = 0.0671
R indices (all data)	R_1 = 0.0378, wR_2 = 0.0723
GOF (F^2)	1.049
Crystal Size	0.26 x 0.24 x 0.22 mm^3
Index ranges	-26<=*h*<=13, -21<=*k*<=25, -16<=*l*<=8
Absorption correction	Semi-empirical from equivalents
Max. and min. transmission	0.639 and 0.595
Refinement method	Full-matrix least-squares on F^2
Data / restraints / parameters	2747 / 0 / 154
Extinction coefficient	n/a
Largest diff. peak and hole	0.379 and -0.207 e.$Å^{-3}$

2.3.4 Thermal and chemical stability

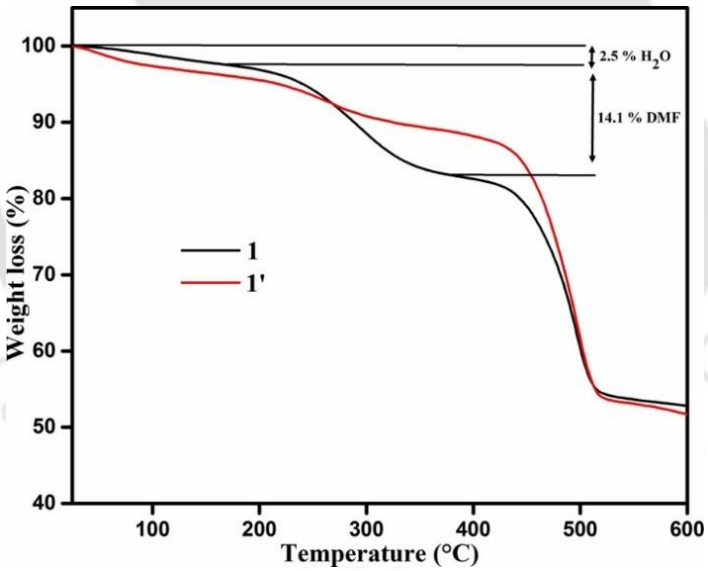

Figure 2.4 TG curves of **1** and **1'** recorded in an argon atmosphere in the temperature range of 25-600 °C with a heating rate of 10 °C/min.

The TGA data clearly suggested that both the samples (i.e., **1** and **1'**) of the compound are stable up to 440 °C. Hence, the MOF material features excellent thermal stability. As evident from the TG curve of **1** (Figure 2.4), the weight loss of 2.5 wt% observed between 25 and 170 °C is due to the removal of 0.5 H_2O molecule per formula unit (calcd.: 2.6 wt%). The second weight loss of 14.1 wt% observed between 170-380 °C is due to the removal of 0.7

DMF molecule per formula unit (calcd.: 15.0 wt%). The decomposition of the framework starts at 440 °C.

The chemical stability of **1'** was checked by stirring it in different solvents as well as in acidic and basic medium (15 mL per 100 mg of **1'**) for 16 h. Here, **1'** was stirred at room temperature in water, methanol, acetic acid, 1(M) HCl and NaOH (at pH = 10) solutions for 16 h. It can be concluded from the XRPD patterns of the recovered samples (Figure 2.5) that the MOF material preserved its structural integrity in all these liquids. The crystallinity of the compound was slightly reduced after stirring in 1(M) HCl solution. The satisfactory chemical and thermal stability of **1'** can be very useful for its practical applications.

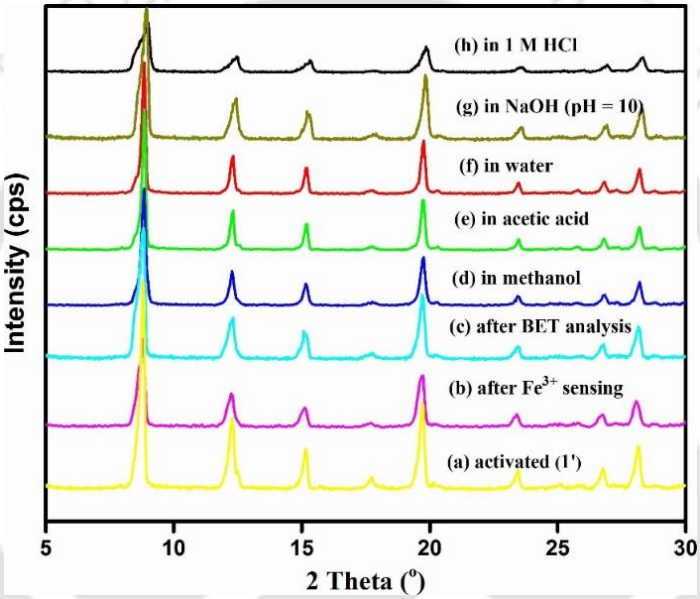

Figure 2.5 XRPD patterns of compound **1** in different forms: (a) activated, (b) after 5 cycles of fluorescence titration experiments with Fe^{3+} solution, (c) after BET analysis, (d) after treatment with methanol, (e) after treatment with acetic acid, (f) after treatment with water, (g) after treatment with NaOH solution (pH = 10), and (h) after treatment with 1(M) HCl.

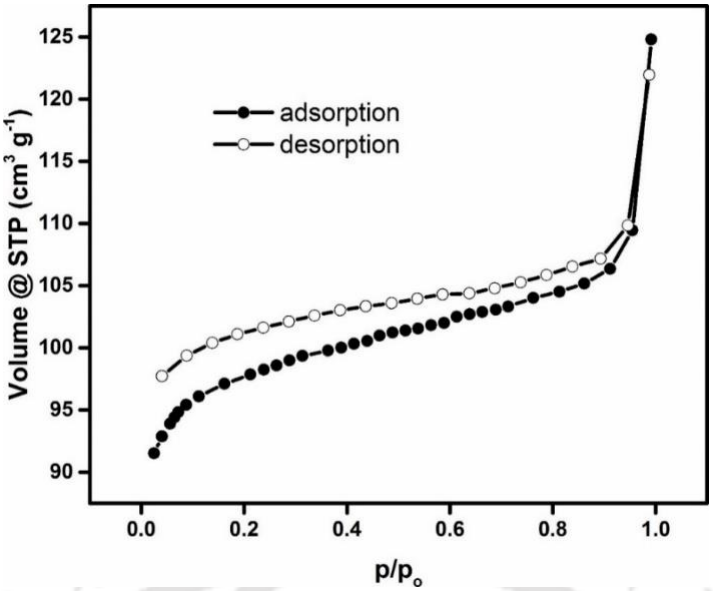

Figure 2.6 N_2 adsorption (filled circles) and desorption (empty circles) isotherms of thermally activated **1'** measured at –196 °C.

2.3.5 Surface area measurement

The nitrogen sorption experiment was performed to determine the extent of microporosity of material **1'**. From this sorption measurement, the specific Brunauer-Emmett-Teller (BET) surface area of **1'** (Figure 2.6) was found to be 292 m^2 g^{-1}. In this way, the permanent microporosity of the framework **1'** was confirmed.

2.3.6 Photoluminescence properties

Figure 2.7 shows solid state excitation and emission spectrum of the H_2QDA linker. The H_2QDA linker give emission peak at 470 nm, when excitation at 330 nm at room temperature. The emission band of the H_2QDA linker could be due to π-π* intra linker electronic transition.[13]

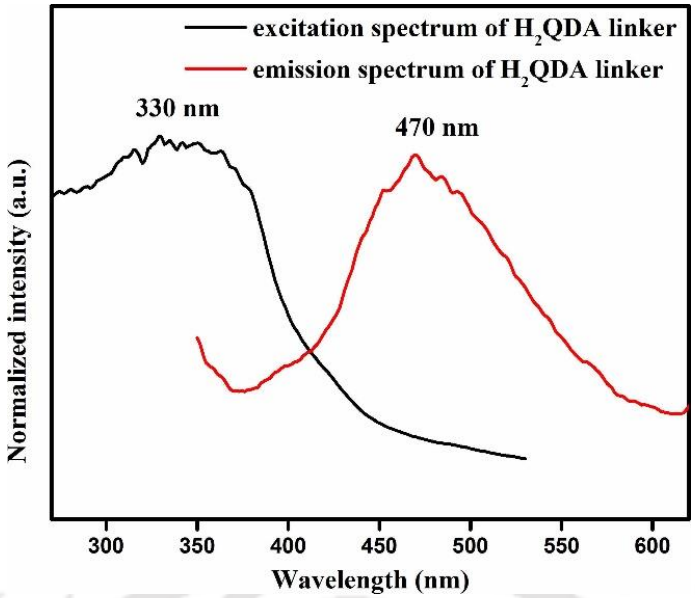

Figure 2.7 Excitation and emission spectra of H_2QDA linker in the solid state.

We also performed the solid state emission spectra of **1**, **1'** and H_2QDA linker as shown in Figure 2.8 When we excited at 310 nm, the both **1** and **1'** gives emission peak at 430 nm and H_2QDA linker gives emission peak at 470 nm. The enhancement in the emission intensity and blue shift in the position of the emission band for **1'** and **1** as compared to the H_2QDA linker might be related to the perturbation in the π–π^* transition due to the coordination of the H_2QDA linker with Zn (II) ions, forming a 3D cubic framework structure.[27]

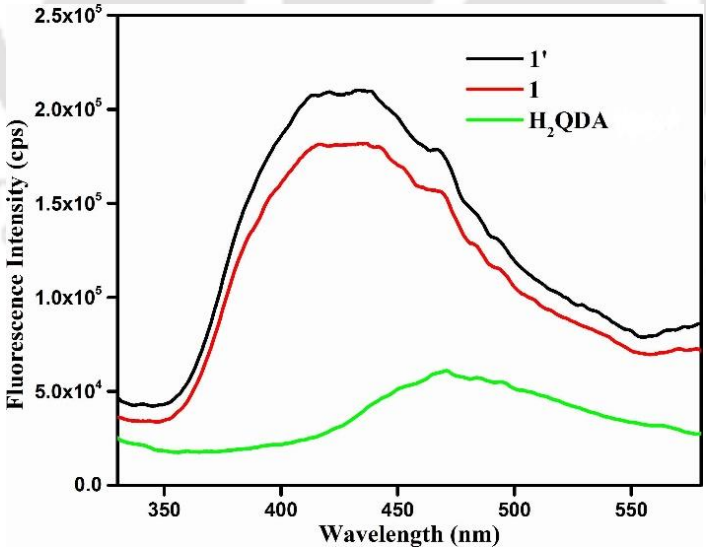

Figure 2.8 Solid state emission spectra of **1**, **1'** and H_2QDA linker (λ_{ex} = 310 nm).

Before investigating the fluorescence sensing behavior of **1'**, we measured the fluorescence emission spectra of **1'** in different organic solvents and water. The chosen organic solvents included DMF, DMA, dimethylsulphoxide, ethanol, methanol, acetonitrile and

dichloromethane. Compound **1'** showed similar emission spectra in most of the organic solvents (Figure 2.9). For the fluorescence sensing studies, methanol was chosen as the solvent, since good selectivity for a particular metal ion was not obtained in the other solvents.

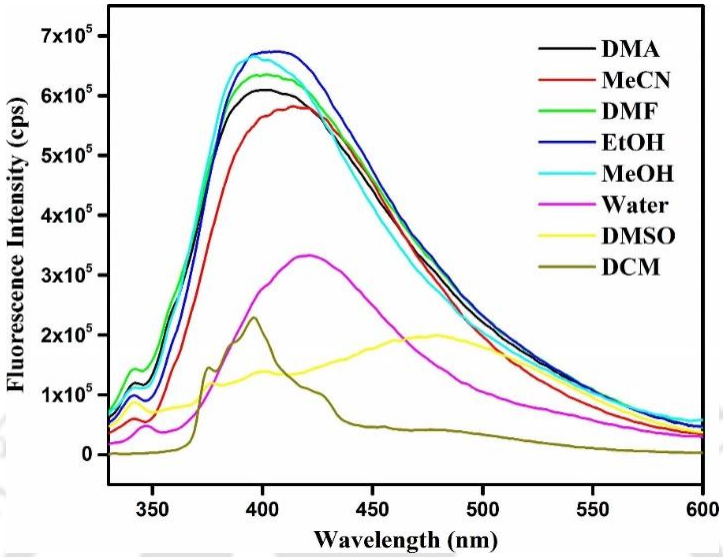

Figure 2.9 Fluorescence emission spectra of **1'** in common organic solvents (λ_{ex} = 310 nm).

2.3.6.1 Detection of metal cations

The twelve metal cations, which were selected for the fluorescence sensing investigations, included K^+, Fe^{2+}, Co^{2+}, Ni^{2+}, Zn^{2+}, Cd^{2+}, Cu^{2+}, Cr^{3+}, Fe^{3+}, Na^+, Pb^{2+} and Mn^{2+}. The solutions of metal cations (10 mM) were prepared in methanol. They were gradually added to the methanolic suspension of **1'**. It was clearly observed that after the addition of 400 µL of 10 mM Fe^{3+} solution to the methanolic suspension of **1'**, almost 97% fluorescence quenching occurred (Figure 2.10). For all the other cations, the fluorescence quenching efficiencies were lower as compared to the Fe^{3+} (Figure 2.11). We have also studied the quenching effect of Fe^{3+} in water. As shown in Figure 2.12, a quenching efficiency of 92% was observed. The percentage of quenching behaviour was almost similar as compared to quenching behaviour in methanol medium. The main reason for using methanol as a solvent for detection experiment is the better selectivity towards Fe^{3+} in methanol (as compare to water) over other competitive metal ions.

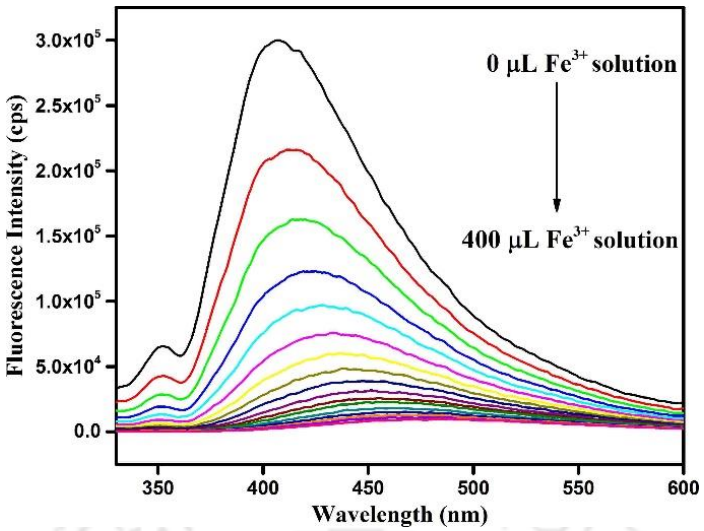

Figure 2.10 Quenching of the fluorescence intensity of the methanolic dispersion of **1'** after incremental addition of 10 mM Fe^{3+} solution.

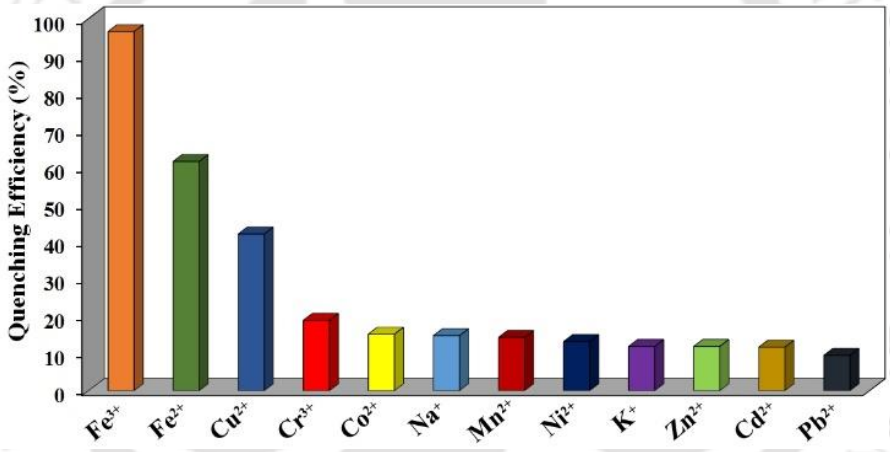

Figure 2.11 The fluorescence quenching efficiencies of different metal cations (400 μL of 10 mM solution) towards the methanolic dispersion of **1'**.

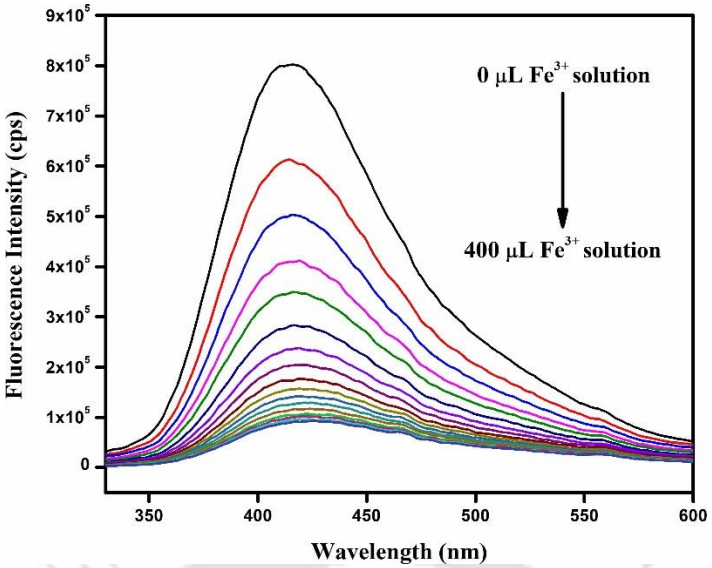

Figure 2.12 Quenching of the fluorescence intensity of the aqueous dispersion of **1'** after incremental addition of 10 mM Fe^{3+} solution.

The selectivity for Fe^{3+} sensing was also examined in the presence of other metal cations. To the methanolic dispersion of **1'**, the solutions of various metal cations were added individually and consequently the solution of Fe^{3+} was added to the mixture. The fluorescence emission spectra of the resulting mixtures were collected. The results of these experiments revealed that the quenching efficiency of Fe^{3+} did not alter considerably even when other metal cations were present in the sensing medium (Figure 2.13). Figure 2.14 shows that at low concentration quenching efficiency increases rapidly than at high concentration (especially in case of Fe^{3+}).

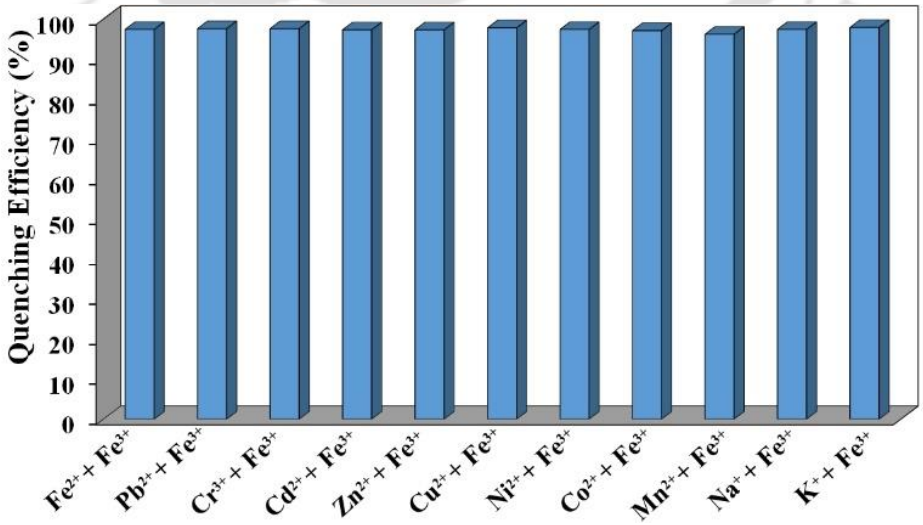

Figure 2.13 The effect of other metal cations on the quenching efficiency of Fe^{3+}.

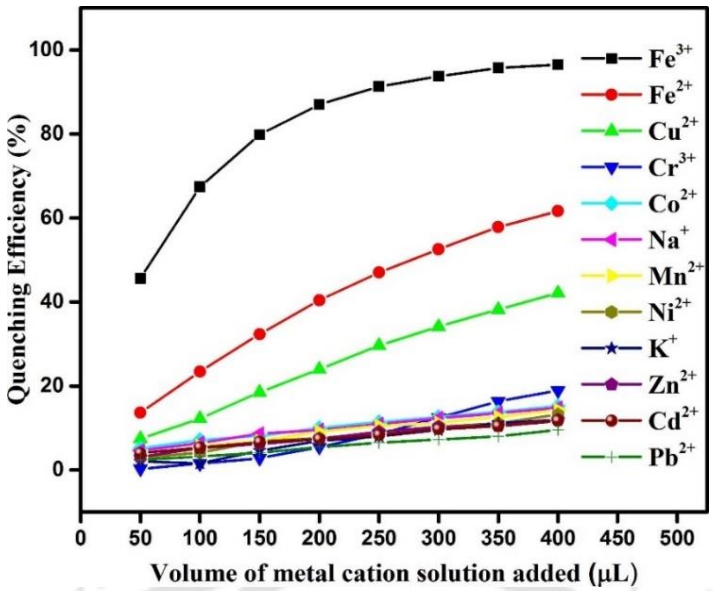

Figure 2.14 Change of fluorescence quenching efficiencies upon gradual addition of 10 mM solution of various metal cations to a 3 mL well-dispersed suspension of **1'** in methanol.

The utilization of the same probe material for multiple times ion is always advantageous for Fe^{3+} detection. We checked the reusability of **1'** up to five cycles. After the first cycle of Fe^{3+} detection investigation, **1'** was recovered by centrifugation from the suspension and washed five times with methanol. Then, the recovered sample was dried in the oven and again suspended in methanol. The suspension was sonicated for 30 min and left without any disturbance for 1 day. The as-prepared stable suspension was used for the subsequent sensing investigation. We repeated the same procedure for five cycles. The recyclability data in Figure 2.15 undoubtedly demonstrate that there was very slight reduction in the original fluorescence intensity of **1'** even after the fifth cycle. The XRPD pattern of the probe after the Fe^{3+} sensing investigation was also analogous as the pattern before the detection experiment (Figure 2.5). These findings indicate that **1'** can be repeatedly used for the Fe^{3+} sensing purpose.

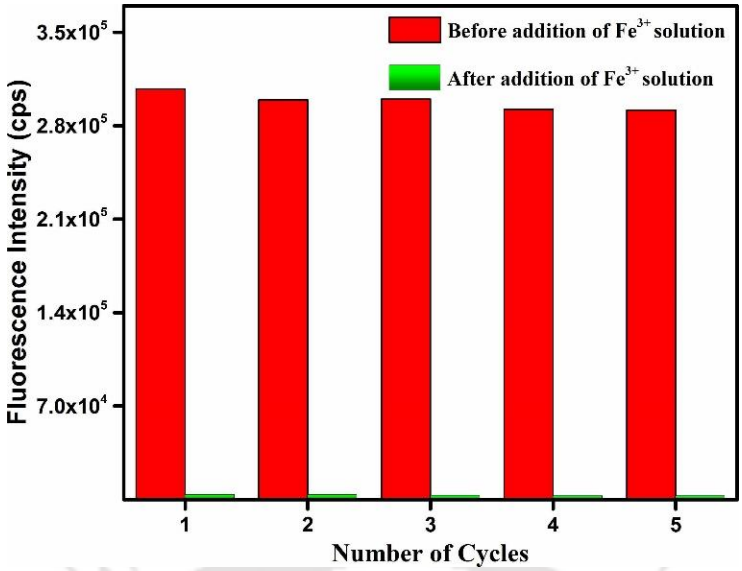

Figure 2.15 Recyclability study for the methanolic suspension of **1'** towards the sensing of Fe^{3+}.

For checking the effect of exposure time on the quenching efficiency, time-dependent fluorescence sensing studies were conducted with four different concentrations of Fe^{3+} solution. Here, 100, 200, 300 and 400 µL of 10 mM Fe^{3+} solution was added individually to the methanolic dispersion of **1'** and the fluorescence spectra were recorded at a regular time interval. The results of the time-dependent sensing investigations (Figure 2.16) definitely dictate the maximum quenching occurred within 40 s of exposure for every concentration of Fe^{3+} solution. The quenching efficiencies became almost constant at longer exposure times, which was irrespective of the concentration of Fe^{3+} solution. Hence, the maximum quenching of the fluorescence intensity occurred instantaneously for each concentration of Fe^{3+} solution. Almost 97% quenching efficiency was observed within 40 s after the addition of 400 µL of 10 mM Fe^{3+} solution.

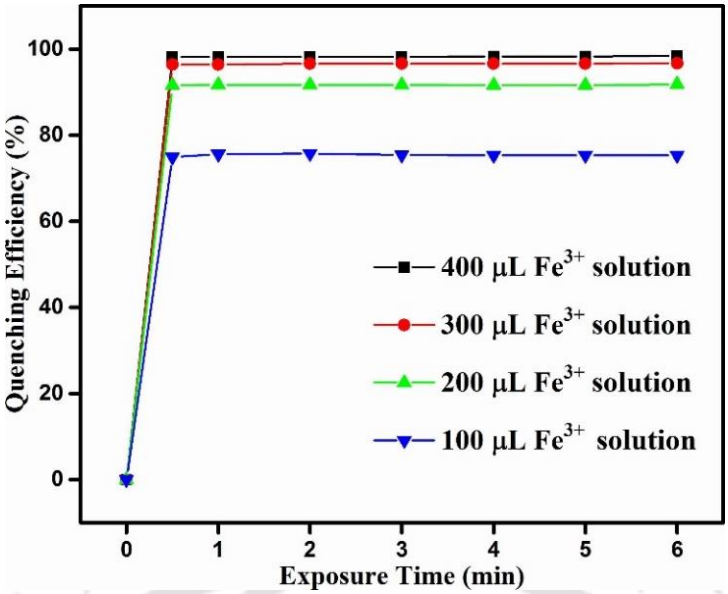

Figure 2.16 The quenching efficiencies of Fe^{3+} solutions having different concentrations towards **1'** as a function of exposure time.

2.3.6.2 Analysis of quenching constant and detection limit for Fe^{3+}

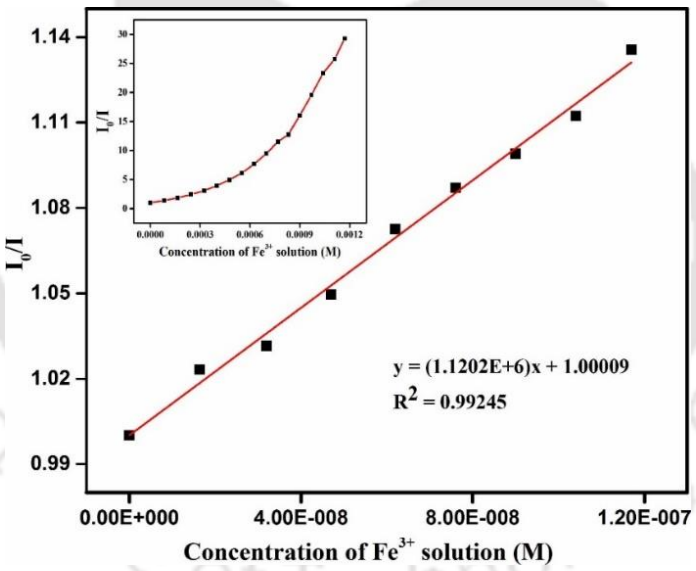

Figure 2.17 Stern-Volmer plot for the quenching of **1'** at lower concentration of Fe^{3+} solution. Inset: non-linearity of the Stern-Volmer plot at higher concentration of Fe^{3+} solution.

The Stern-Volmer (S-V) plot helps to quantify the extent of fluorescence quenching.[46] If the fluorescence intensities in the absence and presence of quencher are represented as I_0 and I respectively, then the S-V plot can be drawn by using the equation[47-48]: $(I_0/I) = K_{sv}[A] + 1$. Here, the molar concentration of the quencher is represented by $[A]$ and the S-V quenching constant is represented by K_{sv}. Figure 2.17 displays the S-V plot for the quenching of **1'** as a function of the concentration of Fe^{3+} solution. The K_{sv} value was found to be 1.12×10^6 M^{-1}

from the linear S-V plot at a lower concentration of Fe^{3+} solution in methanol medium. In water, the K_{sv} value was found to be 0.89×10^6 M^{-1} (Figure 2.18). These values are comparable with the existing MOF based sensors for Fe^{3+} (Table 2.2).[49] [50-56]

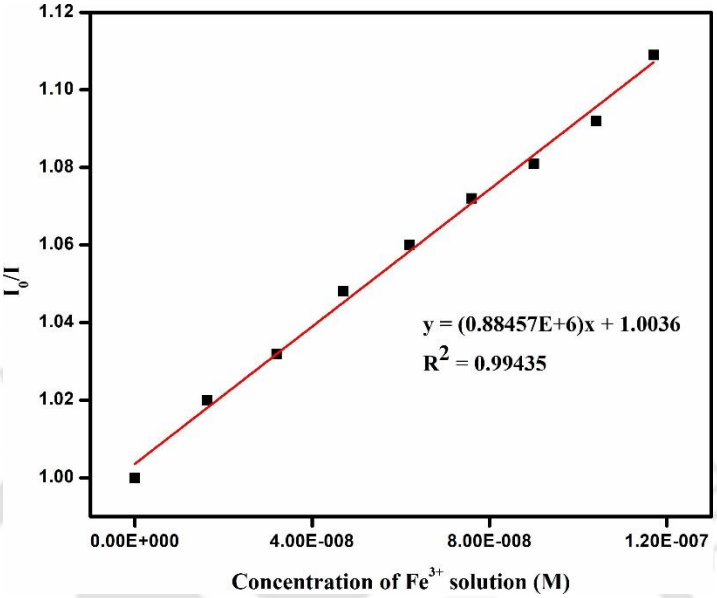

Figure 2.18 Stern-Volmer plot for the quenching of **1'** at lower concentration of Fe^{3+} solution in water.

Table 2.2 A comparison of the Stern-Volmer constant (K_{sv}), detection limit and medium used for the sensing of Fe^{3+} for the MOFs reported till date.

Sl. No.	MOF	K_{sv} (M^{-1})	Detection Limit	Medium Used	Ref.
1.	[Zn(QDA)]·0.3DMF	1.12×10^6	2.3×10^{-8} M	methanol	this work
		0.89×10^6	3.1×10^{-8} M	water	this work
2.	$[La(TPT)(DMSO)_2]\cdot H_2O$	1.36×10^4	-	ethanol	49
3.	$[H(H_2O)_8][DyZn_4(imdc)_4(im)_4]$	2.88×10^4	-	DMSO	57
4.	EuL_3	4.1×10^3	10^{-4} M	ethanol	51
5.	$[Eu_2(MFDA)_2(HCOO)_2(H_2O)_6]\cdot H_2O$	-	3.3×10^{-7} M	DMF	58
6.	$[Cd(H_2L_a)_{0.5}(H_2L_b)_{0.5}(H_2O)]$	-	10^{-5} M	water	59

7.	$[(CH_3)_2NH_2]\cdot[Tb(bptc)]\cdot x$solvents	-	72.76 ppm	ethanol	60
8.	$[Ln_2(Ccbp)_3\cdot 6H_2O]\cdot 3Cl^-\cdot 4H_2O$	1.143×10^5	-	ethanol	61
9.	Eu^{3+}@MIL-124	3.87×10^4	0.3×10^{-6} M	water	62
10.	MIL-53(Al)	-	0.9×10^{-6} M	PBS buffer	63
11.	$[Ln(Hpzbc)_2(NO_3)]\cdot H_2O$	-	2.6×10^{-5} M	ethanol	64
12.	$[Tb(BTB)(DMF)]\cdot 1.5DMF\cdot 2.5H_2O$	-	10^{-5} M	ethanol	65
13.	$[Tb_4(OH)_4(DSOA)_2(H_2O)_8]\cdot(H_2O)_8$	3.5×10^4	-	water	66
14.	Tb^{3+}@Cd-MOF	1.108×10^5	0.010 mM	DMF	67
15.	$[Zr_6O_4(OH)_4(2,7\text{-}CDC)_6]\cdot 19H_2O\cdot 2DMF$	5.5×10^3	9.1×10^{-7} M	water	68
16.	[Cd(*p*-CNPhHIDC)$(4,4'\text{-bipy})_{0.5}$]	1.99×10^3	5×10^{-3} M	water	69
17.	[Zn(*p*-CNPhHIDC)(4,4'-bipy)]	1.37×10^3	5×10^{-3} M	water	69
18.	$[Zr_6O_6(OH)_2(CF_3COO)_2(C_{11}H_5NO_4)_4(H_2O)_4]$	2.25×10^7	1.7×10^{-9} M	water	55
19.	$[Zr_6O_6(OH)_2(CF_3COO)_2(C_{11}H_5NO_4)_4(H_2O)_4]$	1.91×10^7	2.7×10^{-9} M	HEPES buffer	55
20.	$[Al(OH)(BDC\text{-}N_3)]\cdot 1.2H_2O\cdot 0.3DMF$	6.13×10^3	3×10^{-8} M	water	70

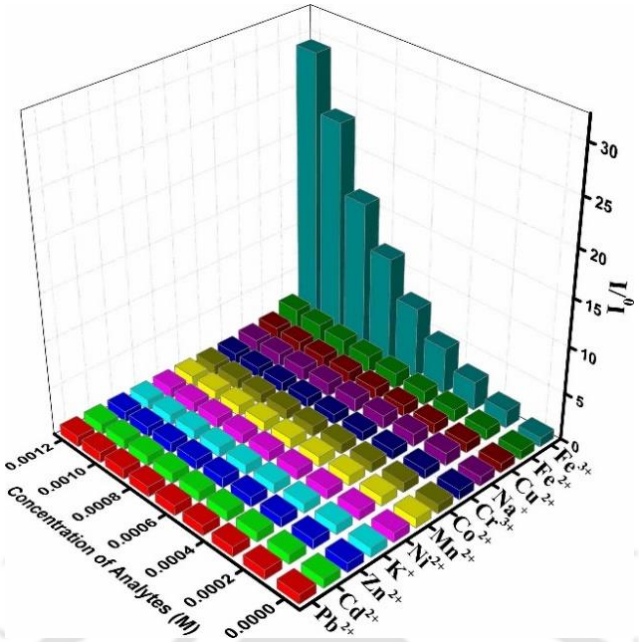

Figure 2.19 Three-dimensional S-V plots for the quenching of **1'** upon the addition of various concentrations of different metal cations.

The 3D S-V plots for all the metal cations are presented in Figure 2.19. The plots are almost linear for the all the metal cations, except Fe^{3+} which showed nonlinearity and linearity at higher and lower concentrations, respectively. The shape of the S-V plot for Fe^{3+} suggests the possibility of both dynamic and static quenching processes.[71]

The time-resolved fluorescence decay measurements were performed to discriminate between these two quenching processes. We conducted the fluorescence lifetime measurements with **1'** in the absence and presence of Fe^{3+} solution in methanol. It can be noticed from Figure 2.20 and Table 2.3 that there is only negligible change in the excited-state lifetime value after the addition of 50 μL of 10 mM Fe^{3+} solution to the methanolic suspension of **1'**, indicating the happening of static quenching (i.e., the formation of a ground-state non-fluorescent complex between **1'** and Fe^{3+}).[53, 72]

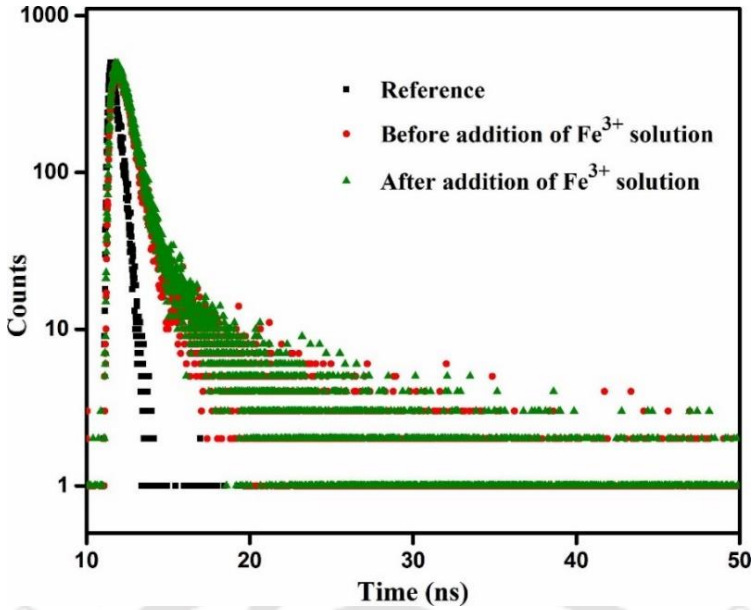

Figure 2.20 Lifetime decay profile of **1'** before and after addition of 50 μL of 10 mM Fe^{3+} solution.

Table 2.3 Average excited-state lifetime (<τ>) values of **1'** before and after the addition of 50 μL of 10 mM Fe^{3+} solution (λ_{ex} = 310 nm).

Volume of 10 mM Fe^{3+} solution added (μL)	B_1	B_2	a_1	a_2	τ_1 (ns)	τ_2 (ns)	<τ>* (ns)	χ^2
0	0.038	0.001	0.812	0.188	0.533	3.092	1.014	1.01
50	0.038	0.002	0.793	0.207	0.564	3.040	1.076	1.08

* $\langle\tau\rangle = a_1\tau_1 + a_2\tau_2$

As shown in Figure 2.19, the plot of the fluorescence intensity of the methanolic suspension of **1'** as a function of the concentration of Fe^{3+} solution at lower concentration range yielded a linear curve. The limit of detection (LOD) was determined as: LOD = $3\sigma/K$.[73] Here, *K* is the slope of the linear curve presented in Figure 2.21 and σ is the standard deviation of the fluorescence intensity of **1'** in the absence of Fe^{3+} solution. The resulting LOD value was 2.3 × 10^{-8} M (9.2 ppb) in methanol medium. We have also calculated the LOD value of **1'** towards Fe^{3+} in water and calculated LOD value was found to be 3.1 × 10^{-8} M (12 ppb) (Figure 2.22). These LOD falls among the lowest LOD values reported in the literature for the MOF-based fluorescence probes for the detection of Fe^{3+} (Table 2.2).[51, 53, 55-56, 58-60, 62-65]

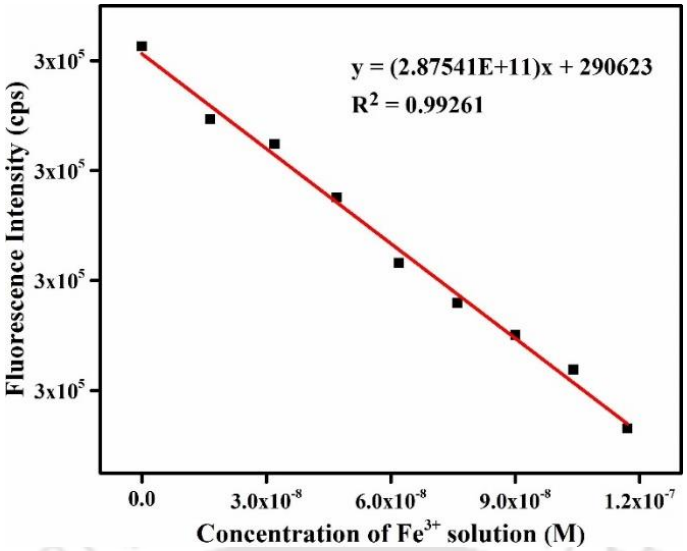

Figure 2.21 Variation in the fluorescence intensity of the methanolic suspension of **1'** as a function of the concentration Fe^{3+} solution.

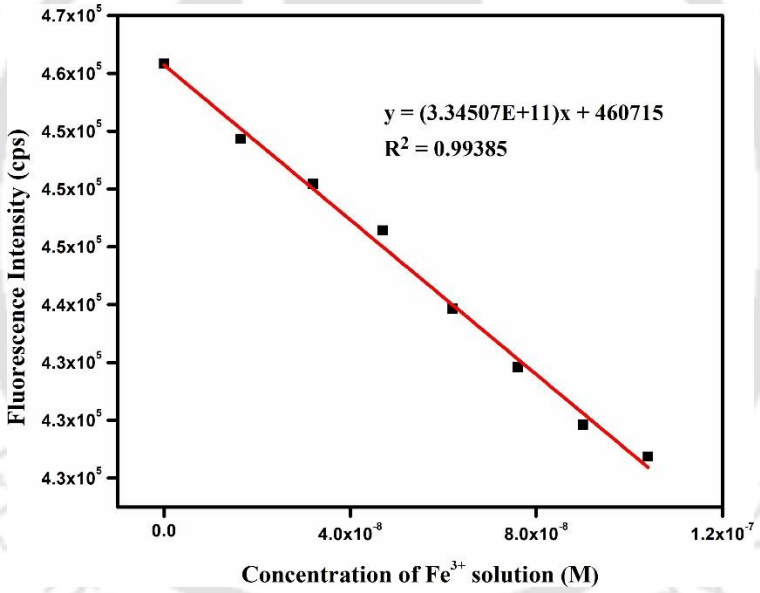

Figure 2.22 Variation in the fluorescence intensity of the aqueous suspension of **1'** as a function of the concentration of Fe^{3+} solution.

2.3.6.3 Mechanisms for Fe^{3+} detection

Finally, we proceeded to explore the mechanism of observed fluorescence quenching property of **1'** by Fe^{3+}. As portrayed in Figure 2.20, the time-resolved fluorescence experiment indicated that the quenching of **1'** by Fe^{3+} is static in nature. We carried out EDX measurement with **1'** obtained after the sensing experiment. The absence of any peak for Fe^{3+} in the EDX spectrum (Figure 2.23) indicated that the Fe^{3+} did not replace any Zn^{2+} present in the framework structure.

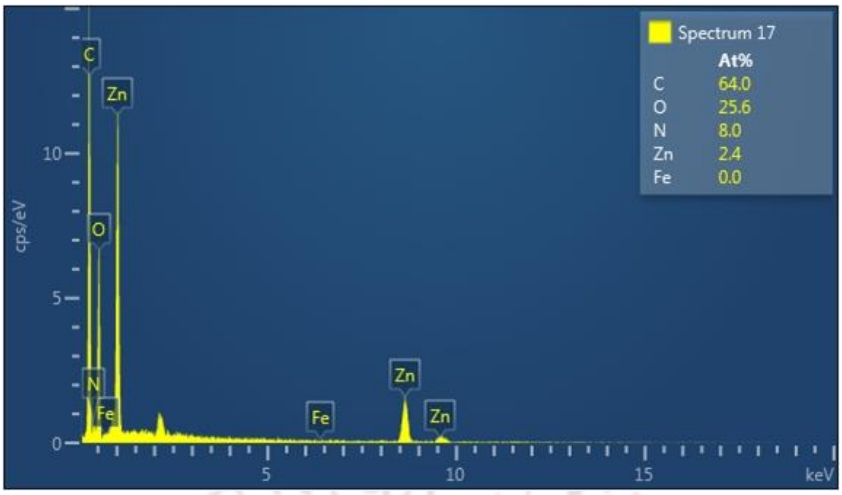

Figure 2.23 EDX spectrum of **1'** after treatment with 10 mM Fe^{3+} solution.

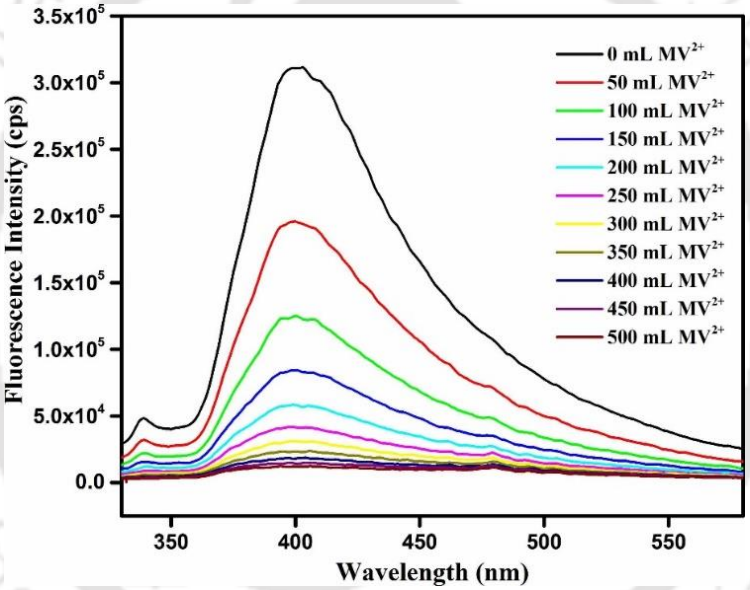

Figure 2.24 Quenching of the fluorescence intensity of **1'** by incremental addition of 10 mM MV^{2+} solution to a 3 mL stable suspension of **1'** in methanol.

The XRPD data of **1'** collected after the Fe^{3+} sensing study showed that the material still maintained its structural robustness after treatment with Fe^{3+} solution. Hence, the quenching process was not caused by the destruction of the framework of **1'**. The photo-induced electron transfer (PET) process may be the reason behind the fluorescence quenching mechanism. In this process, an internal redox reaction occurs between the excited state of the fluorophore with the species which can accept or donate electrons.[48, 74] The Fe^{3+} has a very high positive charge density and hence it has a strong electron withdrawing character as compared to the other metal cations.[75] Hence, we assume that the electron transfer process occurs from the electron-rich linker to the Fe^{3+}, which is responsible for the fluorescence

quenching observed in the system. To confirm the PET process, we carried out fluorescence titration experiments with a very well-known electron acceptor such as methyl viologen (MV^{2+}) dication. The quenching profile by MV^{2+} was same as the quenching profile by Fe^{3+} (Figure 2.24). As MV^{2+} are good electron acceptors, the quenching process occurred through electron transfer process from the electron rich framework to the MV^{2+}.[76] From the similarity of the quenching patterns for both MV^{2+} and Fe^{3+}, we can conclude that the photo-induced electron transfer process from the framework to the Fe^{3+} governs the fluorescence quenching process.

The electron transfer mechanism can be also supported by the slightly red-shifted fluorescence spectra upon Fe^{3+} addition to **1'** (Figure 2.10).[77] There is also a possibility of fluorescence resonance energy transfer (FRET) process which can contribute to the quenching mechanism. In FRET process, the resonance energy is transferred from the fluorophore to the analyte. If there is a substantial overlap between the absorption band of the analyte (acceptor) and the emission band of the flurophore (donor), then FRET process takes place.[78] Figure 2.25 shows the UV-Vis spectra of all the examined metal cations in methanol with the emission spectrum of **1'**. It is clearly indicated from the figure that there is maximum overlap between the electronic absorption spectrum of Fe^{3+} with the emission spectrum of **1'**. These observations suggest that the fluorescence quenching of **1'** by Fe^{3+} takes place through both PET and FRET mechanisms.

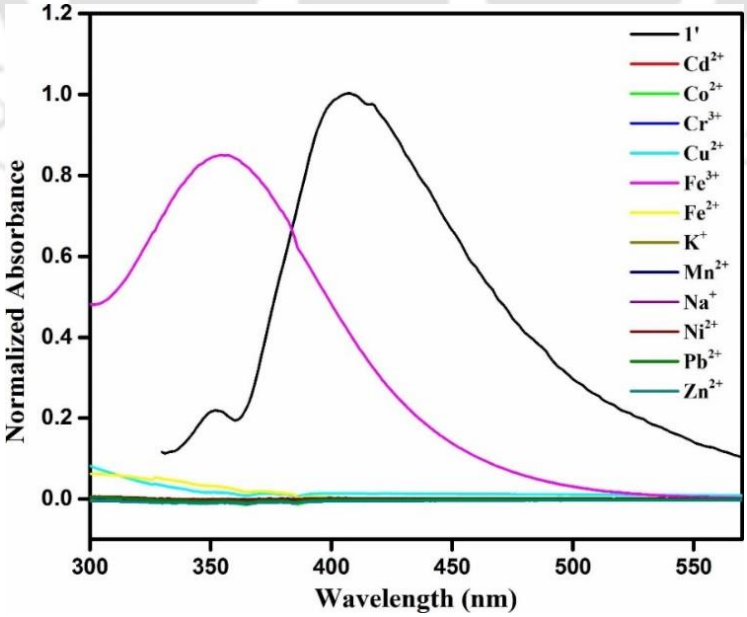

Figure 2.25 UV-Vis absorption spectra of the different metal ions (10×10^{-3} M) solution in methanol. The emission spectra of **1'** (black color) (3 mg) dispersed in methanol (3 mL).

2.4 Conclusions

In this work, a new 3D luminescent MOF (**1**) composed of Zn^{2+} and quinoline-2,6-dicarboxylic acid linker was synthesized by solvothermal method and characterized in detail. Single crystal structure determination disclosed that the 3D framework of **1** possesses PtS topology, in which the Zn^{2+} have distorted square pyramidal geometry with ZnO_4N configuration. The compound exhibited very high chemical stability. It also displayed high thermal stability up to 440 °C. The activated compound (**1'**) showed selective fluorescence sensing behavior for Fe^{3+} with very fast rate of response in methanol. We also demonstrated that the selective sensing property of **1'** for Fe^{3+} is retained in the presence of other competitive metal cations. The LOD for the sensing of Fe^{3+} by **1'** was estimated to be 2.3×10^{-8} M (9.2 ppb), which lies among the lowest values exhibited by the previously reported MOF based fluorescence probes for sensing Fe^{3+}. Recyclability experiments demonstrated that probe **1'** could be recycled for five cycles of fluorescence detection events. The XRPD data confirmed that material **1'** could maintain its structural integrity after the sensing experiment. Spectroscopic studies pointed out that both energy transfer and electron transfer mechanisms play important roles for the selective fluorescence quenching of **1'** by Fe^{3+}. All these experimental results clearly indicate that material **1'** is a promising probe for the practical detection of Fe^{3+}.

2.5 References

1. Furukawa, H.; Cordova, K. E.; O'Keeffe, M.; Yaghi, O. M. The chemistry and applications of metal-organic frameworks *Science* **2013,** *341*, 1230444.

2. Fe´rey, G. Hybrid porous solids: past, present, future. *Chem. Soc. Rev.* **2008,** *37*, 191–214.

3. Zhang, J.; Wu, H.; Emge, T. J.; Li, J. A flexible MMOF exhibiting high selectivity for CO_2 over N_2, CH_4 and other small gases. *Chem. Commun.* **2010,** *46*, 9152-9154.

4. Stock, N.; Biswas, S. Synthesis of metal-organic frameworks (MOFs): routes to various MOF topologies, morphologies, and composites. *Chem. Rev.* **2012,** *112*, 933–969.

5. Ma, L.; Abney, C.; Lin, W. Enantioselective catalysis with homochiral metal–organic frameworks. *Chem. Soc. Rev.* **2009,** *38*, 1248−256.

6. Zeng, L.; Guo, X.; He, C.; Duan, C. Metal−organic frameworks: versatile materials for heterogeneous photocatalysis. *ACS Catal.* **2016,** *6*, 7935–7947.

7. Murray, L. J.; Dincaˇ, M.; Long, J. R. Hydrogen storage in metal–organic frameworks. *Chem. Soc. Rev.* **2009,** *38*, 1294−1314.

8. Sculley, J.; Yuan, D.; Zhou, H.-C. The current status of hydrogen storage in metal–organic frameworks—updated. *Energy Environ. Sci.* **2011,** *4*, 2721–2735.

9. Chen, B.; Xiang, S.; Qian, G. Metal−organic frameworks with functional pores for recognition of small molecules. *Acc. Chem. Res.* **2010,** *43*, 1115–1124.

10. Li, J.-R.; Sculley, J.; Zhou, H.-C. Metal-organic frameworks for separations. *Chem. Rev.* **2012,** *112*, 869–932.

11. Uemura, T.; Yanai, N.; Kitagawa, S. Polymerization reactions in porous coordination polymers. *Chem. Soc. Rev.* **2009,** *38*, 1228−1236.

12. Hu, Z.; Deibert, B. J.; Li, J. Luminescent metal–organic frameworks for chemical sensing and explosive detection. *Chem. Soc. Rev.* **2014,** *43*, 5815− 5840.

13. Allendorf, M. D.; Bauer, C. A.; Bhaktaa, R. K.; Houka, R. J. T. Luminescent metal–organic frameworks. *Chem. Soc. Rev.* **2009,** *38*, 1330−1352.

14. Wales, D. J.; Grand, J.; Ting, V. P.; Burke, R. D.; Edler, K. J.; Bowen, C. R.; Mintova, S.; Burrows, A. D. Gas sensing using porous materials for automotive applications. *Chem. Soc. Rev.* **2015,** *44*, 4290-4321

15. Hao, Z.; Yang, G.; Song, X.; Zhu, M.; Meng, X.; Zhao, S.; Song, S.; Zhang, H. A europium(III) based metal–organic framework: bifunctional properties related to sensing and electronic conductivity. *J. Mater. Chem. A* **2014,** *2*, 237-244

16. Taylor-Pashow, K. M. L.; Rocca, J. D.; Xie, Z.; Tran, S.; Lin, W. Postsynthetic modifications of iron-carboxylate nanoscale metal−organic frameworks for imaging and drug delivery. *J. Am. Chem. Soc.* **2009,** *131*, 14261–14263.

17. Li, A.-L.; Gao, Q.; Xu, J.; Bu, X.-H. Proton-conductive metal-organic frameworks: Recent advances and perspectives. *Coord. Chem. Rev.* **2017,** *344*, 54–82.

18. Zhang, F.-M.; Dong, L.-Z.; Qin, J.-S.; Guan, W.; Liu, J.; Li, S.-L.; Lu, M.; Lan, Y.-Q.; Su, Z.-M.; Zhou, H.-C. Effect of imidazole arrangements on proton-conductivity in metal–organic frameworks. *J. Am. Chem. Soc.* **2017,** *139*, 6183–6189.

19. Zhao, Y. Emerging applications of metal−organic frameworks and covalent organic frameworks. *Chem. Mater.* **2016,** *28*, 8079–8081.

20. Pettinari, C.; Marchetti, F.; Mosca, N.; Tosi, G.; Drozdov, A. Application of metal−organic frameworks. *Polym. Int.* **2017,** *66*, 731–744.

21. Williams, D. E.; Rietman, J. A.; Maier, J. M.; Tan, R.; Greytak, A. B.; Smith, M. D.; Krause, J. A.; Shustova, N. B. Energy Transfer on Demand: Photoswitch-Directed Behavior of Metal−Porphyrin Frameworks. *J. Am. Chem. Soc.* **2014,** *136*, 11886−11889.

22. Cadiau, A.; Adil, K.; Bhatt, P. M.; Belmabkhout, Y.; Eddaoudi, M. A metal-organic framework–based splitter for separating propylene from propane. *Science* **2016,** *353*, 137–140.

23. Guillerm, V.; Kim, D.; Eubank, J. F.; Luebke, R.; Liu, X.; Adil, K.; Lah, M. S.; Eddaoudi, M. A supermolecular building approach for the design and construction of metal–organic frameworks. *Chem. Soc. Rev.* **2014,** *43*, 6141-6172

24. Feng, D.; Gu, Z.-Y.; Chen, Y.-P.; Park, J.; Wei, Z.; Sun, Y.; Bosch, M.; Yuan, S.; Zhou, H.-C. A highly stable porphyrinic zirconium metal−organic framework with shp-a topology. *J. Am. Chem. Soc.* **2014,** *136*, 17714−17717.

25. Greathouse, J. A.; Allendorf, M. D. The Interaction of Water with MOF-5 Simulated by Molecular Dynamics. *J. Am. Chem. Soc.* **2006,** *128*, 10678–10679.

26. Wang, H.; Lustig, W. P.; Li, J. Sensing and capture of toxic and hazardous gases and vapors by metal–organic frameworks. *Chem. Soc. Rev.* **2018,** *47*, 4729-4756.

27. SK, M.; Biswas, S. A thiadiazole-functionalized Zr(IV)-based metal–organic framework as a highly fluorescent probe for the selective detection of picric acid. *CrystEngComm* **2016,** *18*, 3104–3113.

28. Yi, F.-Y.; Chen, D.; Wu, M.-K.; Han, L.; Jiang, H.-L. Chemical sensors based on metal–organic frameworks. *ChemPlusChem* **2016,** *81*, 675-690.

29. B.-Bon, A.; Costero, A. M.; Gil, S.; Parra, M.; Soto, J.; M.-Máñez, R.; Sancenón, F. A new selective fluorogenic probe for trivalent cations. *Chem. Commun.* **2012,** *48*, 3000-3002

30. Hider, R. C.; Kong, X. Iron speciation in the cytosol: an overview. *Dalton Trans.* **2013,** *42*, 3220–3229.

31. Chen, Z.; Sun, Y.; Zhang, L.; Sun, D.; Liu, F.; Meng, Q.; Wang, R.; Sun, D. A tubular europium–organic framework exhibiting selective sensing of Fe^{3+} and Al^{3+} over mixed metal ions. *Chem. Commun.* **2013,** *49*, 11557-11559.

32. Andrews, N. C. Disorders of iron metabolism. *N. Engl. J. Med.* **1999,** *341*, 1986-1995.

33. Carter, K. P.; Young, A. M.; Palmer, A. E. Fluorescent sensors for measuring metal ions in living systems. *Chem. Rev.* **2014,** *114*, 4564–4601.

34. Ulahannan, R. T.; Panicker, C. Y.; Varghese, H. T.; Musiol, R.; Jampilek, J.; Alsenoy, C. V.; War, J. A.; Srivastava, S. K. Molecular structure, FT-IR, FT-Raman, NBO, HOMO and LUMO, MEP, NLO and molecular docking study of 2-[(E)-2-(2-bromophenyl)-ethenyl]quinoline-6-carboxylic acid. *Spectrochim. Acta A* **2015,** *151*, 184–197.

35. Bottino, F. A.; Pasquale, G. D.; Pollicino, A.; Recca, A.; Staniland, P. A. Synthesis and characterization of new quinoline monomers. *J. Heterocyclic Chem.* **1989,** *26*, 929-931.

36. Sheldrick, G. M. Siemens Industrial Automation Inc., Madison, WI,. *SAINT and XPREP, 5.1 ed.* **1995**.

37. Sheldrick, G. M. Crystal structure refinement with SHELXL. *Acta Crystallogr., Sect. C: Struct. Chem.* **2015,** *71*, 3.

38. SAINT, V. S., Version 2.03, Bruker AXS, Inc., Madison, WI,, **2002**.

39. Spek, A. L. Structure validation in chemical crystallography. *Acta Cryst.* **2009,** *D65*, 148–155.

40. Spek, A. L. Single-crystal structure validation with the program PLATON. *J. Appl. Crystallogr.* **2003,** *36*, 7-13.

41. Farrugia, L. J. WinGX suite for small-molecule single-crystal crystallography. *J. Appl. Crystallogr.* **1999,** *32*, 837-838.

42. Dalapati, R.; Kökçam-Demir, Ü.; Janiak, C.; Biswas, S. The effect of functional groups in the aqueousphase selective sensing of Fe(III) ions by thienothiophene-based zirconium metal–organic frameworks and the design of molecular logic gates. *Dalton Trans.* **2018,** *47*, 1159-1170.

43. Nandi, S.; Banesh, S.; Trivedi, V.; Biswas, S. A dinitro-functionalized metal–organic framework featuring visual andfluorogenic sensing of H_2S in living cells, human blood plasma and environmental samples. *Analyst* **2018,** *143*, 1482-1491.

44. Blatov, V. A.; Shevchenko, A. P.; Proserpio, D. M. Applied topological analysis of crystal structures with the program package ToposPro. *Cryst. Growth Des.* **2014,** *14*, 3576–3586.

45. Sluis, P. v. d.; Spek, A. L. BYPASS: an effective method for the refinement of crystal structures containing disordered solvent regions. *Acta Crystallogr., Sect. A: Found. Crystallogr.* **1990,** *46*, 194-201.

46. Keizer, J. Nonlinear Fluorescence Quenching and the Origin of Positive Curvature in Stern-Volmer Plots. *J. Am. Chem. Soc.* **1983,** *105*, 1494-1498.

47. Lin, R.-B.; Li, F.; Liu, S.-Y.; Qi, X.-L.; Zhang, J.-P.; Chen, X.-M. A Noble-Metal-Free Porous Coordination Framework with Exceptional Sensing Efficiency for Oxygen. *Angew. Chem. Int. Ed.* **2013,** *52*, 13429 –13433.

48. III, S. W. T.; Joly, G. D.; Swager, T. M. Chemical Sensors Based on Amplifying Fluorescent Conjugated Polymers. *Chem. Rev.* **2007,** *7*, 1339-1386.

49. Zhang, C.; Yan, Y.; Pan, Q.; Sun, L.; He, H.; Liu, Y.; Liang, Z.; Li, J. A microporous lanthanum metal–organic framework as a bi-functional chemosensor for the detection of picric acid and Fe^{3+} ions. *Dalton Trans.* **2015,** *44*, 13340–13346.

50. Li, Y.-F.; D.Wang; Liao, Z.; Kang, Y.; Ding, W.-H.; Zheng, X.-J.; Jin, L.-P. Luminescence tuning of the Dy–Zn metal–organic framework and its application in the detection of Fe(III) ions. *J. Mater. Chem. C* **2016,** *4*, 4211-4217.

51. Zheng, M.; Tan, H.; Xie, Z.; Zhang, L.; Jing, X.; Sun, Z. Fast Response and High Sensitivity Europium Metal Organic Framework Fluorescent Probe with Chelating Terpyridine Sites for Fe^{3+}. *ACS Appl. Mater. Interfaces* **2013,** *5*, 1078−1083.

52. Wang, K.-M.; Du, L.; Ma, Y.-L.; Zhao, J.-S.; Wang, Q.; Yan, T.; Zhao, Q.-H. Multifunctional chemical sensors and luminescent thermometers based on lanthanide metal–organic framework materials. *CrystEngComm* **2016,** *18*, 2690–2700.

53. Das, A.; Biswas, S. A multi-responsive carbazole-functionalized Zr(IV)-based metal-organic framework for selective sensing of Fe(III), cyanide and p-nitrophenol. *Sens. Actuator B-Chem* **2017,** *250*, 121-131.

54. Weng, H.; Yan, B. A flexible Tb(III) functionalized cadmium metal organic framework as fluorescent probe for highly selectively sensing ions and organic small molecules. *Sens. Actuator B-Chem* **2016,** *228*, 702–708.

55. Gogoi, C.; Biswas, S. A new quinoline based luminescent Zr(IV) metal-organic framework for the ultrasensitive recognition of 4-nitrophenol and Fe(III) ion. *Dalton Trans.* **2018,** *47*, 14696-14705.

56. Das, A.; Banesh, S.; Trivedi, V.; Biswas, S. Extraordinary sensitivity for H_2S and Fe(III) sensing in aqueous medium by Al-MIL-53-N_3 metal–organic framework: in vitro and in vivo applications of H_2S sensing. *Dalton Trans.* **2018,** *47*, 2690–2700.

57. Li, Y.-F.; Wang, D.; Liao, Z.; Kang, Y.; Ding, W.-H.; Zheng, X.-J.; Jin, L.-P. Luminescence tuning of the Dy–Zn metal–organic framework and its application in the detection of Fe(III) ions. *J. Mater. Chem. C* **2016,** *4*, 4211-4217.

58. Zhou, X.-H.; Li, L.; Li, H.-H.; Li, A.; Yanga, T.; Huang, W. A flexible Eu(III)-based metal–organic framework: turn-off luminescent sensor for the detection of Fe(III) and picric acid. *Dalton Trans.* **2013,** *42*, 12403–12409.

59. Wu, Y.; Yang, G.-P.; Zhang, Y.; Shi, N.; Han, J.; Wang, Y.-Y. New luminescent Cd(II)-MOF as highly selective chemical probe for Fe^{3+} in aqueous solution with mixed metal ions. *RSC Adv.* **2015,** *5*, 90772-90777

60. Zhao, X.-L.; Tian, D.; Gao, Q.; Sun, H.-W.; Xu, J.; Bu, X.-H. A chiral lanthanide metal–organic framework for selective sensing of Fe(III) ions. *Dalton Trans.* **2016,** *45*, 1040–1046.

61. Wang, K.-M.; Du, L.; Ma, Y.-L.; Zhao, J.-S.; Wang, Q.; Yan, T.; Zhao, Q.-H. Multifunctional chemical sensors and luminescent thermometers based on lanthanide metal–organic framework materials. *CrystEngComm.* **2016,** *18*, 2690-2700.

62. Xu, X.-Y.; Yan, B. Eu (III)-functionalized MIL-124 as fluorescent probe for highly selectively sensing ions and organic small molecules especially for Fe (III) and Fe (II). *ACS Appl. Mater. Interfaces* **2015,** *7*, 721–729.

63. Yang, C.-X.; Ren, H.-B.; Yan, X.-P. Fluorescent metal–organic framework MIL-53(Al) for highly selective and sensitive detection of Fe^{3+} in aqueous solution. *Anal. Chem.* **2013,** *85*, 7441–7446.

64. Li, G.-P.; Liu, G.; Li, Y.-Z.; Hou, L.; Wang, Y.-Y.; Zhu, Z. Uncommon Pyrazoyl-Carboxyl Bifunctional Ligand-Based Microporous Lanthanide Systems: Sorption and Luminescent Sensing Properties. *Inorg. Chem.* **2016,** *55*, 3952-3959.

65. Xu, H.; Hu, H.-C.; Cao, C.-S.; Zhao, B. Lanthanide organic framework as a regenerable luminescent probe for Fe^{3+}. *Inorg. Chem.* **2015,** *54*, 4585−4587.

66. Dong, X.-Y.; Wang, R.; Wang, J.-Z.; Wang, S.-Q.; Mak, T. C. W. Highly selective Fe^{3+} sensing and proton conduction in a water-stable sulfonate–carboxylate Tb–organic-framework. *J. Mater. Chem. A* **2015,** *3*, 641–647.

67. Weng, H.; Yan, B. A flexible Tb(III) functionalized cadmium metal organic framework as fluorescent probe for highly selectively sensing ions and organic small molecules. *Sens. Actuator B-Chem.* **2016,** *228*, 702–708.

68. Das, A.; Biswas, S. A multi-responsive carbazole-functionalized Zr(IV)-based metal-organic framework for selective sensing of Fe(III), cyanide and p-nitrophenol. *Sens. Actuator B-Chem.* **2017,** *250*, 121-131.

69. Zhang, J.; Zhao, L.; Liu, Y.; Li, M.; Li, G.; Meng, X. Two luminescent transition-metal–organic frameworks with a predesigned ligand as highly sensitive and selective iron(III) sensors. *New J.Chem.* **2018,** *42*, 6839-6847.

70. Das, A.; Banesh, S.; Trivedi, V.; Biswas, S. Extraordinary sensitivity for H_2S and Fe(iii) sensing in aqueous medium by Al-MIL-53-N_3 metal-organic framework: in vitro and in vivo applications of H_2S sensing. *Dalton Trans.* **2018,** *47*, 2690-2700.

71. Mukherjee, P. S.; Acharyya, K. A fluorescent organic cage for picric acid detection. *Chem. Commun.* **2014,** *50*, 15788- 15791.

72. Shangguan, J.; Huang, J.; He, D.; He, X.; Wang, K.; Ye, R.; Yang, X.; Qing, T.; Tang, J. Highly Fe^{3+}-selective fluorescent nanoprobe based on ultrabright N/P codoped carbon dots and Its application in biological samples. *Anal. Chem.* **2017,** *89*, 7477−7484.

73. Buragohain, A.; Yousufuddin, M.; Sarma, M.; Biswas, S. 3D Luminescent Amide-Functionalized Cadmium Tetrazolate Framework for Selective Detection of 2,4,6-Trinitrophenol. *Cryst. Growth Des.* **2016,** *16*, 842−851.

74. Toal, S. J.; Trogler, W. C. Polymer sensors for nitroaromatic explosives detection. *J. Mater. Chem.* **2006,** *16*, 2871-2883

75. Huang, H.; Li, H.; Feng, J.-J.; Feng, H.; Wang, A.-J.; Qian, Z. One-pot green synthesis of highly fluorescent glutathione-stabilized copper nanoclusters for Fe^{3+} sensing. *Sens. Actuator B-Chem* **2017,** *241*, 292–297.

76. Porel, M.; Chuang, C.-H.; Burda, C.; Ramamurthy, V. Ultrafast Photoinduced Electron Transfer between an Incarcerated Donor and a Free Acceptor in Aqueous Solution. *J. Am. Chem. Soc.* **2012,** *134*, 14718−14721.

77. Zhang, Z.; Li, F.; He, C.; Ma, H.; Feng, Y.; Zhang, Y.; Zhang, M. Novel Fe^{3+} fluorescence probe based on the charge-transfer (CT) molecules. *Sens. Actuator B-Chem* **2018,** *255*, 1878–1883.

78. Hussain, S.; Malik, A. H.; Afroza, M. A.; Iyer, P. K. Ultrasensitive detection of nitroexplosive – picric acid via a conjugated polyelectrolyte in aqueous media and solid support. *Chem. Commun.* **2015,** *51*, 7207- 7210.

CHAPTER 3

A pyrazine core-based luminescent Zr(IV)-organic framework for specific sensing of picric acid and $Cr_2O_7^{2-}$

*This chapter represents synthesis and characterization of a new MOF containing Zr(IV) ion and 2,3,5,6-tetrakis(4-carboxyphenyl)pyrazine (H_4**L**) linker by solvothermal method. The results of Pawley refinement confirmed that the as-synthesized compound (**2**) is isostructural with the Zr-CAU-24 MOF, which has been reported previously. The activated compound (**2'**) has a very high BET surface area (1419 m^2/g) and CO_2 adsorption capacity (4.4 mmol/g at 1.4 bar and 0 °C). Being highly water-stable, luminescent **2'** can selectively recognize dichromate ($Cr_2O_7^{2-}$) in water and picric acid (PA) in dimethyl sulfoxide (DMSO), by fluorescence quenching mechanism. The detection limits were found to be 13.08 and 8.58 ppb for PA and $Cr_2O_7^{2-}$, respectively. Moreover, the mechanisms behind this selective detection of analytes were also investigated.*

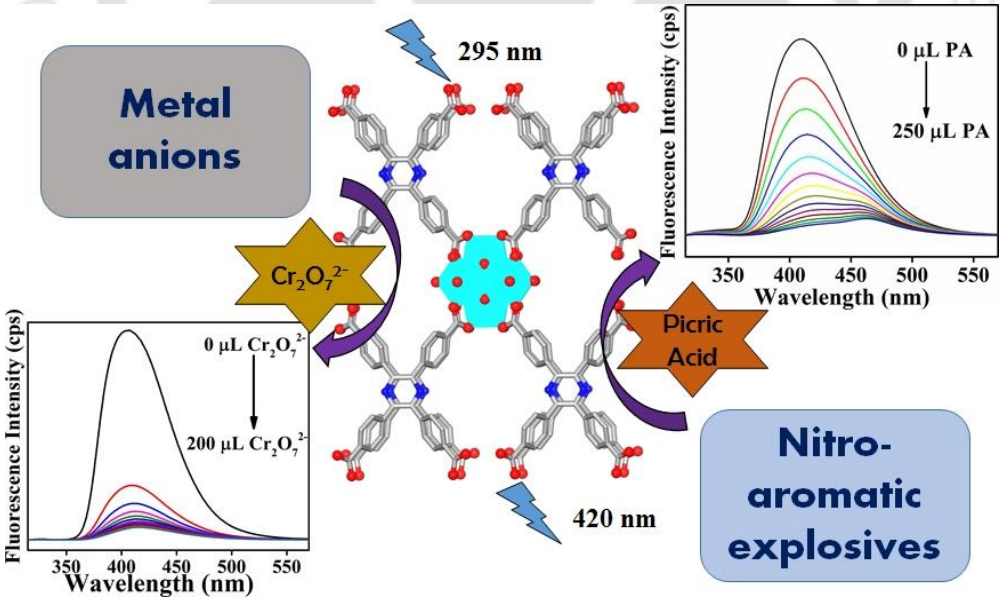

CrystEngComm

C. Gogoi, H. Reinsch and S. Biswas, *CrystEngComm*, 2019, **21**, 6252-6260.

3.1 Introduction

Metal-organic frameworks (MOFs) are a class of inorganic and organic hybrid materials formed by metal ions and organic linkers.[1] The intriguing properties of MOFs are determined by the overall physical properties of the inorganic and organic parts. MOF materials have modular structures by virtue of variation of metal ions and organic linkers. These highly crystalline materials have extraordinarily high porosity as well as vast internal surface area. MOFs are known for their huge applications as functional materials, which include catalysis,[2] gas storage/separation,[3-4] photovoltaic conversion,[5] sensing,[6-9] molecular magnetism,[10-11] conductivity,[12] polymerization[13] and so on. The fluorescence-based sensing of MOFs has emerged as a new generation of sensors for having benefits like high selectivity, quick response, non-destructive nature and simple operational methods.

For security of the native country and safety of the environment, the recognition of nitroaromatic explosives (NAEs) is of paramount importance.[14-15] The NAEs are highly used for the preparation of landmines, military operations and criminal activities. These NAEs can spoil the environment by contamination of water resources as well as soil at toxic levels, which can lead to hazardous effects on living organisms.[16-17] Among the NAEs, picric acid (PA) is a dangerous explosive with high detonation properties and a low safety coefficient. PA is used in rocket fuels, dyes, matches, firework, pesticides, pharmaceutical and leather industries. The by-products during production of these materials cause catastrophic environmental pollution as they contaminate the soil and water, affecting the living system adversely.[18] In the last few years, luminescent MOFs have arisen as favourable materials for PA detection.[19-25] Although there have been significant progress in the field of PA sensing by MOF materials, there is still scope for improvement of selectivity, sensitivity as well as recyclability.

$Cr_2O_7^{2-}$ ion is a well-known carcinogen which is widely used in metallurgy, leather tanning, printing, electroplating industries and so on.[26-27] This highly toxic ion is very harmful to living organisms and also for the environment. It can cause several diseases in human beings such as cancer, deformity and gene mutation.[28] Environmental Protection Agency (EPA)[29] declared that concentration of total chromium in water should be below 100 ppb. Therefore, the detection of $Cr_2O_7^{2-}$ ion in aqueous medium at low ppb level is very essential for the environment.

In the present work, a highly conjugated, π-electron rich 2,3,5,6-tetrakis(4-carboxyphenyl)pyrazine (H_4**L**) linker has been utilized for the synthesis of a Zr(IV) MOF. The

synthesis of the MOF (**2**) was performed by solvothermal technique and it was characterized thoroughly by analytical and spectroscopic methods. In this chapter, the gas adsorption, physicochemical stability and luminescence sensing features of the activated MOF (**2'**) for PA and $Cr_2O_7^{2-}$ will be discussed.

3.2 Experimental section

3.2.1 Materials and physical methods

The 2,3,5,6-tetrakis(4-carboxyphenyl)pyrazine) (H_4**L**) linker was synthesized by using previously reported procedure.[30] All other chemicals were purchased from chemical suppliers and used without any further purification. The Bruker D2 Phaser X-ray diffractometer was employed for X-ray powder diffraction (XRPD) measurements at 30 kV, 10 mA using Cu-Kα (λ = 1.5406 Å) radiation. The Fourier transform infrared (FT-IR) spectra were taken on a Perkin Elmer Spectrum Two FT-IR spectrometer with samples prepared on KBr pellets in the range of 4000-500 cm^{-1}. The characteristic peaks were mentioned using notation like very strong (vs), strong (s), medium (m), shoulder (sh), broad (br) and weak (w). Thermogravimetric analyses (TGA) of **2** and **2'** were carried out by using a SDT Q600 V20.9 Build 20 thermogravimetric analyzer from the temperature range 25 to 700 °C at a heating rate of 10 °C min^{-1} under argon atmosphere. The Brunauer-Emmett-Teller (BET) measurement of **2'** were recorded on a Quantachrome Autosorb iQ-MP volumetric gas adsorption equipment at -196 °C. The CO_2 gas adsorption experiment were carried out using Quantachrome iSorb-HP1 gas sorption analyzer at 0 °C and also at 25 °C. Prior to N_2 and CO_2 adsorption experiments, **2'** was degassed under dynamic vacuum condition for 6 h at 120 °C. The Zeiss (Gemini) SEM equipment and the Hitachi S3400N SEM-EDX instrument were used for the field emission-scanning electron microscopy (FE-SEM) images and the energy dispersive X-ray (EDX) experiment respectively. The fluorescence lifetime measurement was performed using Edinburgh Instrument Life-Spec II spectrometer. During lifetime measurement, the samples were excited at 295 nm and maintaining the emission wavelength at 410 nm. Caution! *NAEs like PA, 4-NP are highly explosive so should be handled very carefully and also used in small amounts.*

3.2.2 Synthesis of $[Zr_6(\mu_3\text{-}O)_4(\mu_3\text{-}OH)_4(OH)_4(H_2O)_4(L)_2]\cdot 3H_2O\cdot 2DMF$ (2)

The microcrystalline powder of **2** was obtained by reacting a mixture of $ZrOCl_2\cdot 8H_2O$ (15 mg, 0.05 mmol), H_4**L** linker (20 mg, 0.04 mmol) and benzoic acid (872 mg) (in 1.25 : 1 : 200 molar ratio) in DMF (3 mL) at 150 °C for 24 h. The reaction was carried out in a Pyrex

tube, which was heated in an oil bath. Before heating, the mixture was thoroughly mixed by sonication for 10 min. After 24 h of solvothermal reaction, the white coloured precipitate was collected by filtration and then washed several times with acetone. It was then dried at 80 °C. The yield of the compound (**2**) was found to be 13 mg (0.01 mmol, 88 %) on the basis of metal salt. Anal. Calcd. for **2** in % : C, 39.42; H, 3.21; N, 3.94. Found: C, 39.04; H, 3.01; N; 3.91. Anal. Calcd. for **2'** in % : C, 39.78; H, 2.50; N, 2.90. Found: C, 39.55; H, 2.29; N, 2.87. FT-IR (KBr, cm^{-1}): 3445 (br), 1653 (sh), 1615(m), 1547 (m), 1410 (vs), 1259(w), 1181 (w), 1111(w), 1015 (w), 871(w), 780 (w), 718 (w), 601 (m).

3.2.3 Activation of compound 2

Compound **2'** was obtained in three stages. Firstly, compound **2** was stirred for 48 h in methanol, which is a low boiling solvent. Secondly, the compound received after filtration was heated in an oven at 90 °C for 12 h. Lastly, the dried compound was kept under high vacuum for 24 h at 120 °C. This desolvated MOF sample (**2'**) was used for further analysis.

3.2.4 Pawley refinement

The XRPD patterns were measured in transmission geometry using a STOE Stadi MP with $CuK\alpha_1$ radiation and equipped with a Mythen detector. Due to the low number of reflections, the pattern could not be reliably indexed, but the data exhibits very strong similarities with the theoretical pattern of the recently reported MOF Zr-CAU-24 which incorporates the linker 1,2,4,5-tetrakis(4-carboxyphenyl)benzene (TCPB) and has the composition $[Zr_6(\mu_3\text{-}O)_4(\mu_3\text{-}OH)_4(OH)_4(H_2O)_4(TCPB)_2]$.[31] Using the cell parameters of Zr-CAU-24 as starting values, the cell parameters for the new compound could be refined by structure-less Pawley refinement using TOPAS academics (Figure 3.1).[32]

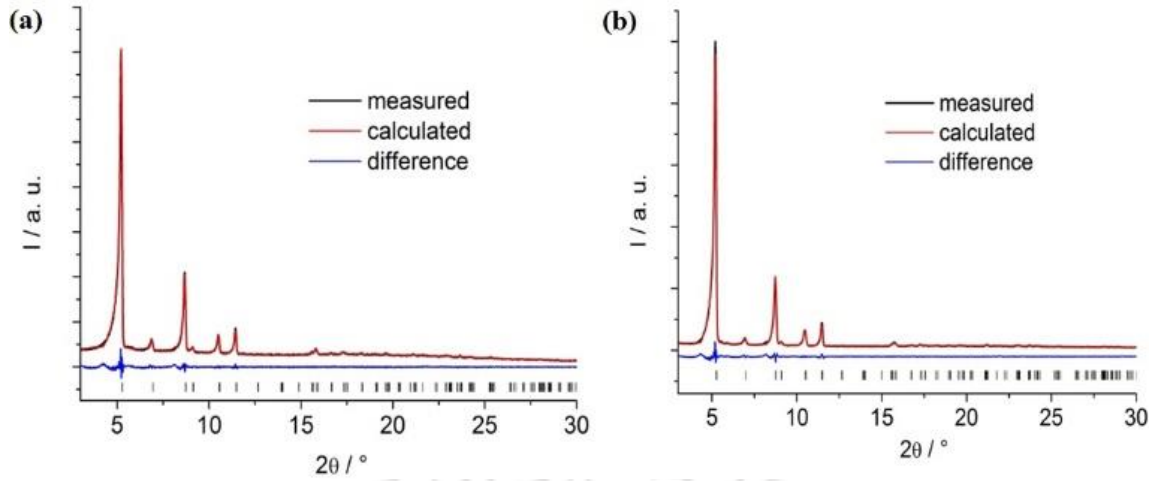

Figure 3.1 Fits for the structure-less Pawley refinement of as-synthesized **2** (left) and activated **2'** (right).

The cell parameters changed only slightly upon activation and the XRPD patterns look virtually identical. A structural model was designed starting from the crystal structure of Zr-CAU-24. The refined unit cell parameters of the activated MOF were imposed and the linker was manipulated into the used molecule based on a pyrazine core. Afterwards the structure was fully optimized by force-field calculations using the universal force-field[33] as implemented in the Forcite routine in the software suite of Materials Studio.[34] An attempted full Rietveld refinement of this model was not possible which we attribute for once to the low number of reflections but also to the presence of residual guest molecules inside the pores of the framework. Such residual electron density was observed during the attempted refinement inside the framework and is also found in the structure of Zr-CAU-24, especially inside the smaller cages. Nevertheless, the simulated XRPD data correlates suitably with the experimental data, albeit the peak intensities deviate for the reasons stated above. The refinement parameters for the structures of **2** and **2'** are provided in Table 3.1.

Table 3.1 Structural refinement parameters for compound **2** and **2'** obtained from Pawley fits.

Sample	Compound **1**	Compound **1'**
Crystal system	orthorhombic	orthorhombic
Space group	*Cmmm*	*Cmmm*
a / Å	19.375(12)	19.492(12)
b / Å	33.376(21)	33.489(20)

c / Å	12.712(12)	12.608(7)
$\alpha = \beta = \gamma$ / °	90	90
V/ Å^3	8220(10)	8230(8)
R_{wp} / %	3.5	4.9
GoF	3.0	2.0

3.2.5 Sensing experiments for NAEs and anions

The suspension of **2'** in water and DMSO were prepared separately in glass vials by dispersing 3 mg of **2'** in 3 mL of solvent. The mixtures were sonicated for 1 h and kept without any disturbance for overnight to get a stable suspension. The luminescence spectra were acquired at an excitation wavelength (λ_{ex}) of 295 nm. The NAEs used for the sensing experiments were 2,6-dinitrotoluene (2,6-DNT), PA, 4-nitrophenol (4-NP), 2,4-dinitrophenol (2,4-DNP), nitrobenzene (NB), 1,3-dinitrobenzene (1,3-DNB), 4-nitrotoluene (4-NT) and 2,4-dinitrotoluene (2,4-DNT). Three millimolar solutions of these NAEs were prepared in DMSO. For sensing of anions, we selected thirteen anions such as $Na_2Cr_2O_7{\cdot}2H_2O$, $KMnO_4$, CH_3COONa, Na_2CO_3, $Na_3PO_4{\cdot}12H_2O$, NaBr, NaCl, NaCN, $NaHCO_3$, $NaNO_2$, NaSCN, Na_2SO_4 and $NaClO_4{\cdot}H_2O$. Three millimolar solutions of these anions were prepared in water. For the sensing of metal anions, 2800 µL of water and 200 µL of aqueous suspension of **2'** were poured in a quartz cuvette and solutions of different cations or anions were added incrementally. Similarly, for sensing of NAEs, same amounts of pure DMSO and suspension of **2'** in DMSO were placed in a quartz cuvette. Thereafter, solutions of selected NAEs were added gradually. The fluorescence quenching efficiency was measured by using formula: $(1-I/I_o) \times 100$ %, in which I_o and I are the fluorescence intensities preceding and following the addition of analyte, respectively.

3.3 Results and discussion

3.3.1 Synthesis and characterization of the MOF

The present compound was obtained in highly crystalline and phase-pure form by using $ZrOCl_2{\cdot}8H_2O$ as a metal source, DMF as a solvent and benzoic acid as a modulator at temperature of 150 °C for 24 h. After completion of reaction, white coloured precipitate (**2**) was collected by filtration. The morphology of the compound was revealed from FE-SEM

analysis as needle type microcrystals (Figure 3.2). The high crystallinity and phase-purity of the compound were confirmed by acquiring its XRPD pattern (Figure 3.3), which looked very similar as the theoretical XRPD data. The XRPD pattern of **2'** indicated that the compound retained its structure after activation.

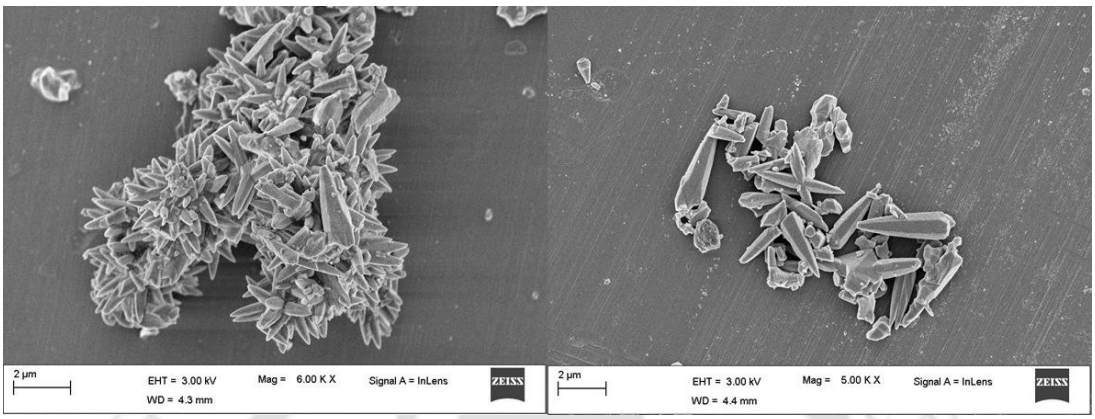

Figure 3.2 FE-SEM images of **2**.

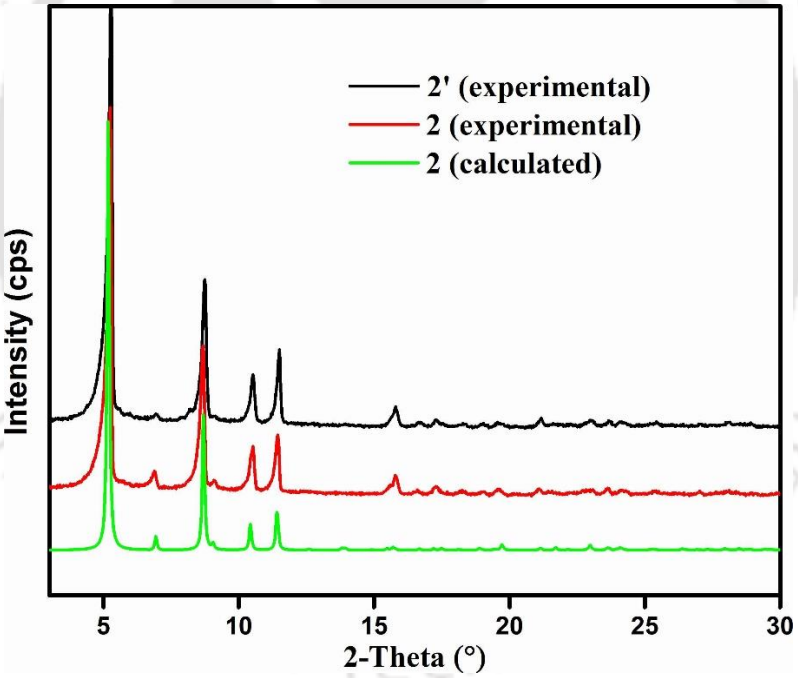

Figure 3.3 Calculated and experimental XRPD patterns of **2** and **2'**.

The FT-IR spectra of **2**, **2'** and H_4**L** linker were examined (Figure 3.4) to check the incorporation of linker into the framework. The strong absorption bands at around 1615 and 1410 cm^{-1} for both **2** and **2'** represent the asymmetric and symmetric $–CO_2$ stretching vibrations of the coordinated H_4**L** linker, respectively. The absence of absorption band at around 1705 cm^{-1} for **2** as compared to H_4**L** linker is indicative of complete deprotonation of the H_4**L** linker during formation of **2**. The carbonyl stretching vibration of DMF molecules present inside the

framework of **2** display band at around 1653 cm^{-1}, which is absent in case of **2'**. This observation implies that **2'** is free from DMF molecules after activation.

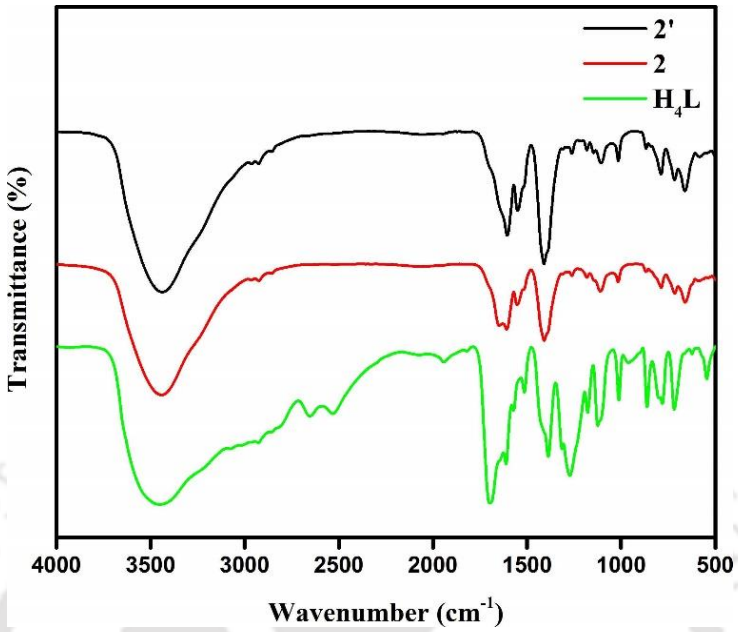

Figure 3.4 FT-IR spectra of H_4**L** linker (green), compound **2** (red) and **2'** (black).

3.3.2 Structure description of 2

We indexed the XRPD pattern of **2** in an orthorhombic crystal system with space group *Cmmm* with *a* = 19.375(12) Å, *b* = 33.376(21) Å, *c* = 12.712(12) Å. The results of Pawley refinement (Figure 3.1) confirmed that the simulated and experimental XRPD data are in good agreement with each other for **2**. The refinement data also point out that **2** is isostructural with the Zr-CAU-24 MOF, which has been reported previously.[31] The main difference between the structure of **2** and Zr-CAU-24 is that the former contains pyrazine-core based tetracarboxylate linker ($\mathbf{L}^{4-}$, Figure 3.5a) whereas the latter consists of benzene-core based $TCPB^{4-}$ linker. Similar to Zr-CAU-24, the crystal structure of **2** contains $[Zr_6(\mu_3\text{-}O)_4(\mu_3\text{-}OH)_4]^{12+}$ clusters. Each Zr_6 cluster is connected with eight carboxylate functionalities from $\mathbf{L}^{4-}$ linkers. In addition to carboxylate groups, the Zr_6 cluster is bonded with OH^- anions and H_2O molecules, which completes the coordination number (8) of each Zr(IV) ion. The asymmetric unit of **2** contains two crystallographically independent Zr atoms, a quarter of $\mathbf{L}^{4-}$ linker and two μ_3-O atoms (Figure 3.5b). The Zr_6 clusters are connected with each other *via* the $\mathbf{L}^{4-}$ linkers forming a 3D polymeric framework (Figure 3.5c and 3.5d), which has C-centered orthorhombic symmetry and **scu** topology. The framework contains rhombic channels having dimensions of 4.7 × 11.2 Å.

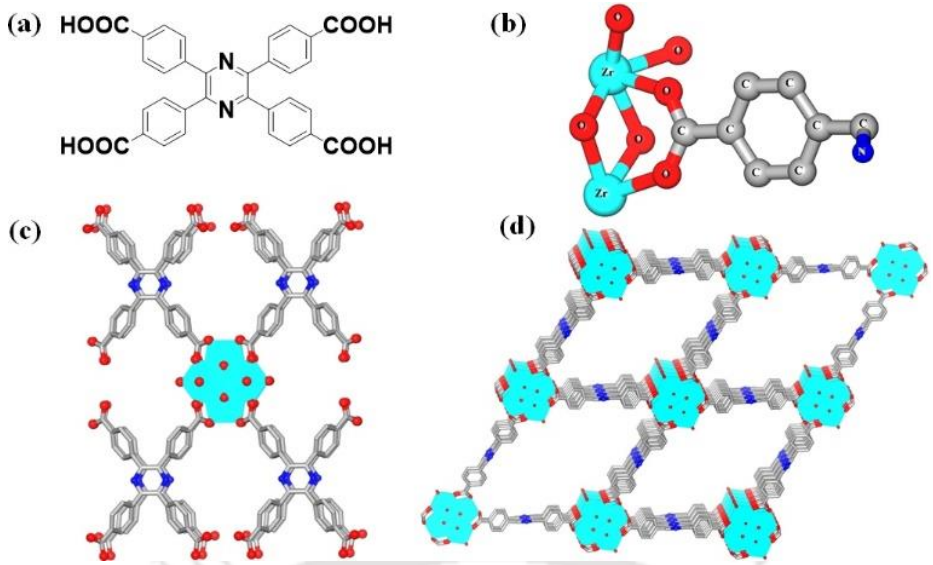

Figure 3.5 (a) Structure of H_4**L** linker, (b) asymmetric unit of **2**, (c) node connectivity in the structural network of **2**, and (d) overall 3D framework of **2** with **scu** topology.

3.3.3 Thermal and chemical stability

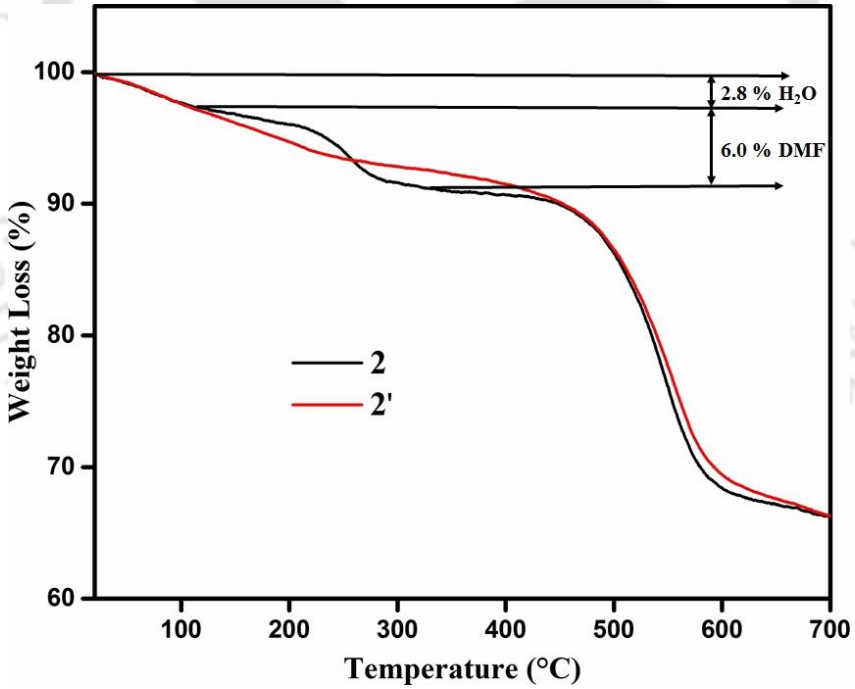

Figure 3.6 TG curves of **2** and **2'** recorded in an argon atmosphere in the temperature range of 25-700 °C with a heating rate of 10 °C/min.

According to the TGA curves, **2** and **2'** are thermally stable up to 440 °C (Figure 3.6) in Ar atmosphere. In the TGA curve of **2**, the first weight loss of 2.8% observed between 25 and 125 °C is because of removal of two molecules of water per formula unit (calcd. 2.5%). From 125 to 340 °C, the weight loss of 6.0% is due to the removal of two DMF guest molecules

per formula unit (calcd. 6.8%). After that no weight loss was observed till 440 °C and **2** started to decompose from this temperature. In case of **2'**, the first weight loss of 3.4% is because of the loss of water molecules which was physically adsorbed during storage in air atmosphere after activation.

The chemical stability of **2'** was tested by stirring it in few liquids like acetone, methanol, ethanol, water, 1 M HCl, 1 M NaOH and acetic acid for 12 h. Later, the compound was recovered through filtration and dried at 90 °C in an air oven. The XRPD data revealed that the framework of **2'** did not decompose after stirring in all these liquids, except 1M NaOH solution (Figure 3.7). Thus, the framework of **2'** is stable in water, selected organic solvents and acidic conditions.

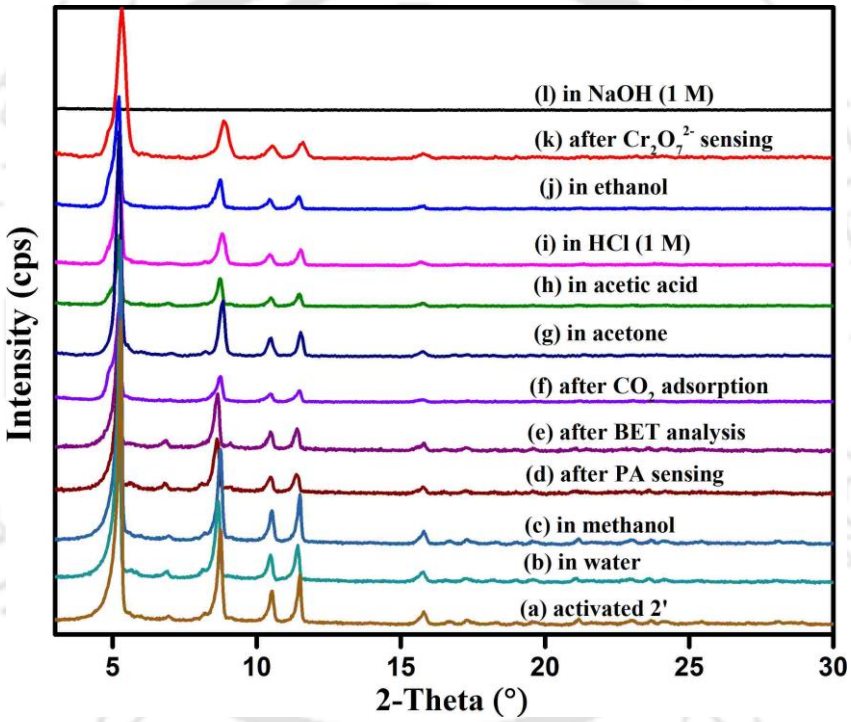

Figure 3.7 XRPD patterns of **2'** in different forms: (a) activated; (b) after treatment with water; (c) after treatment with methanol; (d) after 5 cycles of fluorescence titration experiments with PA; (e) after BET analysis; (f) after CO_2 adsorption; (g) after treatment with acetone; (h) after treatment with acetic acid; (i) after treatment with 1(M) HCl; (j) after treatment with ethanol; (k) after 5 cycles of fluorescence titration experiments with $Cr_2O_7^{2-}$ ions: (l) after treatment with 1(M) NaOH.

3.3.4 Gas adsorption properties

The permanent microporosity of **2'** was examined by N_2 sorption study (at -196 °C) which disclosed type-I adsorption isotherm (Figure 3.8). From the N_2 adsorption isotherm, the BET surface area was found to be 1419 m^2/g. This value indicates that **2'** is highly porous toward N_2. However, this value is somewhat less than the formerly reported and isostructural Zr-CAU-24 MOF with TCPB linker.[31] The CO_2 adsorption isotherm was acquired at 0 and 25 °C up to 1.4 bar. The CO_2 adsorption capacity of **2'** at 1.4 bar was found to be 4.4 mmol/g and 2.5 mmol/g at 0 and 25 °C, respectively (Figure 3.9). [30, 35]

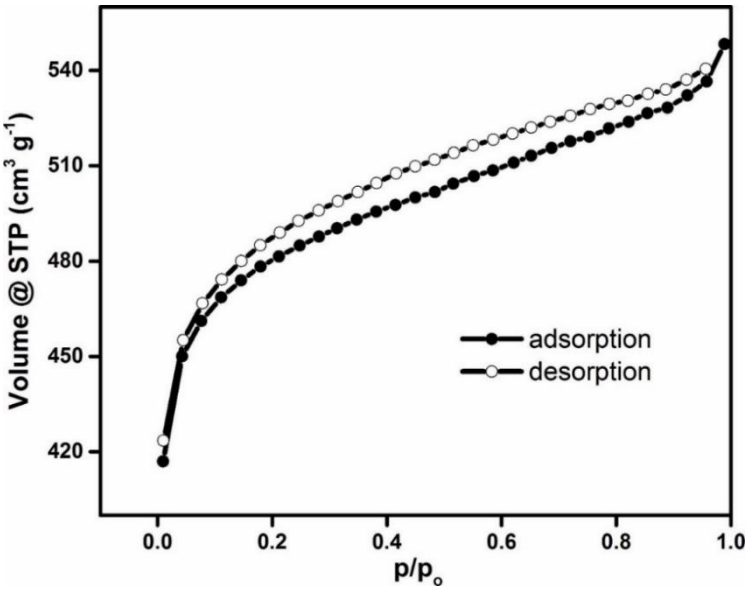

Figure 3.8 N_2 sorption isotherms of **2'** at -196 °C.

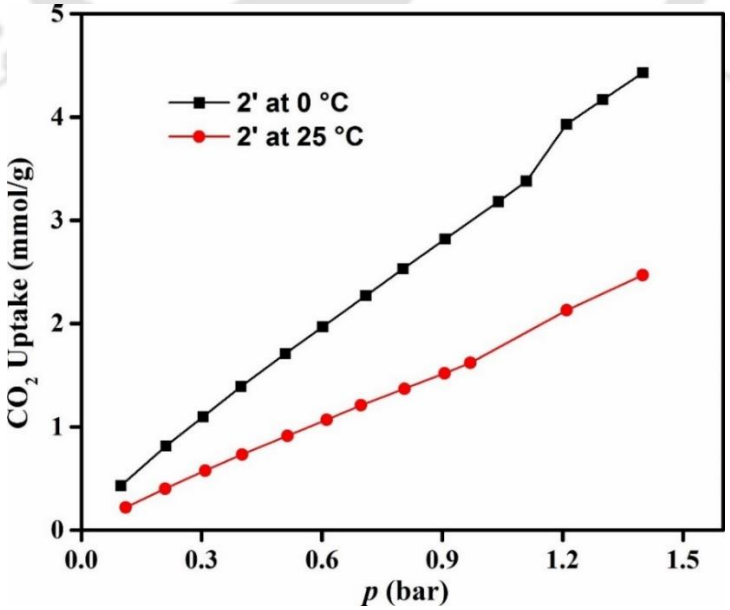

Figure 3.9 CO_2 sorption isotherms of **2'** at 0 °C and 25 °C.

3.3.5 Luminescence behavior

The luminescence behavior of H_4**L** linker and **2'** were examined at room temperature in the solid state. The free H_4**L** linker showed week fluorescence emission at 410 nm when excited at 295 nm. In comparison, the H_4**L** linker coordinated to Zr(IV) ion in the framework of **2'** exhibited emission maximum at 420 nm when excited at the same wavelength (Figure 3.10). The emission maximum of the free H_4**L** linker may be attributed to intralinker $\pi \rightarrow \pi^*$ and $n \rightarrow \pi^*$ transitions.[7] Compound **2'** showed strong emission and slight red shift (10 nm) of the emission maximum as compared to free H_4**L** linker. These changes in emission properties are mainly caused by restriction of the free intramolecular rotation of H_4**L** linker because of coordination of the linker with Zr(IV) ion which in turn perturbs the electronic energy levels. The luminescence properties of **2'** in water and few organic solvents were also investigated. All the selected organic solvents showed similar type of emission spectra (Figure 3.11). For our fluorescence sensing experiments, we chose water for detection of metal anions, and DMSO for the detection of NAEs. The main reason behind the selection of DMSO as a solvent for NAEs sensing is that the required selectivity is not obtained in other solvents. The sensing studies of NAEs were executed in DMSO instead of water due to the poor selectivity exhibited by **2'** for a particular NAE in water.

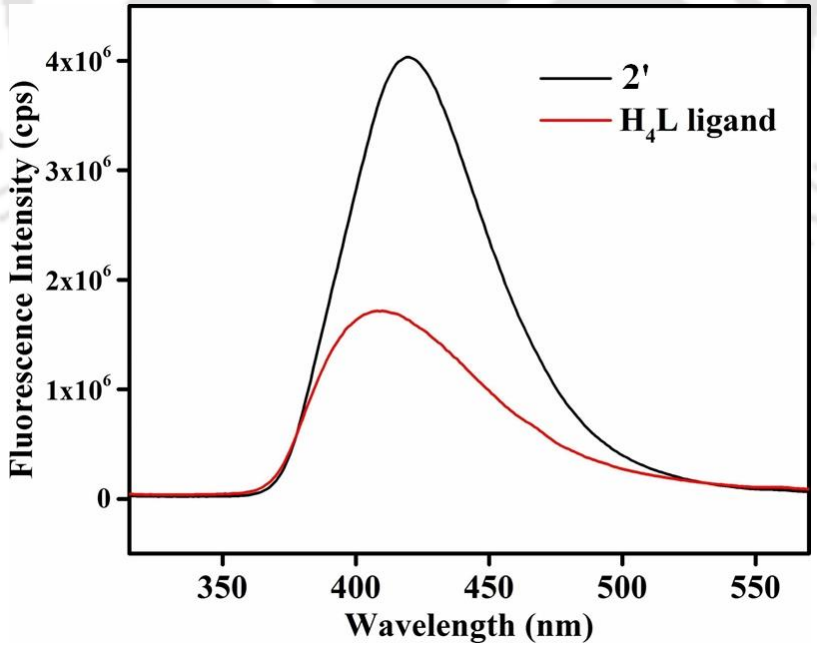

Figure 3.10 The solid-state photoluminescence spectra of H_4**L** linker and **2'** (excited at 295 nm).

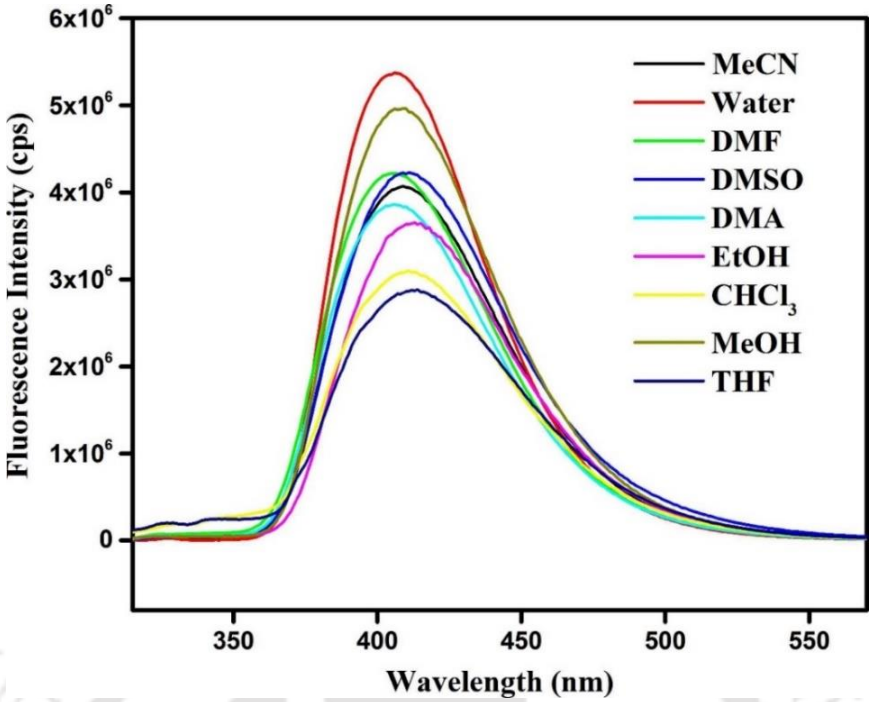

Figure 3.11 Fluorescence emission spectra of **2'** in water and common organic solvents (λ_{ex} = 295 nm).

3.3.6 Detection of NAEs and anions

For the recognition of NAEs, eight NAEs namely PA, 4-NP, 2,4-DNT, 2,6-DNT, 2,4-DNP, 1,3-DNB, 4-NT and NB were selected. Thirteen anions such as $Cr_2O_7^{2-}$, MnO_4^-, AcO^-, CO_3^{2-}, PO_4^{3-}, Br^-, Cl^-, CN^-, HCO_3^-, NO_2^-, SCN^-, SO_4^{2-} and ClO_4^- were chosen for the sensing of anions. The fluorescence spectra were acquired after incremental addition of solutions of NAEs (3 mM in DMSO) and anions (3 mM in water) to the suspension of **2'**. Among all tested NAEs and metal anions, 92% and 94% fluorescence quenching were observed after addition of 250 µL of PA and 200 µL of $Cr_2O_7^{2-}$ solution, respectively (Figure 3.12 and Figure 3.13).

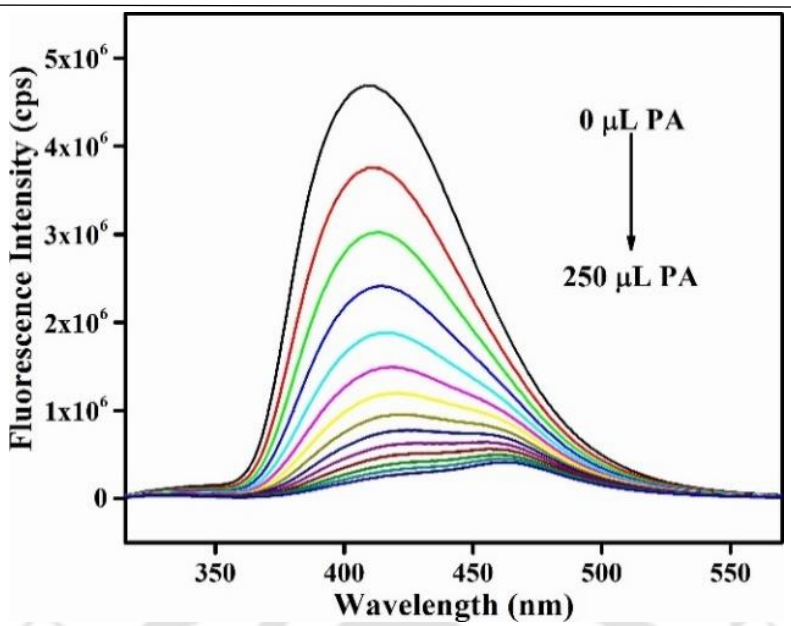

Figure 3.12 Fluorescence reduction for **2'** dispersed in DMSO (1 mg/mL) upon gradual addition of 3 mM PA solution prepared in DMSO.

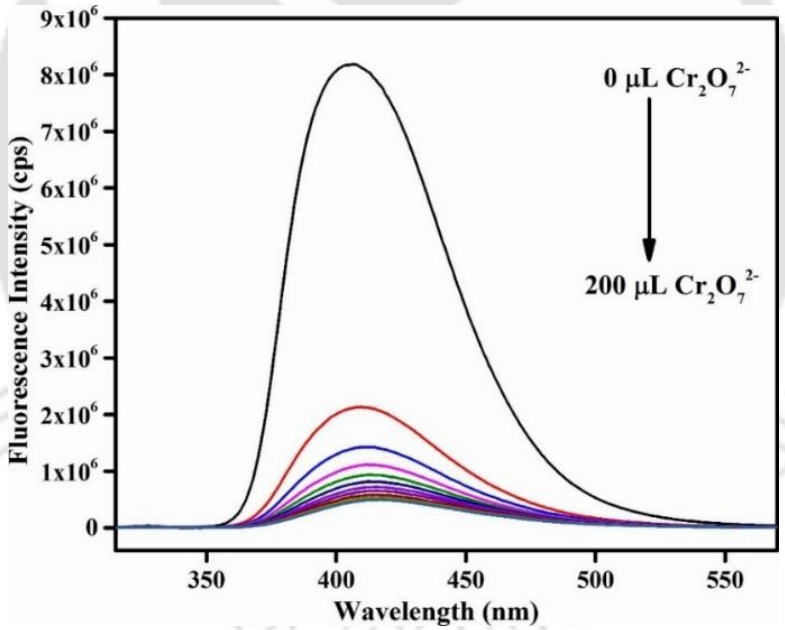

Figure 3.13 Fluorescence reduction for **2'** dispersed in water (1 mg/mL) upon gradual addition of 3 mM $Cr_2O_7^{2-}$ solution prepared in water.

Moreover, the quenching effect of PA in aqueous medium was also studied. As shown in Figure 3.14, a quenching efficiency of 92% was observed for PA in aqueous medium. We chose DMSO for the detection experiment, since the above-mentioned selectivity toward PA was not achieved in aqueous medium.

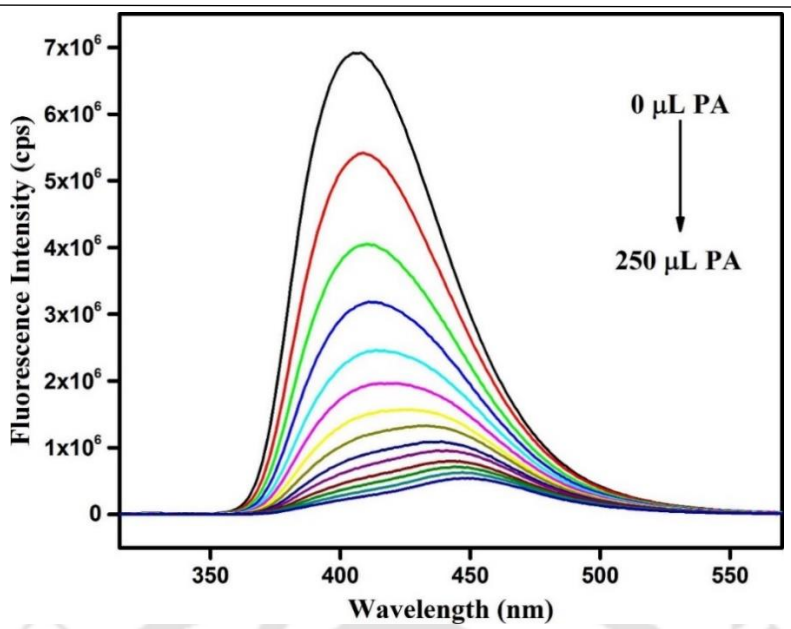

Figure 3.14 Luminescence quenching of **2'** dispersed in water after gradual addition of 3 mM solution of PA in water (250 µL).

All NAEs could quench the fluorescence intensity of **2'** but their quenching efficiencies were different when the identical amount of the solution of NAEs was added (Figure 3.15). By adding the same amount of the solution of different NAEs (in DMSO) was added to the suspension of **2'**, the maximum quenching of fluorescence intensity was observed in case of PA (92%). Thus, the high specificity of **2'** for PA was corroborated. It can be inferred from Figure 3.16 that the great selectivity of the MOF probe for PA was nearly unaffected by the presence of other interfering NAEs.

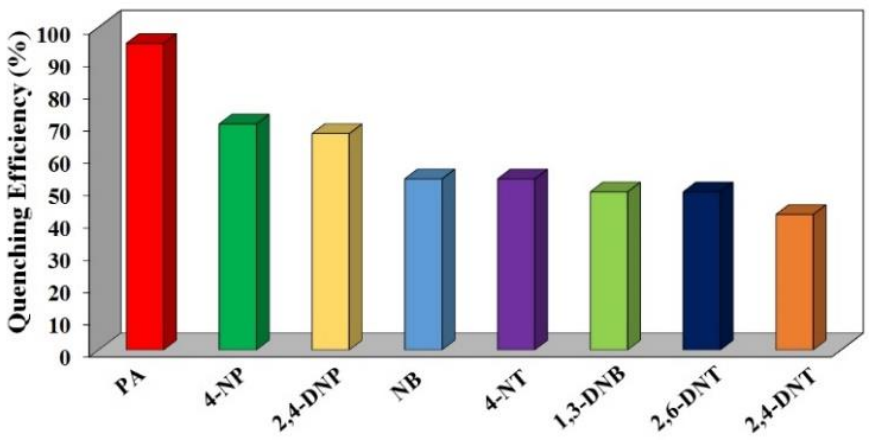

Figure 3.15 Quenching efficiency of **2'** after addition of 3 mM solutions (250 µL) different NAEs in DMSO.

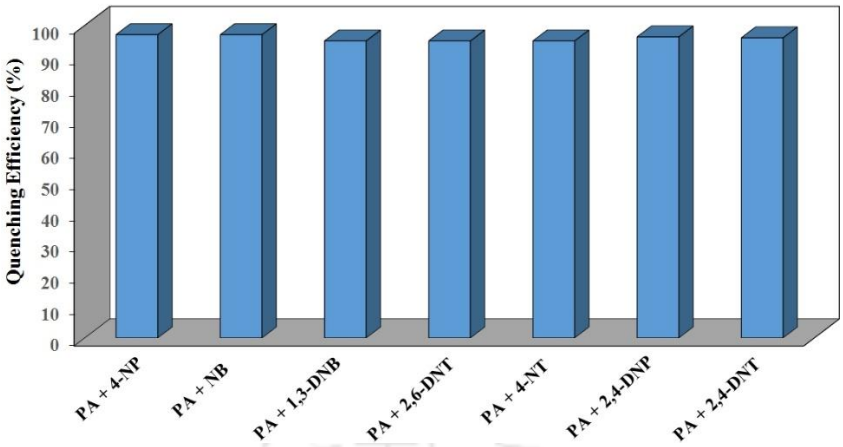

Figure 3.16 Quenching efficiencies of **2'** after addition of equal amounts of different NAEs and PA in DMSO.

The response towards PA was very rapid (30 s), as shown in Figure 3.17. The concentration dependent quenching experiment (Figure 3.18) disclosed that the quenching percentage increased rapidly at lower concentration than that at higher concentration in case of PA. The quenching percentage remained almost invariant for all other intrusive NAEs in the whole concentration range of the experiment.

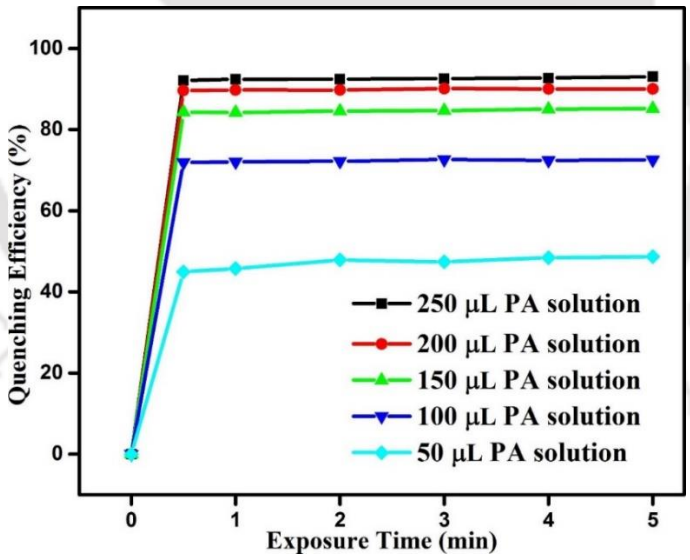

Figure 3.17 Quenching efficiencies of **2'** after addition of 3 mM PA as a function of exposure time in DMSO solvent.

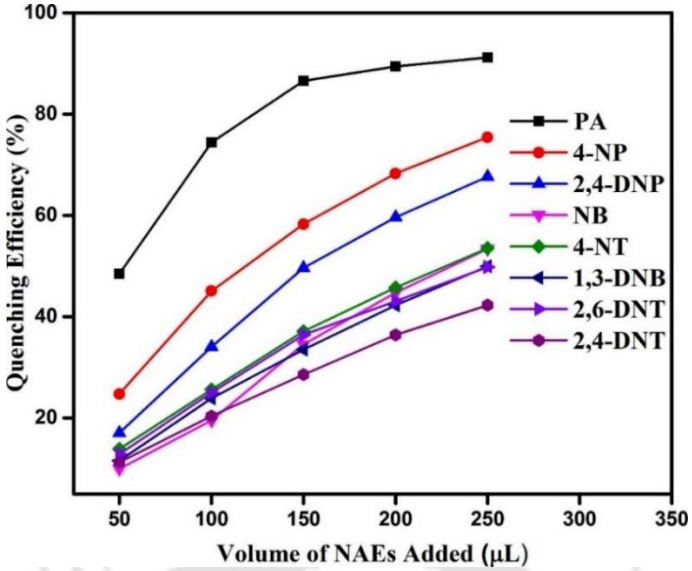

Figure 3.18 Change of quenching efficiency (%) after addition of different volumes of 3 mM.

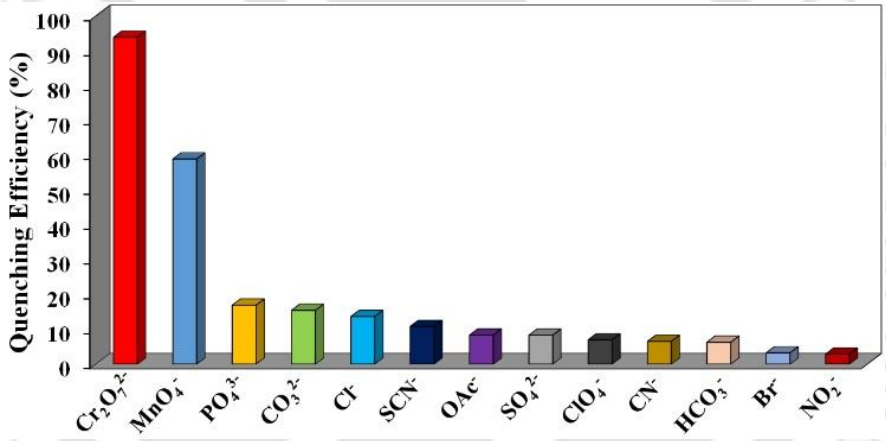

Figure 3.19 Quenching efficiency of **2'** after addition of 3 mM solutions (150 µL) of different anions in aqueous medium.

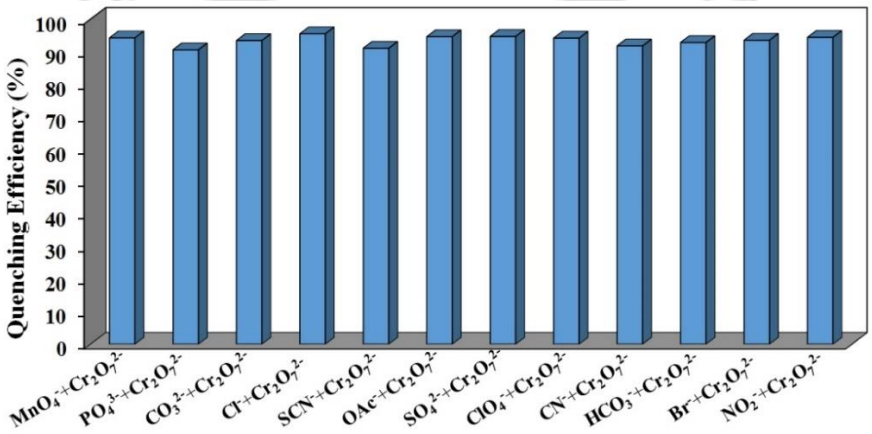

Figure 3.20 Quenching efficiencies of **2'** after addition of equal amounts of other anions and $Cr_2O_7^{2-}$ ion.

The quenching efficiencies of the other competitive metal anions were lower than the quenching efficiency shown by $Cr_2O_7^{2-}$ ion in aqueous medium (Figure 3.19). More than 90% quenching efficiencies were observed for all other metal anions when equal amount of aqueous $Cr_2O_7^{2-}$ solution was added to the suspensions of **2'** where other metal anions were already present (Figure 3.20). We can infer that the presence of other metal anions does not affect the quenching property of $Cr_2O_7^{2-}$ ion. From Figure 3.21, it is observed that **2'** displays very quick response (30 s) towards $Cr_2O_7^{2-}$ ion. The concentration dependent graph (Figure 3.22) shows that the quenching effect is higher at lower concentration of $Cr_2O_7^{2-}$. The quenching effect remains almost the same at higher concentration of $Cr_2O_7^{2-}$.

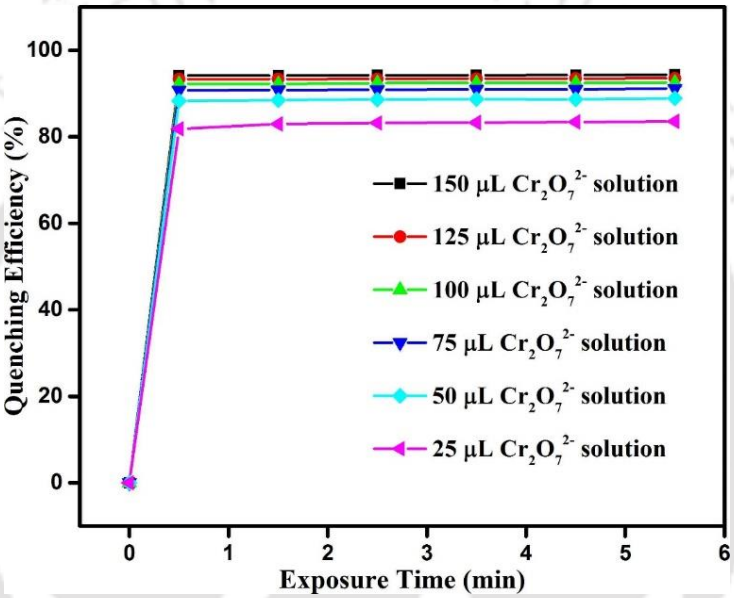

Figure 3.21 Quenching efficiencies of **2'** after addition of 3 mM $Cr_2O_2^{2-}$ as a function of exposure time in water.

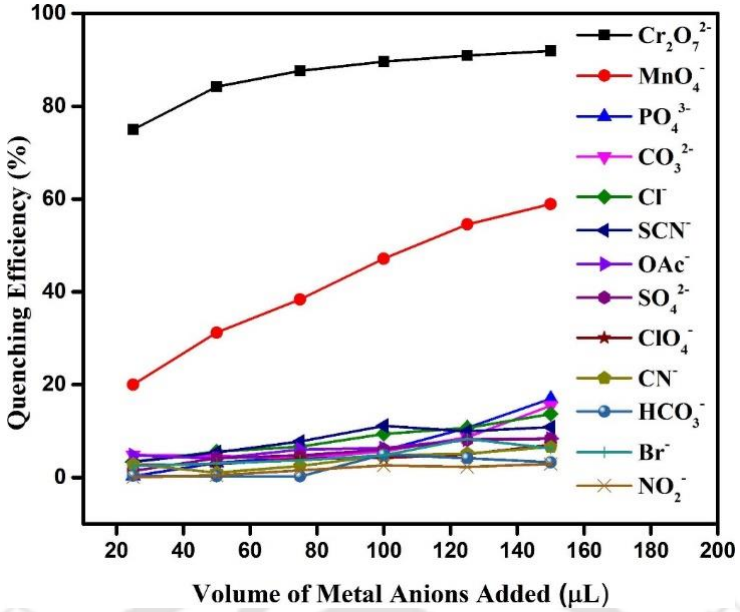

Figure 3.22 Change of quenching efficiency (%) after addition of different volumes of 3 mM different metal anions.

The recyclable property of a fluorescent probe is very important for its practical application in sensing various species. Taking this point into consideration, the recyclability experiments for PA and $Cr_2O_7^{2-}$ were carried out up to 5 cycles. After completion of fluorescence titration experiment, **2'** was filtered, washed with acetone and dried at 90 °C for 12 h. Then, again sensing experiment was carried out with that sample. The initial and final fluorescence intensity of **2'** remained nearly the same for all the three sensing experiments (Figure 3.23 and Figure 3.24). Besides, we acquired the XRPD patterns of **2'** after the 5th cycle of recyclability experiment. The XRPD data show that the framework remained intact even after the 5th cycle (Figure 3.7). These experimental results indicate that **2'** is a highly reusable chemical sensor, which is advantageous for its practical application.

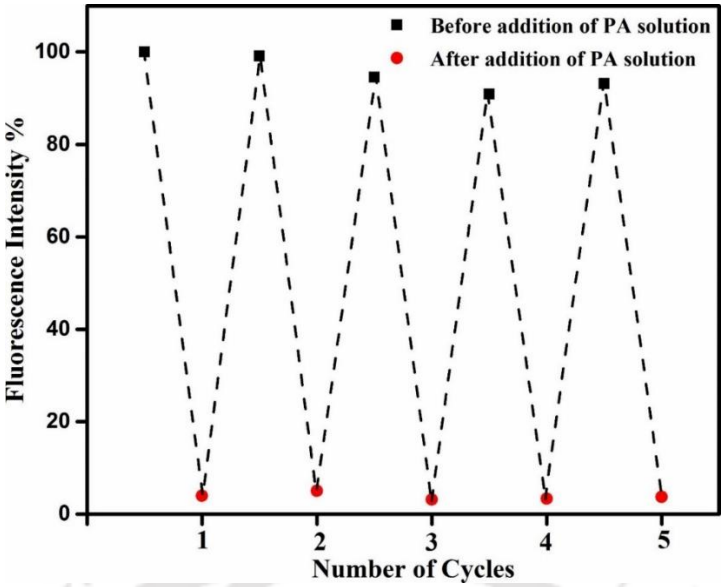

Figure 3.23 Reproducibility test for the aqueous suspension of **2'** towards sensing of PA.

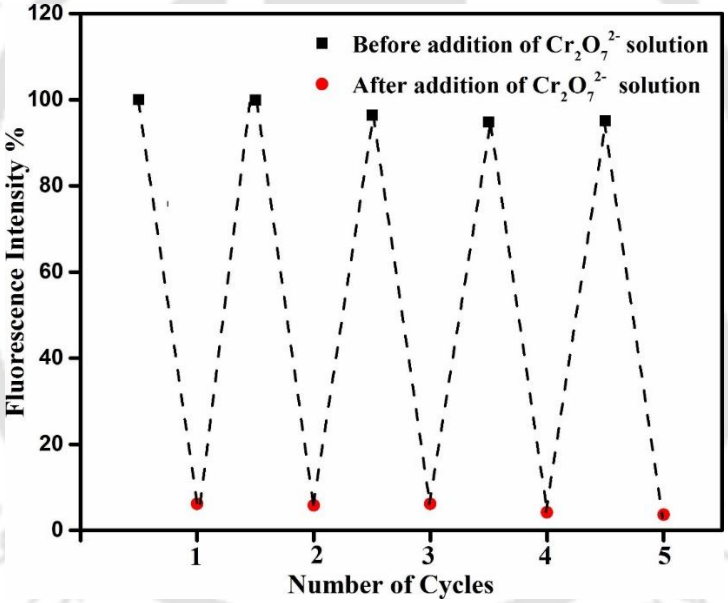

Figure 3.24 Reproducibility test for the aqueous suspension of **2'** towards sensing of $Cr_2O_7^{2-}$ ion.

The quenching effect was further analyzed using Stern-Volmer (S-V) plot. The S-V plot can be drawn on the basis of the equation: $I_0/I = K_{sv}[Q] + 1$, where I_0 is the original fluorescence intensity of **2'** and I is the fluorescence intensity of **2'** in presence of respective analyte.[36] $[Q]$ is the molar concentration of analyte and K_{sv} is the quenching constant. The K_{sv} values for PA, and $Cr_2O_7^{2-}$ were found to be $4.56 \times 10^5\ M^{-1}$ (Figure 3.25) and $1.02 \times 10^6\ M^{-1}$ (Figure 3.26), respectively. The K_{sv} value for PA in water medium was found to be 2.89×10^5

M^{-1} (Figure 3.27). In all three cases, the K_{sv} values are analogous with the other reported MOFs (Tables 3.2-3.3).[8, 18, 20, 22, 24-25, 27, 36-67]

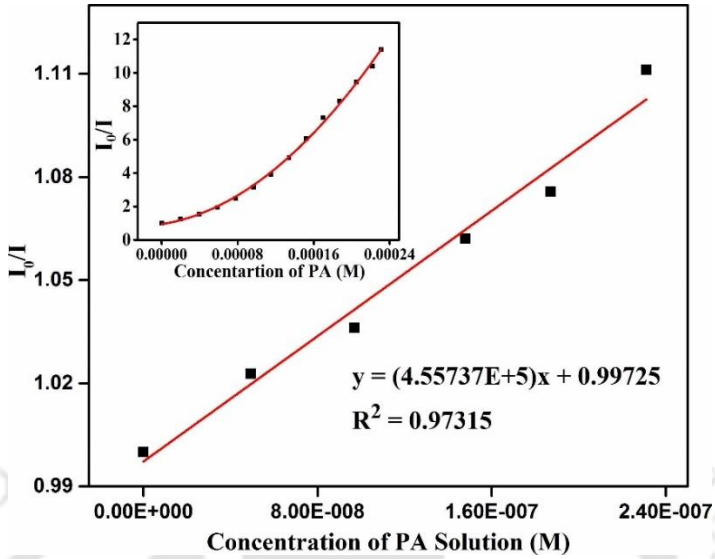

Figure 3.25 S-V plot for the quenching of **2'** at lower concentrations of PA in DMSO. Inset: non linearity of the S-V plot at higher concentrations of PA.

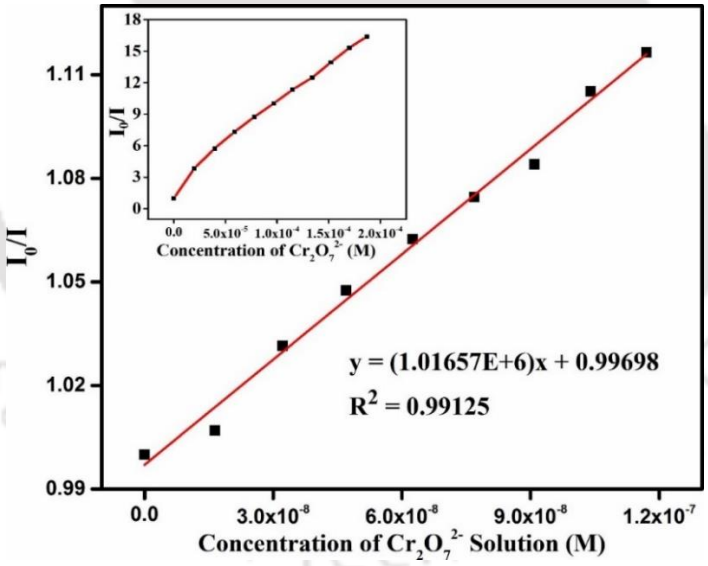

Figure 3.26 S-V plot for the quenching of **2'** at lower concentrations of $Cr_2O_7^{2-}$ ion in water. Inset: non linearity of the S-V plot at higher concentrations of $Cr_2O_7^{2-}$ ion.

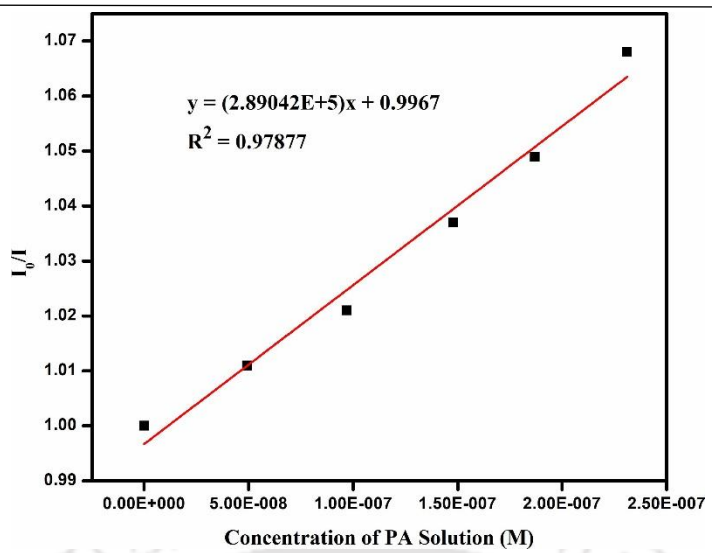

Figure 3.27 S-V plot for the quenching of **2'** at lower concentrations of PA in water.

Table 3.2 A comparison of the Stern-Volmer constant (K_{sv}), detection limit and medium used for PA detection for some MOFs already reported till date.

Sl. No.	MOF	K_{sv} (M^{-1})	Detection Limit	Medium Used	Ref.
1.	$[Zr_6(\mu_3\text{-}O)_4(\mu_3\text{-}OH)_4(OH)_4(H_2O)_4(L)_2]$	4.56×10^5	5.72×10^{-8} M	DMSO	this work
		2.89×10^5	2.00×10^{-8} M	water	this work
2	$[[Cd(ATAIA)]\cdot4H_2O]_n$	1.59×10^7	0.94×10^{-9} M	water	41
3.	EuNDC	3.22×10^4	1.64×10^{-7} M	water	25
4.	AHU-TW1	1.44×10^4	4.05×10^{-6} M	DMF	42
	AHU-TW3	1.48×10^4	3.94×10^{-6} M		
	AHU-TW4	5.0×10^4	1.16×10^{-6} M		
	AHU-TW6	5.31×10^4	1.10×10^{-6} M		
5.	$[Zr_6O_4(OH)_4(BTDB)_6]\cdot8H_2O\cdot6DMF$	2.49×10^4	1.63×10^{-6} M	methanol	68
6.	$[Cd_5Cl_6(L)(HL)_2]\cdot7H_2O$	4.05×10^4	1.87×10^{-7} M	ethanol	19
7.	[Tb(1,3,5-BTC)]	3.41×10^4	8.1×10^{-8} M	ethanol	69

8.	$Zr_6O_4(OH)_4(L)_6$	2.9×10^4	2.6×10^{-6} M	water	43
9.	$[Cd(NDC)_{0.5}(PCA)]_n$	3.5×10^4	-	acetonitrile	21
10.	$[La(TPT)(DMSO)_2] \cdot H_2O$	9.89×10^4	-	ethanol	56
11.	$[[CuL(I)].DMF.H_2O]_n$	1.51×10^5	215 ppb	acetonitrile	70
12.	BUT-12 BUT-13	3.1×10^5 5.1×10^5	23 ppb 10 ppb	water	57
13.	$[Zn_2(NDC)_2(bpy)].Gx$	0.4×10^4	-	ethanol	71
14.	$[Zn_8(ad)_4(BPDC)_6$ $(0.2Me_2NH_2)] \cdot G$	4.6×10^4	12.9×10^{-6} M	water	58
15.	$[Zr_6O_4(OH)_6(L)_6]n$	5.8×10^4	0.4 ppm	water	59
16.	$[Cd_3(TPT)_2(DMF)_2]$ $\cdot 0.5H_2O]_n$	6.56×10^4	-	ethanol	60
17.	$[Zn_2(L)_2(dpyb)]_n$ $[Zn(L)(dipb)](H_2O)_2$	2.40×10^4 2.46×10^4	- -	DMA	61
18.	TB-Zn-CP	4.37×10^4	23 ppb	water	72
19.	$[Pr_2(TATMA)_2 \cdot 4DMF \cdot 4H_2O]_n$	1.6×10^4	-	DMF	73
20.	$[[Zn(C_{34}H_{18}O_8)_{0.5}(C_{20}N_2H_{16})_{0.5}]$ $[0.5(C_{20}N_2H_{16})]]_n$	8.1×10^4	-	DMF	18
21.	$[Zn(NDC)H_2O)]_n$ $[Cd(NDC)(H_2O)]_n$	6×10^4 2.385×10^4	1×10^{-6} M 4×10^{-6} M	water	74
22.	$[Zn_4(DMF)(Ur)_2(2,6\text{-}NDC)_4]_n$	10.83×10^4	1.63 ppm	water	62
23.	H_2ATAIA $H_2AMTAIA$ $H_2DMTAIA$	1.759×10^5 9.875×10^4 1.646×10^4	120 ppb 0.8 ppm 1.2 ppm	water	24
24.	$[Zn_2(TCPP)(DMF)_2]$	3.59×10^4	-	ethanol	30

Table 3.3 A comparison of the Stern-Volmer constant (K_{sv}), detection limit and medium used for $Cr_2O_7^{2-}$ detection for some MOFs already reported till date.

Sl. No	MOF	K_{sv} (M^{-1})	Detection Limit	Medium Used	Ref.
1.	$[Zr_6(\mu_3\text{-}O)_4(\mu_3\text{-}OH)_4(OH)_4(H_2O)_4(L)_2]$	1.02×10^6	2.88×10^{-8} M	water	this work
2.	JLU-MOF60	5.91×10^4	3.78×10^{-7} M	water	27
3.	JLU-MOF50	4.99×10^4	-	water	63
4.	$[(CH_3)_2NH_2]_6[Cd_3L(H_2O)_2]\cdot 12H_2O$	9.19×10^5	-	water	75
5.	NUM-5	9.4×10^4	0.7 ppm	water	64
6.	$[Cd(TIPA)_2(ClO_4^-)_2]\cdot(DMF)_3(H_2O)$	7.15×10^4	8 ppb	water	76
7.	$[Cd(L)(TPOM)_{0.75}].xS$	1.35×10^4	-	water	77
8.	$[Zn(L)(BBI)\cdot(H_2O)_2]$	1.17×10^4	-	water	77
9.	$[Zn_2(TPOM)(NDC)_2]\cdot 3.5H_2O$	9.21×10^4	2.35×10^{-6} M	water	65
10.	BUT-28	1.02×10^5	36 ppb	water	66
11.	534-MOF-Tb	1.37×10^4	0.14×10^{-3} M	water	78
12.	$[Eu(ipbp)_2(H_2O)_3]Br_6H_2O$	8.98×10^3	5.16×10^{-6} M	water	79
13.	$[Zn_2(tpeb)_2(2,3\text{-}ndc)_2]\cdot H_2O\}_n$	-	2.531 ppb	water	80
14.	MOR-2	-	4 ppb	water	81
15.	Zn-MOF-1	2.07×10^4	3.53×10^{-6} M	water	82
16.	[Zn(L)(bpp)]·DMF [Zn(L)(bpe)]·DMF	2.78×10^3 7.91×10^3	3.52×10^{-6} M 4.28×10^{-6} M	DMF	83
17.	$[Eu(L)(HCOO)(H_2O)]_n$ $[Tb(L)(HCOO)(H_2O)]_n$	2.76×10^4 2.13×10^4	1.0×10^{-6} M 2.1×10^{-6} M	water	84
18.	Eu-MOF	1.55×10^4	9.2×10^{-6} M	water	85

19.	Eu^{3+}@MIL-121	4.34×10^3	5.4×10^{-8} M	water	67
20.	$[Zn_7(TPPE)_2(SO_4^{2-})_7](DMF\cdot H_2O)$	1.09×10^4	26.98 ppb	water	86
21.	$[Tb(TATAB)(H_2O)_2]\cdot NMP$	1.11×10^4	-	water	87
22.	$[Zn_3(tza)_2(\mu_2\text{-}OH)_2(H_2O)_2]H_2O$	5.02×10^3	10^{-6} M	water	88
23.	$[Zn(btz)]_n$ $[Zn_2(ttz)H_2O]_n$	3.19×10^3 2.19×10^3	2×10^{-6} M 2×10^{-5} M	water	89
24.	$[Eu(Himdc)(ina)(H_2O)]_n$	2.46×10^3	-	water	90
25.	$[Eu_2(H_2O)(DCPA)_3]_n$	8.7×10^3	1.09×10^{-4} M	water	91
26.	BUT-39	1.57×10^3	1.5×10^{-6} M	water	92

The 3D S-V plots at higher concentration for all the chosen NAEs and metal anions are presented in Figure 3.28 and Figure 3.29 respectively. The linear S-V curve for at lower concentration (Figures 3.25-3.26) indicates that the quenching mechanism is either dynamic or static in nature. But, the deviation of the curve from linearity at higher concentration indicates the occurrence of both quenching mechanisms.

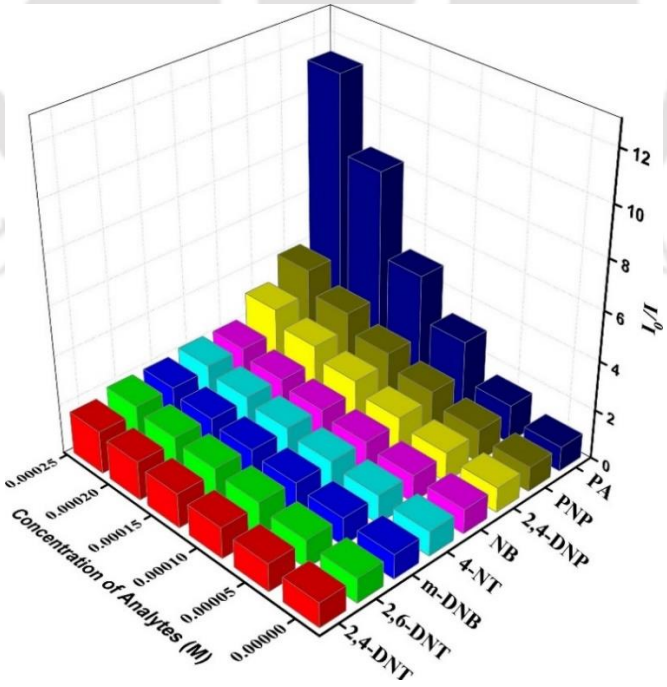

Figure 3.28 3D S-V plots for the quenching of **2'** upon the addition of various concentrations of different NAEs.

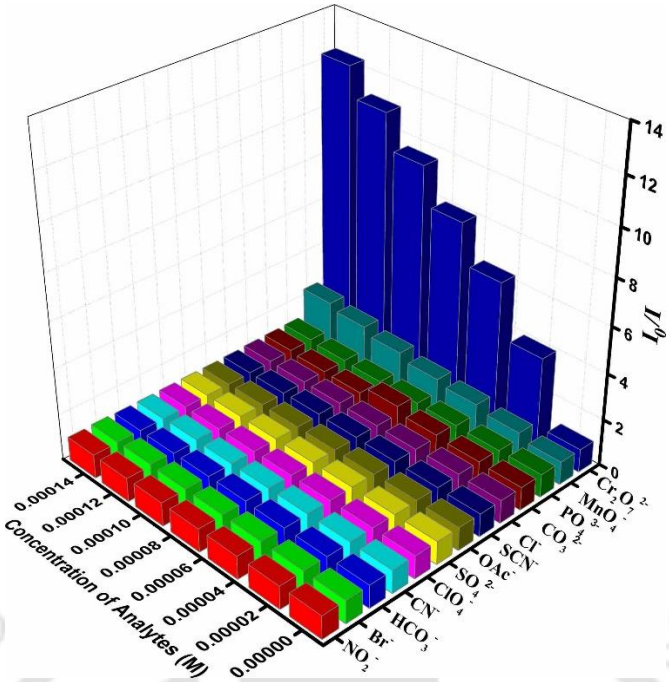

Figure 3.29 3D S-V plots for the quenching of **2'** upon the addition of various concentrations of different metal anions.

We also performed temperature dependent luminescence studies in three different temperature and calculated the K_{SV} values (Figures 3.30-3.31 and tables 3.4-3.5). As it can be seen from the Tables 3.4-3.5, *K*sv values for all three analytes decreases as the temperature is increased. This finding confirmed that all three quenching mechanism is static in nature.[93]

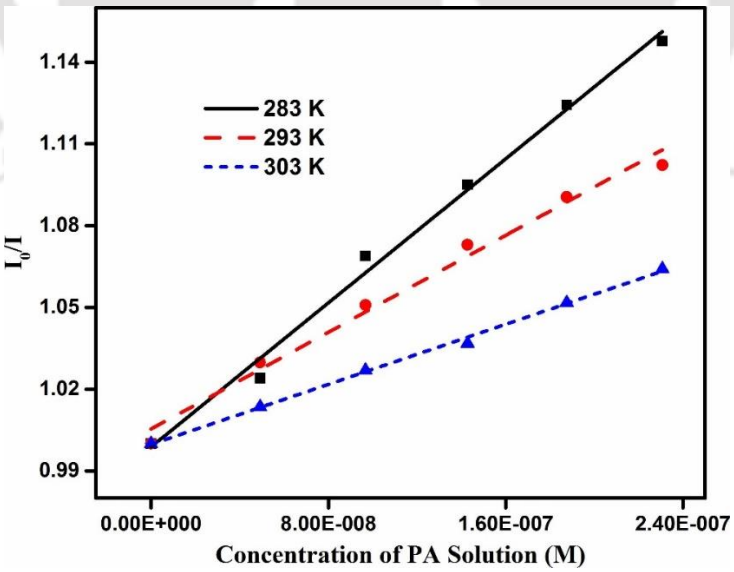

Figure 3.30 S-V plot at different temperature for quenching of **2'** by PA solution.

Table 3.4. Liner regression analysis of S-V plot at different temperatures for quenching of **2'** by PA solution.

T (K)	K_{sv} (M^{-1})×10^5	R^2
283	6.606	0.99158
293	4.443	0.98416
303	2.756	0.99693

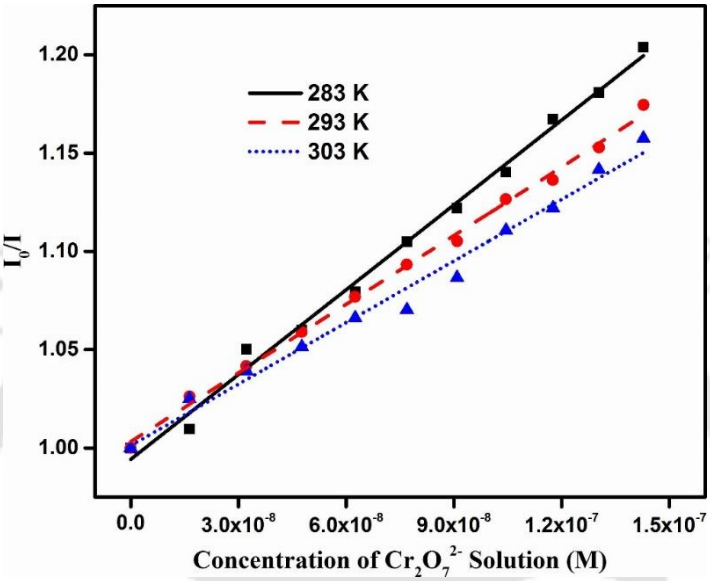

Figure 3.31 S-V plot at different temperature for quenching of **2'** by $Cr_2O_7^{2-}$ solution.

Table 3.5 Liner regression analysis of S-V plot at different temperatures for quenching of **2'** by $Cr_2O_7^{2-}$ solution.

T (K)	K_{sv} (M^{-1})×10^6	R^2
283	1.438	0.99320
293	1.164	0.99669
303	1.044	0.98411

To gain further details about these two quenching mechanisms, we carried out time-resolved fluorescence quenching experiments for both (PA and $Cr_2O_7^{2-}$) quenching processes. Figures 3.32-3.33 reveals that there are negligible changes in the average excited-state lifetime (⟨τ⟩) values of **2'** after treatment with PA or $Cr_2O_7^{2-}$ solution. Before and after addition of PA solution to **2'**, the ⟨τ⟩ values were found to be 0.44 and 0.38 ns, respectively (Table 3.6). For

$Cr_2O_7^{2-}$, these values were 0.76 and 0.53 ns, respectively (Table 3.7). These values of lifetime indicate that both quenching processes are static in nature.

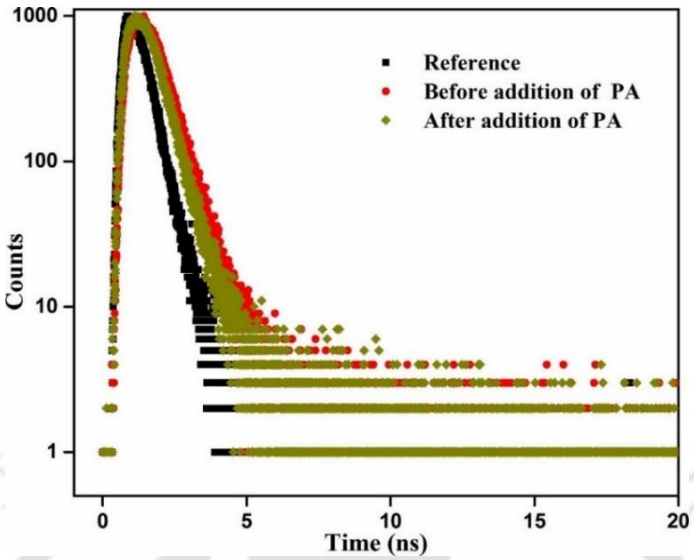

Figure 3.32 Lifetime decay profile of **2'** before and after addition of 200 μL of 10 mM PA in DMSO.

Table 3.6 Average excited state lifetime (<τ>) values of **2'** before and after addition of 200 μL of 10 mM PA solution in DMSO (λ_{ex} = 295 nm).

Volume Added (μL)	B_1	B_2	a_1	a_2	τ_1 (ns)	τ_1 (ns)	<τ>* (ns)	χ^2
0	0.016	0.001	88.52	11.48	0.36	1.06	0.44	1.01
200	0.021	0.001	99.90	9.91	0.28	1.10	0.38	1.03

* $\langle\tau\rangle = a_1\tau_1 + a_2\tau_2$

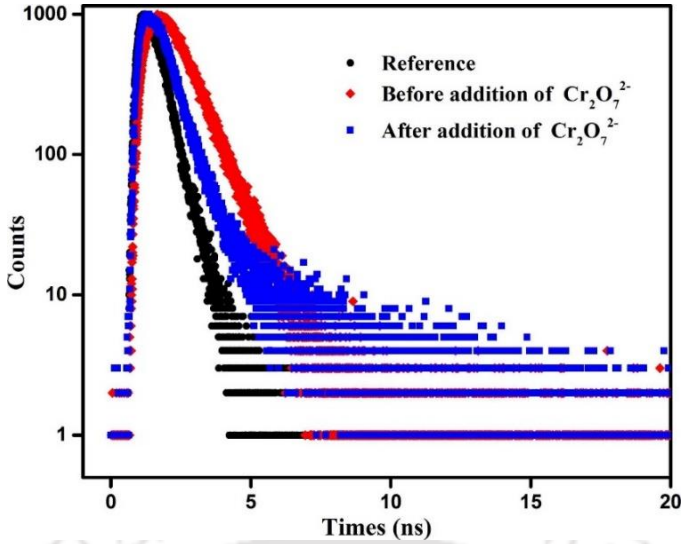

Figure 3.33 Lifetime decay profile of **2'** before and after addition of 150 μL of 3 mM $Cr_2O_7^{2-}$ solution in water.

Table 3.7 Average excited state lifetime (<τ>) values of **2'** before and after addition of 150 μL of 3 mM $Cr_2O_7^{2-}$ solution (λ_{ex} = 295 nm).

Volume Added (μL)	B_1	B_2	a_1	a_2	τ_1 (ns)	τ_1 (ns)	<τ>* (ns)	χ^2
0	0.012	0.001	90.32	9.67	0.69	1.40	0.76	1.01
150	0.020	0.001	92.13	7.66	0.35	2.73	0.53	1.01

* $<\tau> = a_1\tau_1 + a_2\tau_2$

The limit of detection (LOD) of **2'** towards PA and $Cr_2O_7^{2-}$ was calculated using $3\sigma/K$ requirement. Here, *K* is the slope of the plot of fluorescence intensity against concentration of analyte and σ is the standard deviation of the initial fluorescence intensity of **2'**. For these experiments, we gradually added the analytes having very low concentration to the suspension of **2'** and measured the fluorescence intensity. By plotting the fluorescence intensity against concentration, the linear curve (Figures 3.34-3.35) was obtained. The LOD values of **2'** towards PA and $Cr_2O_7^{2-}$ were found to be 5.72×10^{-8} M (13.08 ppb) and 2.88×10^{-8} M (8.58 ppb) respectively. We have also calculated LOD value of **2'** towards PA in water and calculated LOD value was found to be 2.00×10^{-8} M (4.58 ppb) (Figure 3.36). These data are among the lowest LOD values of the previously reported MOFs towards fluorogenic detection of PA and $Cr_2O_7^{2-}$ ion. (Tables 3.2-3.3).[6, 8, 24-25, 27, 36-37, 40-42, 45-51, 53, 57-59, 62, 64-68]

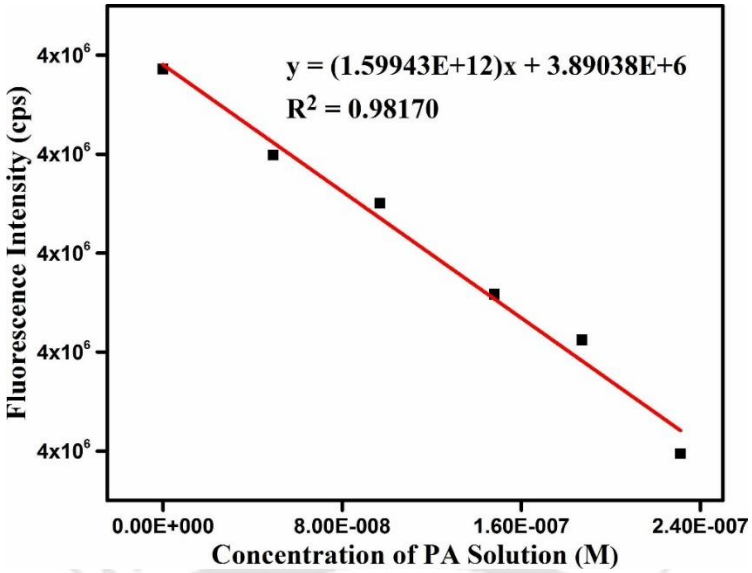

Figure 3.34 Change of fluorescence intensity of **2'** suspension in DMSO as a function of concentration of added PA solution in DMSO.

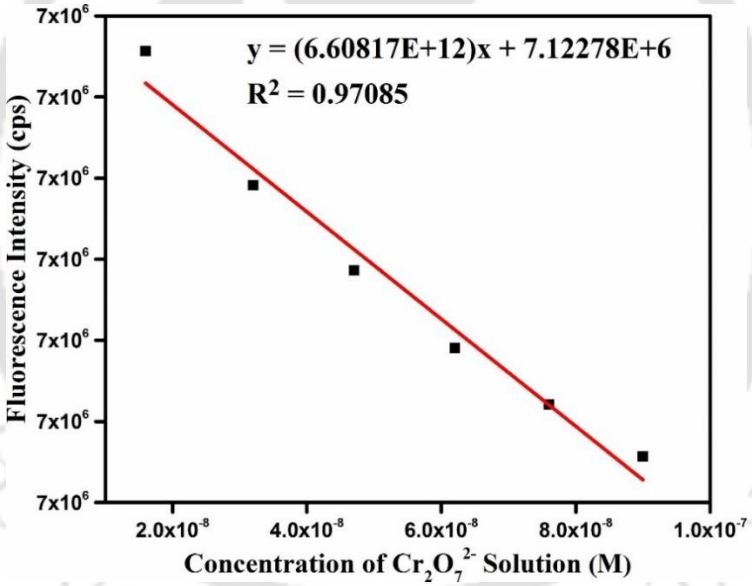

Figure 3.35 Change of fluorescence intensity of aqueous suspension of **2'** as a function of concentration of added $Cr_2O_7^{2-}$ solution in water.

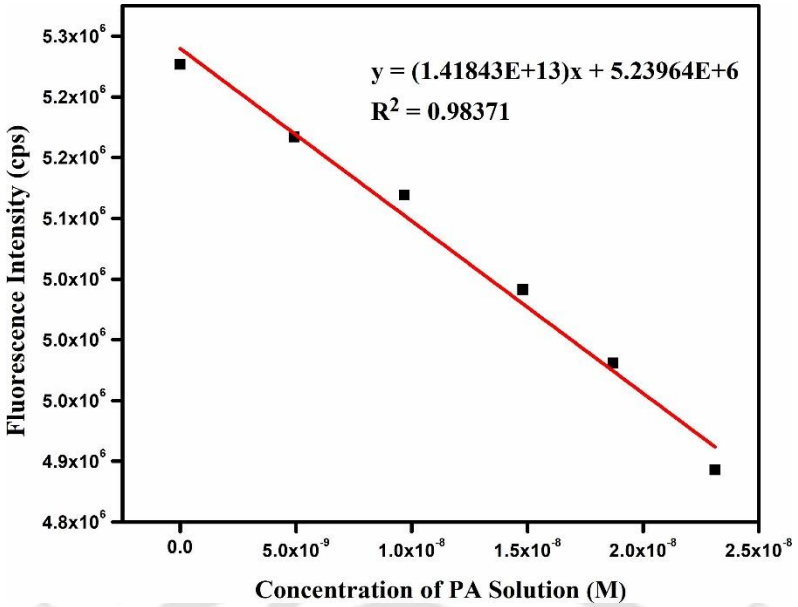

Figure 3.36 Change of fluorescence intensity of **2'** suspension in water as a function of concentration of added PA solution in water.

3.3.7 Mechanisms for the quenching of 2' by PA and $Cr_2O_7^{2-}$

The fluorescence quenching features of **2'** by PA can be considered to occur via PET mechanism from the electron-donor framework to electron-acceptor PA molecule. Fluorescence intensity of the electron-donor fluorophore in **2'** can be effectively quenched by all NAEs through PET mechanism, since all chosen NAEs are nitro-substituted electron-acceptor substrates.[94-95] To verify the plausibility of this mechanism, we calculated the HOMO-LUMO energies of the selected NAEs by density functional theory at the B3LYP/6-31G* accuracy level[96] (Figure 3.37 and Table 3.8). The results of this computational study indicate that the observed maximum fluorescence quenching by PA is due to easy electron transfer from **2'** to the LUMO energy level of PA, which is located at a lower energy level in comparison with other NAEs.[21, 97] However, the experimental order of the fluorescence intensity quenching (i.e. PA > 4-NP > 2,4-DNP > NB > 4-NT > 1,3-DNB > 2,6-DNT > 2,4-DNT) is not in full agreement with the corresponding LUMO energies of the examined NAEs. This result points out that PET is not the sole mechanistic pathway for the fluorescence intensity quenching of **2'**.[21] FRET is another possible mechanism for the fluorescence intensity quenching of **2'** by PA. To check the likelihood of FRET mechanism, we plotted the UV-Vis spectra of all NAEs (measured in water) and emission spectrum of **2'** (recorded in DMSO) in 300-600 nm range (Figure 3.38). As compared to other NAEs, the UV-Vis spectrum of PA showed the largest overlap with the emission spectrum of **2'** which in turn implies that the excitation energy can

be more effectively absorbed by PA than other NAEs. The non-linearity of S-V plot at higher concentration range (Figure 3.28) and the largest spectral overlap for PA indicate that both PET and FRET quenching mechanisms are possibly responsible for the quenching phenomena of **2'** by PA.[19, 98] Furthermore, the acid-base interactions between the acidic hydroxyl group of PA and basic pyrazine core of $\mathbf{L}^{4-}$ linker can play an important role for the fluorescence quenching of **2'**.

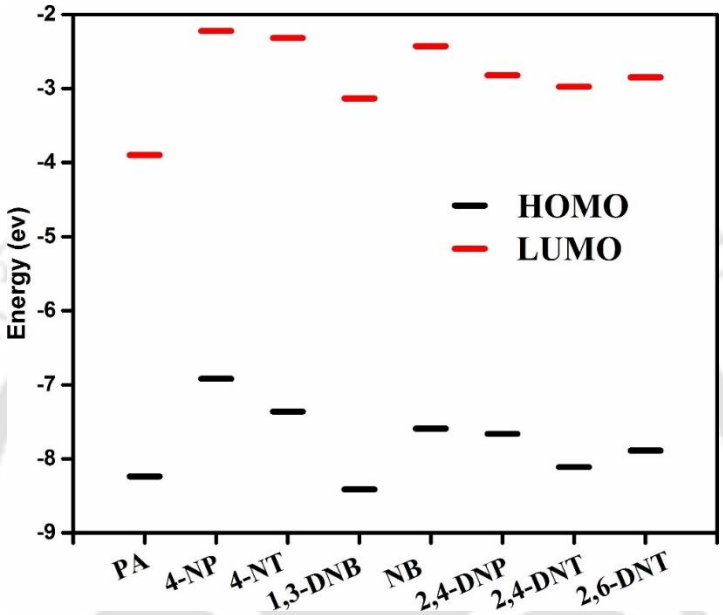

Figure 3.37 HOMO and LUMO energies of the selective NAEs.

Table 3.8 HOMO and LUMO energy levels of selected analytes calculated by density functional theory (DFT) at B3LYP/6-31G* accuracy level using Gaussian 09 package of program.[96]

Analyte	HOMO (eV)	LUMO (eV)	Band Gap (eV)
PA	-8.2374	-3.898	4.3394
4-NP	-6.9207	-2.2213	4.6994
2,4-DNP	-7.6644	-2.8202	4.8442
NB	-7.5917	-2.4294	5.1623
4-NT	-7.3626	-2.3171	5.0454
1,3-DNB	-8.4129	-3.1350	5.2779
2,6-DNT	-7.8913	-2.8501	5.0412

2,4-DNT	-8.1131	-2.9769	5.1362

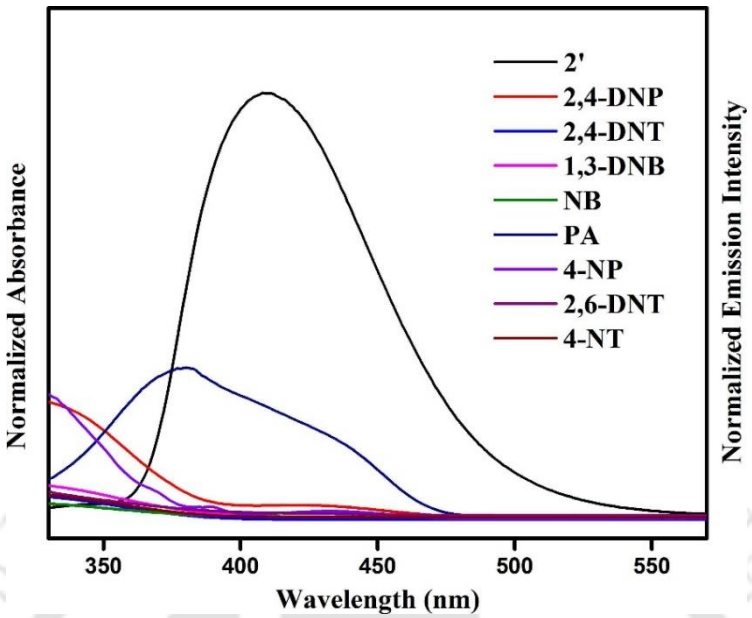

Figure 3.38 UV-Vis absorption spectra of the NAEs in DMSO (3×10^{-3} M). The emission spectrum of **1'** (black curve) (3 mg) dispersed in DMSO (3 mL).

The XRPD pattern of **2'** after $Cr_2O_7^{2-}$ sensing experiment (Figure 3.7) agrees well with that of un-treated **2'**. This result concludes that the quenching effect shown by $Cr_2O_7^{2-}$ is not because of decomposition of the framework. It is found from Figure 3.39 that the absorption spectrum of $Cr_2O_7^{2-}$ overlaps considerably with the emission spectrum of **2'**. This result indicates that $Cr_2O_7^{2-}$ ion can strongly absorb the energy of the excitation light which results in quenching of emission intensity. The absorption spectra of other investigated anions showed lesser overlap with the emission spectrum of **2'** as compared to $Cr_2O_7^{2-}$. Hence, there was lesser resonance energy transfer between the framework and other metal anions. The small change in the lifetime values (Table 3.7) before and after treatment with $Cr_2O_7^{2-}$ ion indicates the static quenching mechanism.

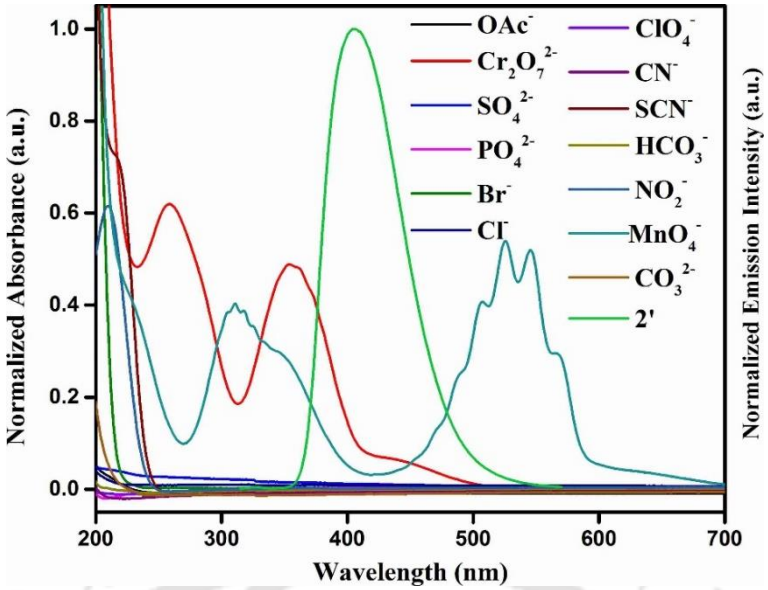

Figure 3.39 UV-Vis absorption spectra of the aqueous solutions (3×10^{-3} M) containing different metal anions. The emission spectrum of **2'** (green curve) (3 mg) dispersed in water (3 mL).

3.4 Conclusions

In conclusion, a highly luminescent Zr(IV) organic framework (**2**) with pyrazine core based tetracarboxylate linker was obtained by solvothermal reaction. Compound **2** was characterized by different spectroscopic and analytical techniques like XRPD analysis, FT-IR spectroscopy and TG analysis. Activated form of the compound (**2'**) exhibited high porosity with BET surface area of 1419 m^2/g and CO_2 adsorption capacity of 4.4 mmol/g at 1.4 bar and 0 °C. Moreover, **2'** exhibited selective and sensitive fluorogenic detection of Fe^{3+} and PA in water and DMSO, respectively. The LOD values of **2'** for PA and $Cr_2O_7^{2-}$ were 5.72×10^{-8} M and 2.88×10^{-8} M, respectively. These data are among the lowest LOD values exhibited by previously reported MOFs for the detection of PA and $Cr_2O_7^{2-}$. Compound **2'** remained intact in its original framework after the quenching experiments, as confirmed by the XRPD experiments. The compound is highly recyclable, since the fluorescence intensity after five cycles of sensing experiments was almost identical with the initial intensity. The possible fluorescence quenching mechanisms of **2'** for PA and $Cr_2O_7^{2-}$ were also investigated. With these features, the new highly porous Zr-MOF can be recognized as an extremely selective and sensitive fluorogenic sensor for PA and $Cr_2O_7^{2-}$ having very short response time.

3.5 References

1. Zhou, H.-C.; Long, J. R.; Yaghi, O. M. Introduction to Metal−Organic Frameworks. *Chem. Rev.* **2012,** *112*, 673−674.

2. Yang, Q.; Xu, Q.; Jiang, H. L. Metal–organic frameworks meet metal nanoparticles: synergistic effect for enhanced catalysis. *Chem. Soc. Rev.* **2017,** *46*, 4774–4808.

3. Banerjee, R.; Phan, A.; Wang, B.; Knobler, C.; Furukawa, H.; O'Keeffe, M.; Yaghi, O. M. High-throughput synthesis of zeolitic imidazolate frameworks and application to CO_2 capture. *Science* **2008,** *319*, 939−943.

4. Sumida, K.; Rogow, D. L.; Mason, J. A.; McDonald, T. M.; Bloch, E. D.; Herm, Z. R.; Bae, T.-H.; Long, J. R. Carbon Dioxide Capture in Metal–Organic Frameworks. *Chem. Rev.* **2012,** *112*, 724–781.

5. Stavila, V.; Talin, A. A.; Allendorf, M. D. MOF-based electronic and optoelectronic devices. *Chem. Soc. Rev.* **2014,** *43*, 5994−6110.

6. Xu, H.; Gao, J.; Qian, X.; Wang, J.; He, H.; Cui, Y.; Yang, Y.; Wang, Z.; Qian, G. Metal–organic framework nanosheets for fastresponse and highly sensitive luminescent sensing of Fe^{3+}. *J. Mater. Chem. A* **2016,** *4*, 10900−10905.

7. Allendorf, M. D.; Bauer, C. A.; Bhakta, R. K.; Houk, R. J. T. Luminescent metal–organic frameworks. *Chem. Soc. Rev.* **2009,** *38*, 1330–1352

8. Wang, J.; Jiang, M.; Yan, L.; Peng, R.; Huangfu, M.; Guo, X.; Li, Y.; Wu, P. Multifunctional luminescent Eu(III)-based metal−organic framework for sensing methanol and detection and adsorption of Fe(III) Ions in aqueous solution. *Inorg. Chem.* **2016,** *55*, 12660−12668.

9. Hu, Z.; Deibert, B. J.; Li, J. Luminescent metal–organic frameworks for chemical sensing and explosive detection. *Chem. Soc. Rev.* **2014,** *43*, 5815-5840.

10. Weng, D.-F.; Wang, Z.-M.; Gao, S. Framework-structured weak ferromagnets. *Chem. Soc. Rev.* **2011,** *40*, 3157−3181.

11. Kurmoo, M. Magnetic metal–organic frameworks. *Chem. Soc. Rev.* **2009,** *38*, 1353-1379.

12. Meng, X.; Wang, H.-N.; Song, S.-Y.; Zhang, H.-J. Proton-conducting crystalline porous materials. *Chem. Soc. Rev.* **2017,** *46*, 464–480.

13. Uemura, T.; Yanai, N.; Kitagawa, S. Polymerization reactions in porous coordination polymers. *Chem. Soc. Rev.* **2009,** *38*, 1228–1236.

14. Smith, K. D.; McCord, B. R.; McCrehan, W. A.; Mount, K.; Rowe, W. F. Detection of smokeless powder residue on pipe bombs by micellar electrokinetic capillary electrophoresis. *J. Forensic Sci.* **1999,** *44*, 789-794.

15. Yew, Y. T.; Ambrosi, A.; Pumera, M. Nitroaromatic explosives detection using electrochemically exfoliated graphene. *Sci. Rep.* **2016,** *6*, 33276-33286.

16. Rodgers, J. D.; Bunce, N. J. Treatment methods for the remediation of nitroaromatic explosives. *Water Res.* **2001,** *35*, 2101– 2111.

17. Germain, M. E.; Knapp, M. J. Optical explosives detection: from color changes to fluorescence turn-on. *Chem. Soc. Rev.* **2009,** *38*, 2543–2555.

18. Sanda, S.; Parshamoni, S.; Biswas, S.; Konar, S. Highly selective detection of palladium and picric acid by a luminescent MOF: a dual functional fluorescent sensor. *Chem. Commun.* **2015,** *51*, 6576-6579.

19. Buragohain, A.; Yousufuddin, M.; Sarma, M.; Biswas, S. 3D luminescent amide-functionalized cadmium tetrazolate framework for selective detection of 2,4,6-trinitrophenol. *Cryst. Growth Des.* **2016,** *16*, 842−851.

20. Ju, P.; Zhang, E.; Jiang, L.; Zhang, Z.; Hou, X.; Zhang, Y.; Yanga, H.; Wang, J. A novel microporous Tb-MOF fluorescent sensor for highly selective and sensitive detection of picric acid. *RSC Adv.* **2018,** *8*, 21671–21678.

21. Nagarkar, S. S.; Joarder, B.; Chaudhari, A. K.; Mukherjee, S.; Ghosh, S. K. Highly selective detection of nitro explosives by a luminescent metal–organic framework. *Angew. Chem. Int. Ed* **2013,** *52*, 2881–2885.

22. Song, X.-Z.; Song, S.-Y.; Zhao, S.-N.; Hao, Z.-M.; Zhu, M.; Meng, X.; Wu, L.-L.; Zhang, H.-J. Single-crystal-to-single-crystal transformation of a europium(III) metal–organic framework producing a multi-responsive luminescent sensor. *Adv. Funct. Mater.* **2014,** *24*, 4034–4041.

23. Zhang, Y.; Li, B.; Ma, H.; Zhang, L.; Zhang, W. An RGH–MOF as a naked eye colorimetric fluorescent sensor for picric acid recognition. *J. Mater. Chem. C* **2017,** *5*, 4661-4669.

24. Das, P.; Mandal, S. K. Understanding the effect of an amino group on the selective and ultrafast detection of TNP in water using fluorescent organic probes. *J. Mater. Chem. C* **2018,** *6*, 3288-3297.

25. Xia, T.; Zhu, F.; Cui, Y.; Yang, Y.; Wang, Z.; Qian, G. Highly selective luminescent sensing of picric acid based on a water-stable europium metal-organic framework. *J. Solid State Chem.* **2017,** *245*, 127–131.

26. Shen, X. C.; Ma, S.; Xia, H.; Shi, Z.; Mu, Y.; Liu, X. M. Cationic porous organic polymers as an excellent platform for highly efficient removal of pollutants from water. *J. Mater. Chem. A* **2018,** *6*, 20653-20658.

27. Liu, J.; Ye, Y.; Sun, X.; Liu, B.; Li, G.; Liang, Z.; Liu, Y. A multifunctional Zr(IV)-based metal–organic framework for highly efficient elimination of Cr(VI) from the aqueous phase. *J. Mater. Chem. A* **2019,** *7*, 16833-16841.

28. Costa, M.; Klein, C. B. Toxicity and carcinogenicity of chromium compounds in humans. *Crit. Rev. Toxicol.* **2006,** *36*, 155-163.

29. *U. S. EPA. Chromium in Drinking Water. March 1,* **2016**.

30. Jiang, Y.; Sun, L.; Du, J.; Liu, Y.; Shi, H.; Liang, Z.; Li, J. Multifunctional zinc metal−organic framework based on designed H_4TCPP ligand with aggregation-induced emission effect: CO_2 adsorption, luminescence, and sensing property. *Cryst. Growth Des.* **2017,** *17*, 2090−2096.

31. Lammert, M.; Reinsch, H.; Murray, C. A.; Wharmby, M. T.; Terraschkea, H.; Stock, N. Synthesis and structure of Zr(IV)- and Ce(IV)-based CAU-24 with 1,2,4,5-tetrakis(4-carboxyphenyl)benzene. *Dalton Trans.* **2016,** *45*, 18822-18826

32. *Topas Academics 4.2* **2007**.

33. Rappe, A. K.; Casewit, C. J.; Colwell, K. S.; III, W. A. G.; Skiff, W. M., UFF, a full periodic table force field for molecular mechanics and molecular dynamics simulations. *J. Am. Chem. Soc.* **1992,** *114*, 10024–10035.

34. Materials Studio Version 5.0 *Accelrys Inc.: San Diego* **2009**.

35. Prasad, R. R. R.; Seidner, S. E.; Cordes, D. B.; Lozinska, M. M.; Dawson, D. M.; Thompson, M.; Düren, T.; Chakarova, K. K.; Mihaylov, M. Y.; Hadjiivanov, K. I.; Hoffmann, F.; Slawin, A. M. Z.; Ashbrook, S. E.; Clarke, M. L.; Wright, P. A. STA-27, a porous Lewis acidic scandium MOF with an unexpected topology type prepared with 2,3,5,6-tetrakis(4-carboxyphenyl)pyrazine. *J. Mater. Chem. A* **2019**, DOI: 10.1039/C8TA10610J

36. Chen, C.-H.; Wang, X.-S.; Li, L.; Huang, Y.-B.; Cao, R. Highly selective sensing of Fe3+ by an anionic metal–organic framework containing uncoordinated nitrogen and carboxylate oxygen sites. *Dalton Trans.* **2018,** *47*, 3452–3458.

37. Ma, A.; Wu, J.; Han, Y.; Chen, F.; Li, B.; Cai, S.; Huang, H.; Singh, A.; Kumar, A.; Liu, J. Rational synthesis of a luminescent uncommon (3,4,6)-c connected Zn(II) MOF: a dual channel sensor for the detection of nitroaromatics and ferric ions. *Dalton Trans.* **2018,** *47*, 9627–9633.

38. Huang, W.-H.; Ren, J.; Yang, Y.-H.; Li, X.-M.; Wang, Q.; Jiang, N.; Yu, J.-Q.; Wang, F.; Zhang, J. Water-stable metal−organic frameworks with selective sensing on Fe^{3+} and nitroaromatic explosives, and stimuli-responsive luminescence on lanthanide encapsulation. *Inorg. Chem.* **2019,** *58*, 1481−1491.

39. Zheng, M.; Tan, H.; Xie, Z.; Zhang, L.; Jing, X.; Sun, Z. Fast response and high sensitivity europium metal organic framework fluorescent probe with chelating terpyridine sites for Fe^{3+}. *ACS Appl. Mater. Interfaces* **2013,** *5*, 1078–1083.

40. Rao, P. C.; Mandal, S. Europium-based metal−organic framework as a dual luminescence sensor for the selective detection of the phosphate anion and Fe^{3+} ion in aqueous media. *Inorg. Chem.* **2018,** *57*, 11855-11858.

41. Das, P.; Mandal, S. K. Strategic design and functionalization of an amine-decorated luminescent metal organic framework for selective gas/vapor sorption and nanomolar sensing of 2,4,6-trinitrophenol in water. *ACS Appl. Mater. Interfaces* **2018,** *10*, 25360−25371.

42. Wang, D.; Hu, Z.; Xu, S.; Li, D.; Zhang, Q.; Ma, W.; Zhou, H.; Wu, J.; Tian, Y. Fluorescent metal–organic frameworks based on mixed organic ligands: new candidates for highly sensitive detection of TNP. *Dalton Trans.* **2019,** *48*, 1900–1905.

43. Nagarkar, S. S.; Desai, A. V.; Ghosh, S. K. A fluorescent metal–organic framework for highly selective detection of nitro explosives in the aqueous phase. *Chem. Commun.* **2014,** *50*, 8915-8918.

44. Zhan, Z.; Liang, X.; Zhang, X.; Jia, Y.; Hu, M. A water-stable europium-MOF as a multifunctional luminescent sensor for some trivalent metal ions (Fe^{3+}, Cr^{3+}, Al^{3+}), PO_4^{3-} ions, and nitroaromatic explosives. *Dalton Trans.* **2019,** *48*, 1786–1794.

45. Gogoi, C.; Biswas, S. A new quinoline based luminescent Zr(IV) metal–organic framework for the ultrasensitive recognition of 4-nitrophenol and Fe(III) ions. *Dalton Trans.* **2018,** *48*, 14696-14705.

46. Dalapati, R.; K.-Demir, Ü.; Janiak, C.; Biswas, S. The effect of functional groups in the aqueousphase selective sensing of Fe(III) ions by thienothiophene-based zirconium metal–organic frameworks and the design of molecular logic gates. *Dalton Trans.* **2018,** *47*, 1159–1170.

47. Das, A.; Banesh, S.; Trivedi, V.; Biswas, S. Extraordinary sensitivity for H_2S and Fe(III) sensing in aqueous medium by Al-MIL-53-N_3 metal–organic framework: in vitro and in vivo applications of H_2S sensing. *Dalton Trans.* **2018,** *47*, 2690–2700.

48. Das, A.; Biswas, S. A multi-responsive carbazole-functionalized Zr(IV)-based metal-organic framework for selective sensing of Fe(III), cyanide and p-nitrophenol. *Sens. Actuator B-Chem.* **2017,** *250*, 121-131.

49. Gogoi, C.; Yousufuddin, M.; Biswas, S. A new 3D luminescent Zn(II)–organic framework containing a quinoline-2,6-dicarboxylate linker for the highly selective sensing of Fe(III) ions. *Dalton Trans.* **2019,** *48*, 1766-1773.

50. Weng, H.; Yan, B. A flexible Tb(III) functionalized cadmium metal organic framework as fluorescent probe for highly selectively sensing ions and organic small molecules. *Sens. Actuator B-Chem.* **2016,** *228*, 702-708.

51. Zhang, J.; Zhao, L.; Liu, Y.; Li, M.; Li, G.; Meng, X. Two luminescent transition-metal–organic frameworks with a predesigned ligand as highly sensitive and selective iron(III) sensors. *New J.Chem.* **2018,** *42*, 6839-6847.

52. Dong, X.-Y.; Wang, R.; Wang, J.-Z.; Wang, S.-Q.; Mak, T. C. W. Highly selective Fe^{3+} sensing and proton conduction in a water-stable sulfonate–carboxylate Tb–organic-framework. *J. Mater. Chem. A* **2015,** *3*, 641–647.

53. Xu, X.-Y.; Yan, B. Eu(III)-Functionalized MIL-124 as Fluorescent Probe for Highly Selectively Sensing Ions and Organic Small Molecules Especially for Fe(III) and Fe(II). *ACS Appl. Mater. Interfaces* **2015,** *7*, 721-729.

54. Wang, K.-M.; Du, L.; Ma, Y.-L.; Zhao, J.-S.; Wang, Q.; Yan, T.; Zhao, Q.-H. Multifunctional chemical sensors and luminescent thermometers based on lanthanide metal–organic framework materials. *CrystEngComm* **2016,** *18*, 2690-2700.

55. Li, Y.-F.; Wang, D.; Liao, Z.; Kang, Y.; Ding, W.-H.; Zheng, X.-J.; Jin, L.-P. Luminescence tuning of the Dy–Zn metal–organic framework and its application in the detection of Fe(III) ions. *J. Mater. Chem. C* **2016,** *4*, 4211-4217.

56. Zhang, C.; Yan, Y.; Pan, Q.; Sun, L.; He, H.; Liu, Y.; Liang, Z.; Li, J. A microporous lanthanum metal–organic framework as a bi-functional chemosensor for the detection of picric acid and Fe3+ ions. *Dalton Trans.* **2015,** *44*, 13340-13346.

57. Wang, B.; Lv, X.-L.; Feng, D.; Xie, L.-H.; Zhang, J.; Li, M.; Xie, Y.; Li, J.-R.; Zhou, H.-C. Highly stable Zr(IV)-based metal-organic frameworks for the detection and removal of antibiotics and organic explosives in water. *J. Am. Chem. Soc.* **2016,** *138*, 6204-6216.

58. Joarder, B.; Desai, A. V.; Samanta, P.; Mukherjee, S.; Ghosh, S. K. Selective and sensitive aqueous-phase detection of 2,4,6-trinitrophenol (TNP) by an amine-functionalized metal–organic framework. *J. Mater. Chem. C* **2014,** *2*, 10073-10081.

59. Nagarkar, S. S.; Desai, A. V.; Samanta, P.; Ghosh, S. K. Aqueous phase selective detection of 2,4,6-trinitrophenol using a fluorescent metal–organic framework with a pendant recognition site. *Dalton Trans.* **2015,** *44*, 15175-15180.

60. Zhang, C.; Sun, L.; Yan, Y.; Li, J.; Song, X.; Liu, Y.; Liang, Z. A luminescent cadmium metal–organic framework for sensing of nitroaromatic explosives. *Dalton Trans.* **2015,** *44*, 230-236.

61. Shi, Z.-Q.; Guo, Z.-J.; Zheng, H.-G. Two luminescent Zn(II) metal–organic frameworks for exceptionally selective detection of picric acid explosives. *Chem. Commun.* **2015,** *51*, 8300-8303.

62. Mukherjee, S.; Desai, A. V.; Manna, B.; Inamdar, A. I.; Ghosh, S. K. Exploitation of guest accessible aliphatic amine functionality of a metal–organic framework for selective detection of 2,4,6-trinitrophenol (TNP) in water. *Cryst. Growth Des.* **2015,** *15*, 4627-4634.

63. Sun, X.; Yao, S.; Yu, C.; Li, G.; Liu, C.; Huo, Q.; Liu, Y. An ultrastable Zr-MOF for fast capture and highly luminescence detection of $Cr_2O_7^{2-}$ simultaneously in an aqueous phase. *J. Mater. Chem. A* **2018,** *6*, 6363-6369.

64. Yao, Z.-Q.; Li, G.-Y.; Xu, J.; Hu, T.-L.; Bu, X.-H. A water-stable luminescent Zn^{II} metal-organic framework as chemosensor for high-efficiency detection of Cr^{VI}-anions ($Cr_2O_7^{2-}$ and CrO_4^{2-}) in aqueous solution. *Chem. Eur. J.* **2018,** *24*, 3192-3198.

65. Lv, R.; Li, H.; Su, J.; Fu, X.; Yang, B.; Gu, W.; Liu, X. Zinc metal-organic framework for selective detection and differentiation of Fe(III) and Cr(VI) ions in aqueous solution. *Inorg. Chem.* **2017,** *56*, 12348-12356.

66. Xu, M.-M.; Kong, X.-J.; He, T.; Wu, X.-Q.; Xie, L.-H.; Li, J.-R. A stable Zr(IV)-based metal-organic framework constructed from C=C bridged di-isophthalate ligand for sensitive detection of $Cr_2O_7^{2-}$ in water. *Inorg. Chem.* **2018,** *57*, 14260-14268.

67. Hao, J.-N.; Yan, B. Ln^{3+} post-functionalized metal–organic frameworks for color tunable emission and highly sensitive sensing of toxic anions and small molecules. *New J. Chem.* **2016,** *40*, 4654-4661.

68. SK, M.; Biswas, S. A thiadiazole-functionalized Zr(IV)-based metal–organic framework as a highly fluorescent probe for the selective detection of picric acid. *CrystEngComm* **2016,** *18*, 3104-3113.

69. Xiao, J.-D.; Qiu, L.-G.; Ke, F.; Yuan, Y.-P.; Xu, G.-S.; Wang, Y.-M.; Jiang, X. Rapid synthesis of nanoscale terbium-based metal–organic frameworks by a combined ultrasound-vapour phase diffusion method for highly selective sensing of picric acid. *J. Mater. Chem. A* **2013,** *1*, 8745-8752.

70. Santra, A.; Francis, M.; Parshamoni, S.; Konar, S. Nanoporous Cu(I) metal–organic framework: selective adsorption of benzene and luminescence sensing of nitroaromatics. *ChemistrySelect* **2017,** *2*, 3200-3206.

71. Asha, K. S.; Bhattacharyya, K.; Mandal, S. Discriminative detection of nitro aromatic explosives by a luminescent metal–organic framework. *J. Mater. Chem. C* **2014,** *2*, 10073-10081.

72. Shanmugaraju, S.; Dabadie, C.; Byrne, K.; Savyasachi, A. J.; Umadevi, D.; Schmitt, W.; Kitchen, J. A.; Gunnlaugsson, T. A supramolecular Troger's base derived coordination zinc polymer for fluorescent sensing of phenolic-nitroaromatic explosives in wate. *Chem. Sci.* **2017,** *8*, 1535-1546.

73. He, H.; Chen, S.-H.; Zhang, D.-Y.; Yang, E.-C.; Zhao, X.-J. A luminescent metal–organic framework as an ideal chemosensor for nitroaromatic compounds. *RSC Adv.* **2017,** *7*, 38871-38876.

74. Ghosh, P.; Saha, S. K.; Roychowdhury, A.; Banerjee, P. Recognition of an explosive and mutagenic water pollutant, 2,4,6-Trinitrophenol, by cost-effective luminescent MOFs. *Eur. J. Inorg. Chem.* **2015**.

75. Lu, B.-B.; Jiang, W.; Yang, J.; Liu, Y.-Y.; Ma, J.-F. Resorcin[4]arene-based microporous metal-organic framework as an efficient catalyst for CO_2 cycloaddition with epoxides and highly selective luminescent sensing of $Cr_2O_7^{2-}$. *ACS Appl. Mater. Interfaces* **2017,** *9*, 39441-39449.

76. Fu, H.-R.; Zhao, Y.; Zhou, Z.; Yang, X.-G.; Ma, L.-F. Neutral ligand TIPA-based two 2D metal–organic frameworks: ultrahigh selectivity of C_2H_2/CH_4 and efficient sensing and sorption of Cr(VI). *Dalton Trans.* **2018,** *47*, 3725-3732.

77. Zhao, Y.; Xu, X.; Qiu, L.; Kang, X.; Wen, L.; Zhang, B. Metal-organic frameworks constructed from a new thiophene functionalized dicarboxylate: luminescence sensing and pesticide removal. *ACS Appl. Mater. Interfaces* **2017,** *9*, 15164-15175.

78. Chen, M.; Xu, W.-M.; Tian, J.-Y.; Cui, H.; Zhang, J.-X.; Liu, C.-S.; Du, M. A terbium(III) lanthanide–organic framework as a platform for a recyclable multi-responsive luminescent sensor. *J. Mater. Chem. C* **2017,** *5*, 2015-2021.

79. Zhang, C.; Sun, L.; Yan, Y.; Shi, H.; Wang, B.; Liang, Z.; Li, J. A novel photo- and hydrochromic europium metal–organic framework with good anion sensing properties. *J. Mater. Chem. C* **2017,** *5*, 8999-9004.

80. Gu, T.-Y.; Dai, M.; Young, D. J.; Ren, Z.-G.; Lang, J.-P. Luminescent Zn(ii) coordination polymers for highly selective sensing of Cr(III) and Cr(VI) in water. *Inorg. Chem.* **2017,** *56,* 4668-4678.

81. Rapti, S.; Sarma, D.; Diamantis, S. A.; Skliri, E.; Armatas, G. S.; Tsipis, A. C.; Hassan, Y. S.; Alkordi, M.; Malliakas, C. D.; Kanatzidis, M. G.; Lazarides, T.; Plakatouras, J. C.; Manos, M. J. All in one porous material: exceptional sorption and selective sensing of hexavalent chromium by using a Zr^{4+} MOF. *J. Mater. Chem. A* **2017,** *5*, 14707-14719.

82. Guo, X.-Y.; Zhao, F.; Liu, J.-J.; Liu, Z.-L.; Wang, Y.-Q. An ultrastable zinc(II)–organic framework as a recyclable multi-responsive luminescent sensor for Cr(III), Cr(VI) and 4-nitrophenol in the aqueous phase with high selectivity and sensitivity. *J. Mater. Chem. A* **2017,** *5*, 20035-20043.

83. Chen, Z. W.; Mi, X. N.; Wang, S. N.; Lu, J.; Li, Y. W.; Li, D. C.; Dou, J. M. Two novel penetrating coordination polymers based on flexible S-containing dicarboxylate acid with sensing properties towards Fe^{3+} and $Cr^{2}O^{72-}$ ions. *J. Solid State Chem.* **2018,** *261*, 75-85.

84. Sun, Z.; Yang, M.; Ma, Y.; Li, L. C. Multi-responsive luminescent sensors based on two-dimensional lanthanide-metal organic frameworks for highly selective and sensitive detection of Cr(III) and Cr(VI) ions and benzaldehyde. *Cryst. Growth Des.* **2017,** *17*, 4326-4335.

85. Gai, Y.-L.; Guo, Q.; Zhao, X.-Y.; Chen, Y.; Liu, S.; Zhang, Y.; Zhuo, C.-X.; Yao, C.; Xiong, K.-C. Extremely stable europium-organic framework for luminescent sensing of $Cr_2O_7^{2-}$ and Fe^{3+} in aqueous systems. *Dalton Trans.* **2018,** *47*, 12051-12055.

86. Wu, X.-X.; Fu, H.-R.; Han, M.-L.; Zhou, Z.; Ma, L.-F. Tetraphenylethylene immobilized metal-organic frameworks: highly sensitive fluorescent sensor for the detection of $Cr_2O_7^{2-}$ and nitroaromatic explosives. *Cryst.Growth Des* **2017,** *17*, 6041-6048.

87. Wen, G.-X.; Han, M.-L.; Wu, X.-Q.; Wu, Y.-P.; Dong, W.-W.; Zhao, J.; Li, D.-S.; Ma, L.-F. A multi-responsive luminescent sensor based on a super-stable sandwich-type terbium(III)–organic framework. *Dalton Trans.* **2016,** *45*, 15492-15499.

88. Song, T.-Q.; Dong, J.; Gao, H.-L.; Cui, J.-Z.; Zhao, B. A unique zinc-organic framework constructed through in situ ligand synthesis for conversion of CO_2 under mild conditions and as a luminescence sensor for $Cr_2O_7^{2-}/CrO_4^{2-}$. *Dalton Trans.* **2017,** *46*, 13862-13868.

89. Cao, C.-S.; Hu, H.-C.; Xu, H.; Qiao, W.-Z.; Zhao, B. Two solvent-stable MOFs as a recyclable luminescent probe for detecting dichromate or chromate anions. *CrystEngComm* **2016,** *18*, 4445-4451.

90. Liu, L.-H.; Qiu, X.-T.; Wang, Y.-J.; Shi, Q.; Sun, Y.-Q.; Chen, Y.-P. NIR emission and luminescent sensing of a lanthanide–organic framework with Lewis basic imidazole and pyridyl sites. *Dalton Trans.* **2017,** *46,* 12106-12113.

91. He, H. M.; Chen, S.-H.; Zhang, D.-Y.; Hao, R.; Zhang, C.; Yang, E.-C.; Zhao, X.-J. A micrometer-sized europium(III)–organic framework for selective sensing of the $Cr_2O_7^{2-}$ anion and picric acid in water systems. *Dalton Trans.* **2017,** *46,* 13502-13509.

92. He, T.; Zhang, Y.-Z.; Kong, X.-J.; Yu, J. M.; Lv, X.-L.; Wu, Y. F.; Guo, Z.-J.; Li, J.-R. Zr(IV)-based metal-organic framework with T-shaped ligand: unique structure, high stability, selective detection, and rapid adsorption of $Cr_2O_7^{2-}$ in water. *ACS Appl. Mater. Interfaces* **2018,** *10,* 16650-16659.

93. Sharma, R. N.; Pancholi, S. S. Protein binding interaction study of olmesartan medoxomil and its metabolite olmesartan by fluorescence spectroscopy. *Int J Pharm Pharm Sci* **2014,** *6,* 726-729.

94. Enkin, N.; Sharon, E.; Golub, E.; Willner, I. Ag nanocluster/DNA hybrids: functional modules for the detection of nitroaromatic and RDX explosives. *Nano Lett.* **2014,** *14,* 4918-4922.

95. Liu, S. G.; Luo, D.; Li, N.; Zhang, W.; Lei, J. L.; Li, N. B.; Luo, H. Q. Water-soluble nonconjugated polymer nanoparticles with strong fluorescence emission for selective and sensitive detection of nitro-explosive picric acid in aqueous medium. *ACS Appl. Mater. Interfaces* **2016,** *8,* 21700-21709.

96. Frisch, M. J.; Trucks, G. W.; Schlegel, H. B.; Scuseria, G. E.; Robb, M. A.; Cheeseman, J. R.; Scalmani, G.; Barone, V.; Mennucci, B.; Petersson, G. A.; Nakatsuji, H.; Caricato, M.; Li, X.; Hratchian, H. P.; Izmaylov, A. F.; Bloino, J.; Zheng, G.; Sonnenberg, J. L.; Hada, M.; Ehara, M.; Toyota, K.; Fukuda, R.; Hasegawa, J.; Ishida, M.; Nakajima, T.; Honda, Y.; Kitao, O.; Nakai, H.; Vreven, T.; Montgomery, J. A.; Peralta, J. E.; Ogliaro, F.; Bearpark, M.; Heyd, J. J.; Brothers, E.; Kudin, K. N.; Staroverov, V. N.; Kobayashi, R.; Normand, J.; Raghavachari, K.; Rendell, A.; Burant, J. C.; Iyengar, S. S.; Tomasi, J.; Cossi, M.; Rega, N.; Millam, J. M.; Klene, M.; Knox, J. E.; Cross, J. B.; Bakken, V.; Adamo, C.; Jaramillo, J.; Gomperts, R.; Stratmann, R. E.; Yazyev, O.; Austin, A. J.; Cammi, R.; Pomelli, C.; Ochterski, J. W.; Martin, R. L.; Morokuma, K.; Zakrzewski, V. G.; Voth, G. A.; Salvador, P.; Dannenberg, J. J.; Dapprich, S.; Daniels, A. D.; Farkas, O.; Foresman, J. B.; Ortiz, J. V.; Cioslowski, J.; Fox, D. J. *Gaussian 09, Gaussian, Inc., Wallingford CT* **2009**.

97. Pramanik, S.; Zheng, C.; Zhang, X.; Emge, T. J.; Li, J. New microporous metal-organic framework demonstrating unique selectivity for detection of high explosives and aromatic compounds. *J. Am. Chem. Soc.* **2011,** *133*, 4153-4155.

98. Cui, Y.; Yue, Y.; Qian, G.; Chen, B. Luminescent functional metal-organic frameworks. *Chem. Rev.* **2012,** *112*, 1126-1162.

CHAPTER 4

Specific fluorescence sensing of hydrogen sulphide by an azide functionalized Zr(IV) MOF with DUT-52 structure

*This chapter describes the synthesis and characterization of an azide functional group containing Zr(IV) based MOF with DUT-52 (DUT = Dresden University of Technology) structure via solvothermal process. The cubic framework has hexanuclear $[Zr_6O_4(OH)_4]^{2+}$ building units. The three-dimensional cubic framework is formed by interconnecting these building units through the carboxylate groups of twelve NDC-N_3 (NDC-N_3 = 1-azidonaphthalene-3,7-dicarboxylic acid) linkers. The data from the fluorescence experiments suggested that activated compound (**3'**) exhibits sensitive and selective detection of H_2S in an aqueous medium. The response time of **3'** is very short (2 min) towards H_2S. By using mass spectrometry, FT-IR and ^1H NMR spectroscopy, the mechanism for the reduction of azide into an amine group was established.*

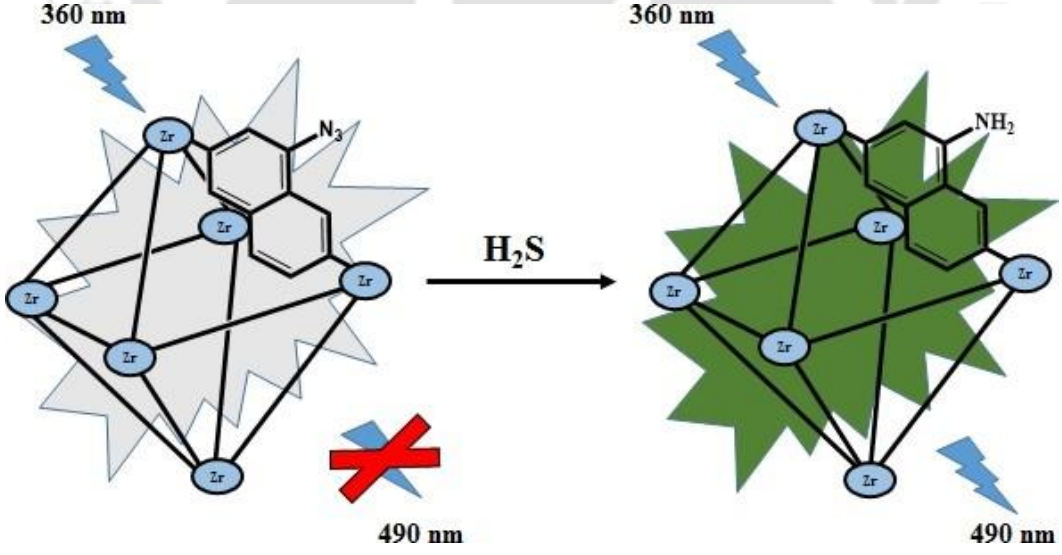

MICROPOROUS AND MESOPOROUS MATERIALS

C. Gogoi, A. Kumar, M. SK, S. Biswas. *Microporous and mesoporous mater.*, 2021, **311**, 110725-110732.

4.1 Introduction

In recent years, the chemistry of porous solids has increased the attention of scientists across the world due to its suitability towards molecular recognition, gas adsorption and purification, catalysis, asymmetric synthesis, *etc*.[1-5] MOFs are a new class of porous solids, which are also called as porous coordination polymers.[6] They are composed of inorganic metal ions or metal clusters and organic linkers, forming insoluble complexes which are assembled in one, two, and three-dimensional frameworks. The high surface area, reasonable stability and fascinating adjustable properties make them useful in many potential applications like catalysis, sensing, drug delivery, gas separation/adsorption, optoelectronics, etc.[7-19] Among all, great efforts have been made for exploring the sensing behavior of MOFs.[14] The primary benefits of MOFs instead of using other porous materials are that MOFs can be designed and tuned through selective choice of different metal ions and organic linkers. The final structures of the MOFs can be influenced by the coordination nature of metal ions, solvents properties, modulators, reaction temperatures, reaction times and so on.[20-21] A particular category of MOFs is LMOFs (LMOF = luminescent metal-organic framework).[8, 22-24] These LMOFs have been used as luminescent probes to detect desired chemical species. When the luminescence intensity increases on addition of any specific analyte, it is called luminescence turn-on whereas the quenching in luminescence intensity is called luminescence turn-off.[25-27]

Modernization of industries releases many hazardous chemicals in the form of gases as well as liquids. Among these gases, H_2S is one of the major pollutants.[28-29] H_2S is a well-known gasotransmitter along with carbon monoxide and nitric oxide in the biological systems.[30] This gas has a hazardous effect on living beings.[31] Acute exposure of H_2S prevents the functioning of Cytochrome oxidase enzyme, which ultimately results in lack of oxygen inside the cells. This gas is originated inside the human body and causes several diseases like diabetes, liver cirrhosis, Alzheimer's disease, cancer, *etc*.[32-34] Until now, detection of H_2S is conducted by methods like gas chromatography, colorimetry, electrochemical analysis and metal-induced precipitation.[35-38] These techniques have an essential requirement of pretreatment of the samples. For selective and non- invasive sensing of H_2S, fluorescence-based method using MOFs has been used in the literature recently.[39] Due to easiness in handling, low cost, simplicity and rapid response, the fluorescence-based technique has attracted more interests over other detection techniques.[40]

An efficient strategy to prepare MOFs for the detection of H_2S is to use azide or nitro functionalized aromatic organic linkers. The concept behind the use of azide or nitro functionality is the reduction of these groups into amine group on treatment with H_2S.[29-30, 41-42] Recently, azide functionalized Zr-based CAU-10, Zr-based UiO-66 and Al-based MIL-53 (CAU = Christian-Albrechts-University) MOFs for the H_2S detection have been reported by our group.[43],[39-40] Herein, a new porous azide functionalized Zr(IV) based DUT-52 MOF (**3**) with 1-azidonaphthalene-3,7-dicarboxylic acid ($H_2NDC\text{-}N_3$) linker has been synthesized and characterized by different spectroscopic techniques. The microporous framework of the activated MOF (**3'**) can selectively detect H_2S over other competitive analytes in aqueous solution. The sensing process is very fast and the MOF exhibits very low detection limit.

4.2 Experimental section

4.2.1 Materials and instrumental techniques

All the reagents and solvents were procured from commercial sources and used without purification except the $H_2NDC\text{-}N_3$ linker. Fourier transform infrared (FT-IR) spectra were collected in the region 400-4000 cm^{-1} on a PerkinElmer Spectrum Two FT-IR spectrometer. The following notations were used for characterization of the bands: broad (br), strong (s), very strong (vs), medium (m) and weak (w). Thermogravimetric analysis (TGA) was carried out with an SDT Q600 V20.9 Build 20 thermogravimetric analyzer in the temperature range of 25-700 °C in an argon atmosphere at the rate of 10 °C min^{-1}. The Bruker D2 Phaser X-ray diffractometer was employed for X-ray powder diffraction (XRPD) measurements at 30 kV, 10 mA using Cu-Kα (λ = 1.5406 Å) radiation. N_2 sorption isotherms were recorded by using Quantachrome Autosorb iQ-MP volumetric gas adsorption equipment at -196 °C. CO_2 adsorption experiments in the low-pressure range were performed by employing a Quantachrome iSorb-HP gas adsorption instrument at 25 °C. Before the sorption analysis, the degassing of the compound was carried out at 80 °C under high vacuum for 5 h. Fluorescence sensing studies were performed with a HORIBA JOBIN YVON Fluoromax-4 spectrofluorometer. A Bruker Avance III 600 NMR spectrometer was used for recording ^{1}H-NMR spectra at 600 MHz. Mass spectra were recorded with an Agilent 6520 Q-TOF highresolution mass spectrometer (HR-MS). Before the HR-MS measurement, 10 mg of un-treated or Na_2S-treated **3'** were separately suspended in 1.0 mL of methanol and 100 µL of 48% HF was added. The organic phase was separated by filtration and diluted with methanol for HR-MS analysis.

4.2.2. Synthesis of $H_2NDC\text{-}N_3$ linker:

The linker was synthesized by using naphthalene-2,6-dicarboxylic acid (H_2NDC) as a starting material. 1-Amino naphthalene-3,7-dicarboxylic acid ($H_2NDC\text{-}NH_2$) was prepared from H_2NDC by following the previsoudly reported procedure (Scheme S1).[44] Then, diazotization of $H_2NDC\text{-}NH_2$ was performed and in the second step, the azide containing linker was prepared from the diazonium salt.

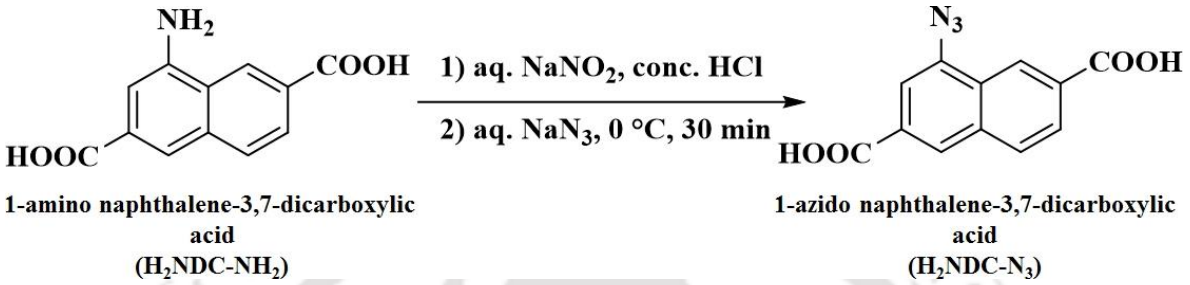

Scheme 4.1 Scheme for the preparation of $H_2NDC\text{-}N_3$ linker.

In the first step, a solution of sodium nitrite (1.021 g, 14.79 mmol) in water (18 mL) was added dropwise into a mixture of $H_2NDC\text{-}NH_2$ (1.40 g, 6.05 mmol) linker, conc. HCl (18 mL), and water (18 mL) at 0 °C. The mixture was stirred for 30 min. In the second step, a solution of sodium azide (0.46 g) in water (18 mL) was added in the reaction mixture. During addition, the temperature of the reaction mixture was maintained at 0 °C. Afterward, the reaction mixture was stirred for overnight at room temperature. The resulting brownish precipitate was collected by vacuum filtration, washed with cold ice-water, and dried under reduced pressure to yield 1-azido naphthalene-3,7-dicarboxylic acid abbreviated as $H_2NDC\text{-}N_3$. The yield was 1.2 g (6.1 mmol, 61 %). ^{1}H-NMR (400 MHz, DMSO-d_6): δ = 7.81 (s, 1H), 8.48 (s, 1H), 8.10 (d, 1H), 8.24 (d, 1H), 8.69 (s, 1H) and 13.47 (s, 2H) ppm. ^{13}C NMR (100 MHz, DMSO-d_6): δ = 167.32, 166.98, 138.16, 135.15, 130.83, 130.78, 130.44, 127.32, 127.12, 127.03, 124.66 and 114.40 ppm. ESI-MS (m/z): 256.058 for $(M\text{-}H)^-$ ion (M = mass of $H_2NDC\text{-}N_3$ linker). The presence of azide functional group in the linker was confirmed by the existence of strong absorption band at 2114 cm^{-1} in the FT-IR spectrum. In Figures 4.1-4.4, the ^{1}H NMR, ^{13}C NMR, mass and FT-IR spectra of $H_2NDC\text{-}N_3$ linker are shown.

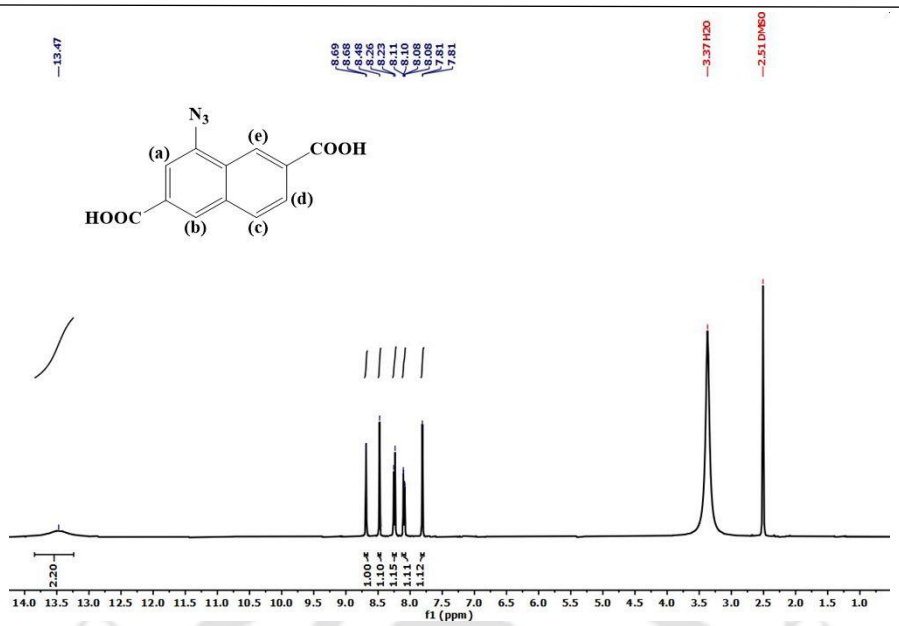

Figure 4.1 ^{1}H NMR spectrum of $H_2NDC\text{-}N_3$ linker in DMSO-d_6.

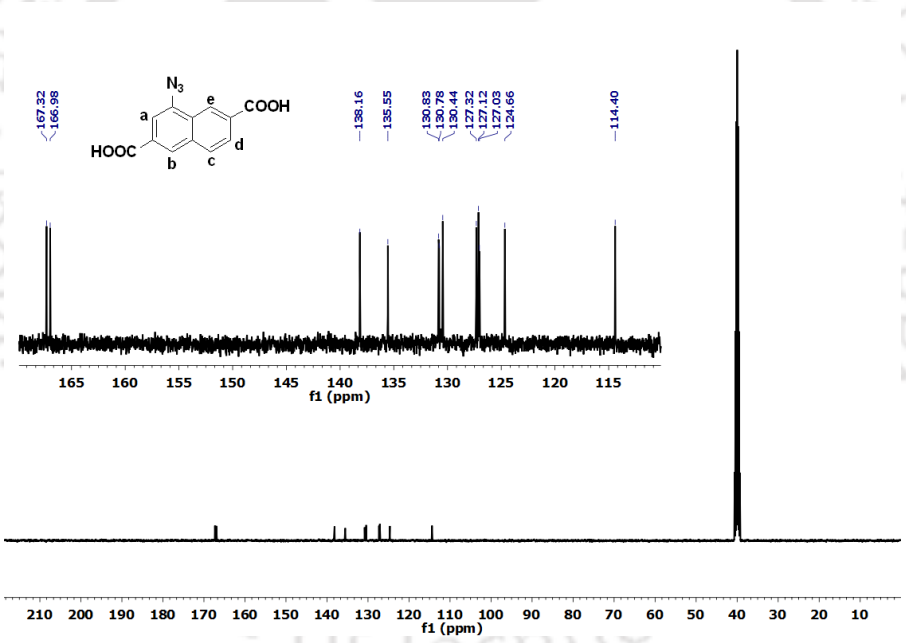

Figure 4.2 ^{13}C NMR spectrum of $H_2NDC\text{-}N_3$ linker in DMSO-d_6.

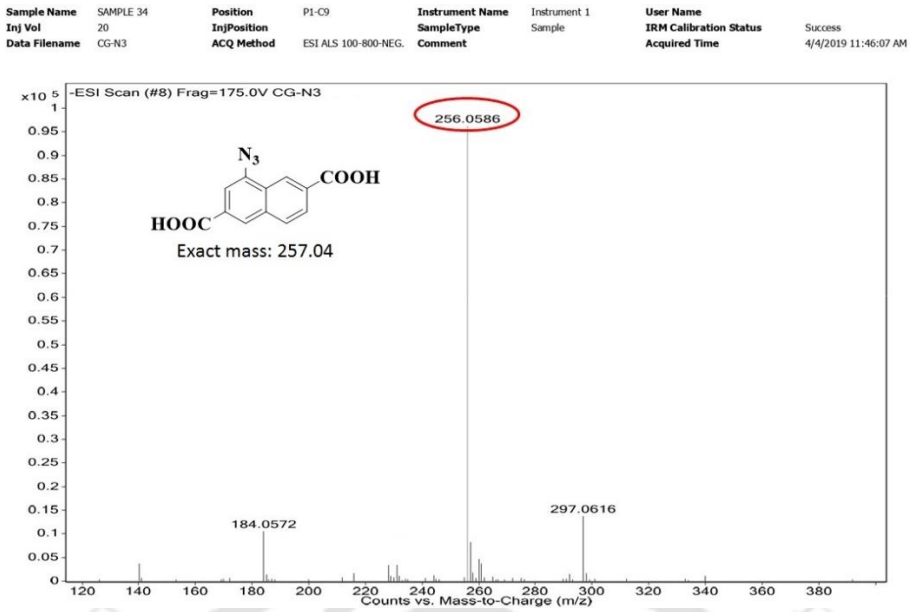

Figure 4.3 HR-MS spectrum of H_2NDC-N_3 linker in MeOH.

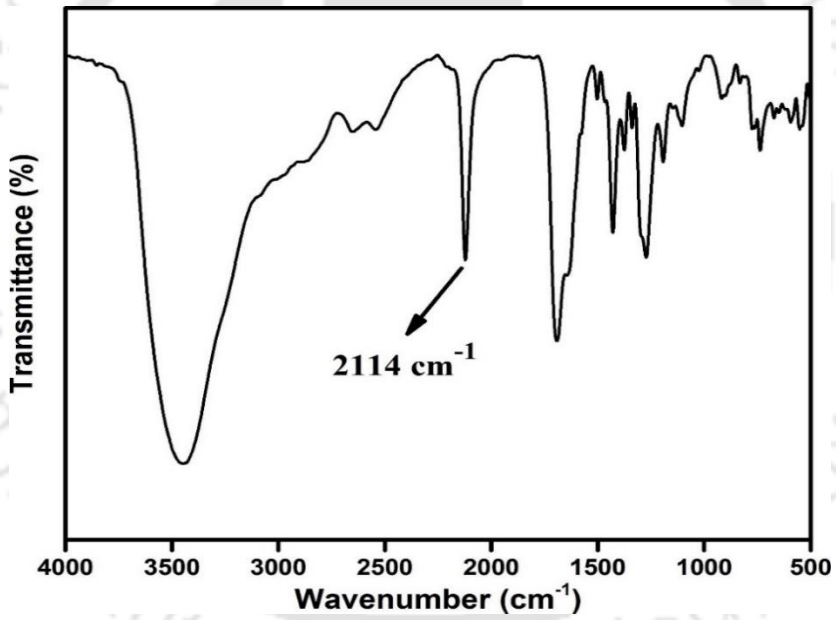

Figure 4.4 FT-IR spectrum of H_2NDC-N_3 linker.

4.2.3 Synthesis of $[Zr_6O_4(OH)_4(NDC\text{-}N_3)_6]\cdot 12H_2O\cdot 10DMF$ (DUT-52-N_3, 3)

For the synthesis of **3**, $ZrCl_4$ (18 mg), H_2NDC-N_3 linker (20 mg), *N*,*N*-dimethylformamide (DMF) (3 mL) and acetic acid (100 µL) were mixed in a glass tube which was sealed and heated at 110 °C for 20 h. After the completion of reaction, the glass tube was allowed to cool to room temperature and the precipitate was collected using vacuum filtration technique. The brown color precipitate was thoroughly washed with acetone. Compound **3** was obtained in dry form after being kept at 50 °C for 5 h inside an oven. The yield of product is

25 mg (0.01 mmol, 85%) based on metal salt. FT-IR (KBr, cm^{-1}): 3432 (br), 2114 (vs), 1656 (s), 1607 (sh), 1585 (sh), 1419 (s), 1288 (w), 1248 (w), 1105 (s), 926 (s), 791 (s), 665 (s), 482 (s).

4.2.4 Activation of 3

In the activation process, **3** (100 mg) was stirred overnight in methanol (20 mL) under ambient conditions. Later on, the compound was filtered off and heated under high vacuum at 80 °C for 5 h. The thermally activated MOF material has been indicated as **3'**.

4.2.5 Fluorescence sensing investigations

In a 5 mL glass vial, 2 mg of **3'** was taken and 4 mL of water was added into it. After that, the mixture was sonicated for 1 h and kept undisturbed at ambient conditions for 24 h to get a stable suspension of the compound for fluorescence titration measurements. In a quartz cuvette, 200 µL of the suspension of **3'** was taken and 2800 µL of water was added to make the solution up to 3 mL. Then, the fluorescence spectrum was recorded. In this 3 mL suspension of ***3'***, solution of Na_2S was added gradually up to 10 equivalents per azide group. Here, we used Na_2S as a source of H_2S. For the selectivity experiments, different selected analytes (3 equivalents) were added gradually and fluorescence spectra were collected. Afterward, we again added 3 equivalents of Na_2S to the cuvette which already contained the competitive analytes. All these experiments were performed upon excitation at 360 nm. All these emission spectra were recorded in the range of 380-700 nm. The fold enhancement of intensity was measured by the formula: I/I_0, in which I_o and I are the fluorescence intensity preceding and following the addition of analyte, respectively.

4.3 Results and discussion

4.3.1 Synthesis and characterization of 3 and 3'

Before determining the optimized procedure for the synthesis of **3**, we performed many reactions by changing three different zirconium salts ($ZrCl_4$, $ZrOCl_2{\cdot}8H_2O$ and $ZrO(NO_3)_2{\cdot}xH_2O$) with modulators like acetic acid, benzoic acid, formic acid and trifluoroacetic acid in two different solvents (DMF and *N,N*-diethylformamide). The optimized conditions were obtained using $ZrCl_4$ as a metal salt and acetic acid as a modulator in DMF. After filtration, a homogeneous phase of octahedral nanosized crystals was obtained (Figure 4.5).

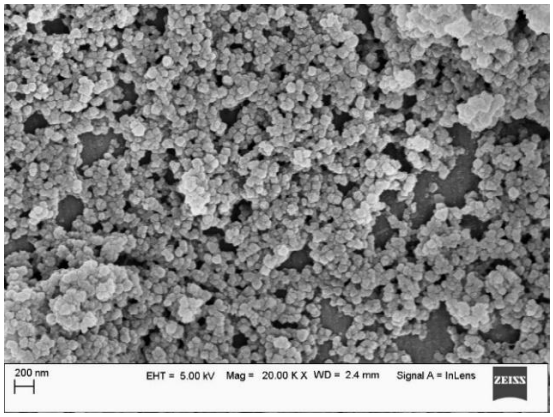

Figure 4.5 FE-SEM image of **3**.

XRPD experiments were performed to check the crystallinity, phase purity and structural integrity of the prepared compound. The XRPD pattern of as-synthesized **3** matches closely with the simulated XRPD pattern of the previously reported DUT-52 compound (Figure 4.6) [45]. We conducted indexing of experimental XRPD data collected at room temperature to obtain the unit cell parameters. Table 4.1 displays the indexing results, which point out that the lattice parameters are comparable with DUT-52. We also performed Pawley fit of the experimental XRPD data (Figure 4.7). The result of Pawley fit showed good similarity with the simulated diffractogram of DUT-52. Hence, the framework of the prepared compound exhibits the same topology as DUT-52. In addition, the evident similarity between the XRPD patterns of the as-synthesized and thermally activated samples of **3** indicates that the compound maintained its integrity of the framework after the thermal activation process (Figure 4.6).

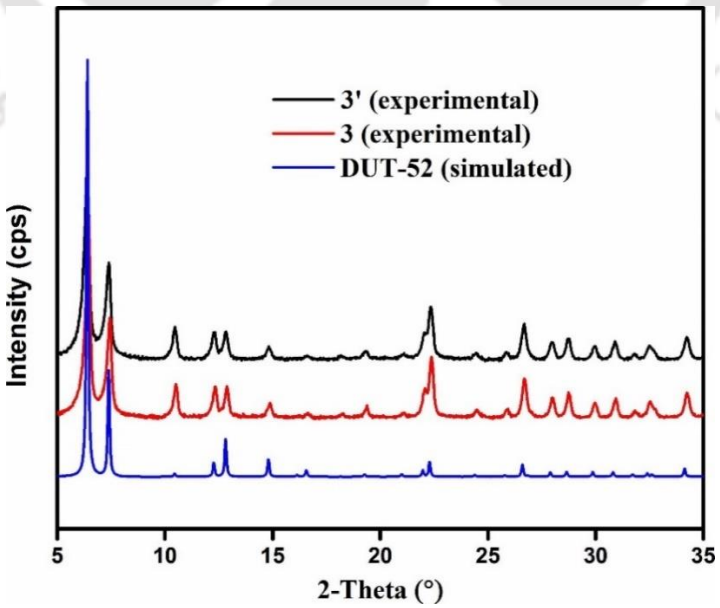

Figure 4.6 Comparison of the experimental XRPD data of **3** and **3'** with simulated XRPD data of DUT-52 MOF.

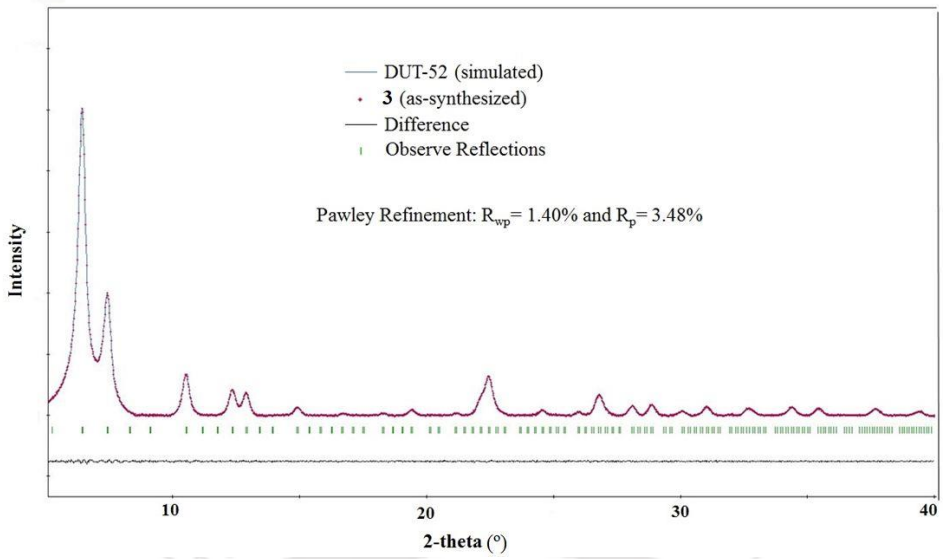

Figure 4.7 Pawley fit for the XRPD pattern of as-synthesized **3**. Blue lines and red dots denote simulated and observed patterns, respectively. The peak positions and difference plot are displayed at the bottom (R_p = 3.48, R_{wp} = 1.40).

Table 4.1 Unit cell parameters of **3** obtained by indexing its XRPD data collected at room temperature. The obtained values have been compared with the SCXRD data of Zr-DUT-52 MOF collected at room temperature.

Compound name	DUT-52-N_3 (**3**)	Zr-DUT-52[45]
Crystal System	Cubic	Cubic
a = b = c (Å)	23.743 (3)	23.910 (3)
V (Å^3)	13384 (29)	13669 (9)

The FT-IR spectra of both **3** and **3'** reveal characteristic frequencies at around 1610 and 1419 cm^{-1}, which correspond to asymmetrical and symmetrical stretching vibrations of coordinated –COO group, respectively. The azide stretching frequency is observed at around 2114 cm^{-1} for **3** and **3'** (Figure 4.8). The absence of absorption band at 1661 cm^{-1} in the IR spectra of **3** and **3'** as compared to free linker (Figure 4.4) indicates that deprotonation of the linker has been accomplished. The sharp peak at 1652 cm^{-1} for **1** is due to the stretching vibration of carbonyl group from DMF molecules. This peak is absent after activation of the compound, which indicates that the activation of the compound has been accomplished.

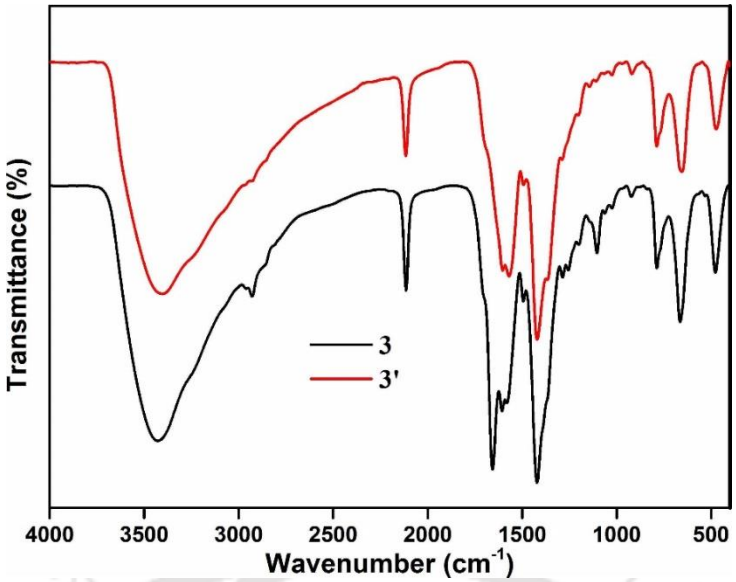

Figure 4.8 FT-IR spectra of **3** (black) and **3'** (red).

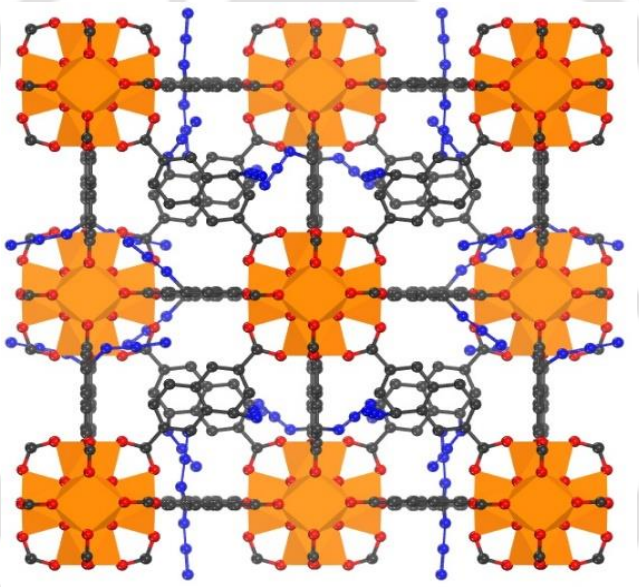

Figure 4.9 Perspective view of the simulated three-dimensional cubic framework of DUT-52-N_3 MOF drawn in ball-and-stick model. Color codes: Zr, orange polyhedra; C, grey; O, red; N, navy blue.

4.3.2 Structure description

The similarity between the XRPD pattern of azide functionalized DUT-52 (DUT-52-N_3, **3**) material with the unfunctionalized DUT-52 compound revealed that **3** has similar structure as the parent DUT-52 MOF.[45] Kaskel and co-workers already reported the structure of unfunctionalized DUT-52 MOF. It has face centered cubic structure with $Fm\bar{3}m$ as space group. The simulated cubic three-dimensional structural framework of **3** is shown in Figure 4.9. The cubic framework of **3** has hexanuclear $[Zr_6O_4(OH)_4]^{2+}$ building units. The three-

dimensional cubic framework is formed by interconnecting these building units through carboxylate groups of twelve NDC-N_3 linkers. Two types of structural voids are observed within the framework: larger octahedral and smaller tetrahedral cages. The linking between these two types of voids occur though triangular widows.

4.3.3 Gas adsorption properties

To establish the permanent microporosity of material **3'**, a nitrogen sorption experiment was performed. Before the gas adsorption experiment, we stir the **3'** with methanol for another 24 h and activated under vacuum at 80 °C for 5 h. As shown in Figure 4.10, the adsorption-desorption isotherms represent typical Type I nature. The surface area was determined by Brunauer-Emmett-Teller (BET) method and it was calculated to be 505 m^2/g. This value is much lower than the pristine Zr-DUT-52 MOF (1399 $m^2\ g^{-1}$).[45] Nevertheless, this value is higher than the previously reported dinitro functionalized Zr-DUT-52 MOF (S_{BET} = 330 m^2g^{-1}).[46] The XRPD pattern (Figure 4.11) revealed that **3'** retained its structural integrity after BET analysis with slight decrease in crystallinity. The lower BET surface area of **3'** can be attributed to the incomplete activation process. The azide groups attached with organic linkers are easily decomposed after prolonged heating at higher temperature, thus disfavouring the activation of azide functionalized MOFs at higher temperature [40, 43, 47-48]. Furthermore, CO_2 adsorption experiments were performed at two different temperatures. As illustrated in Figure 4.12, it was confirmed that the CO_2 uptakes of **3'** were 2.65 and 1.62 mmol/g at 0 and 25 °C, respectively.

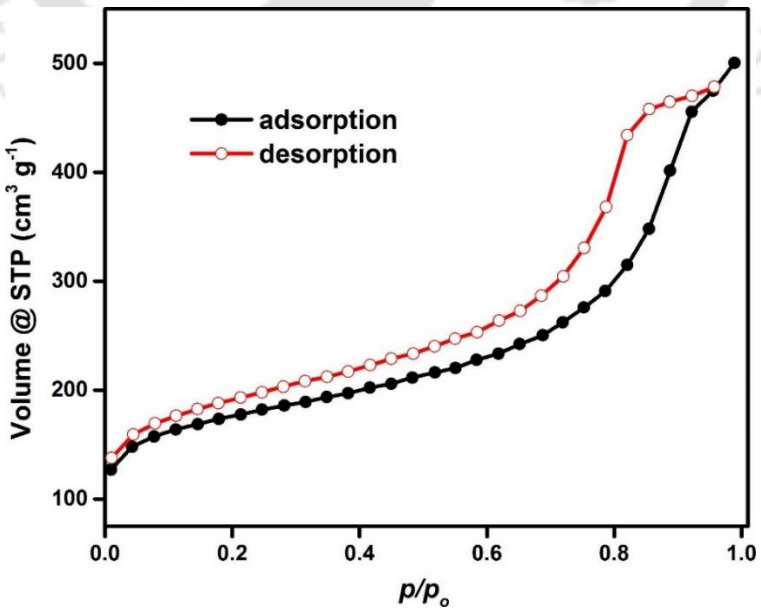

Figure 4.10 N_2 sorption isotherms of **3'** measured at -196 °C.

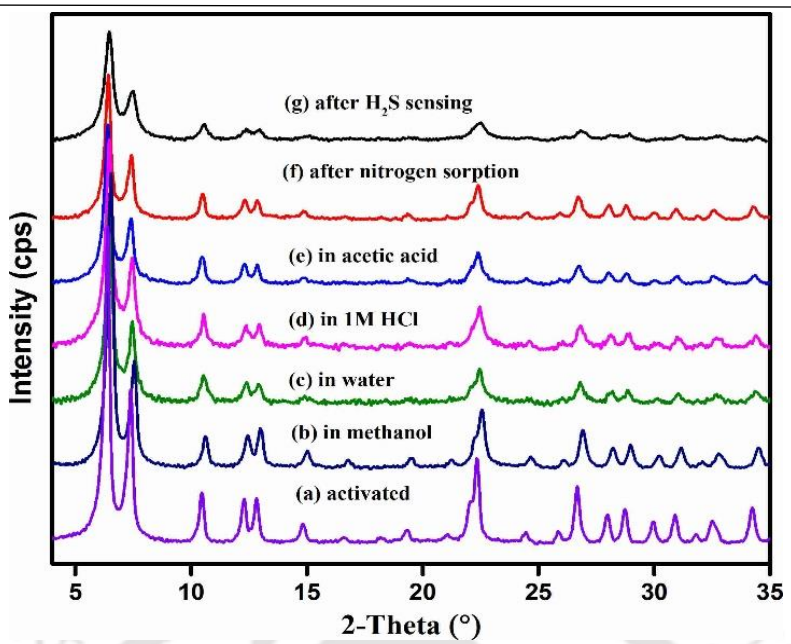

Figure 4.11 Comparison of XRPD data to demonstrate the chemical stability of **3'** in (b) methanol, (c) water, (d) 1M HCl, and (e) 17.4 (M) acetic acid. The XRPD patterns after (f) nitrogen sorption and (g) H_2S sensing are also compared.

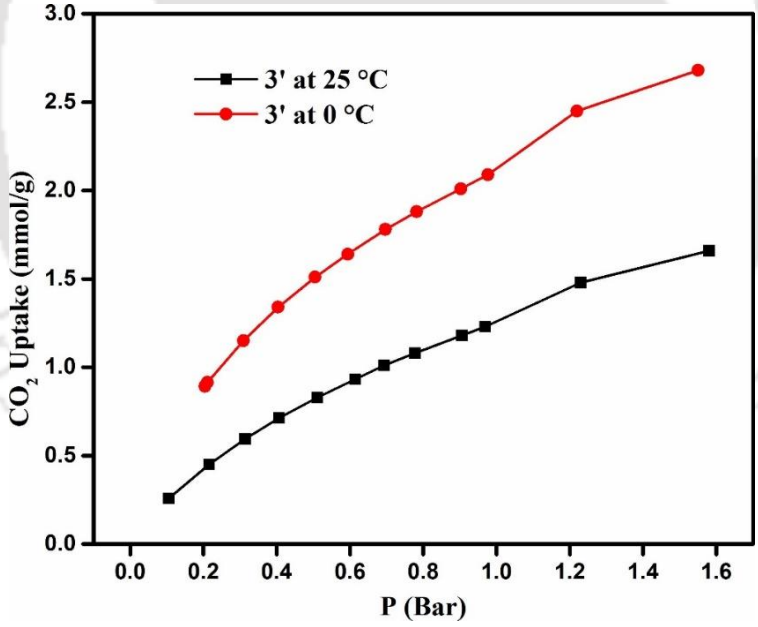

Figure 4.12. CO_2 sorption isotherms of **3'** at 0 °C and 25 °C.

4.3.4 Thermal and chemical stability

Thermogravimetric analyses (TGA) were performed to examine the thermal stability of **3** and **3′**. The experimental observations revealed that **3** and **3'** are thermally stable up to 320 °C under an argon atmosphere (Figure 4.13). In TG curve of **3**, initially from 25-125 °C, 6.7% weight loss is observed due to the removal of twelve water molecules per formula unit

(calculated: 6.8 %). The second weight loss of 22.3% is observed in the range of 128-320 °C due to loss of ten DMF molecules per formula unit (calculated: 23.1%), which was adsorbed inside the pore of the material during synthesis. Afterward, the decomposition of the compound started due to the loss of organic linker. The initial weight loss of 13.7% for **3'** from 25-320 °C was observed because of the loss of water molecules which was absorbed during storage.

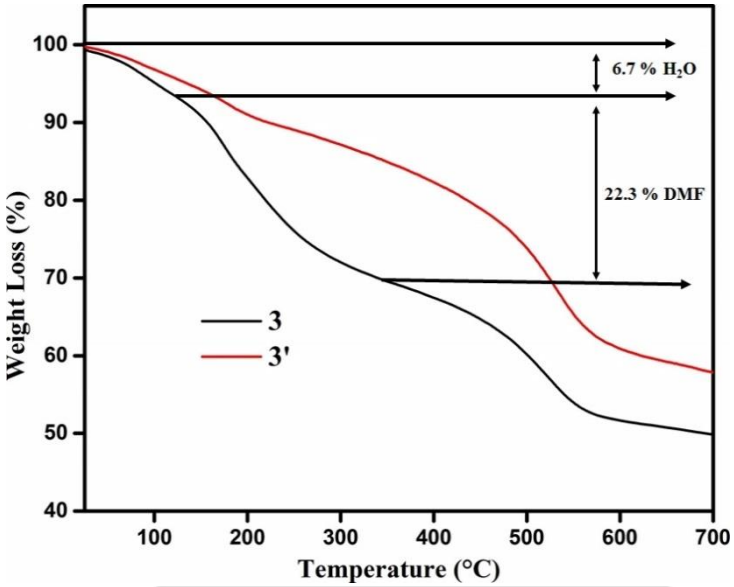

Figure 4.13 TG curves of **3** (black) and **3'** (red) recorded at argon atmosphere in the temperature range 25-700 °C with a heating rate 10 °C min^{-1}.

To examine the chemical stability, **3'** was stirred overnight in water, methanol**,** 1 (M) HCl and 17.4 (M) acetic acid solutions. After that, the samples were collected by vacuum filtration, dried in an oven for 3 h at 80 °C and the structural features of these materials were examined by XRPD technique. As shown in Figure 4.11, the compound retained its structural features (and thus structural durability) after treatment with water, acetic acid, methanol and 1(M) HCl solutions. Similar experiments were also performed after nitrogen sorption and H_2S sensing, which revealed the retention in structural integrity. To evaluate more about the chemical stability, we perform the BET surface area measurement experiment after treatment with these solvents (Figure 4.14). As shown in table 4.2, BET surface area value was reduced from 505 $m^2 g^{-1}$ to 335 $m^2 g^{-1}$ in case of acetic acid whereas other are calculated to be near 450 $m^2 g^{-1}$. There would be possibility of some structure collapse between metal cluster and linker at 17.4 M acetic acid concentration, which in turn decreased the BET surface area. Therefore, the conclusion could be drawn that **3'** is highly stable in methanol, water and 1 M HCl but somewhat less stable in acetic acid although, it retains its XRPD pattern and morphology in acetic acid.

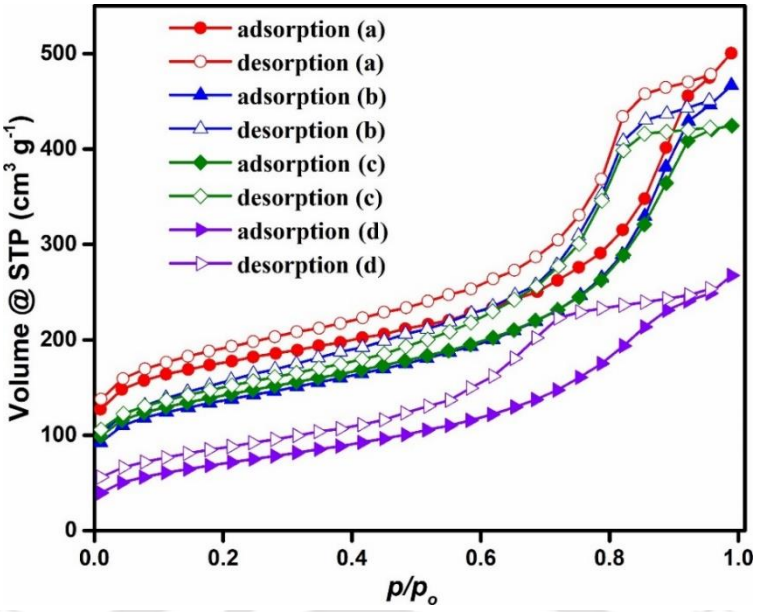

Figure 4.14 N_2 adsorption and desorption isotherm after treatment with (a) methanol, (b) 1 M HCl, (c) water, (d) acetic acid of **3'** measured at -196 °C. (Note- before analysis, each sample was again activated after treatment with these solvents).

Table 4.2 Mass balance before and after treatment with different solvents and corresponding BET surface area of **3'**.

Solvents	Mass of **3'** Taken (mg)	Mass of **3'** Left[(a)] (mg)	BET Surface Area ($m^2\ g^{-1}$)
Methanol	100.0	85.3	505
1 M HCl	100.0	76.2	448
Water	100.0	78.1	463
Acetic acid	100.0	43.1	335

[(a)] **3'** was stir with these solvents for overnight and then again we activated the sample by stirring with methanol for overnight and heated under vacuum at 80 °C for 5 h, then we take the mass of the sample.

4.3.5 Photoluminescence properties

Recently, several Zn(II), Al(III), Zr(IV) and Ce(IV) based MOFs have been reported which have the properties of selective sensing towards H_2S.[40, 43, 46, 49-50] Our group has also investigated azide functionalized CAU-10, UiO-66 and MIL-53 MOFs for the sensitive and quick fluorogenic detection of H_2S.[40, 43, 50]

The emission and excitation spectra of **3'** were measured at room temperature in water (Figure 4.15). The excitation spectrum (black line, obtained monitoring the emission at 490 nm) showed a sharp peak at 360 nm. The emission spectrum (red line, obtained by excitation at 360 nm) showed emission band at 490 nm, which was generated by the organic linker.

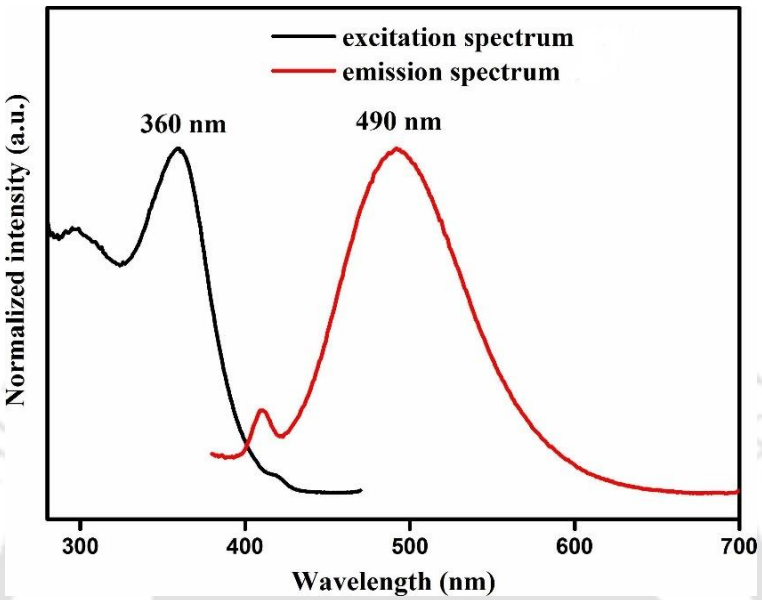

Figure 4.15 Excitation and emission spectrum of **3'**.

To check the sensing properties towards H_2S, we have executed fluorescence experiments with DUT-52-N_3 (**3'**). Before the treatment with H_2S, **3'** suspension showed weak fluorescence. But, after the treatment with H_2S, azide moiety has been reduced to amine group. Hence, the fluorescence intensity of **3'** was enhanced dramatically by H_2S treatment (Figure 4.16). The reason for such enhancement in intensity is the donation of electrons into naphthalene ring by amine group.[46, 51] To determine the concentration of H_2S required to attain saturation in the fluorescence emission intensity, fluorescence titration experiments were accomplished. We used Na_2S as the source of H_2S. We collected the fluorescence spectra of **3'** in the range of 380-700 nm (λ_{ex} = 360 nm and λ_{em} = 490 nm) upon gradual addition of Na_2S solution (0 to 10 equivalents per azide group). As demonstrated in Fig. 4, after addition of 3 equivalents of Na_2S, saturation in fluorescence intensity was observed. After adding 3 equivalents of Na_2S, there was an increment of almost 33 folds in fluorescence intensity of **3'** in water. We have also examined the fold increment of fluorescence intensity after the addition of Na_2S solution in HEPES buffer (pH = 7.4, 10 mM) (Figure 4.17). The fluorescence intensity of **3'** in HEPES buffer increased by 9 folds after the addition of 10 equivalents of Na_2S. Since the fold increment of emission intensity is higher in water as compared to HEPES buffer, we conducted all other fluorescence detection experiments in water.

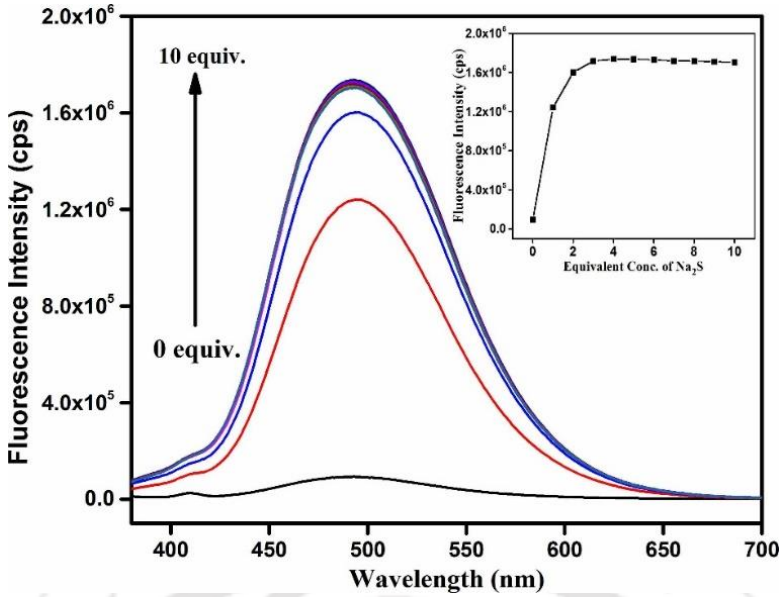

Figure 4.16 Fluorescence rise of **3'** in water with increasing concentration of Na_2S (λ_{ex} = 360 nm, λ_{em} = 490 nm). Inset: fluorescence intensity is plotted against concentration of Na_2S.

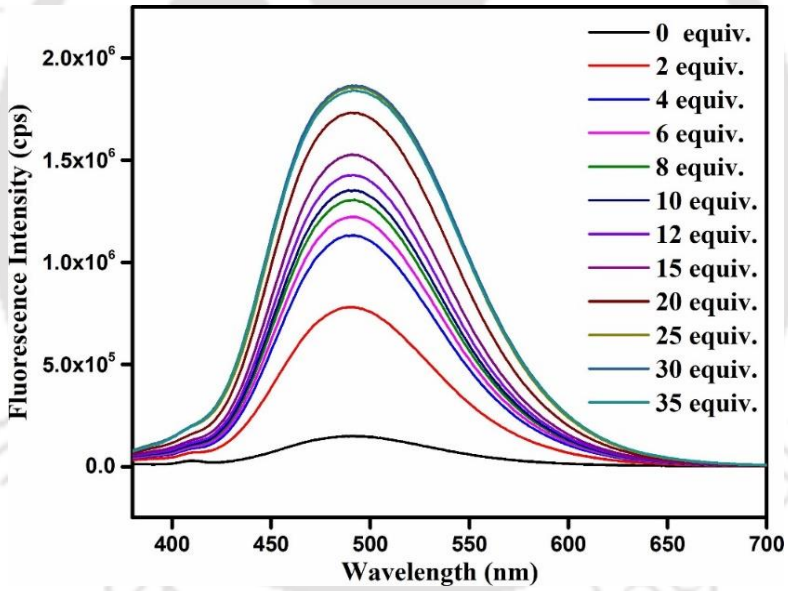

Figure 4.17 Fluorescence increment of **3'** in 10 mM HEPES buffer (pH = 7.4) with increasing concentration of Na_2S (λ_{ex} = 360 nm, λ_{em} = 490 nm).

Time dependent H_2S sensing experiments were conducted to determine the response time of the probe for H_2S. In a cuvette, 200 µL of **3'** dispersion was added to 2800 µL of water and fluorescence spectra were measured. Afterward, Na_2S solution (3 equivalents per azide group) was added into the suspension and again fluorescence spectra were collected with a time interval of 1 min for 15 min. The addition of Na_2S solution led to gradual enhancement in the intensity from "turn-off" state to the "turn-on" state (Figure 4.18). The enhancement in intensity was observed until 2 min. After that, saturation in fluorescence intensity was

observed. This means that within 2 min, almost all the azide groups were converted into amine groups. The response time is faster than that of most of the reported MOFs for H_2S sensing (Table 4.3).[40, 52-57] The result proved that this DUT-52-N_3 MOF is a very promising fluorescent "turn-on" probe towards H_2S sensing.

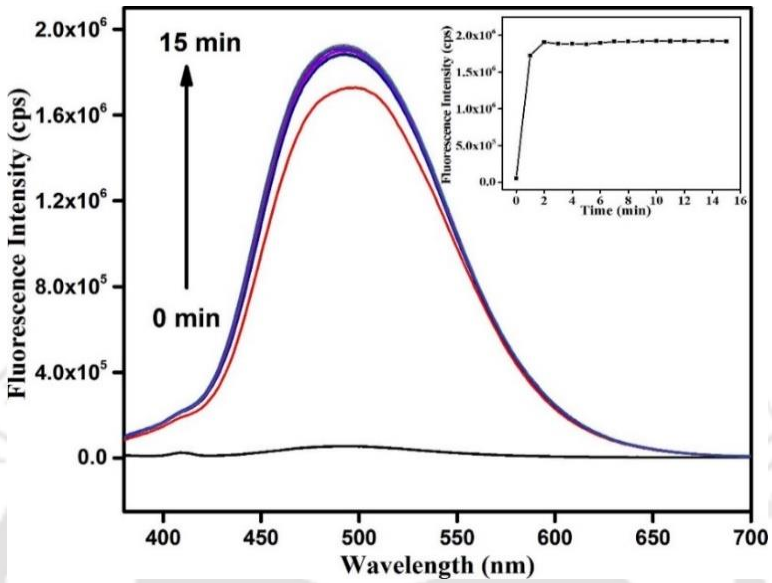

Figure 4.18 Fluorescence variation of **3'** after gradual addition of Na_2S (3 equiv. per azide group) with a time interval of 1 min up to 15 min. Inset: plot of fluorescence intensity versus time (λ_{ex} = 360 nm and λ_{em} = 490 nm).

Table 4.3 Comparison of the response time, detection limit and analyte used of various existing MOFs and other materials for the fluorescence detection of H_2S.

Sl. No.	Sensor Material	Type of Material	Method Used	Response Time (s)	LOD	Linear Range	Analyte	Ref.
1	Ce-UiO-66-N_3	MOF	fluorescence	760	12.2 µM	-	NaSH	58
2	Ce-UiO-66-NO2	MOF	fluorescence	760	34.84 µM	-	NaSH	58
3	CAU-10-N_3	MOF	fluorescence	420	2.65 µM	-	Na_2S	43
4	Eu^{3+}/Cu^{2+}@ UiO-66-$(COOH)_2$	MOF	fluorescence	30	5.45 µM	0-625 µM	NaSH	59

5	DUT-52-N_3	MOF	fluorescence	120	0.50 µM	0-1.67 µM	Na_2S	this work
6	Zr-UiO-66-N_3	MOF	fluorescence	180	118 µM	-	Na_2S	56
7	DUT-52-$(NO_2)_2$	MOF	fluorescence	3300	20 µM	100-700 µM	Na_2S	60
8	IRMOF-3-N_3	MOF	fluorescence	<120	28.3 µM	-	NaSH	61
9	Zr-UiO-66-NO_2	MOF	fluorescence	460	188 µM	-	Na_2S	62
10	Zr-UiO-66-$(NO_2)_2$	MOF	fluorescence	2400	14.14 µM	-	Na_2S	39
11	Al-MIL-53-N_3	MOF	fluorescence	180	0.09 µM	-	Na_2S	40
12	Tb^{3+}@Cu-MOF	MOF	fluorescence	120	1.2 µM	0-5 mM	Na_2S	52
13	$[EuCu(pydc)_2(ox)_{0.5}(H_2O)_3 \cdot 1.5H_2O]_{2n}$	MOF	fluorescence	120	0.13 µM	130 nM, +∞	H_2S	63
14	MN-ZIF-90	MOF	fluorescence	510	25 µM	-	H_2S	54
15	$[CuL(AlOH)_2]_n$	MOF	fluorescence	360	0.02 µM	-	NaSH	64
16	Al-MIL-101-N_3	MOF	fluorescence	-	100 µM	-	Na_2S	65
17	MN-ZIF-90	MOF	fluorescence	-	-	-	-	66
18	Al-TCPP-Cu	MOF	fluorescence	-	-	0-100 µM	-	67
19	CAU-10-V-H	MOF	fluorescence	10	1.65 µM	-	NaSH	68

20	UiO-66-$CH=CH_2$	MOF	fluorescence	10	6.46 µM	10-600 mM	NaSH	69
21	SHS-M1 SHS-M2	organic molecule	fluorescence	- -	0.2 µM 0.4 µM	-	Na_2S	70
22	NHS1	organic molecule	fluorescence	4800	0.02 µM	0.2-5 µM	NaSH	71
23	Cy-N_3	organic molecule	fluorescence	1200	0.08 µM	-	NaSH	72
24	SFP-1 SFP-1	organic molecule	fluorescence	7200 14400	- -	- -	Na_2S	73
25	WSP5	organic molecule	fluorescence	-	0.047 µM	-	NaSH	74
26	probe 1	organic molecule	fluorescence	3600	2.4 µM	-	NaSH	75
27	QCM coated with PPy/TiO_2 film	quartz-crystal microbalance	Frequency shift	-	10 ppm	-	H_2S	76
28	polymer P1	semiconducting polymer	conductivity impedance	-	1 ppb	-	H_2S	77
29	polyaniline nanowires-gold nanoparticles	conducting polymer	conductivity impedance	<120	0.1 ppb	0.1-100 ppb	H_2S	78
30	nafion membrane (H_2SO_4 treated)	solid polymer electrolyte	amperometry	9	100 ppb	0.1-100 ppm	H_2S	79
31	In_2O_3 whiskers	semi conducting oxide	conductivity impedance	120-210	200 ppb	-	H_2S	80

32	CuO-BSST	semi conducting oxide	conductivity impedance	10	4-10 ppb	-	H_2S	81
33	ZnO rod	semi conducting oxide	conductivity impedance	-	50 ppb	-	H_2S	82
34	bare gold NPs	nanoparticles	UV-vis spectroscopy	-	0.08 µM	0.5-10 µM	Na_2S	83
35	PSS-PA-Cu NC aggregates	Nano cluster aggregates	fluorescence	-	0.65 µM	1-20 µM	Na_2S	84
36	SF4	organic molecule	fluorescence	-	0.125 µM	-	NaSH	85
37	π-conjugation rhodamine-NBD	organic molecule	fluorescence	-	0.37 µM	-	Na_2S	86
38	CTN	organic molecule	fluorescence	-	90 nM	0-36 µM	NaSH	87
39	DNS-Az	organic molecule	fluorescence	-	1 µM	-	Na_2S	88
40	cpGFP-Tyr66pAzF	organic molecule	fluorescence	420	-	-	NaSH	89

To estimate the selectivity of **3'** towards H_2S over other competitive analytes, we conducted a series of fluorescence experiments after the addition of equal amounts of all selected analytes. As shown in Figure 4.19, other selected competitive analytes (alanine, cystine, NaCl, NaBr, NaI, $Na_2S_2O_3$, $Na_2S_2O_3{\cdot}5H_2O$, $NaHSO_3$, $NaNO_2$, $NaNO_3$, Na_2SO_3, Na_2SO_4, serine and glutathione) have very less effects on the emission intensity of **3'** as compared to Na_2S. The fluorescence intensity increased by only 1 to 3 folds after addition of other interfering analytes. In contrast, a remarkable luminescence increment up to 33 folds was observed for **3'** after addition of Na_2S. These experimental results corroborate the great selectivity of the DUT-52-N_3 probe for fluorometric H_2S detection.

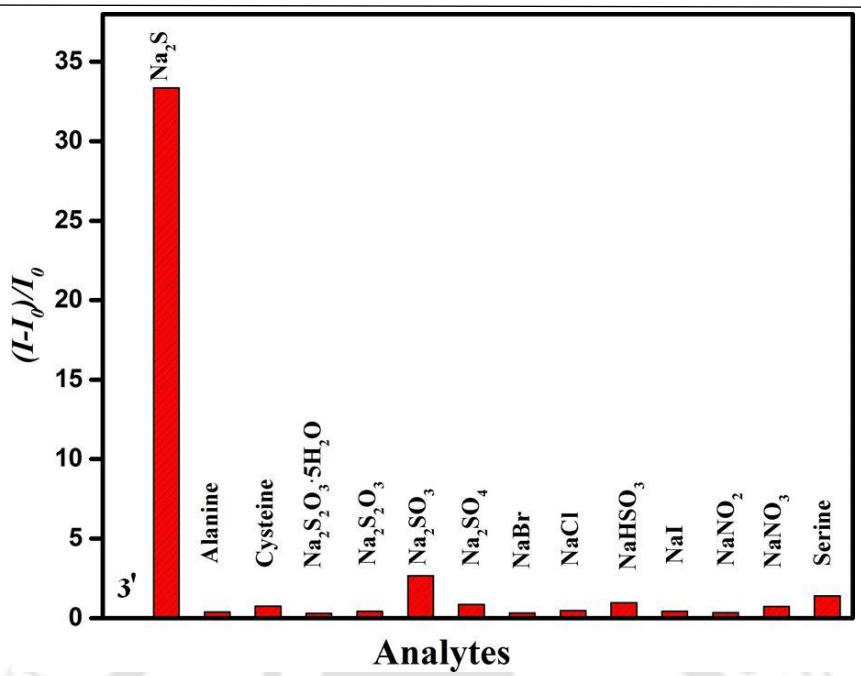

Figure 4.19 Relative fluorescence intensity enhancement of **3'** in water towards addition of different analytes (3 equivalents for each azide group).

Competitive fluorometric detection experiments were conducted to determine the selectivity of **3'** for H_2S in presence of other biologically relevant analytes. We recorded the fluorescence spectra of **3'** in presence of different selected analytes (3 equivalents per azide functionality). After that, Na_2S (3 equivalents per azide functionality) was added into those solutions which already consisted the competitive analytes and emission spectra were collected. It is clearly seen from Figure 4.20 that other biologically relevant analytes did not increase the fluorescence intensity of **3′**. Indeed, the fluorescence of **3'** increased significantly after the addition of Na_2S solution into the solution consisting of **3'** and other analytes. This is not surprising to observe that glutathione showed strong reducing behavior towards **3'**. Glutathione is a strong reducing agent.[90-92] It is expected that glutathione can react with the azide group of probe before reaction of the probe with Na_2S. Hence, in case of glutathione, lower turn-on fluorescence intensity of **3'** was observed. Similar interference from glutathione was previously observed for MOF type H_2S probes.[39, 46]

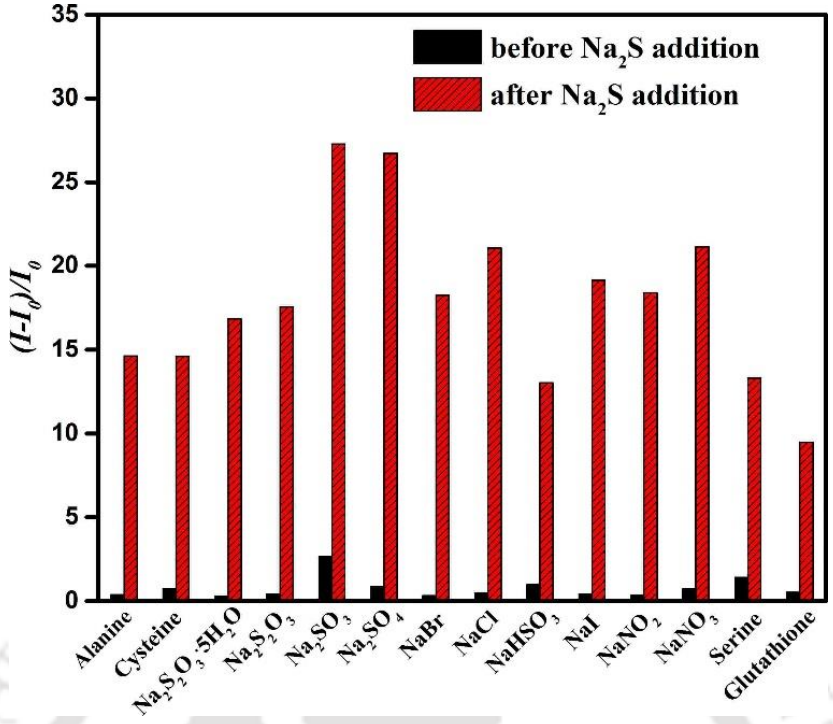

Figure 4.20 Fluorescence enhancement properties of **3'** in water upon addition of different analytes (black) and further addition of H_2S into the same mixture (red).

The detection limit value was estimated for H_2S at a lower concentration, which showed the effectiveness of **3'** towards detection of H_2S. A linear curve was obtained by plotting the fluorescence intensity against the concentration of Na_2S in lower range (Figure 4.21). We carried out this experiments in triplicate to determine stahdard deviation of measurements and the reoroducibility of the analytical process. The error bar in Figure 4.21 represent three standard deviation. The formula used for the calculation of limit of detection (LOD) was $3\sigma/K$, where σ stands for standard deviation and *K* stands for slope of the linear curve.[93] The observed LOD for **3'** was 0.50 μM. This LOD value for H_2S detection is lower than the previously reported dinitro functionalized DUT-52 MOF (LOD = 20 μM).[46] This LOD value also lies among the lowest concentration range for the fluorogenic sensing of H_2S by MOFs (Table 4.3).[39, 43, 53, 56-57] Although some other type of materials showed lower detection limit values, the response time is relatively short for our MOF probe. Thes results demonstrate that probe **3′** has a clear-cut advantages (in terms of sensitivity and response time) over existing fluorescent probes for sensing of H_2S.

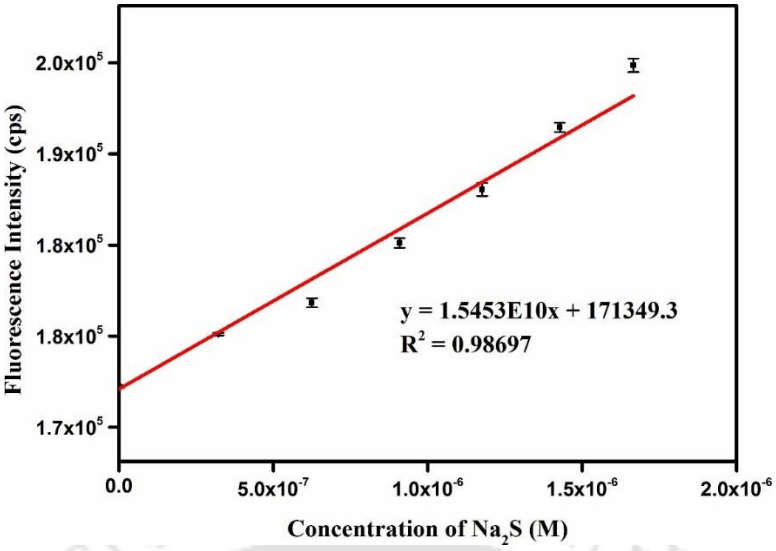

Figure 4.21 Change of fluorescence intensity of the aqueous suspension of **3'** against concentration of Na_2S. This curve is relevant for the estimation of LOD. The error bars indicate the standard deviations of three measurements.

4.3.6 Mechanism for sensing of H_2S

The expected mechanism of H_2S sensing is the reduction of azide functionality (present in **3'**) to an electron donating amine group. To prove this mechanism, we conducted mass spectrometry, FT-IR and ^1H NMR analyses. The FT-IR spectroscopic data revealed that when Na_2S was added to **3'**, the characteristics signal of azide at 2114 cm^{-1} disappeared almost completely, which was observed before the treatment of **3'** with Na_2S (Figure 4.22). In the absence of Na_2S, the digested sample of **3'** showed the most intense peak at m/z = 256.1773 (negative ion mode) in its mass spectrum, which can be assigned to the $(M-H)^-$ ion of H_2NDC-N_3 linker (Figure 4.23). In contrast, the mass spectrum of the digested sample of **3'** after treatment with Na_2S showed peak at m/z = 230.1745 (negative ion mode), which corresponds to $(M-H)^-$ ion of reduced H_2NDC-N_3 linker i.e. $H_2NDC-NH_2$ (Figure 4.24). From this experiment, we can conclude that the azide groups of sensor **3′** have been completely converted into amine groups. It is observed from the ^1H NMR spectra (Figure 4.25) that the aromatic protons of $NDC-NH_2$ linker in **3'** (after treatment with Na_2S) are upfield shifted as compared to $NDC-N_3$ linker in **3'** (**3'** was digested in DMSO/HF for NMR measurement). The peak for the protons from $–NH_2$ functionality is absent, which can be attributed to their rapid exchange with D_2O.[94] In the digested Na_2S-treated material, no peak for the aromatic protons of the azide functionalized NDC was observed. Hence, we can conclude that azide functionalized NDC is fully converted to amine functionalized NDC during H_2S sensing.

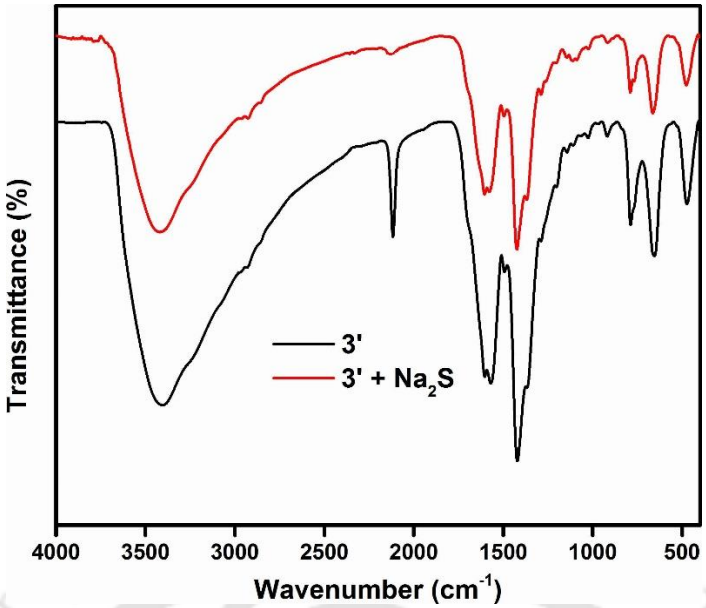

Figure 4.22 FT-IR spectra of **3'** before and after treatment with Na_2S.

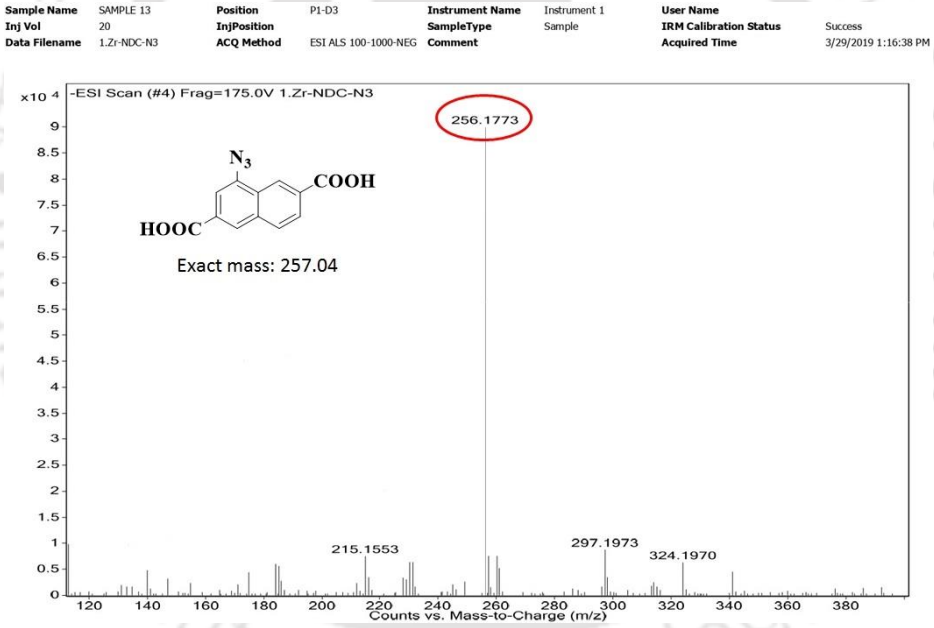

Figure 4.23 HR-MS spectrum of **3'** (digested in MeOH/HF) showing m/z peak at 256.1773 (negative ion mode), which corresponds to $(M-H)^-$ ion (M = mass of $H_2NDC\text{-}N_3$ linker).

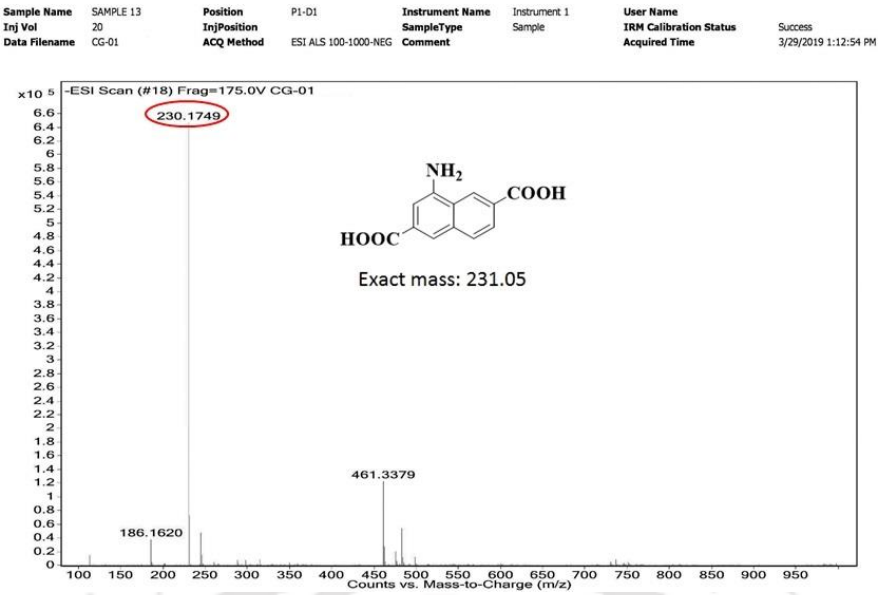

Figure 4.24 HR-MS spectrum of Na_2S-treated **3'** (digested in MeOH/HF) showing m/z (negative ion mode) peak at 230.1749, which correspond to $(M-H)^-$ ion of reduced H_2NDC-N_3 linker i.e. $H_2NDC-NH_2$.

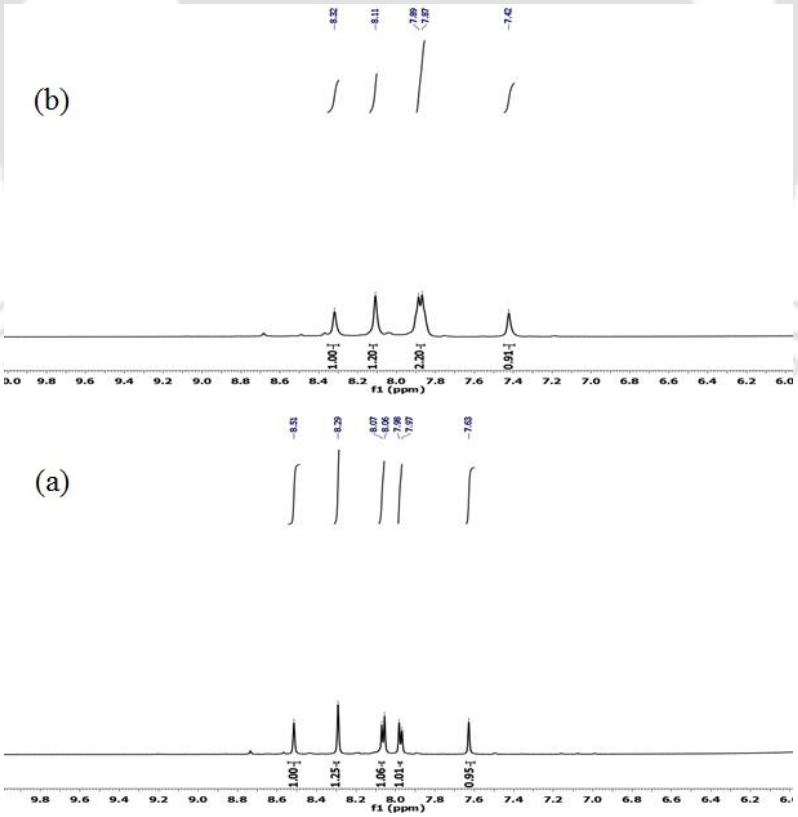

Figure 4.25 ^1H NMR spectra of (a) un-treated **3'** and (b) Na_2S-treated **3'** after digestion in DMSO-d_6/HF.

4.4 Conclusions

A highly stable Zr(IV) MOF (**3**) with DUT-52 topology and azide functionalization was synthesized and characterized extensively. Compound **3** was activated by exchanging guest solvent molecules with methanol followed by heating under vacuum. The TG analyses revealed that both the activated and as-synthesized forms of the compound are thermally stable up to 320 °C. The sensing of H_2S in aqueous medium showed that the activated MOF sample is a fluorescent "turn-on" type probe. Upon rection with Na_2S, almost 33-fold enhancement in the fluorescence intensity of **3'** was observed. The compound showed great specificity for H_2S detection even in the presence of other interfering analytes. The calculated limit of detection of **3'** towards H_2S is 0.50 μM, which is lower than the previously reported dinitro-functionalized DUT-52 MOF. The response time of **3'** is very short (2 min) towards H_2S. By using mass spectrometry, FT-IR and ^1H NMR spectroscopy, the mechanism for the reduction of azide into an amine group was established.

4.5 References

1. Yu, J.-T.; Chen, Z.; Sun, J.; Huang, Z.-T.; Zheng, Q.-Y. Cyclotricatechylene based porous crystalline material: Synthesis and applications in gas storage. *J. Mater. Chem.* **2012,** *22*, 5369-5373.
2. Li, P.-Z.; Wang, X.-J.; Zhang, K.; Nalaparaju, A.; Zou, R.; Zou, R.; Jiang, J.; Zhao, Y. ''Click''-extended nitrogen-rich metal–organic frameworks and their high performance in CO_2-selective capture. *Chem. Commun.* **2014,** *50*, 4683-4685.
3. Manju; Roy, P. K.; Ramanan, A.; Rajagopal, C. Core-shell polysiloxane-MOF 5 microspheres as a stationary phase for gas-solid chromatographic separation. *RSC Adv.* **2014,** *4*, 17429–17433.
4. Ma, L.; Abney, C.; Lin, W. Enantioselective catalysis with homochiral metal–organic frameworks. *Chem. Soc. Rev.* **2009,** *38*, 1248-1256.
5. Zhao, Y. Emerging applications of metal-organic frameworks and covalent organic frameworks. *Chem. Mater.* **2016,** *28*, 8079-8081.
6. Zhou, H.-C.; Long, J. R.; Yaghi, O. M. Introduction to metal-organic frameworks. *Chem. Rev.* **2012,** *112*, 673−674.
7. Furukawa, H.; Ko, N.; Go, Y. B.; Aratani, N.; Choi, S. B.; Choi, E.; Yazaydin, A. Ö.; Snurr, R. Q.; O'Keeffe, M.; Kim, J.; Yaghi, O. M. Ultrahigh porosity in metal-organic frameworks. *Science* **2010,** *329*, 424-428.

8. Allendorf, M. D.; Bauer, C. A.; Bhakta, R. K.; Houk, R. J. T. Luminescent metal–organic frameworks. *Chem. Soc. Rev.* **2009,** *38*, 1330-1352.

9. Li, J.-R.; Sculley, J.; Zhou, H.-C. Metal-organic frameworks for separations. *Chem. Rev.* **2012,** *112*, 869-932.

10. Kreno, L. E.; Leong, K.; Farha, O. K.; Allendorf, M.; Duyne, R. P. V.; Hupp, J. T. Metal-organic framework materials as chemical sensors. *Chem. Rev.* **2012,** *112*, 1105-1125.

11. Corma, A.; García, H.; Xamena, F. X. L. Engineering metal organic frameworks for heterogeneous catalysis. *Chem. Rev.* **2010,** *110*, 4606-4655.

12. Furukawa, H.; Ko, N.; Go, Y. B.; Aratani, N.; Choi, S. B.; Choi, E.; Yazaydin, A. O.; Snurr, R. Q.; O'Keeffe, M.; Kim, J.; Yaghi, O. M. Ultrahigh porosity in metal-organic frameworks. *Science* **2010,** *329*, 424-428.

13. Mueller, U.; Schubert, M.; Teich, F.; Puetter, H.; Schierle-Arndt, K.; Pastre, J. Metal-organic frameworks-prospective industrial applications. *J. Mater. Chem.* **2006,** *16*, 626-636.

14. Zhao, D.; Cui, Y.; Yang, Y.; Qian, G. Sensing-functional luminescent metal–organic frameworks. *CrystEngComm* **2016,** *18*, 3746–3759.

15. Falcaro, P.; Ricco, R.; Doherty, C. M.; Liang, K.; Hill, A. J.; Styles, M. J. MOF positioning technology and device fabrication. *Chem. Soc. Rev.* **2014,** *43*, 5513-5560.

16. Yu, J.; Cui, Y.; Xu, H.; Yang, Y.; Wang, Z.; Chen, B.; Qian, G. Confinement of pyridinium hemicyanine dye within an anionic metal-organic framework for two-photon-pumped lasing. *Nat. Commun.* **2013,** *4*, 2719.

17. Gao, J.; Qian, X.; Lin, R.-B.; Krishna, R.; Wu, H.; Zhou, W.; Chen, B. Mixed metal-organic framework with multiple binding sites for efficient C_2H_2/CO_2 separation. *Angew. Chem. Int. Ed.* **2020,** *59*, 4396-4400.

18. Li, C.; Xu, H.; Gao, J.; Du, W.; Shangguan, L.; Zhang, X.; Lin, R.-B.; Wu, H.; Zhou, W.; Liu, X.; Yaoa, J.; Chen, B. Tunable titanium metal–organic frameworks with infinite 1D Ti–O rods for efficient visible-lightdriven photocatalytic H_2 evolution. *J. Mater. Chem. A* **2019,** *7*, 11928-11933.

19. Li, Y.; Zhao, T.; Lu, M.; Wu, Y.; Xie, Y.; Xu, H.; Gao, J.; Yao, J.; Qian, G.; Zhang, Q. Enhancing oxygen evolution reaction through modulating electronic structure of trimetallic electrocatalysts derived from metal–organic frameworks. *Small* **2019,** *15*, 1901940.

20. Peng, D.; Yin, L.; Hu, P.; Li, B.; Ouyang, Z. W.; Zhuang, G. L.; Wang, Z. X. Series of highly stable lanthanide-organic frameworks constructed by a bifunctional linker: synthesis, crystal structures, and magnetic and luminescence properties. *Inorg. Chem.* **2018,** *57*, 2577-2200.

21. Senchyk, G. A.; Lysenko, A. B.; Krautscheid, H.; Rusanov, E. B.; Chernega, A. N.; Krämer, K. W.; Liu, S. X.; Decurtins, S.; Domasevitch, K. V. Functionalized adamantane tectons used in the design of mixed ligand copper(II) 1,2,4-triazolyl/carboxylate metal-organic frameworks. *Inorg. Chem.* **2013,** *52*, 863-872.

22. Cui, Y.; Yue, Y.; Qian, G.; Chen, B. Luminescent functional metal-organic frameworks. *Chem. Rev.* **2012,** *112*, 1126–1162.

23. Rocha, J.; Carlos, L. D.; Paza, F. A. A.; Ananiasab, D. Luminescent multifunctional lanthanides-based metal–organic frameworks. *Chem. Soc. Rev.* **2011,** *40*, 926–940.

24. Lustig, W. P.; Mukherjee, S.; Rudd, N. D.; Desai, A. V.; Li, J.; Ghosh, S. K. Metal–organic frameworks: functional luminescent and photonic materials for sensing applications. *Chem. Soc. Rev.* **2017,** *46*, 3242-3285.

25. Wang, H.; Lustig, W. P.; Li, J. Sensing and capture of toxic and hazardous gases and vapors by metal–organic frameworks. *Chem. Soc. Rev.* **2018,** *47*, 4729-4756.

26. Gogoi, C.; Yousufuddin, M.; Biswas, S. A new 3D luminescent Zn(II)–organic framework containing a quinoline-2,6-dicarboxylate linker for the highly selective sensing of Fe(III) ions. *Dalton Trans.* **2019,** *48*, 1766-1773.

27. Wuttke, S.; Dietl, C.; Hinterholzinger, F. M.; Hintz, H.; Langhals, H.; Bein, T. Turn-on fluorescence triggered by selective internal dye replacement in MOFs. *Chem. Commun.* **2014,** *50*, 3599-3601.

28. Guo, L.; Wang, M.; Cao, D. A novel Zr-MOF as fluorescence turn-on probe for real-time detecting H_2S gas and fingerprint identification. *Small* **2018,** *14*, 1703822-1703828.

29. Li, J.; Yin, C.; Huo, F. Chromogenic and fluorogenic chemosensors for hydrogen sulfide: review of detection mechanisms since the year 2009. *RSC Adv.* **2015,** *5*, 2191–2206.

30. Zheng, K. B.; Lin, W. Y.; Tan, L. A phenanthroimidazole-based fluorescent chemosensor for imaging hydrogen sulfide in living cells. *Org. Biomol. Chem.* **2012,** *10*, 9683-9688.

31. S. K. Pandey, K. H. K. a. K. T. T. A review of sensor-based methods for monitoring hydrogen sulfide. *TrAC, Trends Anal.* **2012,** *32*, 87-99.

32. Eto, K.; Asada, T.; Arima, K.; Makifuchi, T.; Kimura, H. Brain hydrogen sulfide is severely decreased in Alzheimer's disease. *Biochem. Biophys. Res. Commun.* **2002,** *293*, 1485–1488.

33. Ishigami, M.; Hiraki, K.; Umemura, K.; Ogasawara, Y.; Ishii, K.; Kimura, H. A source of hydrogen sulfide and a mechanism of its release in the brain. *Antioxid. Redox Signaling* **2009,** *11*, 205-214.

34. Eto, K.; Asada, T.; Arima, K.; Makifuchi, T.; Kimura, H. Brain hydrogen sulfide is severely decreased in Alzheimer's disease. *Biochem. Biophys. Res. Commun.* **2002,** *293*, 1485-1488.

35. Radford-Knoery, J.; Cutter, G. A. Determination of carbonyl sulfide and hydrogen sulfide species in natural waters using specialized collection procedures and gas chromatography with flame photometric detection. *Anal. Chem.* **1993,** *65*, 976-982.

36. Brub, P. R.; Parkinson, P. D.; Hall, E. R. Measurement of reduced sulphur compounds contained in aqueous matrices by direct injection into a gas chromatograph with a flame photometric detector. *J. Chromatogr. A* **1999,** *830*, 485-489.

37. Lawrence, N. S.; Davis, J.; Jiang, L.; Jones, T. G. J.; Davies, S. N.; Compton, R. G. The electrochemical analog of the methylene blue reaction: a novel amperometric approach to the detection of hydrogen sulfide. *Electroanalysis* **2000,** *12*, 1453-1460.

38. Spilker, B.; Randhahn, J.; Grabow, H.; Beikirch, H.; Jeroschewski, P. New electrochemical sensor for the detection of hydrogen sulfide and other redox active species. *J. Electroanal. Chem.* **2008,** *612*, 121-130.

39. Nandi, S.; Banesh, S.; Trivedi, V.; Biswas, S. A dinitro-functionalized metal–organic framework featuring visual and fluorogenic sensing of H_2S in living cells, human blood plasma and environmental samples. *Analyst* **2018,** *143*, 1482-1491.

40. Das, A.; Banesh, S.; Trivedi, V.; Biswas, S. Extraordinary sensitivity for H_2S and Fe(III) sensing in aqueous medium by Al-MIL-53-N_3 metal–organic framework: in vitro and in vivo applications of H_2S sensing. *Dalton Trans.* **2018,** *47*, 2690-2700.

41. Yu, F.; Li, P.; Song, P.; Wang, B. S.; Zhao, J. Z.; Han, K. An ICT-based strategy to a colorimetric and ratiometric fluorescence probe for hydrogen sulfide in living cells. *Chem.Commun.* **2012,** *48*, 2852-2854.

42. Hartman, M. C. T.; Dcona, M. M. A new, highly water-soluble, fluorescent turn-on chemodosimeter for direct measurement of hydrogen sulfide in biological fluids. *Analyst* **2012,** *137*, 4910-4912.

43. Nandi, S.; Reinsch, H.; Banesh, S.; Stock, N.; Trivedi, V.; Biswas, S. Rapid and highly sensitive detection of extracellular and intracellular H_2S by an azide-functionalized Al(III)-based metal–organic framework. *Dalton Trans.* **2017,** *46*, 12856-12864.

44. Sim, J.; Yim, H.; Ko, N.; Choi, S. B.; Oh, Y.; Park, H. J.; Park, S. Y.; Kim, J. Gas adsorption properties of highly porous metal–organic frameworks containing functionalized naphthalene dicarboxylate linkers. *Dalton Trans.* **2014,** *43*, 18017-18024.

45. Bon, V.; Senkovska, I.; Weiss, M. S.; Kaskel, S. Tailoring of network dimensionality and porosity adjustment in Zr- and Hf-based MOFs. *CrystEngComm* **2013,** *15*, 9572-9577.

46. Dalapati, R.; Balaji, S. N.; Trivedi, V.; Khamari, L.; Biswas, S. A dinitro-functionalized Zr(IV)-based metal-organic framework as colorimetric and fluorogenic probe for highly selective detection of hydrogen sulphide. *Sens. Actuators B* **2017,** *245*, 1039-1049.

47. Buragohain, A.; Biswas, S. Cerium based azide- and nitro-functionalized UiO-66 frameworks as turn-on fluorescent probes for the sensing of hydrogen sulphide. *CrystEngComm* **2016,** *18*, 4374.

48. Gotthardt, M. A.; Grosjean, S.; Brunner, T. S.; Kotzel, J.; Gänzler, A. M.; Wolf, S.; Bräse, S.; Kleist, W. Synthesis and post-synthetic modification of amine-, alkyne-, azide- and nitro-functionalized metal–organic frameworks based on DUT-5. *Dalton Trans.* **2015,** *44*, 16802-16809

49. Song, R.; Hou, L.; Wang, Y.; Li, Y.; Wang, X.; Zang, Y.; Zang, Y.; Wang, X.; Yan, S. Fluorescence Zn-based metal–organic frameworks for the detection of hydrogen sulfide in natural gas. *Anal. Methods* **2017,** *9*, 3914-3919.

50. Buragohain, A.; Biswas, S. Cerium-Based Azide- and NitroFunctionalized UiO-66 Frameworks as Turn-On Fluorescent Probes for the Sensing of Hydrogen Sulphide. *CrystEngComm* **2016,** *18*, 4374-4381.

51. Karmakar, A.; Samanta, P.; Dutta, S.; Ghosh, S. K. Fluorescent "turn-on" sensing based on metal–organic frameworks (MOFs). *Chem. Asian J.* **2019,** *14*, 4506-4519.

52. Zheng, X.; Fan, R.; Song, Y.; Wang, A.; Xing, K.; Du, X.; Wang, P.; Yang, Y. A highly sensitive turn-on ratiometric luminescent probe based on postsynthetic modification of Tb^{3+}@Cu-MOF for H_2S detection. *J. Mater. Chem. C* **2017,** *5*, 9943-9951.

53. Nagarkar, S. S.; Desai, A. V.; Ghosh, S. K. A nitro-functionalized metal–organic framework as a reaction-based fluorescence turn-on probe for rapid and selective H_2S detection. *Chem. Eur. J.* **2015,** *21*, 9994-9997.

54. Li, H.; Feng, X.; Guo, Y.; Chen, D.; Li, R.; Ren, X.; Jiang, X.; Dong, Y.; Wang1, B. A malonitrile-functionalized metal-organic framework for hydrogen sulfide detection and selective amino acid molecular recognition. *Sci. Rep.* **2014,** *4*, 4366-4371.

55. Ma, Y.; Su, H.; Kuang, X.; Li, X.; Zhang, T.; Tang, B. Heterogeneous nano metal-organic framework fluorescence probe for highly selective and sensitive detection of hydrogen sulfide in living cells. *Anal. Chem.* **2014,** *86*, 11459-11463.

56. Nagarkar, S. S.; Saha, T.; Desai, A. V.; Talukdar, P.; Ghosh, S. K. Metal-organic framework based highly selective fluorescence turn-on probe for hydrogen sulphide. *Sci. Rep.* **2014,** *4*, 7053-7058.

57. Zhang, X.; Hu, Q.; Xia, T.; Zhang, J.; Yang, Y.; Cui, Y.; Chen, B.; Qian, G. Turn-on and ratiometric luminescent sensing of hydrogen sulfide based on metal-organic frameworks. *ACS Appl. Mater. Interfaces* **2016,** *8*, 32259-32265.

58. Buragohain, A.; Biswas, S. Cerium-based azide- and nitro-functionalized UiO-66 frameworks as turn-on fluorescent probes for the sensing of hydrogen sulphide. *CrystEngComm* **2016,** *18*, 4374-4381

59. Zhang, X.; Hu, Q.; Xia, T.; Zhang, J.; Yang, Y.; Cui, Y.; Chen, B.; Qian, G. Turn-on and Ratiometric Luminescent Sensing of Hydrogen Sulfide Based on Metal-Organic Frameworks. *ACS Appl. Mater. Interfaces* **2016,** *8*, 32259-32265.

60. Dalapati, R.; Balaji, S. N.; Trivedi, V.; Khamari, L.; Biswas, S. A dinitro-functionalized Zr(IV)-based metal-organic framework as colorimetric and fluorogenic probe for highly selective detection of hydrogen sulphide. *Sens. Actuators., B* **2017,** *245*, 1039-1049.

61. Zhang, X.; Zhang, J.; Hu, Q.; Cui, Y.; Yang, Y.; Qian, G. Post synthetic modification of metal–organic framework for hydrogen sulfide detection. *Appl. Surf. Sci.* **2015,** *355*, 814-819.

62. Nagarkar, S. S.; Desai, A. V.; Ghosh, S. K. A nitro-functionalized metal-organic framework as a reaction based fluorescence turn-on probe for rapid and selective H_2S Detection. *Chem. Eur. J.* **2015,** *21*, 9994-9997.

63. Zheng, X.; Fan, R.; Song, Y.; Xing, K.; Wang, P.; Yang, Y. Dual-emitting Eu(III)-Cu(II) heterometallic-organic framework: simultaneous, selective, and sensitive detection of hydrogen sulfide and ascorbic acid in a wide range. *ACS Appl. Mater. Interfaces* **2018,** *10*, 32698-32706.

64. Ma, Y.; Su, H.; Kuang, X.; Li, X.; Zhang, T.; Tang, B. Heterogeneous nano metal-organic framework fluorescence probe for highly selective and sensitive detection of hydrogen sulfide in living cells. *Anal. Chem.* **2014,** *86*, 11459-11463.

65. Legrand, A.; Pastushenko, A.; Lysenko, V.; Geloen, A.; Quadrelli, E. A.; Canivet, J.; Farrusseng, D. Enhanced ligand-based luminescence in metal-organic framework sensor. *ChemNanoMat* **2016,** *2*, 866-872.

66. Li, H.; Feng, X.; Guo, Y.; Chen, D.; Li, R.; Ren, X.; Jiang, X.; Dong, Y.; Wang, B. A malonitrile-functionalized metal-organic framework for hydrogen sulfide detection and selective amino acid molecular recognition. *Sci. Rep.* **2014,** *4*, 4366-4370.

67. Ma, Y.; Su, H.; Kuang, X.; Li, X.; Zhang, T.; Tang, B. Heterogeneous nano metal–organic framework fluorescence probe for highly selective and sensitive detection of hydrogen sulfide in living cells. *Anal. Chem.* **2014,** *86*, 11459-11463.

68. Nandi, S.; Reinsch, H.; Biswas, S. A vinyl functionalized mixed linker CAU-10 metal-organic framework acting as a fluorescent sensor for the selective detection of H_2S and palladium(II). *Microporous and Mesoporous Materials* **2020,** *293*, 109790.

69. Li, Y.; Zhang, X.; Zhang, L.; Jiang, K.; Cui, Y.; Yang, Y.; Qian, G. A nanoscale Zr-based fluorescent metal-organic framework for selective and sensitive detection of hydrogen sulfide. *J. Solid State Chem.* **2017,** *255*, 97-101.

70. Bae, S. K.; Heo, C. H.; Choi, D. J.; Sen, D.; Joe, E.-H.; Cho, B. R.; Kim, H. M. A ratiometric two-photon fluorescent probe reveals reduction in mitochondrial H_2S production in parkinson's disease gene knockout astrocytes. *J. Am. Chem. Soc.* **2013,** *135*, 9915-9923.

71. Mao, G.-J.; Wei, T.-T.; Wang, X.-X.; Huan, S.; Lu, D.-Q.; Zhang, J.; Zhang, X.-B.; Tan, W.; Shen, G.-L.; Yu, R.-Q. High-sensitivity naphthalene-based two-photon fluorescent probe suitable for direct bioimaging of H_2S in living cells. *Anal. Chem.* **2013,** *85*, 7875-7881.

72. Yu, F.; Li, P.; Song, P.; Wang, B.; Zhao, J.; Han, K. An ICT-based strategy to a colorimetric and ratiometric fluorescence probe for hydrogen sulfide in living cells. *Chem. Commun.* **2012,** *48*, 2852-2854.

73. Qian, Y.; Karpus, J.; Kabil, O.; Zhang, S.-Y.; Zhu, H.-L.; Banerjee, R.; Zhao, J.; He, C. Selective fluorescent probes for live-cell monitoring of sulphide. *Nat. Commun.* **2011,** *2*, 495.

74. Peng, B.; Chen, W.; Liu, C.; Rosser, E. W.; Pacheco, A.; Zhao, Y.; Aguilar, H. C.; Xian, M. Fluorescent probes based on nucleophilic substitution–cyclization for hydrogen sulfide detection and bioimaging. *Chem. Eur. J.* **2014,** *20*, 1010-1016.

75. Jiang, Y.; Wu, Q.; Chang, X. A ratiometric fluorescent probe for hydrogen sulfide imaging in living cells. *Talanta* **2014,** *121*, 122-126.

76. Cui, S.; Yang, L.; Wang, J.; Wang, X. Fabrication of a sensitive gas sensor based on PPy/TiO_2 nanocomposites films by layer-by-layer self-assembly and its application in food storage. *Sens. Actuators B* **2016,** *233*, 337-346.

77. Lv, A.; Wang, M.; Wang, Y.; Bo, Z.; Chi, L. Investigation into the sensing process of high-performance H_2S sensors based on polymer transistors. *Chem. Eur .J.* **2016,** *22*, 3654-3659.

78. Shirsat, M. D.; Bangar, M. A.; Deshusses, M. A.; Myung, N. V.; Mulchandani, A. Polyaniline nanowires-gold nanoparticles hybrid network based chemiresistive hydrogen sulfide sensor. *Appl. Phys. Lett.* **2009,** *94*, 083502-083504.

79. Yu, C.; Wang, Y.; Hua, K.; Xing, W.; Lu, T. Electrochemical H_2S sensor with H_2SO_4 pre-treated nafion membrane as solid polymer electrolyte. *Sens. Actuators B* **2002,** *96*, 259-265.

80. Kaur, M.; Jain, N.; Sharma, K.; Bhattacharya, S.; Roy, M.; Tyagi, A. K.; Gupta, S. K.; Yakhmi, J. V. Room-temperature H_2S gas sensing at ppb level by single crystal In_2O_3 whiskers. *Sens. Actuators B* **2008,** *133*, 456-461.

81. Jain, G. H.; Patil, L. A. CuO-doped BSST thick film resistors for ppb level H_2S gas sensing at room temperature. *Sens. Actuators B* **2007,** *123*, 246-253.

82. Wang, C.; Chu, X.; Wu, M. Detection of H_2S down to ppb levels at room temperatureusing sensors based on ZnO nanorods. *Sens. Actuators B* **2006,** *113*, 320-323.

83. Deng, H.-H.; Weng, S.-H.; Huang, S.-L.; Zhang, L.-N.; Liu, A.-L.; Lin, X.-H.; Chen, W. Colorimetric detection of sulfide based on target-induced shieldingagainst the peroxidase-like activity of gold nanoparticles. *Anal. Chim. Acta* **2014,** *852*, 218-222.

84. Chen, P.-C.; Li, Y.-C.; Ma, J.-Y.; Huang, J.-Y.; Chen, C.-F.; Chang, H.-T. Size-tunable copper nanocluster aggregates and their application in hydrogen sulfide sensing on paper-based devices. *Sci. Rep.* **2016,** *6*, 24882-24890.

85. Lin, V. S.; Lippert, A. R.; Chang, C. J. Cell-trappable fluorescent probes for endogenous hydrogen sulfide signaling and imaging H_2O_2-dependent H_2S production. *Proc. Natl. Acad. Sci. U. S. A.* **2013,** *110*, 7131-7135.

86. Ismail, I.; Chen, Z.; Ji, X.; Sun, L.; Yi, L.; Xi, Z. A fast-response red shifted fluorescent probe for detection of H_2S in living cells. *Molecules* **2020,** *25*, 437.

87. Cui, J.; Zhang, T.; Sun, Y.-Q.; Li, D.-P.; Liu, J.-T.; Zhao, B.-X. A highly sensitive and selective fluorescent probe for H_2S detectionwith large fluorescence enhancement. *Sens. Actuators. B* **2016,** *232*, 705-711.

88. Peng, H.; Cheng, Y.; Dai, C.; King, A. L.; Predmore, B. L.; Leferand, D. J.; Wang, B. A fluorescent probe for fast and quantitative detection of hydrogen sulfide in blood. *Angew. Chem. Int. Ed.* **2011,** *50*, 9672-9675.

89. Chen, S.; Chen, Z.-j.; Ren, W.; Ai, H.-w. Reaction-based genetically encoded fluorescent hydrogen sulfide sensors. | *J. Am. Chem. Soc.* **2012,** *134*, 9589-9592.

90. Xun, L.; Topp, E.; Orser, C. S. Glutathione is the reducing agent for the reductive dehalogenation of tetrachloro-p-hydroquinone by extracts from a Flavobacterium sp@. *Biochem. Biophys. Res. Commun.* **1992,** *182*, 361-366.

91. Baker, L. M.; Baker, P. R.; Golin-Bisello, F.; Schopfer, F. J.; Fink, M.; Woodcock, S. R.; Branchaud, B. P.; Radi, R.; Freeman, B. A. Nitro-fatty acid reaction with glutathione and cysteine Kinetic analysis of thiol alkylation by a Michael addition reaction. *J. Biol. Chem.* **2007,** *282*, 31085-31093.

92. Appenzeller-Herzog, C. Glutathione- and non-glutathione-based oxidant control in the endoplasmic reticulum. *J. Cell Sci.* **2011,** *124*, 847-855.

93. Gogoi, C.; Biswas, S. A new quinoline based luminescent Zr(IV) metal–organic framework for the ultrasensitive recognition of 4-nitrophenol and Fe(III) ions. *Dalton Trans.* **2018,** *47*, 14696-14705.

94. Lagodzinskaya, G. V.; Yunda, N. G.; Manelis, G. B. NMR study of proton exchange, hydrogen bonding, and dissociation of water in hydrazine solutions. *Bulletin of the Academy of Sciences of the USSR, Division of chemical science* **1980,** *29*, 532-539.

CHAPTER 5

A Zr-based metal-organic framework with DUT-52 structure containing a trifluoroacetamido functionalized linker for aqueous phase fluorescence sensing of cyanide ion and aerobic oxidation of cyclohexane

*This chapter describes the synthesis and characterization of a zirconium (Zr) metal-organic framework having DUT-52 structure with face-centred cubic (fcu) topology and bearing the rigid 1-(2,2,2-trifluoroacetamido) naphthalene-3,7-dicarboxylic acid linker. Fluorescence titration experiments showed that after the addition of cyanide solution to activated compound (**4'**), the emission intensity increased as well as a significant bathochromic shift of 63 nm was observed. The new emission band at 490 nm indicated that the nucleophilic addition at trifluoroacetamide group took place by cyanide anion. Furthermore, the aerobic oxidation of cyclohexane was performed with **4'** under mild reaction conditions, observing higher activity than analogous DUT-52 solid under identical conditions.*

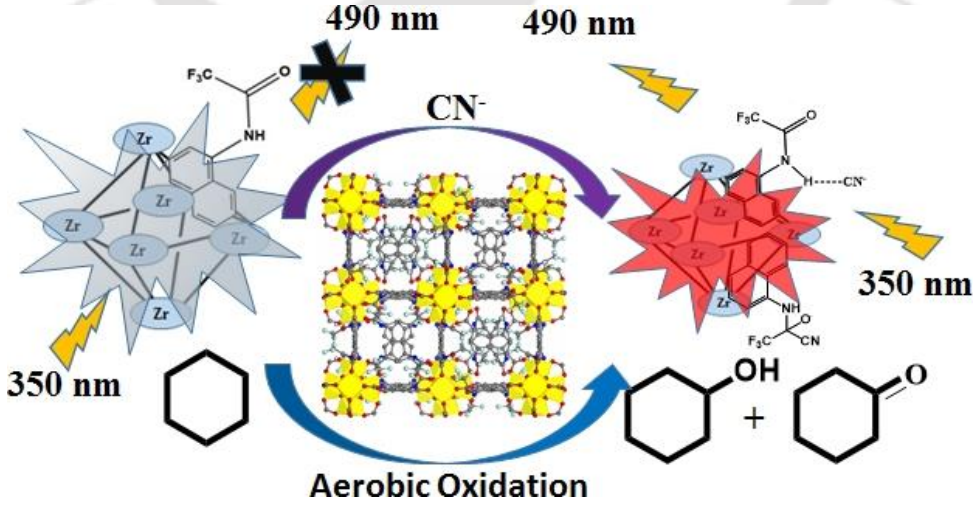

Inorganic Chemistry including bioinorganic chemistry

C. Gogoi, N. Nagarjun, S. Roy, M. SK, D. Volkmer, A. Dhakshinamoorthy, S. Biswas. *Inorg. Chem.* 2021, **60**, 4539-4550.

5.1 Introduction

According to Environment Protection Agency (EPA) and World Health Organization (WHO), cyanide ion (CN^-) is one of the most hazardous chemical species and extremely poisonous to living animals.[1-2] The effect of CN^- ion is so much that it can easily induce the inhibition of respiration which can change the normal functions of the lungs and brain by binding with Fe^{3+} ion of the cytochrome oxidase.[3] The tissues having the fastest oxygen metabolism like cardiac muscle and the brain can easily be affected by the inhalation and ingestion of CN^- ion.[4] According to the guidelines of WHO, the maximum acceptable concentration of CN^- ion in drinking water is 1.9 μM.[1, 5] Nevertheless, despite of its toxicity, cyanide is frequently used in industrial sectors for gold mining, electroplating, metallurgy, synthetic fibers, synthesis of nylon, etc.[6-7] The cyanide-contaminated waste materials of industry and wastewater from natural/artificial processes may pollute water resources. Cyanide can be used as a terrorist weapon of mass destruction. CN^- ion is also listed as CWA (chemical warfare agent). It is vital to monitor and control CN^- level.[8-9] Hence, significant attention has been paid for the detection and quantification of CN^- ion.

Metal-organic frameworks (MOFs), also known as porous coordination polymers (PCPs), are porous, crystalline coordination polymers having open frameworks with potential voids, which are constructed via self-assembly of single metal cations (primary building unit) or metal clusters (SBU) and multi-topic organic linkers.[10-12] In this class of materials, the coordination mode of the metal ions in the SBUS and binding mode of the linkers decide the framework topology of the resulting extended structure, having potential void.[13-14] These robust materials possess interesting physical and chemical properties like optical absorbance, large surface area, tunable porosity, highly chemical and thermal stability, luminescence, conductivity, magnetism and so on.[15-17] Because of their unique properties, they have been extensively used in various applications like molecular recognition, sensing of analytes, gas adsorption and purification, catalysis, asymmetric synthesis, drug delivery and so on.[18-20] Among all, MOFs as a chemical sensor is one of the most explored fields now-a-days. The properties like luminescence, non-toxicity, wide range of chemical stability, diverse pore sizes, biodegradability, open metal-sites for interaction and presence of different functional group make MOFs good chemical sensors in real applications.[21-22] In recent decades, luminescent MOFs (LMOFs) have turned out to be an important category of compounds to detect different guest targets like small organic molecules, solvents, gases, cations, anions, explosives and organic molecules.[23-29] In the presence of different analytes, luminescence of LMOFs may be

increased (turn-on) or quenched (turn-off). This situation depends on the sensitivity of the reaction of analytes with probes.[22, 30-32]

Based on literature data, many different methods like spectrophotometry, electrochemistry, atomic absorption spectroscopy, gas chromatography, voltammetry and fluorometry have been used for the detection of different analytes and organic pollutants. Among all these techniques, fluorometric method is more suitable due to its high sensitivity, short response time, convenience and low cost.[33] There have been a large number of fluorescent based sensors developed so far for CN^- ion.[34-41] But, many fluorescent sensors are organic fluorescent molecules which mainly work in organic media.[36, 42-44] As a result, in several cases, the real-life applications of the probes are hampered. An aqueous medium is highly preferred for biological and medical utilization purposes. Among the many types of fluorescent based sensors that have been developed up to now, the most effective class of sensors is MOFs for aqueous medium sensing.[39, 45-47] Although aqueous phase cyanide sensors are still rare, there are some reports on cyanide sensing, where cyanide is fluorometrically sensed in aqueous or aqueous-organic media by small organic probes.[48] A few MOF sensors have been investigated for aqueous phase cyanide detection including carbazole-functionalized UiO-67,[46] hyrdazine-functionalized CAU-10,[45] hemicyanine-functionalized mixed-linker PCN-700,[38] bio-MOF-1⊃DAAC,[49] and Tb-ADP-Bipy[47]. Based on some literature reports, few small organic molecules with trifluoroaceatmido group as the reaction site were utilized for the detection of cyanide ion.[35, 42, 50]

One of the unique properties of MOFs is the facile introduction of functional groups in the linker that can dominate the catalytic activity or can be combined with metal node as dual active sites for cascade reactions.[51] Among the various applications of MOFs in organic transformations, one of the highly explored reactions is aerobic oxidation of hydrocarbons, in particular cycloalkanes. This is mainly due to the commercial interest of the oxidized products for the preparation of polymers. Hence, a wide range of MOF-based catalysts has been reported as heterogeneous catalysts for the oxidation of cyclohexane. For example, MIL-101(Cr),[52] Salen-Co(II) complex incorporated over MIL-101(Cr)-NH_2,[53] Au@MIL-101(Cr),[54] MIL-100(Fe),[55] Fe(BTC)/MIL-100(Fe),[56] Fe_2(dobdc),[57] NHPI/Fe(NTC) (NHPI: N-hydroxyphthalimide)[58] and MIL-125(Ti)[59]. Although many catalysts have been reported for oxidation of hydrocarbons using MOF based solid catalysts,[60-61] the aerobic oxidation of cyclohexane is still a challenging reaction because of the achievement of high alcohol/ketone selectivity under mild reaction conditions.

Stimulated by the above stated realities, we present a Zr(IV) based MOF bearing the rigid hydrophobic $H_2NDC\text{-}NHCOCF_3$ linker and a comprehensive study on its synthesis, characterization and fluorescence sensing properties for cyanide. It is a trifluoroacetamido functionalized Zr(IV) based MOF having DUT-52 structure with **fcu** topology.[62] It has been named as DUT-52-$NHCOCF_3$ (**4**). Activated (**4'**) form of this MOF has been explored towards the fluorometric sensing of toxic CN^- ion in water. Apart from its great sensitivity, compound **4'** showed high specificity towards sensing of CN^- in aqueous medium. In this chapter, we would also like to present the catalytic performance of **4'** in aerobic oxidation of cyclohexane under mild reaction conditions to achieve high selectivity of alcohol/ketone. Catalyst stability as well as the benefits of grating hydrophobic cavities within the framework of **4'** are also demonstrated with additional control experiments.

5.2 Experimental section

5.2.1 Materials and general methods

All the reagents and solvents were procured from commercial sources and used without purification, except the $H_2NDC\text{-}NHCOCF_3$ linker. Fourier transform infrared (FT-IR) spectra were collected in the region 400-4000 cm^{-1} on a PerkinElmer Spectrum Two FT-IR spectrometer. The following notations were used for characterization of the bands: broad (br), strong (s), very strong (vs), medium (m), weak (w) and shoulder (sh). Thermogravimetric analyses (TGA) were performed under air atmosphere at a heating rate of 5 °C min^{-1} in a temperature region of 25-1000 °C by employing a Netzsch STA-409CD thermal analyser. Rigaku Smartlab X-ray diffractometer (model TTRAX III) was employed for X-ray powder diffraction (XRPD) measurements at 50 kV, 100 mA using Cu-*K*α (λ = 1.5406 Å) radiation. N_2 sorption isotherms were recorded by using Quantachrome Quadrasorb evo surface area analyser at −196 °C. Before the sorption analysis, the degassing of the compound was carried out at 100°C under high vacuum for 12 h. Fluorescence sensing studies were performed with a HORIBA JOBIN YVON Fluoromax-4 spectrofluorometer. A BrukerAvance III 600 NMR spectrometer was used for recording ^1H NMR spectra at 600 MHz. Mass spectra were recorded with an Agilent 6520 Q-TOF high resolution mass spectrometer (HR-MS). Pawley refinement was carried out using Materials Studio software.[63] Indexing of XPRD patterns were performed by using the DIVCOL program[64] which is embedded in STOE's WinXPow software package.[65] Contact angle experiments were performed by employing a KRUSS Drop Shape Analyzer-DSA25 instrument with an automatic liquid dispenser at ambient temperature.

5.2.2 Synthesis of $H_2NDC\text{-}NHCOCF_3$ linker:

By following the protocol reported in the literature, 1-aminonaphthalene-3,7-dicarboxylic acid ($H_2NDC\text{-}NH_2$) was prepared from naphthalene-2,6-dicarboxylic acid (H_2NDC).[66] In a 100 mL round-bottom flask, 10 mmol (2.31 g) of $H_2NDC\text{-}NH_2$ was taken and 15 mL of trifluoroacetic anhydride was added to the flask slowly at room temperature. The reaction mixture was stirred for 4 h. After that 20 mL of ice cold water was added to the reaction mixture, resulting in precipitation. The obtained solid product ($H_2NDC\text{-}NHCOCF_3$ linker) was filtered, washed with a large amount of water and dried in oven at 60 °C. The reaction scheme for the preparation of $H_2NDC\text{-}NHCOCF_3$ linker shown in Scheme S1.

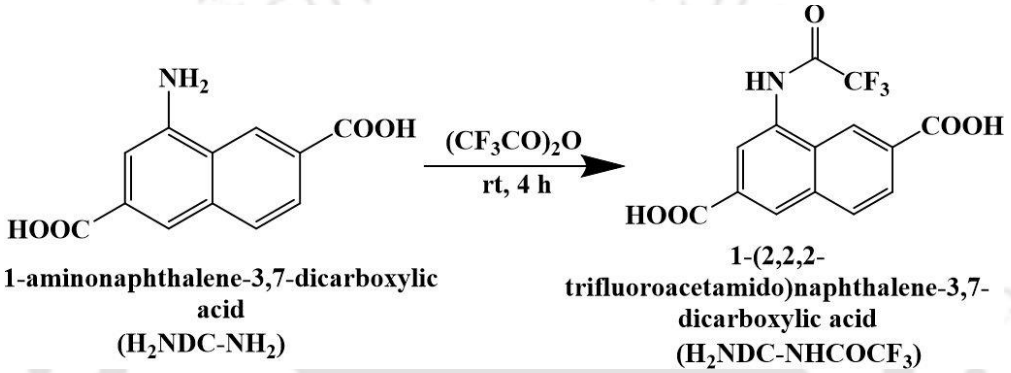

Scheme S1. Syntheis of $H_2NDC\text{-}NHCOCF_3$ linker.

The characterization of the linker was carried out by mass spectrometry, ^1H NMR, ^{13}C NMR and ^{19}F NMR spectroscopy. The ^1H NMR spectrum (Figure 5.1) confirmed the presence of six types of protons in $H_2NDC\text{-}NHCOCF_3$ linker. The naphthalene moiety contains five types of protons and one proton is present at the nitrogen atom of acetamido functionality. The six kind of protons are marked as a, b, c, d, e and f. The chemical shift values are observed at 11.79 (s, 1H, -NH), 8.70 (s, 1H, Ar-H), 8.12 (d, 1H, Ar-H), 8.33 (d, 1H, Ar-H), 8.58 (s, 1H, Ar-H) and 8.10 (s, 1H, Ar-H) ppm, respectively. Since there are no additional protons in the ^1H NMR spectrum, the formation of by-products is ruled out. The ^{13}C NMR spectrum (Figure 5.2) revealed that there are fourteen types of carbon atoms present in the linker. The observed chemical shift values are 115.13, 117.99, 124.37, 125.32, 126.90, 130.36, 130.95, 131.07, 132.77, 135.47, 156.48, 156.85, 166.98 and 167.42 ppm. The ^{19}F NMR spectrum (Figure 5.3) showed an intense peak at -73.70 ppm due to the same type of fluorine atoms present in trifluoroacetamido moiety. In the mass spectrum of the linker (Figure 5.4), the most intense peak was found at m/z = 326.004 (measured in negative ion mode), which corresponds to $(M\text{-}H)^-$ ion (M is the mass of $H_2NDC\text{-}NHCOCF_3$ linker). The theoretically calculated mass of the

linker is 327.22 g mol^{-1}. Therefore, it can be concluded that the desired $H_2NDC\text{-}NHCOCF_3$ linker has been synthesized.

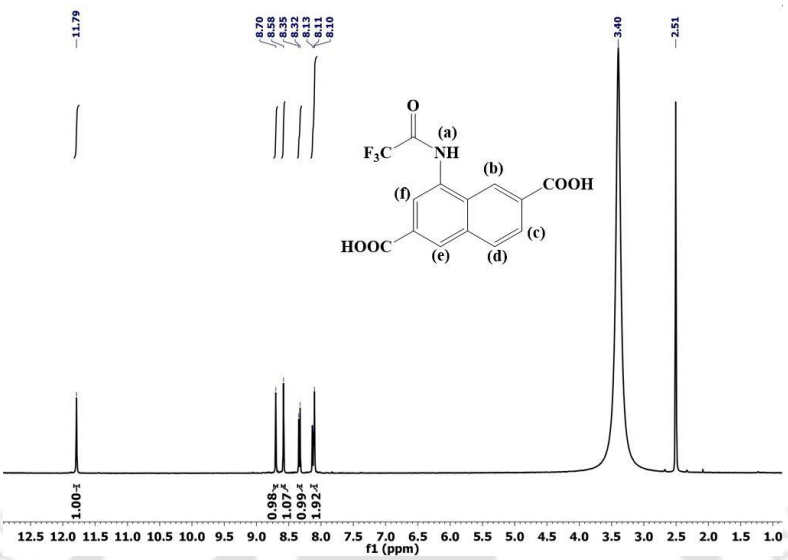

Figure 5.1 ^{1}H NMR spectrum of $H_2NDC\text{-}NHCOCF_3$ linker measured in DMSO-d_6.

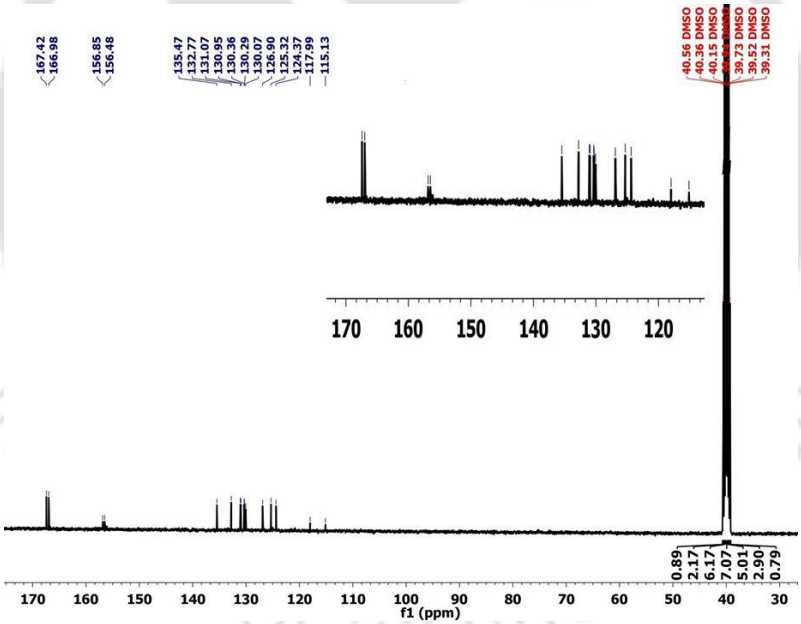

Figure 5.2 ^{13}C NMR spectrum of $H_2NDC\text{-}NHCOCF_3$ linker measured in DMSO-d_6.

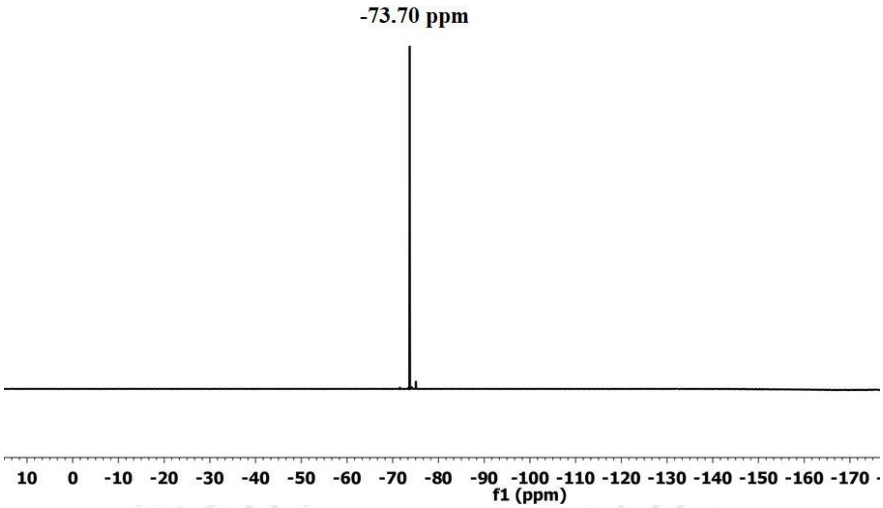

Figure 5.3 ^{19}F NMR spectrum of $H_2NDC\text{-}NHCOCF_3$ linker measured in DMSO-d_6.

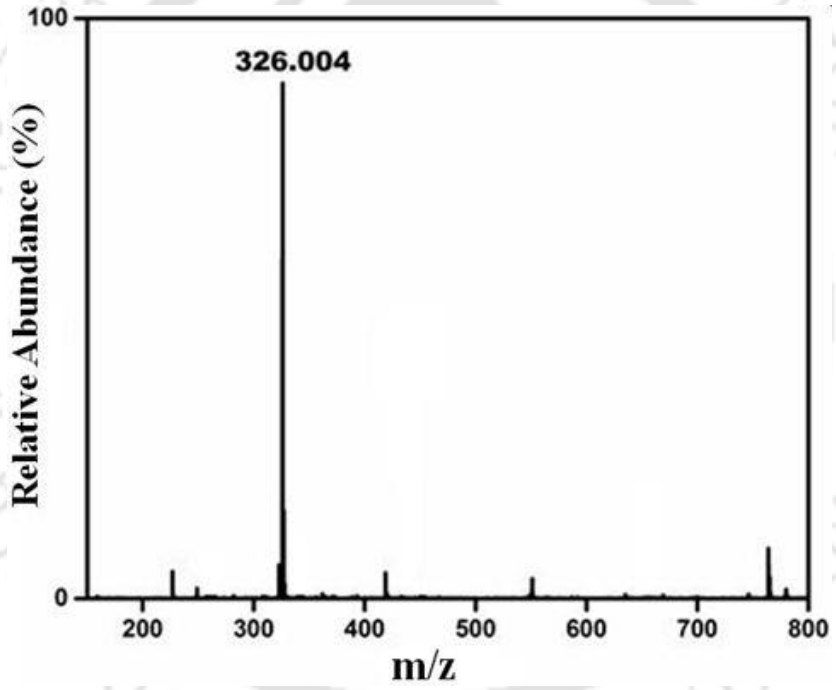

Figure 5.4 Mass spectrum of $H_2NDC\text{-}NHCOCF_3$ linker.

5.2.3 Synthesis of $[Zr_6O_4(OH)_4(NDC\text{-}NHCOCF_3)_6]\cdot 3H_2O\cdot 2DMF$ (4)

In a sealed tube, $ZrOCl_2\cdot 8H_2O$ (20 mg, 0.06 mmol), $H_2NDC\text{-}NHCOCF_3$ linker (20 mg, 0.06 mmol) and benzoic acid (223 mg, 1.82 mmol) as a modulator were taken. Then, 3 mL of *N*,*N*-dimethylformamide (DMF) was poured into the tube, which was kept in an ultrasonic bath for homogenization for 15 min. The tube was properly sealed and kept for 24 h at 120 °C in a block heater. After cooling the sealed tube down to room temperature, light yellow coloured powder of compound **4** was obtained by filtration. Compound **4** was then dried at 80 °C for 6 h. Yield: 25 mg (0.01 mmol, 77%). The yield was calculated based on the zirconium salt. Anal.

Calcd. for **4** ($C_{90}H_{60}F_{18}N_8O_{43}Zr_6$, molecular weight: 2830.78 g mol^{-1}) in %: C, 38.19; H, 2.14; N, 3.96. Found: C, 38.04; H, 2.19; N; 3.88. Anal.Calcd. for **4'** ($C_{84}H_{40}F_{18}N_6O_{38}Zr_6$, molecular weight: 2630.55 g mol^{-1}) in %: C, 38.35; H, 1.53; N, 3.19. Found: C, 38.91; H, 1.87; N, 3.29. FT-IR (KBr, cm^{-1}): 3418 (br), 1720 (s), 1653 (sh), 1613 (br), 1577 (vs), 1420 (s), 1368 (w), 1211 (w), 1170 (s), 924 (w), 786 (s), 723 (w), 664 (s), 550 (w), 478 (s).

5.2.4 Activation of 4

In the activation process, **4** (100 mg) was stirred overnight in methanol (20 mL) under ambient conditions. Later on, the compound was filtered off and heated for 5 h in high vacuum at 80 °C. The thermally activated MOF material has been indicated as **4'**.

5.2.5 Details of structural simulation for compound 4

The experimental XRPD pattern of compound **4** could be indexed in cubic crystal system (Table S1). Therefore, a structural model based on the related compound Zr-CCA (CSD code: XAPFOM; H_2CCA: 4-carboxycinnamic acid), which crystallized in the space group $Pn\bar{3}$, was used as the starting model.[67] The universal force field method of Materials Studio software was used to create a structural model for DUT-52-$NHCOCF_3$ (compound **4**) by force field optimization.[68] Due to the symmetry operators in the cubic space group $Pn\bar{3}$, the structural plot shows a double substitution of the –$NHCOCF_3$ groups. For the structural simulation, the atomic occupancy factors of the –$NHCOCF_3$ groups have been set to an occupancy factor of 0.5 each.

5.2.6 Fluorescence sensing investigation

In a typical experimental set-up, 1 mg of compound **4'** was dispersed in 5 mL of water in a small glass vial. After sonication, the mixture was kept undisturbed for 24 h at ambient conditions to get a stable dispersion. This stable dispersion was used for all the fluorescence measurements. For a typical experiment, 200 µL of the dispersion of **4'** was taken in a quartz cuvette. The total volume of the cuvette was made up to 3 mL by adding 2800 µL of water and the fluorescence spectrum was recorded. In this 3 mL dispersion of **4'**, 10 mM of NaCN (in water) solution was added. After every incremental addition of NaCN solution, fluorescence spectra were recorded. The NaCN solution was added gradually up to saturation in fluorescence intensity. Here, we used NaCN as a source of CN^- ion. To investigate interference from other anions, intrusive anions (10 mM solutions) were added to the dispersion of probe kept in a cuvette and fluorescence spectra were recorded. Afterward, we added a definite amount of 10 mM solution of NaCN to the same cuvette and after a definite interval, fluorescence emission

spectra were measured. All these experiments were performed upon excitation at 350 nm and emission spectra were acquired in the range of 370-650 nm. The fold enhancement of emission intensity was calculated by the formula: I/I_0, in which I_0 and I are the initial fluorescence intensity and fluorescence intensity after the addition of anion solution, respectively. For CN^- sensing in real water samples, tap and drinking water were collected from our laboratory. Lake water was collected from Serpentine lake, IIT Guwahati and river water was obtained from Brahmaputra River, Assam, India. The collected samples were filtered twice before performing the fluorescence experiments.

5.2.7 Reaction procedure for catalysis study

Aerobic oxidation of cyclohexane was performed in a 25 mL two-necked round bottom flask by loading 20 mg of **4'**, acetonitrile (2.5 mL) and cyclohexane (1 mmol). To this mixture, $AgBF_4$ (26 mg) was also added, thoroughly mixed and sealed with a silicon septum. Later, this slurry was kept on a silicon oil bath maintained at 60 °C. This heterogeneous suspension was purged with molecular oxygen (99.99% purity). This reaction mixture was stirred for the different time intervals up to 24 h and the reaction temperature was monitored continuously. After 24 h, the reaction was cooled down to room temperature. Later, the reaction slurry was diluted with acetonitrile (3 mL), stirred for 30 min and filtered. This sample was analyzed by gas chromatography (operation conditions: HP-5 capillary column, oven temperature: 50 to 300 °C, ramp rate: 10 °C/min; inlet temperature 250 °C) to determine conversion and selectivity using internal standard method. The oxidation products were identified by GC-MS using similar conditions employed for GC. Reusability tests were carried out as indicated above with the recovered solid after catalytic reaction. The separation of cyclohexanol and cyclohexanone from the crude mixture of cyclohexane oxidation was performed with HPLC Shimadzu LC-6AD (model: CBM-20A) with wavelength absorbance detector. Separations were achieved with a hyperclone 5u MOS (C_8) 120A column (column dimension 150 × 4.6 mm). The elution rate was 1.0 mL/min and cyclohexanone and cyclohexanol were detected at 274 and 254 nm, respectively with the absorbance detector. Solvent programming was used to establish the optimum solvent ratio. The elution solvent consisted of HPLC grade of acetonitrile-water (3:1) to obtain adequate resolution. ^{1}H-NMR spectra were recorded with 400 MHz NMR using $CDCl_3$ as solvent.

5.3 Results and discussion

5.3.1 Synthesis and characterization

We used two zirconium salts namely, $ZrCl_4$ and $ZrOCl_2 \cdot 8H_2O$ and DMF as a solvent to get optimized synthesis conditions. Main purpose of using zirconium based salts is that among the family of MOFs, zirconium MOFs show high physicochemical stability, rich structural types, large porosity, intriguing properties and functions.[69] Different modulators like acetic acid, benzoic acid, formic acid and trifluoroacetic acid were used to increase the crystallinity of the MOFs.[70] Herein, the optimized reaction conditions were obtained by using $ZrOCl_2 \cdot 8H_2O$ as a metal salt, benzoic acid as a modulator and DMF as a solvent. After heating the reaction mixture for 24 h at 120 °C, nanocrystals with octahedral morphology and almost uniform size were obtained (Figure 5.5).

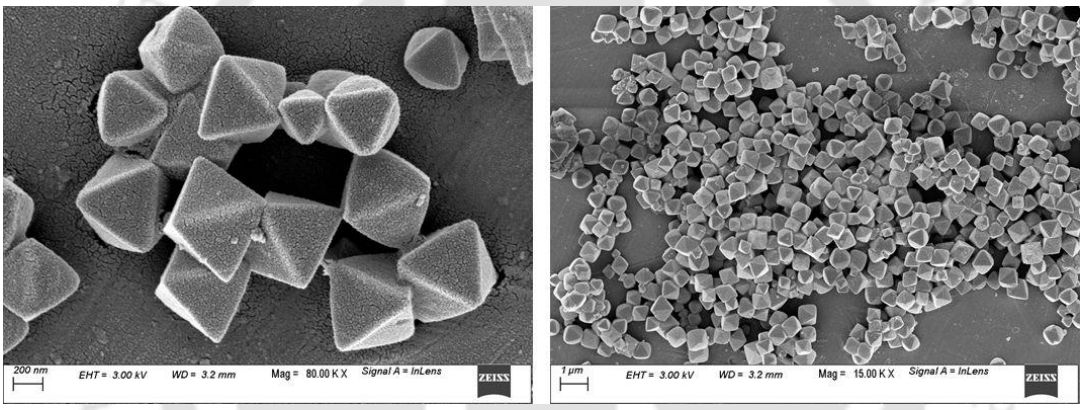

Figure 5.5 FE-SEM images of **4**.

The phase purity was confirmed by the XRPD experiment. The as-synthesized material (**4**) showed a good resemblance with the XRPD pattern of the earlier reported parent DUT-52 compound (Figure 5.6). Therefore, it was concluded that as-synthesized compound **4** is isostructural with DUT-52. The XRPD pattern of activated material **4'** was also collected. It is well-matched with the reported DUT-52 MOF material. This implies that guest-free form of **4** has the same structural framework as the parent compound.

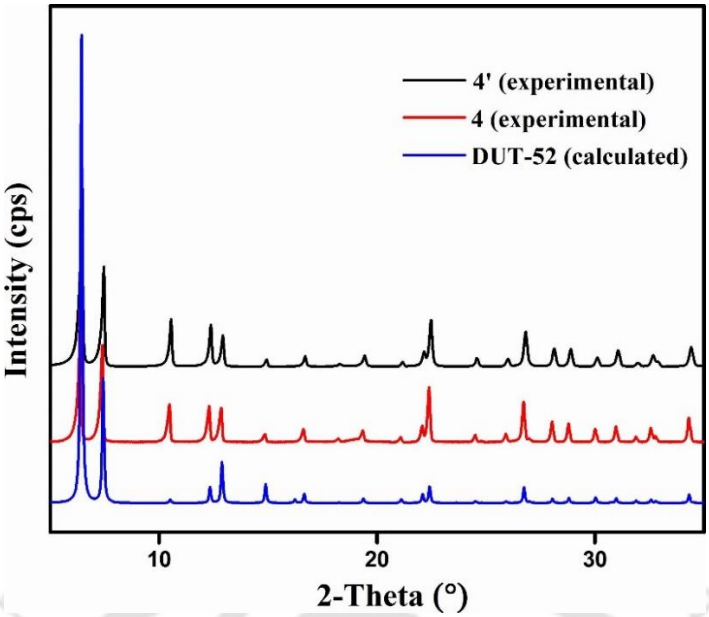

Figure 5.6 The simulated XRPD data of pristine DUT-52 MOF and experimental XRPD data of **4** and **4'**.

In the FT-IR spectra, **4** and **4'** showed frequencies at around 1577 and 1420 cm^{-1}, which correspond to the asymmetrical and symmetrical stretching vibrations of coordinated –COO group, respectively (Figure 5.7). A sharp peak for carbonyl stretching frequency of trifluoroacetamido group was observed at 1720 cm^{-1}.[71] Before activation, **4** contained solvent molecules (DMF) trapped inside the pore. Hence, in case of **4**, the carbonyl stretching frequency of DMF molecules appeared at 1653 cm^{-1}. This peak disappeared for activated compound, which indicated the full removal of trapped DMF molecules. Therefore, the compound was fully free from guest molecules after thermal activation.

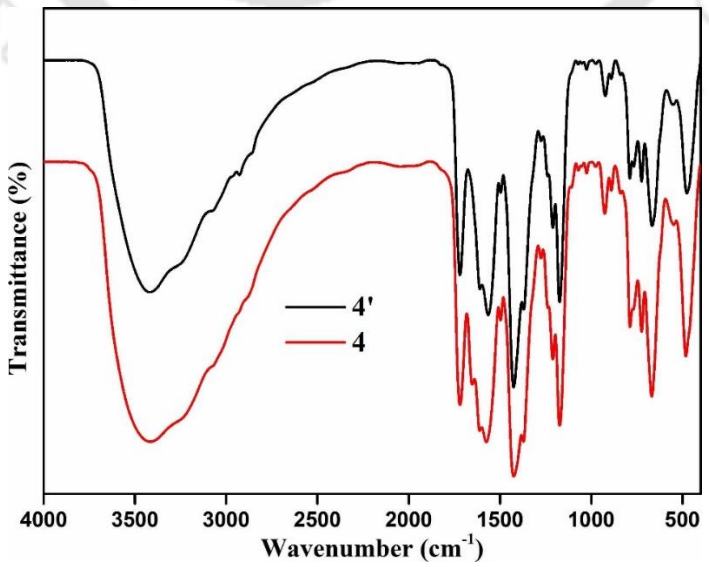

Figure 5.7 FT-IR spectra of as-synthesized **4** (red) and activated **4'** (black).

5.3.2 Structure Description

Zr(IV)-based MOFs are very attractive framework compounds with exceptionally high thermal, chemical and hydrolytic stability.[72] Among the few types of SBUs reported for Zr(IV)-based MOFs, the hexanuclear $[Zr_6O_4(OH)_4]^{12+}$ building unit is the most common. This SBU features 12-connected node and it is mainly found in the UiO-n (UiO stands for University of Oslo) family of robust, porous framework solids.[72] The structural framework of UiO-66 is obtained by the connection of $[Zr_6O_4(OH)_4]^{12+}$ SBUs with the carboxylates of twelve BDC linkers to produce 3-D framework with cubic close-packed structure. The framework of DUT-52 MOF is structurally related to UiO-66.[62] DUT-52 framework is made up of hexanuclear $[Zr_6O_4(OH)_4]^{12+}$ SBUs and un-functionalized NDC linkers (NDC is a longer version of BDC linker). The DUT-52 MOF was first synthesized by Kaskel *et al.* in 2013. According to the single-crystal X-ray diffraction analysis data of DUT-52, Kaskel and his group reported that it crystallized in cubic space group $Fm\bar{3}m$ (a = 23.910 (3) Å).[62] The crystal structure of compound **4** is exactly simiar as DUT-52 compound. The 3-D cubic framework of compound **4** (Figure 5.8) is formed by interconnecting hexanuclear $[Zr_6O_4(OH)_4]^{12+}$ building units through carboxylate groups of twelve NDC-$NHCOCF_3$ linkers. We also conducted indexing of the experimental XRPD data to obtain the unit cell parameters. Table 5.1 displays the indexing results, which point out that the lattice parameters are comparable with DUT-52. Pawley fit of as-synthesized XRPD data showed good similarity with the simulated XRPD pattern of DUT-52 (Figure 5.9). From these results, we can conclude that compound **4** is isostructural with DUT-52.

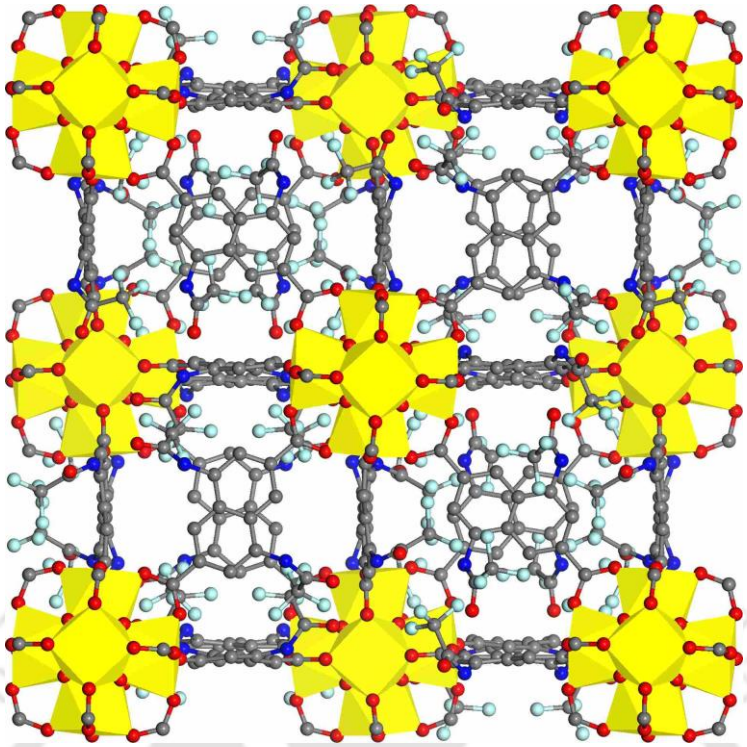

Figure 5.8 The simulated cubic framework structure of DUT-52-NHCOCF$_3$ MOF (**4**) in ball and stick model. The C, O, N and F atoms are shown as grey, red, blue, aquamarine colored balls, respectively. The Zr clusters are displayed as yellow polyhedra. The packing plot shows a double substitution of the –NHCOCF$_3$ groups and this is due to the symmetry operators in the cubic space group $Pn\bar{3}$. For the structural simulation, the atomic occupancy factors of the –NHCOCF$_3$ groups have been set to an occupancy factor of 0.5 each. The structure was simulated by Materials Studio software.[73]

Table 5.1 Unit cell parameters of **4** obtained by indexing its XRPD data. The obtained values have been compared with Zr-DUT-52 MOF.

Compound Name	DUT-52-NHCOCF$_3$ (**4**)	Zr-DUT-52[62]
Crystal System	cubic	cubic
a = b = c (Å)	23.785(3)	23.910(3)
V (Å^3)	13456.3(26)	13669(9)

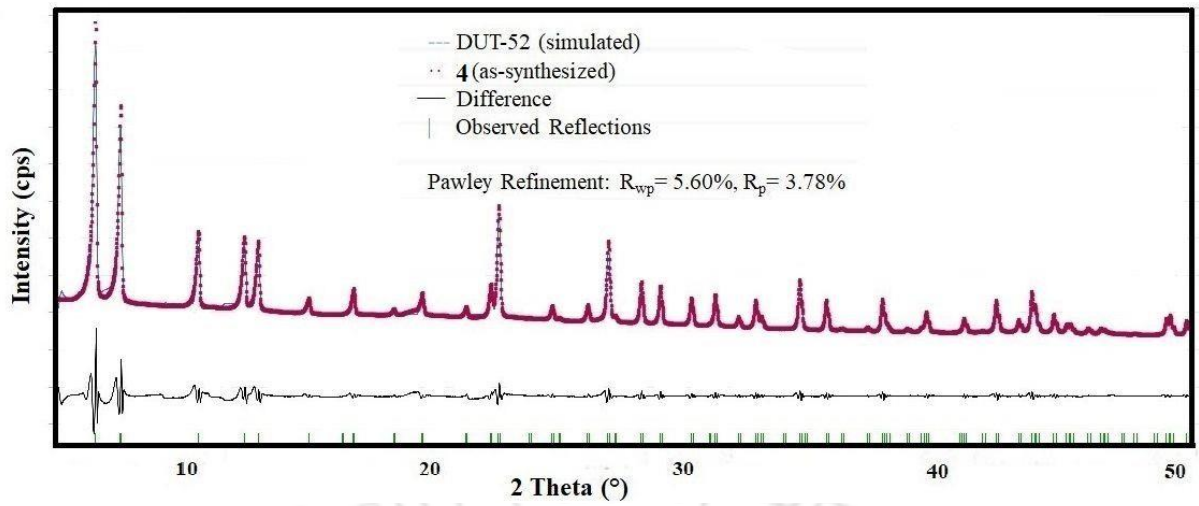

Figure 5.9 Pawley fit for the XRPD pattern of as-synthesized **4**. Blue lines and red dots denote simulated and observed patterns, respectively. The peak positions and difference plot are displayed at the bottom (R_p = 3.78, R_{wp} = 5.60).

5.3.3 Chemical stability

The chemical stability of **4'** was examined in different solvents by stirring it in water, ethanol, methanol, acetone, water, tetrahydrofuran (THF), dichloromethane (DCM), dimethyl sulfoxide (DMSO), DMF, 1(M) HCl, toluene, acetonitrile and acetic acid. After 12 h of stirring, the compound was filtered and dried at 80 °C. The structural features of the collected materials were examined by the XRPD technique. All the XRPD patterns were compared with the XRPD patterns of compound **4'**. As shown in Figure 5.10, the structural integrity was retained after the treatment with different solvent media. XRPD experiments were also performed after treating **4'** in different pH media (Figure 5.11) as well as after BET and CN^- sensing studies. The recorded XRPD patterns revealed the retention in structural integrity in all these cases. Hence, **4'** displayed amazing chemical stability in various solvents and at wide pH range.

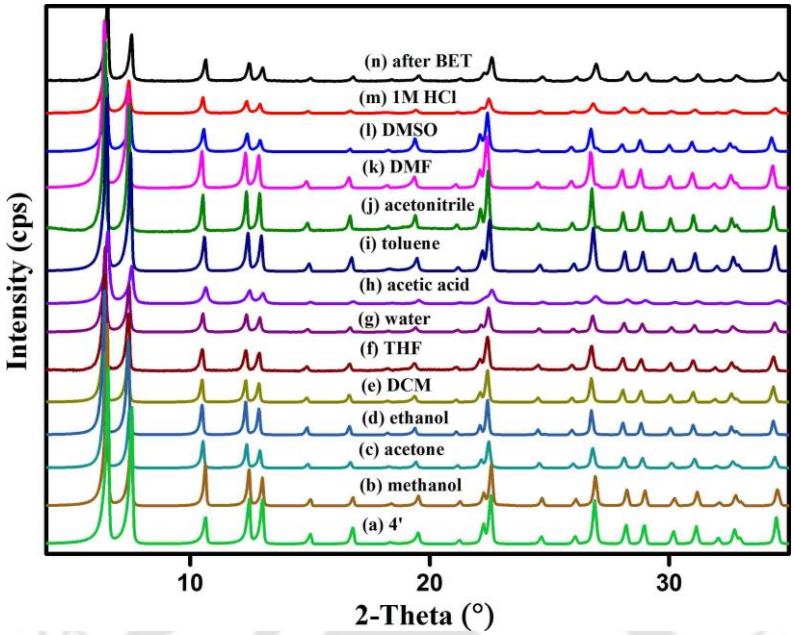

Figure 5.10 XRPD patterns of (a) **4'** showing its chemical stability in (b) methanol, (c) acetone, (d) ethanol, (e) DCM, (f) THF, (g) water, (h) acetic acid, (i) toluene, (j) acetonitrile, (k) DMF, (l) DMSO, and (m) 1M HCl. The XRPD pattern of **4'** after (n) checking the BET surface area.

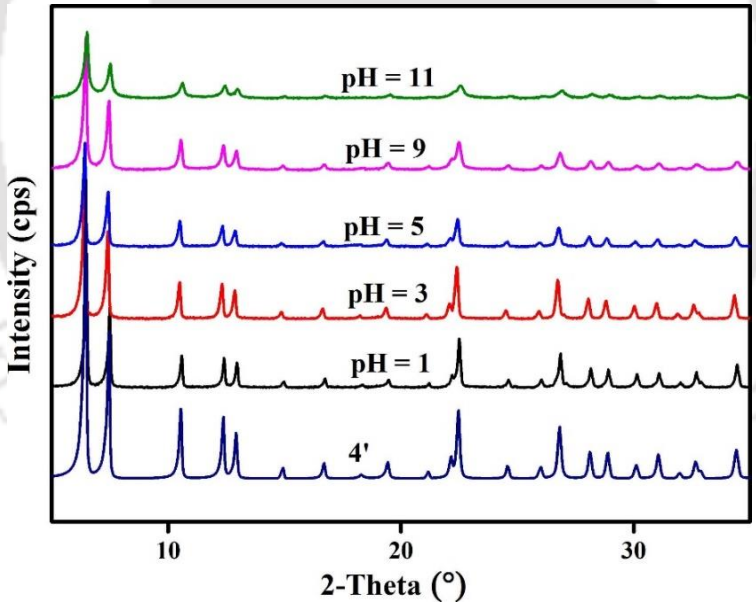

Figure 5.11 XRPD patterns of **4'** showing its chemical stability in different pH media.

5.3.4 Thermal stability

TGA of **4** and **4'** revealed that **4** and **4'** are thermally stable up to 300 °C under an air atmosphere (Figure 5.12). In the TGA curve of **4**, initially from 25-130 °C, 1.9% of weight loss is observed due to the removal of 3 water molecules per formula unit (calculated: 1.9%). Another weight loss (5.4%) for 2 DMF molecules per formula unit is observed in the range of

130-300 °C (calculated: 5.2%). These DMF molecules were trapped inside the pores of the material during its solvothermal preparation. Afterward (from 300 °C), the decomposition of compound starts due to the loss of organic linker. During the storage after desolvation, some water molecules were adsorbed by **4'**. The loss of these water molecules was observed in case of **4'** as the first weight loss step.

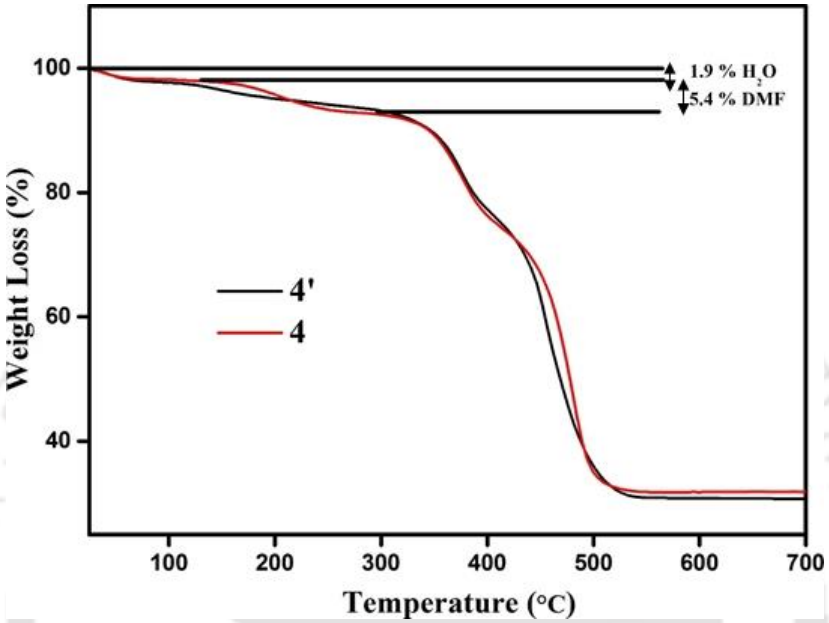

Figure 5.12 TG curves of as-synthesized **4** (red) and activated **4'** (black) recorded in an air atmosphere in the temperature range of 25-1000 °C at a heating rate of 5 °C min^{-1}.

The TGA data might provide some quantitative information about the linker defects in the structure. To quantify the linker defects, the previously reported calculation method was applied.[74] The molecular weight of an ideal, solvent free, dehydroxylated hexanuclear Zr_6 cluster is 3.51 times higher than $6ZrO_2$. Thus, if the end weight of a TGA run is normalized to 100%, the theoretical plateau ($W_{Ideal.\ Plat.}$) should be found at 351% on the TGA trace. The experimental plateau ($W_{Exp.\ Plat.}$) was found to be at 311% (Figure 5.13). Thus, the framework is lighter than that formulated by idealized equation. As seen in Figure 5.14, no additional broad peaks in the low 2-theta region suggested the absence of any missing-cluster defect.[75-76] The observed tendency hence suggests that the presence of only missing linker defects in the framework which helped in the catalytic reaction. The number of linker defects per Zr_6 formula unit has been calculated to be 0.96.

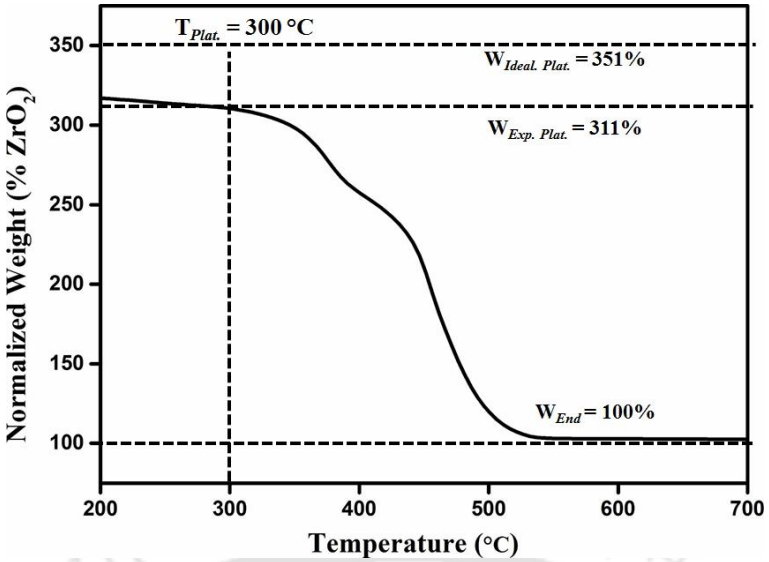

Figure 5.13 Calculation of missing linker defects from the TG curve of activated **4'**. The vertical dashed line pinpoints $T_{Plat.}$, the temperature at which the plateau ($W_{Exp. Plat.}$) is reached. The horizontal dashed lines pinpoint the relevant TGA plateaus.

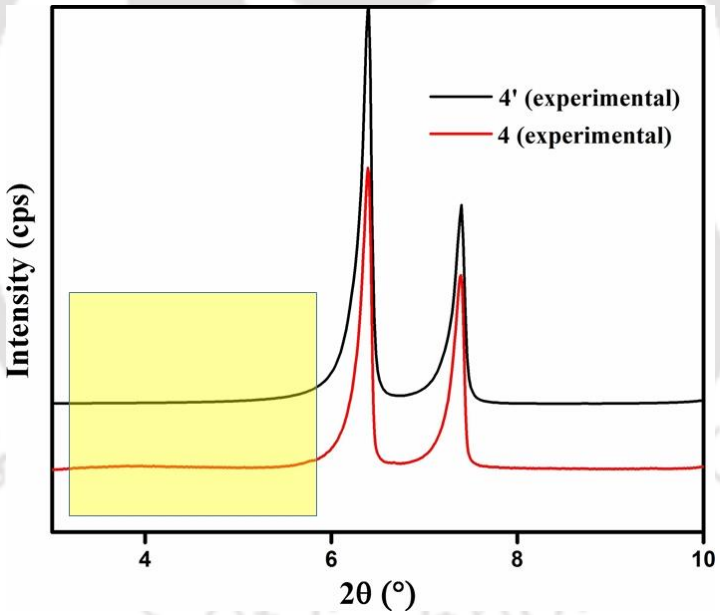

Figure 5.14 Low angle (2θ = 3-10°) region of the XRPD patterns of **4** and **4'**.

5.3.5 Nitrogen sorption study

The permanent porosity of activated compound **4'** was investigated by N_2 sorption studies. It showed type-I N_2 sorption isotherms (Figure 5.15). The sorption isotherm shown by **4'** is the characteristic property of microporous open network materials. The BET surface area was found to be 1105 m^2 g^{-1}. The value of micropore volume at p/p_0 = 0.5 was estimated as 0.60 cm^3 g^{-1}. As anticipated, the BET surface area value of our compound is lesser than the

parent compound, i.e. Zr-DUT-52 (1399 $m^2 g^{-1}$).[62] Nevertheless, this value is quite higher than previously reported dinitro functionalized Zr-DUT-52 MOF (S_{BET} = 330 m^2g^{-1}).[77] Density functional theory (DFT) pore size distribution analysis data revealed that, the pore size distribution of **4'** is mainly distributed below 1 nm (Figure 5.16) and with average pore radius is 1.09 nm.

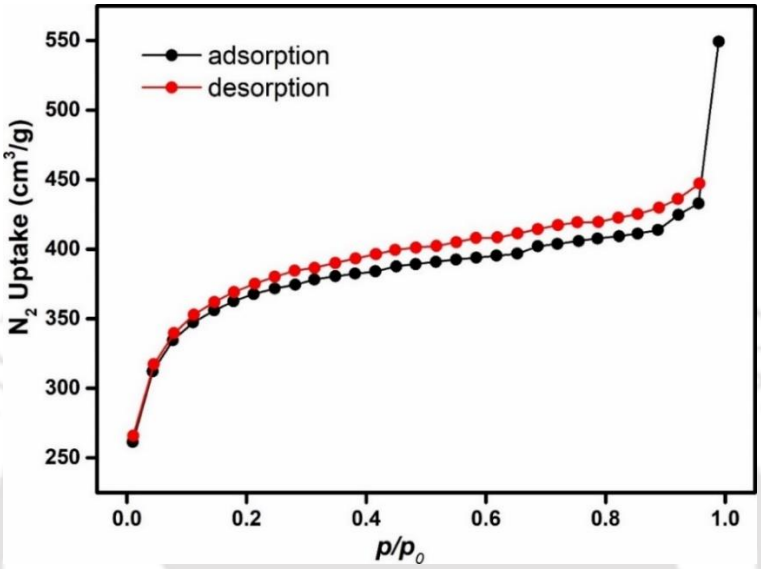

Figure 5.15 N_2 adsorption (black circles) and desorption (red circles) isotherms of thermally activated **4'** recorded at –196 °C.

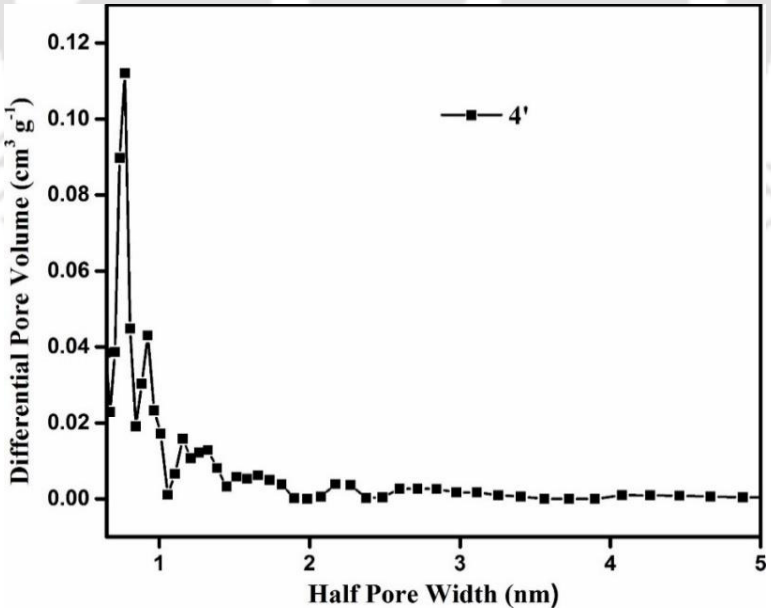

Figure 5.16 Density functional theory (DFT) pore size distribution analysis based on the N_2 adsorption data of **4'** recorded at –196 °C.

5.3.6 Hydrophobicity study

The functionalization of the NDC linker with a trifluoroacetamido group led to a highly hydrophobic framework. The hydrophobicity of the framework was demonstrated by the water-contact angle (WCA) measurement (Figure 5.17). Materials with contact angles below 90° are considered as hydrophilic, in between 90-150° are considered as hydrophobic and above 150° are considered as superhydrophobic.[78] The advancing contact angle of **4'** was measured to be 163° with a contact angle hysteresis of 7°. This result confirmed that our material is superhydrophobic in nature.

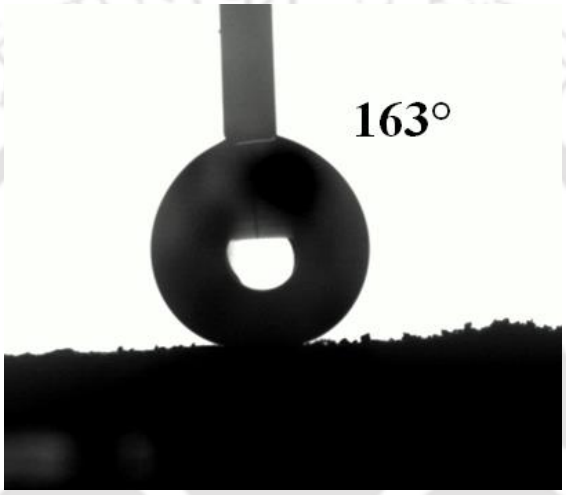

Figure 5.17 Water contact angle (WCA) measurement of **4'**.

5.3.7 Luminescence sensing of CN^-

The $H_2NDC\text{-}NHCOCF_3$ linker was selected to build LMOFs, which was targeted for sensing application due to its conjugated napthelene ring and trifluoroacetamido group as binding sites with CN^- ion. As shown in Figure 5.18, after dispersing **4'** into deionized water, it showed strong emission peak at 430 nm when we excited at 350 nm. The room temperature luminescence properties of **4'** and free $H_2NDC\text{-}NHCOCF_3$ linker were studied in the solid state (Figure 5.19). As expected, upon excitation at 350 nm, $H_2NDC\text{-}NHCOCF_3$ linker showed a weak and wide emission band as compared to **4'** under the same measurement conditions.[79] A slight blue shift was observed in case of **4'** from free $H_2NDC\text{-}NHCOCF_3$ linker (emission centered at 490 nm and 512 nm, respectively). The fluorescence intensity of **4'** is mainly due to the fluorescence emission of the organic linker. The enhancement of fluorescence intensity occurred upon the formation of the ordered 3D MOF structure.[80]

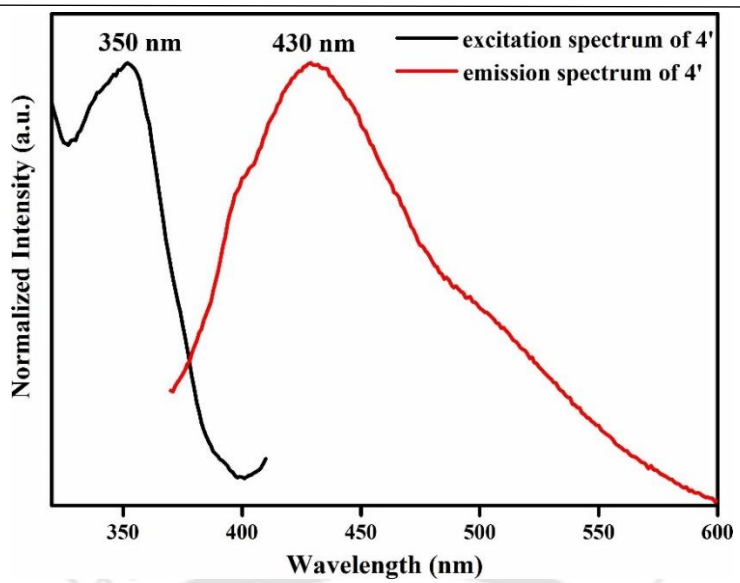

Figure 5.18 Fluorescence excitation and emission spectra of **4'**.

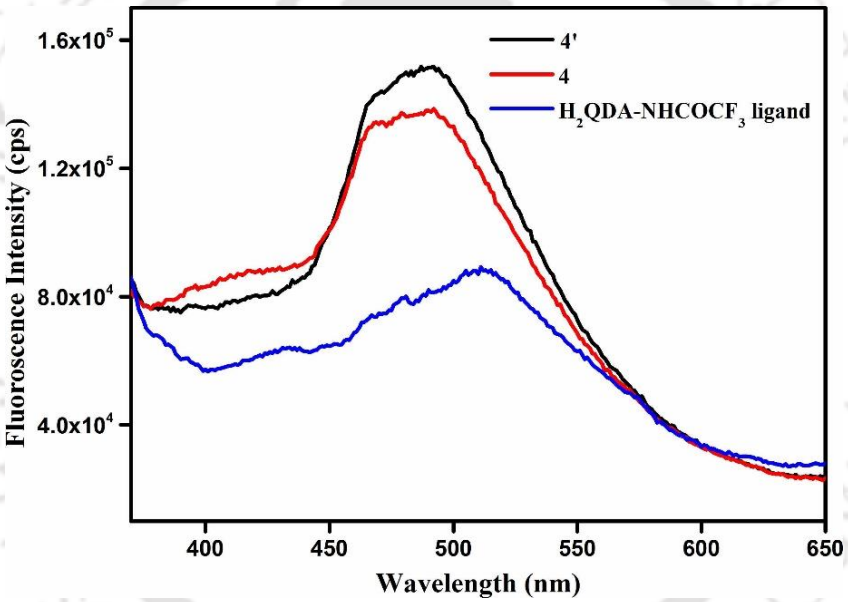

Figure 5.19 Fluorescence emission spectra of **4'** and H_2NDC-NHCOCF_3 linker in the solid state (λ_{ex} = 350 nm).

Due to its high stability in water as well as non-toxic nature of **4'**, we decided to explore the detection capacity of CN^- ion by **4'** in water. The CN^- ion detection behaviour of **4'** in water was examined by monitoring the emission spectrum of stable aqueous dispersion of **4'** after addition of 10 mM solution of NaCN in water. A sudden increase in the emission intensity was noticed after continual addition of CN^- ion solution. As shown in Figure 5.20, upon addition of 200 μL of 10 mM aqueous NaCN solution, almost 3-fold increment was observed for fluorescence emission intensity. On further addition of CN^- ion solution (10 mM), no further increase in the emission intensity observed. As shown in Figure 5.20, upon excitation at 350

nm, the emission band of compound **4'** was found at 427 nm. After addition of cyanide solution to **4'**, the emission intensity increased as well as a significant bathochromic shift of 63 nm was observed. This emission band at 490 nm indicated that the nucleophilic addition at trifluoroacetamide group took place by cyanide anion.[81]

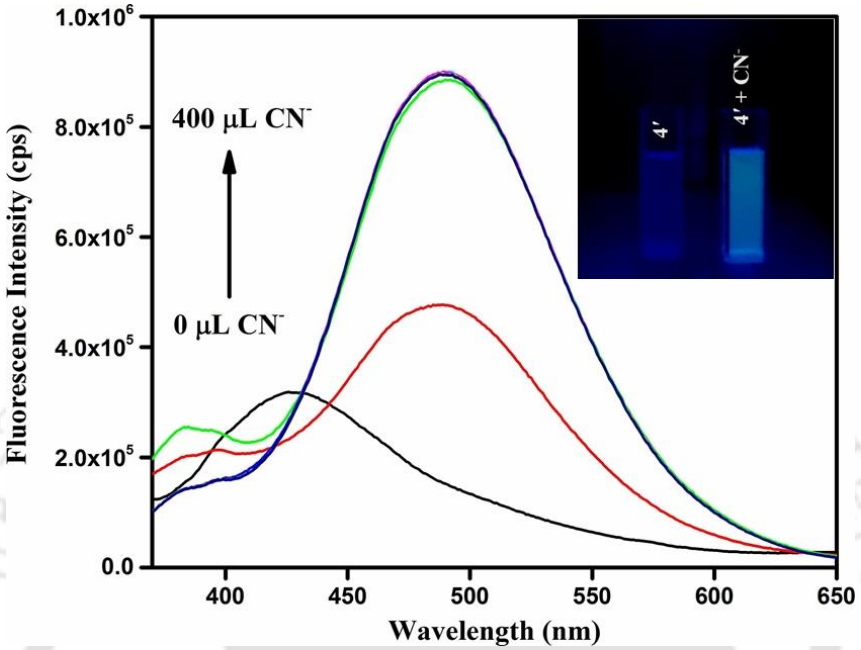

Figure 5.20 Fluorescence emission spectra of **4'** (in water) after incremental addition of aqueous CN^- solution (10 mM). Inset: digital images of cuvettes containing **4'** dispersion with and without CN^- solution under a UV lamp.

A time dependent study was carried out in which the fluorescence of **4'** dispersion was checked as a function of time after the addition of 200 µL of 10 mM cyanide solution. A gradual enhancement of fluorescence was observed up to 2 min. After that, there was no further increase in intensity as shown in Figure 5.21. Hence, we can state that saturation point for fluorescence intensity was achieved after 2 min. The result proved that **4'** is a promising fluorescent "turn-on" probe for CN^- with short response time. This response time is comparable with the previously reported MOF based CN^- sensors (Table 5.2).[38, 45, 47]

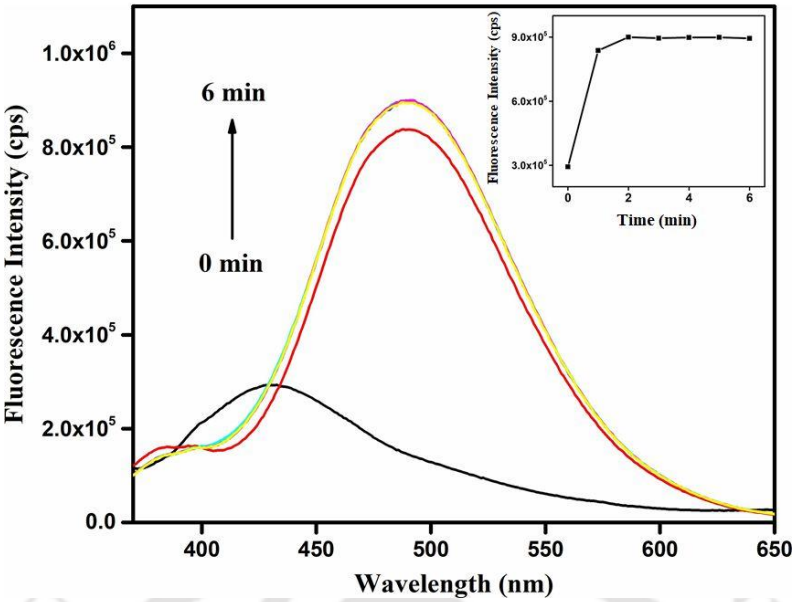

Figure 5.21 Turn-on fluorescence response of **4'** (in water) towards gradual addition of 200 µL of 10 mM cyanide solution at a regular time interval of 1 min up to 6 min. Inset: time dependence of the fluorescence emission intensity.

Table 5.2 Comparison of response time and detection limit of various fluorescent probes for cyanide sensing.

Sl. No.	Name of MOF	Medium Used	Response Time	Detection Limit	Ref.
1	DUT-52-NH-$COCF_3$	water	2 min	0.23 µM	this work
2	CAU-10-N_2H_3	water	2 min	0.48 µM	45
3	carbazole-functionalized UiO-67	water	-	0.14 µM	46
4	M-ZIF-90	DMSO/water	-	2 µM	39
5	Bio-MOF-1⊃DAAC	HEPES buffer	-	5.2 ppb	49
6	Tb-ADP-Bipy	water	10 s	30 nM	47
7	hemicyanine-functionalized mixed-ligand PCN-700	water	1 min	0.05 µM	38

8	**P-1'**	THF/water	5 min	0.35 µM	82

The selectivity of compound **4'** towards CN^- ion was also investigated. The fluorescence spectra of **4'** were recorded after addition of 200 µL of other competitive anions (10 mM) like NO_3^-, HCO_3^-, SO_4^{2-}, F^-, ClO_4^-, SCN^-, I^-, AcO^-, NO_2^-, CH_3O^-, Br^-, Cl^- and $S_2O_3^{2-}$. For all other anions except CN^-, the increase in fluorescence intensity was negligible (0.7-0.9 fold) relative to CN^- (Figure 5.22). It is clearly noticed that the competitive anions have very little impact on the fluorescence of the probe. Hence, the selectivity of the MOF sensor for CN^- over other intrusive anions in aqueous medium is noticeable. We also examined the effect of turn-on behaviour of **4'** for CN^- ion when other interfering anions are present in the medium. For that purpose, fluorescence spectra were recorded by adding the same amount (200 µL of 10 mM solutions) of selected anions and cyanide sequentially to the stable dispersion of compound **4'**. Figure 5.23 revealed that after the addition of aqueous CN^- solution to the mixture containing other anions, the fluorescence intensity of **4'** drastically increased along with a bathochromic shift of the emission band up to 63 nm. The bathochromic shift in the fluorescence emission maximum of **4'** in the presence of CN^- ion provides evidence of nucleophilic addition at the trifluoroacetamide group by CN^- ion.[81] All these results imply that the probe maintained high specificity for CN^- even when the sensing medium contained other competing anions.

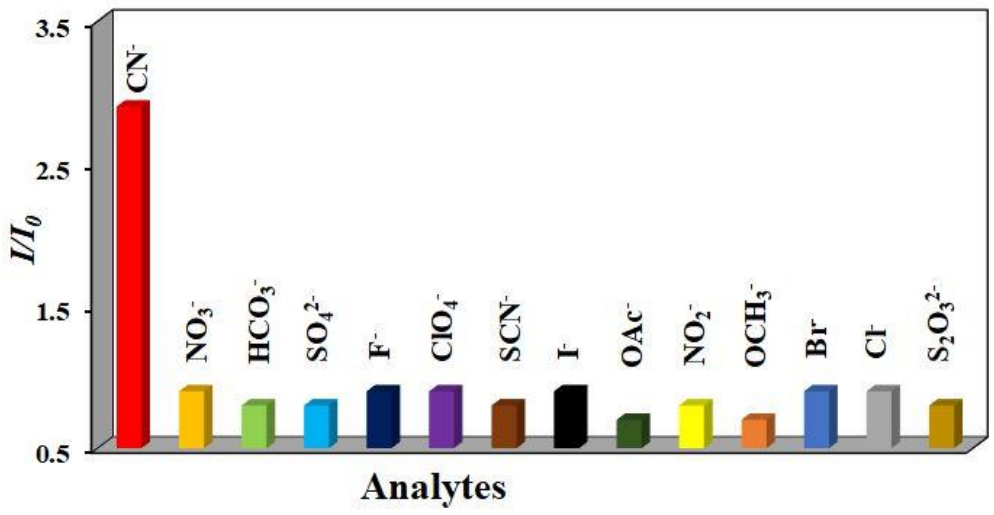

Figure 5.22 Fluorescence turn-on response of **4'** dispersion towards different anions (200 µL of 10 mM in water).

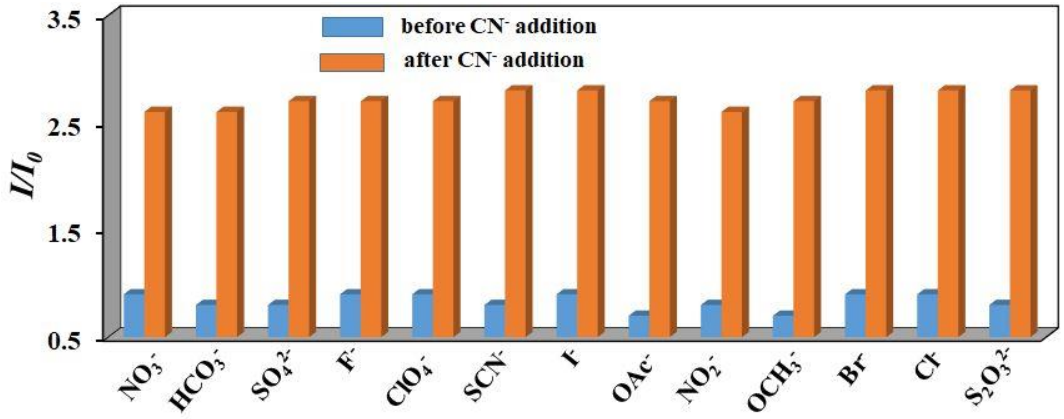

Figure 5.23 Comparison of fluorescence turn-on response of **4'** dispersion towards CN^- (200 µL of 10 mM solution in water) in presence of other potentially competitive anions (200 µL of 10 mM solutions in water).

To estimate the limit of detection (LOD) of **4'** as an efficient fluorescent probe for the sensing of CN^- ion, fluorescence titration experiments were conducted using low concentrations of aqueous NaCN solution. The LOD value was calculated by using formula: LOD = $3\sigma/K$, where σ is the standard deviation of the blank dispersion and K is the slope of the graph drawn between the fluorescence intensity and concentration of CN^- solution (Figure 5.24).[45] The final LOD value was found to be 0.23 µM, which is lower than the maximum acceptable concentration of CN^- ion in drinking water as permitted by WHO.[5]

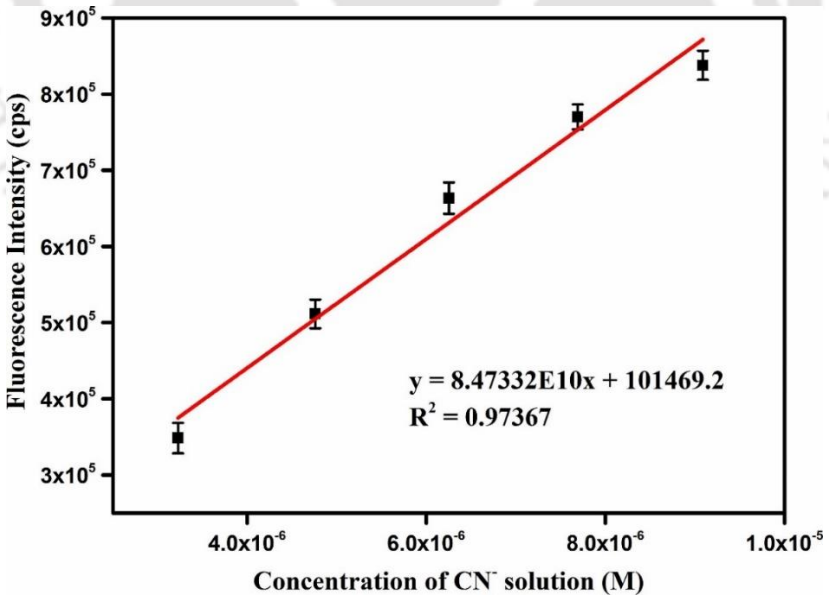

Figure 5.24 Fluorescence intensity of **4'** in water as a function of NaCN concentration. The error bars indicate the standard deviations of three measurements.

We also examined the fluorescence responses of **4'** at different pH ranging from 2 to 11. As shown in Figure 5.25, the fluorescence intensities of the MOF before and after CN^- addition are almost similar in the pH ranging from 3 to 9. These results indicate that our probe can be used for cyanide detection in the pH range from 3 to 9. At highly acidic pH (pH = 2), the –NH proton may undergo protonation and thus the deprotonation by CN^- ion is prevented. Thus, the fluorescence intensity of the probe did not increase upon CN^- addition. After pH 9, the hydroxide ion deprotonates the –NH proton and hence the probe already showed turn-on fluorescence before addition of CN^- ion. Thus, after pH 9, the fluorescence intensity of the probe did not increase significantly after the addition of CN^- solution. The visual changes (under UV lamp) in fluorescence intensity of the probe after addition of CN^- solution in different pH media are shown in Figure 5.26.

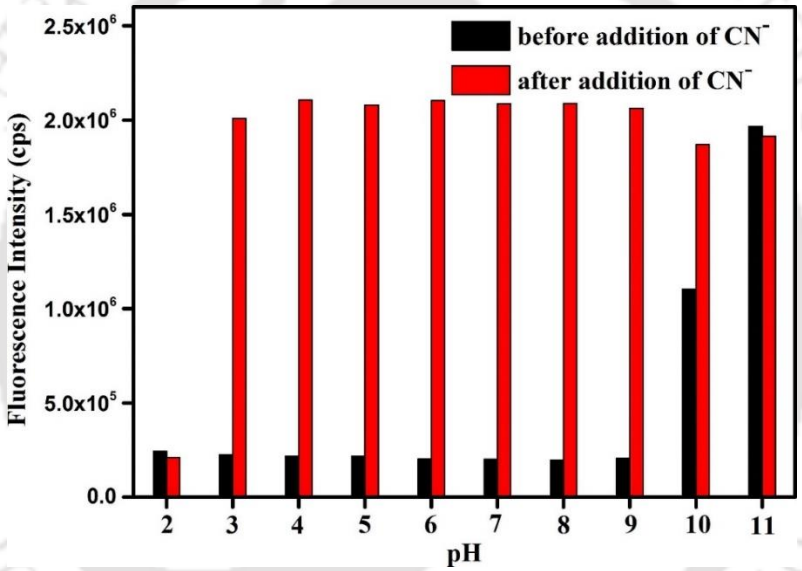

Figure 5.25 Effect of pH on the fluorescence emission intensity of **4'** before and after the addition of 10 mM cyanide solution (400 µL).

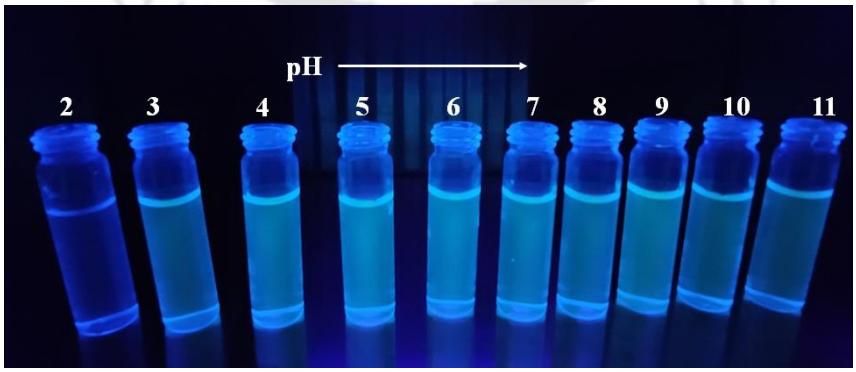

Figure 5.26 Visual changes (under UV lamp) observed for the dispersion of **4'** upon addition of 400 µL of 10 mM CN^- solution at different pH.

5.3.8 Sensing of CN^- in real water samples and paper strips

The practicability of the method was demonstrated by detection of CN^- ions directly in four different environmental water samples (tap, drinking, lake and river water). As shown in Figure 5.27, different water samples containing **4'** were spiked with different concentrations of CN^- solution. After addition of CN^- solution, the fluorescence intensity increased effectively in all different water samples. With increase in the concentration of CN^- solution, the fluorescence intensity also increased. These experimental results suggest that **4'** can be used for the recognition of CN^- ion in environmental water samples. Subsequently, to investigate the on-site detection of CN^- ion in real field, a portable paper strip method was developed. The MOF dispersion in water was coated on a paper strip (using Whatman filter paper) and the paper strip was dried completely. Then, 200 μL of 10 mM CN^- solution was applied using micropipette. As shown in Figure 5.28, the fluorescence colour of the MOF-coated paper strip (under UV lamp) gradually changed from colourless to bright blue with the addition of 10 mM of CN^- solution. Thus, this portable paper strip can be easily used by people for the on-site detection of CN^- at any moment.

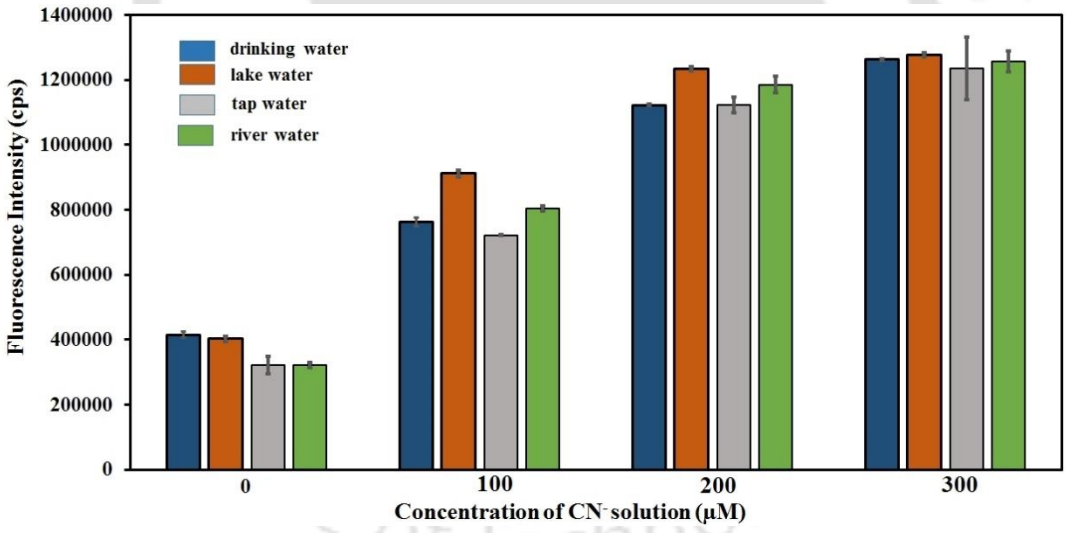

Figure 5.27 Fluorescent detection of CN^- ion in drinking, lake, tap and river water samples by **4'**. The error bars suggest the standard deviations of three measurements.

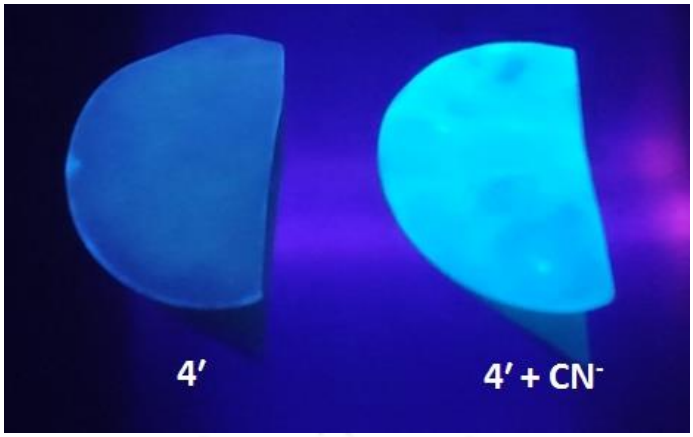

Figure 5.28 Fluorescence changes of **4'**-coated portable paper strips for detecting aqueous NaCN solution under UV lamp at room temperature.

5.3.9 Mechanism for turn-on detection of CN^- ion

It has been previously reported for trifluoroacetamido functionalized organic molecules that the presence of strong electron-withdrawing trifluoroacetyl moiety makes the trifluoroacetamide as electron-withdrawing group.[83-84] Hence, the electron-withdrawing trifluoroacetamide group attached to aromatic ring weakens the emission intensity due to photo-induced electron transfer (PET) process from the aromatic system towards the trifluoroacetamide group.[35, 71, 81] Therefore, the aqueous dispersion of **4'** showed fluorescence weak emission band at 427 nm upon excitation at 350 nm. After addition of CN^- to **4'** dispersion, a notable increase in emission intensity with a significant bathochromic shift of 63 nm (Figure 5.20). It has been reported in the literature that the trifluoroacetamide functionalized organic molecules have strong affinity towards cyanide ion and the trifluoroacetamide group is easily converted into cyanohydrin adduct through nucleophilic addition by cyanide ion.[50, 71, 81, 85-86] The trifluoroacetamide group becomes strong electron-donating moiety after nucleophilic addition of CN^- ion (Scheme 5.2). Thus, the PET process is inhibited. As a result, the drastic increment of fluorescent intensity as well as significant red shift (63 nm) of emission band. As a control experiment, we performed the same fluorescence experiment with unfunctionalized DUT-52 MOF (Figure 5.29). After incremental addition up to 400 μL of 10 mM CN^- solution, there was a slight decrease in fluorescence intensity for parent DUT-52 whereas a remarkable increase in fluorescence intensity was observed for the present probe. To investigate the possible mechanism, ^{1}H NMR titration experiments were carried out with digested **4'** at room temperature (Figure 5.30). With increase in the equivalent concentration of CN^-, the intensity of the peak at 11.79 ppm for –NH proton decreased and gradually shifted

towards the up-field region. After the addition of one equivalent of CN^- solution, the peak for the –NH proton almost vanished. At the same time, the peaks for the aromatic region protons also shifted towards up-field after the addition of CN^- solution. In the ^{13}C NMR spectrum of digested **4'** (Figure 5.31), the peak for the carbonyl carbon of trifluoroacetyl group was highly up-field at 57.95 ppm, indicating the formation of cyanohydrin adduct.[35] The bathochromic shift in the fluorescence emission maximum of **4'** in the presence of CN^- ion also provides the evidence of nucleophilic addition at the trifluoroacetamide group by CN^- ion (Figure 5.20). It can be seen from Figure 5.25 that, under highly basic conditions, **4'** shows enhancement of fluorescence intensity even before the addition of cyanide solution. This enhancement may be due to the deprotonation of –NH proton by the hydroxide ion. Thus, based on the obtained experimental results, we can conclude that the possible mechanisms of CN^- detection by **4'** are the nucleophilic addition of CN^- to the trifluoroacetamide group and the deprotonation of the –NH proton of trifluoroacetamide group.

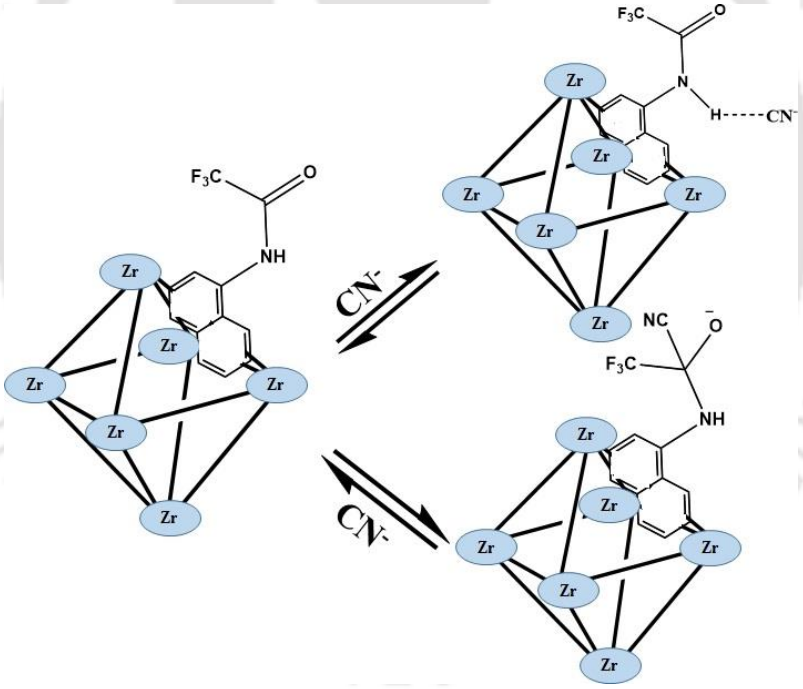

Scheme 5.2 Possible mechanisms of CN^- sensing by **4'**.

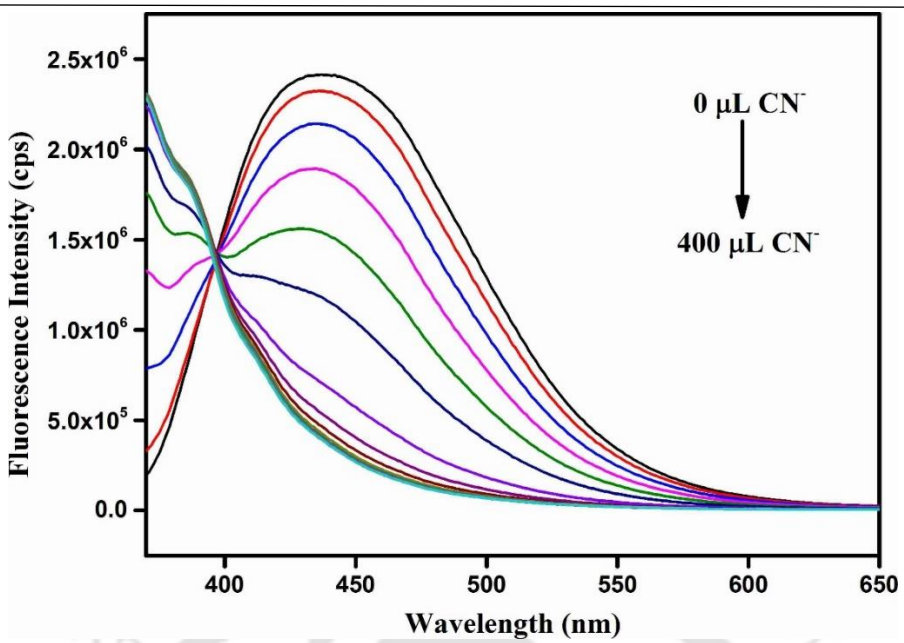

Figure 5.29 Change in the fluorescence intensity of DUT-52 MOF dispersed in water after the addition of 10 mM aqueous NaCN solution.

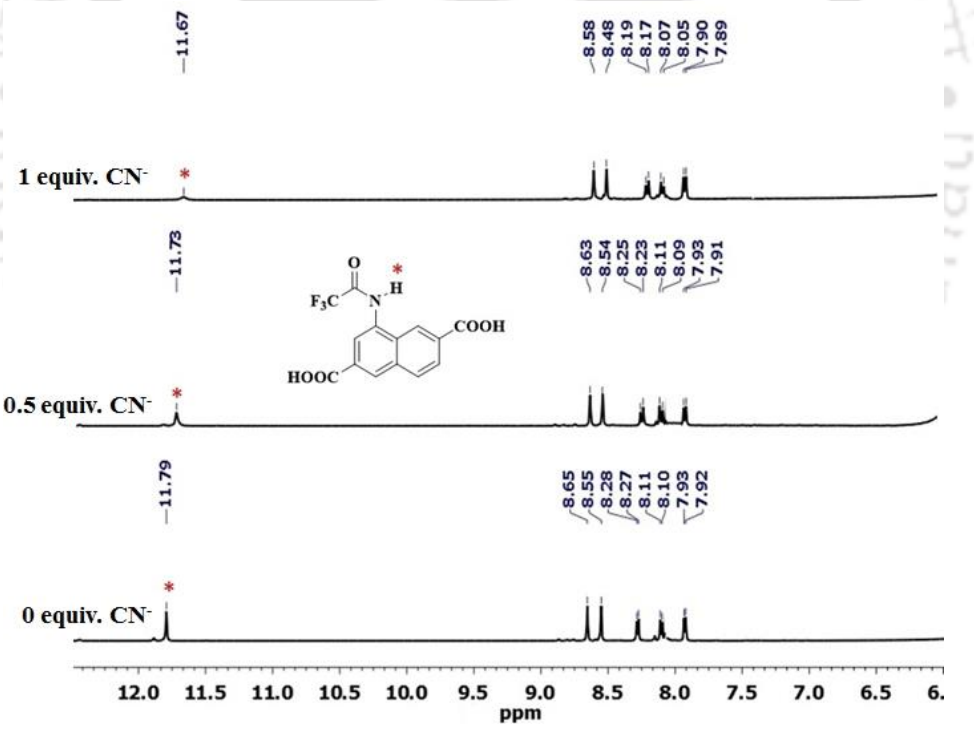

Figure 5.30 Extended view of stacked ^{1}H NMR spectra of NaCN-treated **4'** after digestion in DMSO-d_6/HF.

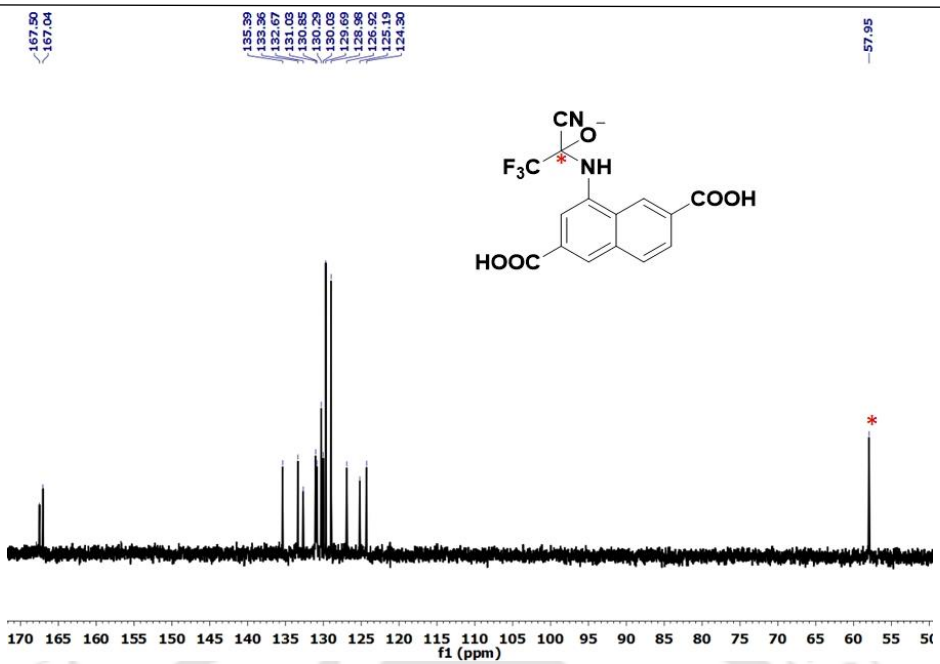

Figure 5.31 ^{13}C NMR spectrum of digested **4'** after treatment with CN^- ion.

5.4 Aerobic oxidation of cyclohexane

Aerobic oxidation of cycloalkanes with very high selectivity of their respective alcohols/ketones is one of the challenging reactions in organic chemistry. In particular, aerobic oxidation of cyclohexane has received tremendous attention due to the commercial importance of its products as the feedstock for the preparation of polymers. Although many efforts have been made to increase the selectivity of alcohol/ketone during the oxidation of cyclohexane, one of the strategies to functionalize the linker with fluorine atoms is to create hydrophobic cavities within the pores of MOFs. This idea was successful in accommodating high population of hydrophobic cyclohexane molecules by increasing the close proximity between the redox sites and cyclohexane. In one of the examples, PCN-222(Fe)-F7 showed 50% conversion of cyclohexane with 90% selectivity of alcohol/ketone in the presence of TBHP as initiator at 80 °C in acetonitrile with $AgBF_4$ as cocatalysts.[87] Very recently, another strategy was developed for the aerobic oxidation of cyclohexane. PCN-224(Mn) was subjected to linker exchange reaction with 2,2'-bis(trifluoromethyl)-4,4'-diphenyl phthalate (L) to introduce hydrophobic cavities in PCN-224(Mn)-L. The aerobic oxidation of cyclohexane was performed with PCN-224(Mn)-L solid and observing 51% conversion with 90% selectivity of alcohol/ketone using TBHP as initiator at 80 °C in acetonitrile using $AgBF_4$ as cocatalyst.[88] The conversion of cyclohexane was reduced to 16% with PCN-224(Mn) with 79% selectivity of alcohol/ketone under identical conditions. This significant decrease in the conversion and selectivity is due to

the lack of hydrophobic cavities, thereby decreasing the contact between the redox sites with cyclohexane since most of the cyclohexane molecules remains on its surface.

These interesting precedents prompted us to prepare **4'** and to evaluate its catalytic activity in the aerobic oxidation of cyclohexane under similar conditions followed in these precedents. The catalytic data of cyclohexane conversion and the selectivity of cyclohexanol and cyclohexanone are presented in Table 5.3. The aerobic oxidation of cyclohexane was negligible (1%) using **4'** as solid catalyst in the absence of TBHP as a radical initiator. In contrast, the conversion of cyclohexane in the presence of **4'** was boosted to 21% with 84% selectivity of alcohol/ketone with 8 µL of TBHP under similar conditions while the conversion was two-fold lower in the absence of $AgBF_4$ (Figure 5.32). On other hand, the conversion of cyclohexane was doubled with slight difference in the alcohol/ketone selectivity (81%) with 20 µL of TBHP using **4'** as solid catalyst under identical conditions. Furthermore, the aerobic oxidation of cyclohexane was performed with 8 µL of TBHP by purposely adding pyridine as a catalytic poison. As it can be seen from Table 5.3, the addition of pyridine to the reaction mixture completely stopped the reaction. This observation is due to the poisoning of uncoordinated metal sites due to the missing linkers as evidenced from TGA studies, which is primarily responsible for the activation of TBHP to initiate the radical oxidation process. On the other hand, the activity of the metal precursor and the functionalized linker was also tested under identical conditions. Although the conversion of cyclohexane was relatively lower than **4'**, the milder activity of the metal precursor arose due to its mild Lewis acidic nature to activate TBHP. Furthermore, the activity of the metal precursor was inhibited after 12 h, while the conversion still progressed with **4'**. These results clearly indicate the advantage of installing the metal nodes within the MOF without undergoing deactivation.

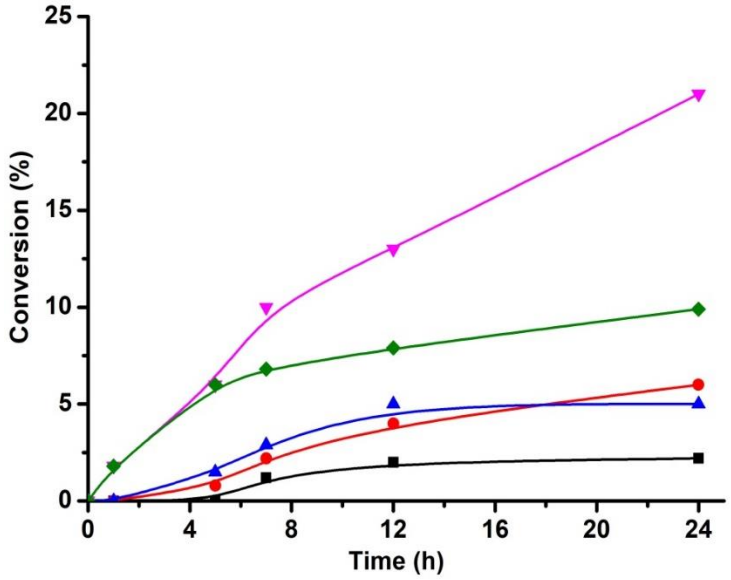

Figure 5.32 Time conversion profile for the aerobic oxidation of cyclohexane. (■) without catalyst (blank), (▲) in the presence of $ZrOCl_2 \cdot 8H_2O$, (●) in the presence of DUT-52 (identical linker without $-NHCOCF_3$ group), (►) in the presence of **1′** and (♦) upon filtration of **4'** solid after 5 h and the reaction mixture stirred without catalyst under identical conditions. Reaction conditions: cyclohexane (1 mmol), catalyst (20 mg), CH_3CN (2.5 mL), $AgBF_4$ (26 mg), O_2 Purging, 60 °C, Reflux, 24 h.

Table 5.3. Aerobic oxidation of cyclohexane using **4'** and analogous catalysts.[a]

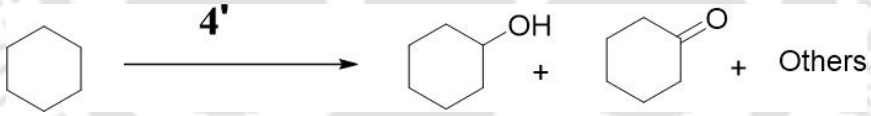

Entry	Catalyst	TBHP (µL)	Conversion[b] (%)	Selectivity[b] (%)	
				ol	one
1	**4'**	0	1	-	-
2	**4'**	8	21, 19,[c] 17[d]	29, 32,[c] 33[d]	55,51,[c] 47[d]
3	**4'**	20	42	33	48
4[e]	**4'**	8	-	-	-
5	DUT-52	8	6	32	48
6[f]	$ZrOCl_2 \cdot 8H_2O$	8	5	34	49

7[g]	$H_2NDC\text{-}NHCOCF_3$	8	3.5	36	46
8[h]	**4'**	8	11	36	47
9[i]	**4'**	8	15	25	51
10[j]	**4'**	8	11	28	47

[a] Reaction conditions: cyclohexane (1 mmol), catalyst (20 mg), CH_3CN (2.5 mL), $AgBF_4$ (26 mg), O_2 Purging, 60 °C, 24 h.

[b] Conversion and selectivity were determined by GC. Selectivity corresponds to the mixture of cyclohexanol and cyclohexanone. Other products are 2-hydroxycyclohexanone and adipic acid.

[c] First reuse.

[d] Second reuse.

[e] Pyridine (50 µL).

[f] 14 mg of $ZrOCl_2 \cdot 8H_2O$.

[g] 15 mg of $H_2NDC\text{-}NHCOCF_3$.

[h] Without $AgBF_4$.

[i]Cycloheptane as a substrate.

[j]Cyclooctane as a substrate.

In order to prove the influence of hydrophobic fluorinated groups in **4'** to promote cyclohexane oxidation, adsorption of cyclohexane was performed with **4'** and DUT-52 under identical conditions employed for catalytic experiments (Table 5.4, Supporting Information). These results clearly indicate that **4'** favours more adsorption of cyclohexane facilely compared to DUT-52 due to the presence of hydrophobic groups in the former solid. On the other hand, the activity of DUT-52 was tested in the aerobic oxidation of cyclohexane as a control experiment under identical conditions. DUT-52 exhibited much lower activity (6%) under similar conditions (Figure 5.32) due to the lack of hydrophobic cavities as well as poor adsorption of cyclohexane compared to **4'**. These experimental results are in good agreement with earlier reports,[87-88] thus demonstrating the facile diffusion of cyclohexane within the pores

of **4'** due to the assistance provided by hydrophobic cavities to enhance the conversion of cyclohexane.

Table 5.4 Adsorption of cyclohexane over **4'** and DUT-52 under similar conditions used for catalytic experiments.

Time (h)	mmol of cyclohexane adsorbed by DUT-52	mmol of cyclohexane adsorbed by **4'**
1	0.015	0.17
3	0.1	0.33
5	0.19	0.5
7	0.28	0.62

Reaction conditions: cyclohexane (1 mmol), catalyst (20 mg), CH_3CN (2.5 mL), O_2 Purging, 60 °C.

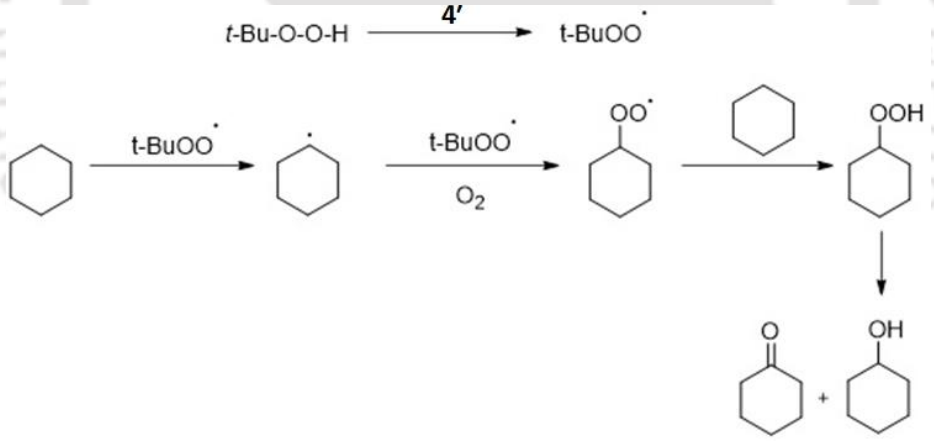

Scheme 5.3 Proposed mechanism for the aerobic oxidation of cyclohexane by **4'** with TBHP.

The observed experimental results shown in Table 5.3 prompted us to propose a reaction mechanism as shown in Scheme 5.3. The aerobic oxidation of cyclohexane was negligible with **4'** as solid catalyst in the absence of TBHP. In contrast, the oxidation of cyclohexane with **4'** in the presence of TBHP promoted the oxidation reaction. The uncoordinated metal sites due to the missing linkers (from TGA results) in **4'** activate TBHP[52, 89] to produce t-BuOO•, which later abstracts hydrogen to afford cyclohexyl radical. This upon reaction with molecular oxygen gives oxygen based radical intermediate, followed by

hydrogen abstraction from cyclohexane affords to the corresponding hydroperoxide. Finally, this hydroperoxide decomposes to cyclohexanol and cyclohexanone in the presence of **4'**. Although these processes are similar with DUT-52 and **4'** solids, the superior activity of the later catalyst is due to the facile diffusion of cyclohexane with the assistance of hydrophobic groups. Further to support these observations, two control experiments were carried out with TEMPO and hydroquinone as radical trapping agents under similar conditions. The catalytic results of cyclohexane oxidation using **4'** with these radical trappers suggested that the conversion (<2 %) is significantly suppressed, thus supporting the above.[56, 88]

Besides the oxidation of cyclohexane, other cycloalkanes were also tested to study the influence of molecular dimension of these substrates for size-selective.[90] From the results shown in Table 5.3 and Figure 5.33, the conversion of cycloalkane is decreased upon increasing the ring size from cyclohexane to cyclooctane. These results prove that the molecular dimension of a cycloalkane plays an important role in the oxidation reaction. Furthermore, a more bulky substrate like phenylcyclohexane was tested under similar conditions and observing 2% conversion with no desired oxidation products. Interestingly, this substrate exhibited long induction period compared to other cycloalkanes tested under similar conditions (Figure 5.33). Thus, the poor conversion along with long induction period clearly indicates the diffusion limitation of phenylcyclohexane. These results prove that the size of a substrate is one of the factors influencing the final conversion of cycloalkanes and size-selective catalysis is operative with cyclohexane due to its smaller dimension (0.6 nm) than the average pore size of **4'** (1.09 nm) (Figure 5.16).

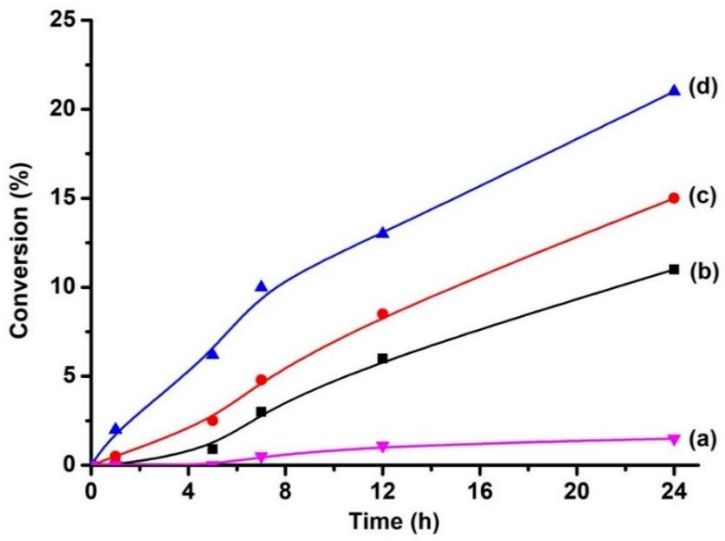

Figure 5.33 Time conversion profile for the aerobic oxidation of a) phenylcyclohexane, b) cyclooctane, (c) cycloheptane and (d) cyclohexane.

Comparing the data obtained in the present study with those reports in the literature clearly indicate some superiority of this work. The comparable catalytic activity in the oxidation of cyclohexane was achieved in the present work even at 60 °C while earlier reports[87-88] required 80 °C. On other hand, the increase of TBHP concentration showed gradual increase in cyclohexane conversion while decreasing alcohol/ketone selectivity in these two reports.[87-88] However, the present catalyst showed two-fold increase in conversion of cyclohexane without affecting the selectivity of the oxidized products. This is due to the milder redox ability of Zr than Fe and Mn-based MOFs without favouring the oxidation of the primarily formed oxidation products. Interestingly, the present catalyst clearly proved that the conversion of cyclohexane was enhanced with **4'** due to its fluorinated linker as well as afforded higher selectivity to alcohol/ketone due to mild oxidizing ability of Zr by controlling the over-oxidation of the primary products.

Catalyst stability is often checked by reusing the recovered solid in repeated cycles under the optimized reaction conditions. In this context, the stability of **4'** was tested by reusing the solid in subsequent runs and the observed results are shown in Table 5.3 These catalytic results clearly indicate that the catalyst retains its activity mostly and the minor decrease in its activity may be due to the loss in the recovery step. This hypothesis was further confirmed by performing a control experiment with the recovered solid after second reuse using a proportionate amount of cyclohexane under similar catalytic conditions. The conversion of cyclohexane in the third reuse is identical to the second reuse, thus confirming that the minor decrease in the 1st and 2nd reuse experiments is not due to the loss of structural integrity (Table 5.5). Furthermore, ICP analysis of the fresh and two times reused solids showed no change in the Zr content, thus confirming the integrity of the solid. This result was also in correlation with the leaching experiment showing the inhibition of the reaction upon removal of the catalyst (Figure 5.32). These results were further proved by XRPD and FE-SEM analysis (Figure 5.34-5.35). The structural integrity of the two times reused solid remained identical to the fresh catalyst. On the other hand, the surface morphology of the two times reused crystals was mostly similar to the fresh solid. Although SEM micrograph of the two times reused solid showed the formation of significant amounts of smaller crystallites due to the mechanical stress, this does not hinder the conversion of cyclohexane.

Table 5.5 Recovery rate of **4'** in reuse experiments and conversion of cyclohexane.

Run	Recovery of **4'**	Conversion (%)
Fresh	-	21
1st reuse	18	19
2nd reuse	17	17
3rd reuse[a]	16	17

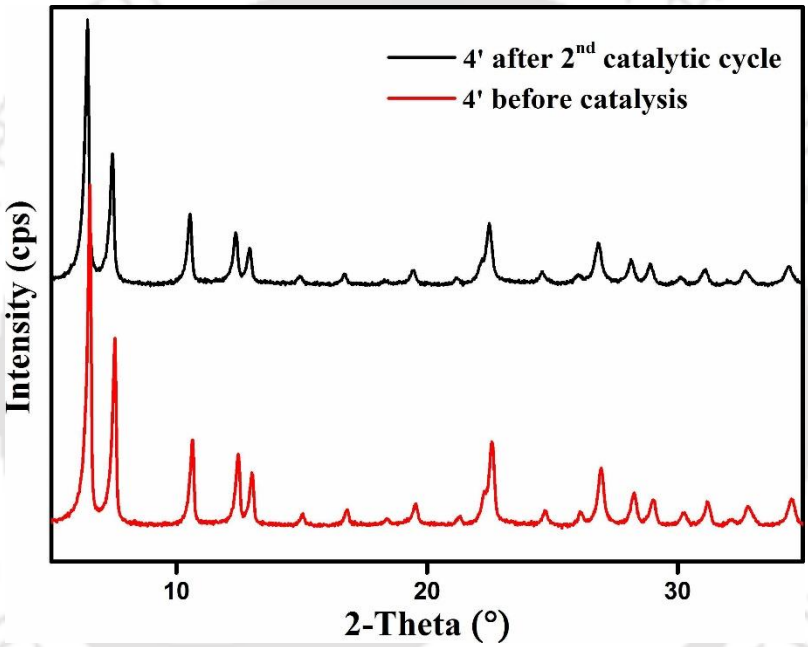

Figure 5.34 XRPD patterns of **4'** before and after catalysis.

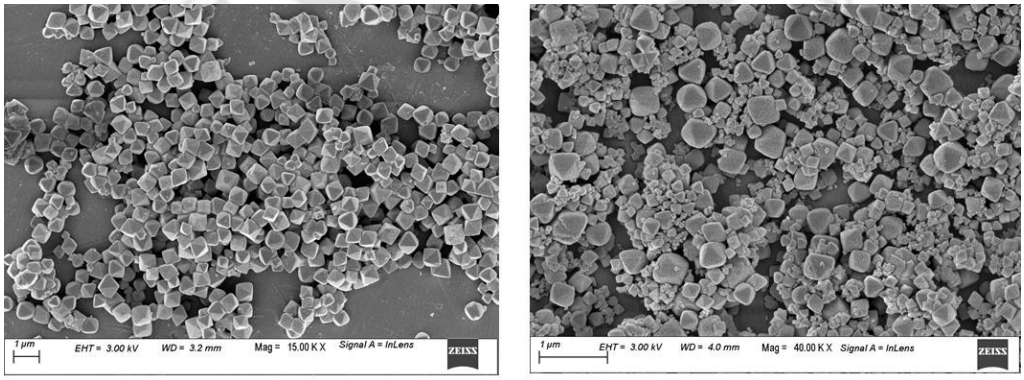

(a) 4′ before catalysis **(b) 4′ after catalysis**

Figure 5.35 FE-SEM images of **4'** (a) before and (b) after two reuses.

5.5 Conclusions

In summary, a Zr(IV) MOF bearing rigid $H_2NDC\text{-}NHCOCF_3$ linker was successfully designed, synthesized and conducted comprehensive characterization. Both **4** and **4'** were stable in different chemical environments and also exhibited very high thermal stability. They are thermally stable up to 300 °C. The N_2 sorption experiment showed that the BET surface area of **4'** is 1105 $m^2\ g^{-1}$. The fluorescence titration experiments showed that probe **4'** can act as a turn-on fluorescent probe for CN^- ion in aqueous medium. The probe showed excellent selectivity for CN^- ion even in presence of other potentially competitive anions in aqueous medium. The MOF can detect CN^- ion in water very quickly (response time = 2 min). The detection limit was 0.23 µM, which is lower than the maximum acceptable concentration of CN^- ion in drinking water as regulated by WHO. **4'** can also be effectively used for CN^- sensing in real water samples and on-site detection of CN^- by using portable paper strips. The experimental studies about the possible sensing mechanisms revealed that the deprotonation of –NH proton of the functional group of linker as well as nucleophilic addition of CN^- to the trifluoroacetamide moiety play key roles in increasing the fluorescence intensity after the addition of CN^-. The catalytic activity of **4'** was tested in the aerobic oxidation of cyclohexane and the observed catalytic data are comparable to earlier reports even at lower temperature. This work clearly highlighted the benefits of functionalizing the linker with fluorine atoms to increase cyclohexane conversion and mild redox behaviour of Zr to increase alcohol/ketone selectivity. The catalyst was reusable for two times with no appreciable change in its conversion/selectivity. Also, the structural integrity and morphology of two-times reused solids remained similar to the fresh solid. In addition, ICP analysis indicated no change in the Zr content before and after the oxidation reaction, thus showing the stability of the framework.

5.6 References

1. *Guidelines for Drinking-Water Quality*, World Health Organization, Geneva, Switzerland, 1996.

2. Jo, J.; Lee, D. Turn-on fluorescence detection of cyanide in water: activation of latent fluorophores through remote hydrogen bonds that mimic peptide β-yurn motif. *J. Am. Chem. Soc.* **2009,** *44*, 16283–16291.

3. Chen, Y.-R.; Deterding, L. J.; Tomer, K. B.; Mason, R. P. Nature of the inhibition of horseradish peroxidase and mitochondrial cytochrome c oxidase by cyanyl radical. *Biochemistry* **2000,** *39*, 4415-4422.

4. Ballantyne, B. The influence of exposure route and species on the acute lethal toxicity and tissue concentrations of cyanide," Developments in Toxicology and Environmental Science. *Developments in Toxicology and Environmental Science* **1989,** *11*, 583–586.

5. Zhang, H.-L.; Wei, T.-B.; Li, W.-T.; Qu, W.-J.; Leng, Y.-L.; Zhang, J.-H.; Lin, Q.; Zhang, Y.-M.; Yao, H. Phenazine-based colorimetric and fluorescent sensor for the selective detection of cyanides based on supramolecular self-assembly in aqueous solution. *Spectrochim. Acta, Part A* **2017,** *175*, 117-124.

6. Dutra, A. J. B.; Rocha, G. P.; Pombo, F. R. Copper recovery and cyanide oxidation by electrowinning from a spent copper-cyanide electroplating electrolyte. *J Hazard Mate* **2008,** *152*, 648-655.

7. Dash, R. R.; Gaur, A.; Balomajumder, C. Cyanide in industrial wastewaters and its removal: a review on biotreatment. *J. Hazard. Mater.* **2009,** *163*, 1-11.

8. Szinicz, L. History of chemical and biological warfare agents. *Toxicology* **2005,** *214*, 167-181.

9. W, C. B.; Blackledge, C. W.; Griesel, A.; Mahon, S. B.; Brenner, M.; Pilz, R. B.; Boss, G. R. A new facile method to measure cyanide in blood. *Anal Chem.* **2010,** *82*, 4216-4221.

10. Foo, M. L.; Matsuda, R.; Kitagawa, S. Functional hybrid porous coordination polymers. *Chem. Mater.* **2014,** *26*, 310-322.

11. Tranchemontagne, D. J.; M.-Corte´s, J. L.; O'Keeffe, M.; Yaghi, O. M. Secondary building units, nets and bonding in the chemistry of metal–organic frameworks. *Chem. Soc. Rev.* **2009,** *38*, 1257-1283.

12. Yaghi, O. M.; O'Keeffe, M.; Ockwig, N. K.; Chae, H. K.; Eddaoudi, M.; Kim, J. Reticular synthesis and the design of new materials. *Nature* **2003,** *423*, 705-714.

13. Ha, J.; Lee, J. H.; Moon, H. R. Alterations to secondary building units of metal-organic frameworks for the development of new functions. *Inorg. Chem. Front.* **2020,** *7*, 12-27.

14. Bauer, C. A.; Timofeeva, T. V.; Settersten, T. B.; Patterson, B. D.; Liu, V. H.; Simmons, B. A.; Allendorf, M. D. Influence of connectivity and porosity on ligand-based luminescence in zinc metal-organic frameworks. *J. Am. Chem. Soc.* **2007,** *129*, 7136-7144.

15. Allendorf, M. D.; Bauer, C. A.; Bhakta, R. K.; Houk, R. J. T. Luminescent metal-organic frameworks. *Chem. Soc. Rev.* **2009,** *38*, 1330-1252.

16. Furukawa, H.; Cordova, K. E.; O'Keeffe, M.; Yaghi, O. M. The chemistry and applications of metal-organic frameworks. *Science* **2013,** *341*, 1230444.

17. Kumar, P.; Deep, A.; Kim, K.-H. Metal organic frameworks for sensing applications. *trac-trend anal. chem.* **2015,** *73*, 39-53.

18. Du, M.; Chen, M.; Yang, X.-G.; Wen, J.; Wang, X.; Fang, S.-M.; Liu, C.-S. A channel-type mesoporous In(iii)–carboxylate coordination framework with high physicochemical stability for use as an electrode material in supercapacitors. *J. Mater. Chem. A* **2014,** *2*, 9828-9834.

19. Yuan, S.; Chen, Y.-P.; Qin, J.-S.; Lu, W.; Zou, L.; Zhang, Q.; Wang, X.; Sun, X.; Zhou, H.-C. Linker installation: engineering pore environment with precisely placed functionalities in zirconium MOFs. *J. Am. Chem. Soc.* **2016,** *138*, 8912–8919.

20. Liu, Y.; Zhao, Y.; Liu, X.-H.; Kang, Y.-S.; Wang, P.; Sun, W.-Y. Novel metal-organic frameworks with high stability for selectively sensing nitroaromatics. *Dalton Trans.* **2018,** *47*, 15399-15404.

21. McKinlay, A. C.; Morris, R. E.; Horcajada, P.; Frey, G.; Gref, R.; Couvreur, P.; Serre, C. BioMOFs: metal–organic frameworks for biological and medical applications. *Angew. Chem. Int. Ed.* **2010,** *49*, 6260-6266.

22. Liu, Y.; Xie, X.-Y.; Cheng, C.; Shao, Z.-S.; Wang, H.-S. Strategies to fabricate metal-organic framework (MOF)-based luminescent sensing platforms. *J. Mater. Chem. C* **2019,** *7*, 10743-10763.

23. Cui, Y.; Zhang, J.; He, H.; Qian, G. Photonic functional metal–organic frameworks. *Chem. Soc. Rev.* **2018,** *47*, 5740-5785.

24. Czaja, A. U.; Trukhan, N.; Mu¨ller, U. Industrial applications of metal–organic frameworks. *Chem. Soc. Rev.* **2009,** *38*, 1284-1293.

25. Hu, Z.; Deibert, B. J.; Li, J. Luminescent metal–organic frameworks for chemical sensing and explosive detection. *Chem. Soc. Rev.* **2014,** *43*, 5815-5840.

26. Britt, D.; Tranchemontagne, D.; Yaghi, O. M. Metal-organic frameworks with high capacity and selectivity for harmful gases. *PNAS* **2008,** *105*, 11623-11627.

27. Kuppler, R. J.; Timmons, D. J.; Fang, Q.-R.; Li, J.-R.; Makal, T. A.; Young, M. D.; Yuan, D.; Zhao, D.; Zhuang, W.; Zhou, H.-C. Potential applications of metal-organic frameworks. *Coord. Chem. Rev* **2009,** *253*, 3042-3066.

28. Kukkar, D.; Vellingiri, K.; Kim, K. H.; Deep, A. Recent progress in biological and chemical sensing by luminescent metal-organic frameworks. *Sens. Actuators B* **2018,** *273*, 1346-1370.

29. Gogoi, C.; Biswas, S. A new quinoline based luminescent Zr(iv) metal–organic framework for the ultrasensitive recognition of 4-nitrophenol and Fe(iii) ions. *Dalton Trans.* **2018,** *47*, 14696-14705.

30. Wuttke, S.; Dietl, C.; Hinterholzinger, F. M.; Hintz, H.; Langhals, H.; Bein, T. Turn-on fluorescence triggered by selective internal dye replacement in MOFs. *Chem. Commun.* **2014,** *50*, 3599-3601.

31. Shustova, N. B.; McCarthy, B. D.; Dinca, M. Turn-on fluorescence in tetraphenylethylene-based metal–organic frameworks: an alternative to aggregation-induced emission. *J. Am. Chem. Soc.* **2011,** *133*, 20126-20129.

32. Gogoi, C.; Reinsch, H.; Biswas, S. A pyrazine core-based luminescent Zr(IV) organic framework for specific sensing of Fe^{3+}, picric acid and $Cr_2O_7^{2-}$. *CrystEngComm* **2019,** *21*, 6252-6260.

33. Germain, M. E.; Knapp, M. J. Optical explosives detection: from color changes to fluorescence turn-on. *Chem. Soc. Rev.* **2009,** *38*, 2543-2555.

34. Anzenbacher, P.; Tyson, D. S.; Jursı´kova´, K.; Castellano, F. N. Luminescence lifetime-based sensor for cyanide and related anions. *J. Am. Chem. Soc.* **2002,** *124*, 6232-6233.

35. Li, H.; Li, B.; Jin, L.-Y.; Kan, Y.; Yin, B. A rapid responsive and highly selective probe for cyanide in the aqueous environment. *Tetrahedron* **2011,** *67*, 7348-7353.

36. Wang, L.; Zhu, L.; Cao, D. A colorimetric probe based on diketopyrrolopyrrole and tert-butyl cyanoacetate for cyanide detection. *New J. Chem.* **2015,** *39*, 7211-7218.

37. Men, G.; Han, W.; Chen, C.; Liang, C.; Jiang, S. A cyanide-sensing detector in aqueous solution based on anion–π interaction-driven electron transfer. *Analyst* **2019,** *144*, 2226-2230.

38. Li, J.; Yuan, S.; Qin, J.-S.; Pang, J.; Zhang, P.; Zhang, Y.; Huang, Y.; Drake, H. F.; Liu, W. R.; Zhou, H.-C. Stepwise assembly of turn-on fluorescence sensors in multicomponent metal–organic frameworks for in vitro cyanide detection. *Angew. Chem. Int. Ed.* **2020,** *59*, 1-6.

39. Karmakar, A.; Kumar, N.; Samanta, P.; Desai, A. V.; Ghosh, S. K. A post-synthetically modified MOF for selective and sensitive aqueous-phase detection of highly toxic cyanide ions. *Chem. Eur. J.* **2016,** *22*, 864-868.

40. Al-Agel, F. A.; Mahmoud, W. E. "Turn-off-on" fluorescence probe based functionalized InP quantum wires for detection of cyanide anions. *Sens. Actuators B* **2013,** *183*, 441-445.

41. Jin, W. J.; Arguelles, M. T. F.; Fernandez, J. M. C.; Pereiro, R.; Medel, A. S. Photoactivated luminescent CdSe quantum dots as sensitive cyanide probes in aqueous solutions. **2005,** *Chem. Commun.*, 883-885.

42. Hao, Y.; Nguyen, K. H.; Zhanga, Y.; Zhanga, G.; Fana, S.; Lia, F.; Guo, C.; Lu, Y.; Song, X.; Qu, P.; Liu, Y.-N.; Xu, M. A highly selective and ratiometric fluorescent probe for cyanide by rationally altering the susceptible H-atom. *Talanta* **2018,** *176*, 234-241.

43. Sessler, J. L.; Cho, D. G. The benzil rearrangement reaction: trapping of a hitherto minor product and its application to the development of a selective cyanide anion indicator. *Org. Lett.* **2008,** *10*, 73-75.

44. Tomasulo, M.; Sortino, S.; White, A. J. P.; Raymo, F. M. Chromogenic oxazines for cyanide detection. *J. Org. Chem.* **2006,** *71*, 744-753.

45. Dalapati, R.; Nandi, S.; Reinsch, H.; Bhunia, B. K.; Mandal, B. B.; Stock, N.; Biswas, S. Fluorogenic naked-eye sensing and live-cell imaging of cyanide by a hydrazine-functionalized CAU-10 metal–organic framework. *CrystEngComm* **2018,** *20*, 4194-4201.

46. Das, A.; Biswas, S. A multi-responsive carbazole-functionalized Zr(IV)-based metal-organic framework for selective sensing of Fe(III), cyanide and p-nitrophenol. *Sens. Actuators, B* **2017,** *250*, 121-131.

47. Wang, L.; Wang, S.; Chen, Y. Detection of cyanide via extended π-conjugation-induced fluorescence enhancement of a metal organic framework composed of terbium(III), bipyridyl and adenosine diphosphate. *Microchim. Acta* **2017,** *184*, 4597-4602.

48. Panja, S.; Panja, A.; Ghosh, K. Supramolecular gels in cyanide sensing: a review. *Mater. Chem. Front.* **2020**, DOI: 10.1039/d0qm00551g.

49. Karmakar, A.; Joarder, B.; Mallick, A.; Samanta, P.; Desai, A. V.; Basu, S.; Ghosh, S. K. Aqueous phase sensing of cyanide ions using a hydrolytically stable metal–organic framework. *Chem. Commun.* **2017,** *53*, 1253-1256.

50. Niu, H.-T.; Jiang, X.; He, J.; Cheng, J.-P. A highly selective and synthetically facile aqueous-phase cyanide probe. *Tetrahedron Lett.* **2008,** *49*, 6521-6524.

51. Dhakshinamoorthy, A.; Garcia, H. Cascade reactions catalyzed by metal organic frameworks. *ChemSusChem* **2014,** *2014*, 2392-2410.

52. Maksimchuk, N. V.; Kovalenko, K. A.; Fedin, V. P.; Kholdeeva, O. A. Cyclohexane selective oxidation over metal–organic frameworks of MIL-101 family: superior catalytic activity and selectivity. *Chem. Commun.* **2012,** *48*, 6812-6814.

53. Sun, Z.; Li, G.; Liu, H.-o.; Liu, L. Salen-Co(II) complex incorporated into amino-functionalized MIL-101(Cr) through postsynthetic modification as a cooperative catalyst for cyclohexane selective oxidation. *Appl. Catal. A Gen.* **2013,** *466*, 98-104.

54. Sun, Z.; Li, G.; Liu, L.; Liu, H.-O. Au nanoparticles supported on Cr-based metal-organic framework as bimetallic catalyst for selective oxidation of cyclohexane to cyclohexanone and cyclohexanol. *Catal. Commun.* **2012,** *27*, 200-205.

55. Kim, A.-R.; Ahn, S.; Yoon, T.-U.; Notestein, J. M.; Farha, O. K.; Bae, Y.-S. Fast cyclohexane oxidation under mild reaction conditions through a controlled creation of redox-active Fe(II/III) sites in a metal-organic framework. *ChemCatChem* **2019,** *11*, 5650-5656.

56. Dhakshinamoorthy, A.; Alvaro, M.; Garcia, H. Metal organic frameworks as efficient heterogeneous catalysts for the oxidation of benzylic compounds with t-butylhydroperoxide. *J. Catal.* **2009,** *267*, 1-4.

57. Xiao, D. J.; Oktawiec, J.; Milner, P. J.; Long, J. R. Pore environment effects on catalytic cyclohexane oxidation in expanded Fe_2(dobdc) analogues. *J. Am. Chem. Soc.* **2016,** *43*, 14371-14379.

58. Mikami, Y.; Dhakshinamoorthy, A.; Alvaro, M.; Garcia, H. Superior performance of Fe(BTC) with respect to other metal-containing solids in the N-Hydroxyphthalimide- promoted heterogeneous aerobic oxidation of cycloalkanes. *ChemCatChem* **2013,** *5*, 1964-1970.

59. Maksimchuk, N.; Lee, J. S.; Ayupov, A.; Chang, J.-S.; Kholdeeva, O. Cyclohexene oxidation with H_2O_2 over metal-organic framework MIL-125(Ti): The effect of protons on reactivity. *Catalysts* **2019,** *9*, 324.

60. Dhakshinamoorthy, A.; Alvaro, M.; Garcia, H. Metal–organic frameworks as heterogeneous catalysts for oxidation reactions. *Catal. Sci. Technol.* **2011,** *1*, 856-867.

61. Dhakshinamoorthy, A.; Asiri, A. M.; Garcia, H. Metal–organic frameworks as catalysts for oxidation reactions. *Chem. Eur. J.* **2016,** *22*, 8012-8024.

62. Bon, V.; Senkovska, I.; Weiss, M. S.; Kaskel, S. Tailoring of network dimensionality and porosity adjustment in Zr- and Hf-based MOFs. *CrystEngComm* **2013,** *15*, 9572-9577.

63. *Materials Studio Version 5.0.*, Accelrys Inc.: San Diego: 2009.

64. Boultif, A.; Louër, D. Indexing of powder diffraction patterns for low-symmetry lattices by the successive dichotomy method. *J. Appl. Crystallogr.* **1991,** *24*, 987-993.

65. *STOE WinXPOW version 2.11*, Stoe & Cie GmbH, Darmstadt, Germany, 2005.

66. Sim, J.; Yim, H.; Ko, N.; Choi, S. B.; Oh, Y.; Park, H. J.; Park, S. Y.; Kim, J. Gas adsorption properties of highly porous metal–organic frameworks containing functionalized naphthalene dicarboxylate linkers. *Dalton Trans.* **2014,** *43*, 18017-18024.

67. Wang, H.; Wang, Q.; Teat, S. J.; Olson, D. H.; Li, J. Synthesis, Structure, and Selective Gas Adsorption of a Single-Crystalline Zirconium Based Microporous Metal–Organic Framework. *Cryst. Growth Des.* **2017,** *17*, 2034–2040.

68. Dassault Systemes BIOVIA. Materials Studio, 7.0. . *San Diego: Dassault Systemes* **2020**.

69. Bai, Y.; Dou, Y.; Xie, L.-H.; Rutledge, W.; Li, J.-R.; Zhou, H.-C. Zr-based metal–organic frameworks: design, synthesis, structure, and applications. *Chem. Soc. Rev.* **2016,** *45*, 2327-2367.

70. Tsuruoka, T.; Furukawa, S.; Takashima, Y.; Yoshida, K.; Isoda, S.; Kitagawa, S. Nanoporous nanorods fabricated by coordination modulation and oriented attachment growth. *Angew. Chem. Int. Ed.* **2009,** *48*, 4739-4743.

71. Yu, H.; Zhao, Q.; Jiang, Z.; Qin, J.; Li, Z. A ratiometric fluorescent probe for cyanide: Convenient synthesis and the proposed mechanism. *Sens. Actuators B Chem* **2010,** *148* 110-116.

72. Valenzano, L.; Civalleri, B.; Chavan, S.; Bordiga, S.; Nilsen, M. H.; Jakobsen, S.; Lillerud, K. P.; Lamberti, C. Disclosing the complex structure of UiO-66 metal organic framework : a synergic combination of experiment and theory. *Chem. Mater.* **2011,** *23*, 1700-1718.

73. Dassault Systemes BIOVIA. Materials Studio, 7.0 *San Diego : Dassault Systemes* **2020**.

74. Shearer, G. C.; Chavan, S.; Bordiga, S.; Svelle, S.; Olsbye, U.; Lillerud, K. P. Defect engineering: tuning the porosity and composition of the metal-organic Framework UiO-66 via modulated synthesis. *Chem. Mater.* **2016,** *28*, 3749-3761.

75. Fu, Y.; Wu, J.; Du, R.; Guo, K.; Ma, R.; Zhang, F.; Zhu, W.; Fan, M. Temperature modulation of defects in NH_2-UiO-66(Zr) for photocatalytic CO_2 reduction. *RSC Adv.* **2019,** *9*, 37733-37738.

76. Wang, J.; Liu, L.; Chen, C.; Dong, X.; Wang, Q.; Alfilfil, L.; AlAlouni, M. R.; Yao, K.; Huang, J.; Zhang, D.; Han, Y. Engineering effective structural defects of metal-organic frameworks to enhance their catalytic performances. *J. Mater. Chem. A* **2020,** *8*, 4464-4472.

77. Dalapati, R.; Balaji, S. N.; Trivedi, V.; Khamari, L.; Biswas, S. A dinitro-functionalized Zr(IV)-based metal-organic framework as colorimetric and fluorogenic probe for highly selective detection of hydrogen sulphide. *Sens. Actuators B Chem* **2017,** *245*, 1039-1049.

78. Fernandez, C. A.; Nune, S. K.; Annapureddy, H. V.; Dang, L. X.; McGrail, B. P.; Zheng, F.; Polikarpov, E.; King, D. L.; Freeman, C.; Brooks, K. P. Hydrophobic and moisture-stable metal–organic frameworks. *Dalton Trans.* **2015,** *44*, 13490-13497.

79. Gogoi, C.; Yousufuddin, M.; Biswas, S. A new 3D luminescent Zn(ii)-organic framework containing a quinoline-2,6-dicarboxylate linker for the highly selective sensing of Fe(iii) ions. *Dalton Trans.* **2019,** *48*, 1766-1773.

80. Zhu, X.-D.; Zhang, K.; Wang, Y.; Long, W.-W.; Sa, R.-J.; Liu, T.-F.; Lü, J. Fluorescent metal-organic framework (MOF) as a highly sensitive and quickly responsive chemical sensor for the detection of antibiotics in simulated wastewater. *Inorg. Chem.* **2018,** *57*, 1060-1065.

81. Duan, Y.-L.; Zheng, Y.-S. A new sensitive and selective fluorescence probe for detection of cyanide. *Talanta* **2013,** *107*, 332-337.

82. Dalapati, R.; Nandi, S.; Biswas, S. Post-synthetic modification of a metal–organic framework with a chemodosimeter for the rapid detection of lethal cyanide via dual emission. *Dalton Trans.* **2020,** *49*, 8684-8692.

83. Kim, J. S.; Quang, D. T. Calixarene-derived fluorescent probes. *Chem. Rev.* **2007,** *107*, 3780-3799.

84. Wu, J.; Liu, W.; Ge, J.; Zhang, H.; Wang, P. New sensing mechanisms for design of fluorescent chemosensors emerging in recent years. *Chem. Soc. Rev.* **2011,** *40*, 3483-3495.

85. Peng, L.; Wang, M.; Zhang, G.; Zhang, D.; Zhu, D. A fluorescence turn-on detection of cyanide in aqueous solution based on the aggregation-induced emission. *Org. Lett. 2009* **2009,** *11*, 1943-1946.

86. Chung, Y. M.; Raman, B.; Kim, D.-S.; Ahn, K. H. Fluorescence modulation in anion sensing by introducing intramolecular H-bonding interactions in host-guest adducts. *Chem. Commun.* **2006**, 186-188.

87. Li, L.; Yang, Q.; Chen, S.; Hou, X.; Liu, B.; Lu, J.; Jiang, H.-L. Boosting selective oxidation of cyclohexane over a metal–organic framework by hydrophobicity engineering of pore walls. *Chem. Commun.* **2017,** *53*, 10026-10029.

88. Ji, J.; Liu, F.; Yang, W.; Tan, M.; Luo, W.; Yin, S.-F. Incorporation of functional groups in porphyrinic metal-organic frameworks by post-modification for highly efficient oxidation catalysis. *ChemCatChem* **2020,** *12*, 4331-4338.

89. Kholdeeva, O. A. Liquid-phase selective oxidation catalysis with metal-organic frameworks. *Catalysis Today* **2016,** *278*, 22-29.

90. Dhakshinamoorthy, A.; Asiri, A. M.; Garcia, H. Catalysis in confined spaces of metal organic frameworks. *ChemCatChem* **2020,** *12*, 4732-4753.

Conclusions

In Chapter 1, we have discussed the literature study, design and synthetic strategies of water-stable MOFs. In 1995, Yaghi and co-workers coined the term 'MOF'. These porous materials are formed by strong bonds between metal ions and organic linkers. They have some outstanding properties like very high surface area, high porosities, high thermal and chemical stability, various pore size and shape, etc. Because of their excellent chemical and physical properties, this remarkable class of porous materials has a wide range of applications like catalysis, gas storage, separation, polymerization, sensing, proton conductivity, drug delivery, bioimaging, etc. MOFs have a high degree of customizability because they can be tailored by selecting different linkers and metal ions. Because of the tunable nature, MOFs can be tailored with precisely controlled pore size, shape and functionality for the specific application. Here, we have discussed the various synthesis methods of MOFs. The solvents, temperature, modulators and reaction time play very important roles in determining the crystallinity, porosity and stability of MOFs. During the synthesis of MOFs, we should be more concerned about the stability of the framework. The unsatisfactory chemical stability of most of the MOFs hinders some of the fundamental studies and also hinders the implementation of MOFs for practical applications. In many areas, MOFs have shown excellent advantages over traditional materials and potential values for commercialization. Water stability is a crucial property for any kind of material to be applicable in the real world. Hence, water-stable MOFs have been in great demand among the scientific community. In the last few decades, a great deal of effort has been devoted to explore the feasibility of luminescent MOFs (LMOFs) for sensing applications. MOF-based sensors have been directly used for the detection of gases, vapors, small molecules, metal ions, nitroaromatics, nerve agents and pesticides. The novel class of MOFs consisting of d^{10} or rare-earth metal centers and conjugated organic linkers can be potentially employed as photoluminescent materials to sense specific metal ions and small organic molecules because of their excellent luminescence emission properties. The frameworks can be judiciously functionalized by specific functionality with the specially functionalized linker, which in turn can act as recognition sites for the targeted analytes. In catalysis, MOFs are promising heterogeneous catalysts due to the presence of unsaturated coordinated metal sites and/or special functional groups of linkers. The unsaturated coordinated metal sites can be prepared by some special treatment like heating at high temperature and linker exchange which in turn activate the metal nodes by removing the weakly coordinated

linkers from the nodes. The activated catalytic sites can also be made by introducing a specific modification of linker such as bipyridine, porphyrin etc.

In Chapter 2, a 3D zinc-organic framework [Zn(QDA)]·0.7DMF·0.5H_2O was synthesized under solvothermal conditions. The single crystal X-ray diffraction analysis reveals that the 3D framework structure has PtS topology and contains Zn(II) ions having distorted square pyramidal geometry with ZnO_4N configuration. The bulk compound was thoroughly characterized using several analytical tools. The activated compound (**1'**) is stable up to 440 °C and also shows excellent chemical stability. Compound **1'** exhibited a very quick fluorescence quenching response after the addition of Fe^{3+} solution. This quenching was not affected by the presence of other competitive metal cations. A very low detection limit of 9.2 ppb was observed for Fe^{3+}, which is among the lowest values documented in the literature for MOF-based fluorescence probes. Both fluorescence resonance energy transfer (FRET) as well as photo-induced electron transfer (PET) processes play major roles in the selective detection of Fe^{3+}. The recyclability experiment suggested that **1'** can be used for the long-term detection of Fe^{3+}.

In Chapter 3, a MOF with Zr(IV) ion containing 2,3,5,6-tetrakis(4-carboxyphenyl)pyrazine (H_4**L**) linker was prepared by a solvothermal method. $ZrOCl_2·8H_2O$ was employed along with H_4**L** linker and benzoic acid (modulator) in DMF to synthesize the title compound. The as-synthesized compound has the formula $[Zr_6(\mu_3\text{-}O)_4(\mu_3\text{-}OH)_4(OH)_4(H_2O)_4(\mathbf{L})_2]·3H_2O·2DMF$ (**2**). The activation of **2** was carried out by using methanol exchange and subsequent heating under a high vacuum at 130 °C. Both **2** and activated samples (**2'**) were characterized by X-ray powder diffraction (XRPD), Fourier transform infrared (FT-IR) and thermogravimetric analysis (TGA). They displayed high chemical stability and thermal stability. Both **2** and **2'** are stable up to 440 °C. Compound **2'** has a very high BET surface area (1419 m^2/g) and CO_2 adsorption capacity (4.4 mmol/g at 1.4 bar and 0 °C). Being highly water-stable, luminescent **2'** can selectively recognize dichromate ($Cr_2O_7^{2-}$) in water and picric acid (PA) in dimethyl sulfoxide (DMSO), by fluorescence quenching mechanism. The detection limits were found to be 13.08 and 8.58 ppb for PA and $Cr_2O_7^{2-}$, respectively. Moreover, the mechanisms behind this selective detection of all three analytes were also investigated. In both the cases, the compound showed reusability up to five cycles without any loss of sensing efficacy. These experimental data vividly depict that **2'** can be considered as a promising sensing material for PA and $Cr_2O_7^{2-}$.

CONCLUSIONS & FUTURE PROSPECTS

In Chapter 4, we synthesized an azide functional group containing Zr(IV) based metal-organic framework (MOF) with DUT-52 (DUT = Dresden University of Technology) topology *via a* solvothermal process. Acetic acid was used as a modulator to increase crystallinity. The synthesized compound (**3**) was activated by exchanging occluded molecules with methanol and heating at 80 °C for 5 h. Both **3** and activated compounds (**3'**) were characterized by X-ray powder diffraction (XRPD), Fourier transform infrared (FT-IR) and thermogravimetric analysis (TGA). Both **3** and **3'** are thermally stable up to 320 °C and chemically stable in solvents like methanol, acetic acid, 1 (M) HCl and water. The Brunauer-Emmett-Teller (BET) surface area of **3'** was found to be 505 m^2 g^{-1}. The data from fluorescence experiments suggested that **3'** exhibits sensitive and selective detection of H_2S in an aqueous medium. The limit of detection (LOD) value was found to 0.50 µM. This value lies in the lowest range of H_2S detection by known MOFs. Moreover, the possible mechanism behind the enhancement of fluorescence intensity after addition of Na_2S in **3'** was also examined.

In chapter 5, a zirconium (Zr) metal-organic framework having DUT-52 (DUT stands for Dresden University of Technology) structure with face-centred cubic (**fcu**) topology and bearing the rigid 1-(2,2,2-trifluoroacetamido) naphthalene-3,7-dicarboxylic acid (H_2NDC-NHCOCF_3) linker was prepared and its solid structure was characterized with the help of X-ray powder diffraction technique. Other characterization methods like thermogravimetric analysis (TGA) and Fourier transform infrared (FT-IR) spectroscopy were applied to verify the phase purity of the compound. In order to get the solvent-free compound (**4'**), **4** was stirred with methanol for overnight and subsequently heated at 100 °C for overnight under a vacuum. As-synthesized (**4**) and activated (**4'**) compounds are thermally stable up to 300 °C. The BET surface area of **4'** was found to be 1105 m^2 g^{-1}. Fluorescence titration experiments showed that **4'** exhibits highly selective and sensitive fluorescence turn-on behaviour towards cyanide (CN^-) anion. The interference experiments suggested that other anions did not interfere in the detection of CN^-. Moreover, a very short response time (2 min) was shown by probe **4'** for CN^- detection. The detection limit was found to be 0.23 µM. **4'** can also be effectively used for CN^- detection in real water samples. The mechanism for the selective detection of CN^- was investigated systematically. Furthermore, the aerobic oxidation catalysis was performed with **4'** under mild reaction conditions, observing higher activity than analogous DUT-52 solid under identical conditions. These experiments clearly indicate the benefits of hydrophobic cavities of **4'** in achieving higher conversion and selectivity. Catalyst stability was proved by

two consecutive reuses and comparing the structural integrity of **4'** before and after reuses by XRPD study.

The thesis work mainly focuses on the design and synthesis of water-stable MOFs. We explored the synthesis and comprehensive characterization of water-stable MOFs and utilized the luminescence property of MOFs for selective and sensitive detection of toxic ions like Fe^{3+}, $Cr_2O_7^{2-}$, CN^- and nitroaromatic explosives. The thesis also explored the application of the hydrophobic cavity of a water-stable MOF for the heterogeneous catalysis reaction.

Future prospects:

In the future, we are planning to prepare MOFs based on the paramagnetic Co^{2+}, Cu^{2+}, Mn^{2+} and Ni^{2+} ions and polycarboxylate linkers, which are expected possess interesting magnetic properties. We have planned to prepare water-stable MOFs with the relatively unexplored multicarboxylate linkers having functional groups like acetoxy, maleimide, phthalimide etc. which can be utilized for the detection of toxic compounds. We are also planning to prepare MOFs with nitrogen-rich linkers such as amines, imidazoles, pyridines, triazoles, tetrazoles, which can show significantly high capability for CO_2 adsorption. The hydrophobic property of MOFs containing fluorine as the functional group in the linker can be used to form composites with fabric, sponge or reduced graphene-oxide. These hydrophobic composites can be used for oil-water separation. We are also planning to prepare MOFs with organic linkers which contain hydrophilic acidic functional groups such as sulfonate, phosphinate, etc. These types of MOFs can show good proton conductivity as hydrophilic acidic functional groups serve as effective proton conduction sites. The defect-containing MOFs always provide better catalytic sites. Hence, the creation of defects (on purpose) at metal nodes can improve the catalytic activity of MOFs in many organic catalysis reactions.

Annexure I

SPRINGER NATURE LICENSE
TERMS AND CONDITIONS

Mar 16, 2021

This Agreement between Mr. Chiranjib Gogoi ("You") and Springer Nature ("Springer Nature") consists of your license details and the terms and conditions provided by Springer Nature and Copyright Clearance Center.

License Number	5030740659047
License date	Mar 16, 2021
Licensed Content Publisher	Springer Nature
Licensed Content Publication	Nature
Licensed Content Title	Reticular synthesis and the design of new materials
Licensed Content Author	Omar M. Yaghi et al
Licensed Content Date	Jun 12, 2003
Type of Use	Thesis/Dissertation
Requestor type	academic/university or research institute
Format	print and electronic
Portion	figures/tables/illustrations
Number of figures/tables/illustrations	1

High-res required	no
Will you be translating?	no
Circulation/distribution	1 - 29
Author of this Springer Nature content	no
Title	Synthesis and Characterization of Some Zn(II) and Zr(IV) Metal-Organic Frameworks and Their Applications in Fluorescence Sensing and Catalysis
Institution name	IIT Guwahati
Expected presentation date	Jun 2021
Order reference number	76
Portions	Figure 1.2
Requestor Location	Mr. Chiranjib Gogoi IIT Guwahati Guwahati, 781039 India Attn: IIT Guwahati
Total	0.00 USD

Terms and Conditions

Springer Nature Customer Service Centre GmbH
Terms and Conditions

This agreement sets out the terms and conditions of the licence (the **Licence**) between you and **Springer Nature Customer Service Centre GmbH** (the **Licensor**). By clicking 'accept' and completing the transaction for the material (**Licensed Material**), you also confirm your acceptance of these terms and conditions.

Annexure I

1. Grant of License

1. 1. The Licensor grants you a personal, non-exclusive, non-transferable, world-wide licence to reproduce the Licensed Material for the purpose specified in your order only. Licences are granted for the specific use requested in the order and for no other use, subject to the conditions below.

1. 2. The Licensor warrants that it has, to the best of its knowledge, the rights to license reuse of the Licensed Material. However, you should ensure that the material you are requesting is original to the Licensor and does not carry the copyright of another entity (as credited in the published version).

1. 3. If the credit line on any part of the material you have requested indicates that it was reprinted or adapted with permission from another source, then you should also seek permission from that source to reuse the material.

2. Scope of Licence

2. 1. You may only use the Licensed Content in the manner and to the extent permitted by these Ts&Cs and any applicable laws.

2. 2. A separate licence may be required for any additional use of the Licensed Material, e.g. where a licence has been purchased for print only use, separate permission must be obtained for electronic re-use. Similarly, a licence is only valid in the language selected and does not apply for editions in other languages unless additional translation rights have been granted separately in the licence. Any content owned by third parties are expressly excluded from the licence.

2. 3. Similarly, rights for additional components such as custom editions and derivatives require additional permission and may be subject to an additional fee. Please apply to Journalpermissions@springernature.com/bookpermissions@springernature.com for these rights.

2. 4. Where permission has been granted **free of charge** for material in print, permission may also be granted for any electronic version of that work, provided that the material is incidental to your work as a whole and that the electronic version is essentially equivalent to, or substitutes for, the print version.

2. 5. An alternative scope of licence may apply to signatories of the STM Permissions Guidelines, as amended from time to time.

3. Duration of Licence

3. 1. A licence for is valid from the date of purchase ('Licence Date') at the end of the relevant period in the below table:

Scope of Licence	Duration of Licence
Post on a website	12 months
Presentations	12 months
Books and journals	Lifetime of the edition in the language purchased

4. Acknowledgement

4. 1. The Licensor's permission must be acknowledged next to the Licenced Material in print. In electronic form, this acknowledgement must be visible at the same time as the figures/tables/illustrations or abstract, and must be hyperlinked to the journal/book's homepage. Our required acknowledgement format is in the Appendix below.

5. Restrictions on use

5. 1. Use of the Licensed Material may be permitted for incidental promotional use and minor editing privileges e.g. minor adaptations of single figures, changes of format, colour and/or style where the adaptation is credited as set out in Appendix 1 below. Any other changes including but not limited to, cropping, adapting, omitting material that affect the meaning, intention or moral rights of the author are strictly prohibited.

5. 2. You must not use any Licensed Material as part of any design or trademark.

5. 3. Licensed Material may be used in Open Access Publications (OAP) before publication by Springer Nature, but any Licensed Material must be removed from OAP sites prior to final publication.

6. Ownership of Rights

6. 1. Licensed Material remains the property of either Licensor or the relevant third party and any rights not explicitly granted herein are expressly reserved.

7. Warranty

IN NO EVENT SHALL LICENSOR BE LIABLE TO YOU OR ANY OTHER PARTY OR ANY OTHER PERSON OR FOR ANY SPECIAL, CONSEQUENTIAL, INCIDENTAL OR INDIRECT DAMAGES, HOWEVER CAUSED, ARISING OUT OF OR IN CONNECTION WITH THE DOWNLOADING, VIEWING OR USE OF THE MATERIALS REGARDLESS OF THE FORM OF ACTION, WHETHER FOR BREACH OF CONTRACT, BREACH OF WARRANTY, TORT, NEGLIGENCE, INFRINGEMENT OR OTHERWISE (INCLUDING, WITHOUT LIMITATION, DAMAGES BASED ON LOSS OF PROFITS, DATA, FILES, USE, BUSINESS OPPORTUNITY OR CLAIMS OF THIRD PARTIES), AND
WHETHER OR NOT THE PARTY HAS BEEN ADVISED OF THE POSSIBILITY OF SUCH DAMAGES. THIS LIMITATION SHALL APPLY NOTWITHSTANDING ANY FAILURE OF ESSENTIAL PURPOSE OF ANY LIMITED REMEDY PROVIDED HEREIN.

8. Limitations

8. 1. ***BOOKS ONLY:*** Where **'reuse in a dissertation/thesis'** has been selected the following terms apply: Print rights of the final author's accepted manuscript (for clarity,

NOT the published version) for up to 100 copies, electronic rights for use only on a personal website or institutional repository as defined by the Sherpa guideline (www.sherpa.ac.uk/romeo/).

8. 2. For content reuse requests that qualify for permission under the STM Permissions Guidelines, which may be updated from time to time, the STM Permissions Guidelines supersede the terms and conditions contained in this licence.

9. Termination and Cancellation

9. 1. Licences will expire after the period shown in Clause 3 (above).

9. 2. Licensee reserves the right to terminate the Licence in the event that payment is not received in full or if there has been a breach of this agreement by you.

Appendix 1 — Acknowledgements:

For Journal Content:
Reprinted by permission from [**the Licensor**]: [**Journal Publisher** (e.g. Nature/Springer/Palgrave)] [**JOURNAL NAME**] [**REFERENCE CITATION** (Article name, Author(s) Name), [**COPYRIGHT**] (year of publication)

For **Advance Online Publication papers:**
Reprinted by permission from [**the Licensor**]: [**Journal Publisher** (e.g. Nature/Springer/Palgrave)] [**JOURNAL NAME**] [**REFERENCE CITATION** (Article name, Author(s) Name), [**COPYRIGHT**] (year of publication), advance online publication, day month year (doi: 10.1038/sj.[JOURNAL ACRONYM].)

For Adaptations/Translations:
Adapted/Translated by permission from [**the Licensor**]: [**Journal Publisher** (e.g. Nature/Springer/Palgrave)] [**JOURNAL NAME**] [**REFERENCE CITATION** (Article name, Author(s) Name), [**COPYRIGHT**] (year of publication)

Note: For any republication from the British Journal of Cancer, the following credit line style applies:

Reprinted/adapted/translated by permission from [**the Licensor**]: on behalf of Cancer Research UK: : [**Journal Publisher** (e.g. Nature/Springer/Palgrave)] [**JOURNAL NAME**] [**REFERENCE CITATION** (Article name, Author(s) Name), [**COPYRIGHT**] (year of publication)

For **Advance Online Publication** papers:
Reprinted by permission from The [**the Licensor**]: on behalf of Cancer Research UK: [**Journal Publisher** (e.g. Nature/Springer/Palgrave)] [**JOURNAL NAME**] [**REFERENCE CITATION** (Article name, Author(s) Name), [**COPYRIGHT**] (year of publication), advance online publication, day month year (doi: 10.1038/sj.[JOURNAL ACRONYM])

For Book content:
Reprinted/adapted by permission from [**the Licensor**]: [**Book Publisher** (e.g.

Palgrave Macmillan, Springer etc) [**Book Title**] by [**Book author**(s)]
[**COPYRIGHT**] (year of publication)

Other Conditions:

Version 1.3

Questions? customercare@copyright.com or +1-855-239-3415 (toll free in the US) or +1-978-646-2777.

Annexure II

ELSEVIER LICENSE
TERMS AND CONDITIONS

Mar 16, 2021

This Agreement between Mr. Chiranjib Gogoi ("You") and Elsevier ("Elsevier") consists of your license details and the terms and conditions provided by Elsevier and Copyright Clearance Center.

License Number	5030800500413
License date	Mar 16, 2021
Licensed Content Publisher	Elsevier
Licensed Content Publication	Coordination Chemistry Reviews
Licensed Content Title	Potential applications of metal-organic frameworks
Licensed Content Author	Ryan J. Kuppler,Daren J. Timmons,Qian-Rong Fang,Jian-Rong Li,Trevor A. Makal,Mark D. Young,Daqiang Yuan,Dan Zhao,Wenjuan Zhuang,Hong-Cai Zhou
Licensed Content Date	Dec 1, 2009
Licensed Content Volume	253
Licensed Content Issue	23-24
Licensed Content Pages	25
Start Page	3042
End Page	3066

Annexure II

Type of Use	reuse in a thesis/dissertation
Portion	figures/tables/illustrations
Number of figures/tables/illustrations	1
Format	both print and electronic
Are you the author of this Elsevier article?	No
Will you be translating?	No
Title	Synthesis and Characterization of Some Zn(II) and Zr(IV) Metal-Organic Frameworks and Their Applications in Fluorescence Sensing and Catalysis
Institution name	IIT Guwahati
Expected presentation date	Jun 2021
Order reference number	79
Portions	1.4
Requestor Location	Mr. Chiranjib Gogoi IIT Guwahati Guwahati, 781039 India Attn: IIT Guwahati
Publisher Tax ID	GB 494 6272 12
Total	0.00 USD

Terms and Conditions

INTRODUCTION

1. The publisher for this copyrighted material is Elsevier. By clicking "accept" in connection with completing this licensing transaction, you agree that the following terms and conditions apply to this transaction (along with the Billing and Payment terms and conditions established by Copyright Clearance Center, Inc. ("CCC"), at the time that you opened your Rightslink account and that are available at any time at http://myaccount.copyright.com).

GENERAL TERMS

2. Elsevier hereby grants you permission to reproduce the aforementioned material subject to the terms and conditions indicated.

3. Acknowledgement: If any part of the material to be used (for example, figures) has appeared in our publication with credit or acknowledgement to another source, permission must also be sought from that source. If such permission is not obtained then that material may not be included in your publication/copies. Suitable acknowledgement to the source must be made, either as a footnote or in a reference list at the end of your publication, as follows:

"Reprinted from Publication title, Vol /edition number, Author(s), Title of article / title of chapter, Pages No., Copyright (Year), with permission from Elsevier [OR APPLICABLE SOCIETY COPYRIGHT OWNER]." Also Lancet special credit - "Reprinted from The Lancet, Vol. number, Author(s), Title of article, Pages No., Copyright (Year), with permission from Elsevier."

4. Reproduction of this material is confined to the purpose and/or media for which permission is hereby given.

5. Altering/Modifying Material: Not Permitted. However figures and illustrations may be altered/adapted minimally to serve your work. Any other abbreviations, additions, deletions and/or any other alterations shall be made only with prior written authorization of Elsevier Ltd. (Please contact Elsevier's permissions helpdesk here). No modifications can be made to any Lancet figures/tables and they must be reproduced in full.

6. If the permission fee for the requested use of our material is waived in this instance, please be advised that your future requests for Elsevier materials may attract a fee.

7. Reservation of Rights: Publisher reserves all rights not specifically granted in the combination of (i) the license details provided by you and accepted in the course of this licensing transaction, (ii) these terms and conditions and (iii) CCC's Billing and Payment terms and conditions.

8. License Contingent Upon Payment: While you may exercise the rights licensed immediately upon issuance of the license at the end of the licensing process for the transaction, provided that you have disclosed complete and accurate details of your proposed use, no license is finally effective unless and until full payment is received from you (either by publisher or by CCC) as provided in CCC's Billing and Payment terms and conditions. If full payment is not received on a timely basis, then any license preliminarily granted shall be deemed automatically revoked and shall be void as if never granted. Further, in the event that you breach any of these terms and conditions or any of CCC's Billing and Payment terms and conditions, the license is automatically revoked and shall be void as if never

granted. Use of materials as described in a revoked license, as well as any use of the materials beyond the scope of an unrevoked license, may constitute copyright infringement and publisher reserves the right to take any and all action to protect its copyright in the materials.

9. Warranties: Publisher makes no representations or warranties with respect to the licensed material.

10. Indemnity: You hereby indemnify and agree to hold harmless publisher and CCC, and their respective officers, directors, employees and agents, from and against any and all claims arising out of your use of the licensed material other than as specifically authorized pursuant to this license.

11. No Transfer of License: This license is personal to you and may not be sublicensed, assigned, or transferred by you to any other person without publisher's written permission.

12. No Amendment Except in Writing: This license may not be amended except in a writing signed by both parties (or, in the case of publisher, by CCC on publisher's behalf).

13. Objection to Contrary Terms: Publisher hereby objects to any terms contained in any purchase order, acknowledgment, check endorsement or other writing prepared by you, which terms are inconsistent with these terms and conditions or CCC's Billing and Payment terms and conditions. These terms and conditions, together with CCC's Billing and Payment terms and conditions (which are incorporated herein), comprise the entire agreement between you and publisher (and CCC) concerning this licensing transaction. In the event of any conflict between your obligations established by these terms and conditions and those established by CCC's Billing and Payment terms and conditions, these terms and conditions shall control.

14. Revocation: Elsevier or Copyright Clearance Center may deny the permissions described in this License at their sole discretion, for any reason or no reason, with a full refund payable to you. Notice of such denial will be made using the contact information provided by you. Failure to receive such notice will not alter or invalidate the denial. In no event will Elsevier or Copyright Clearance Center be responsible or liable for any costs, expenses or damage incurred by you as a result of a denial of your permission request, other than a refund of the amount(s) paid by you to Elsevier and/or Copyright Clearance Center for denied permissions.

LIMITED LICENSE

The following terms and conditions apply only to specific license types:

15. **Translation**: This permission is granted for non-exclusive world **English** rights only unless your license was granted for translation rights. If you licensed translation rights you may only translate this content into the languages you requested. A professional translator must perform all translations and reproduce the content word for word preserving the integrity of the article.

16. **Posting licensed content on any Website**: The following terms and conditions apply as follows: Licensing material from an Elsevier journal: All content posted to the web site must maintain the copyright information line on the bottom of each image; A hyper-text must be included to the Homepage of the journal from which you are licensing at http://www.sciencedirect.com/science/journal/xxxxx or the Elsevier homepage for books at http://www.elsevier.com; Central Storage: This license does not include permission for a

scanned version of the material to be stored in a central repository such as that provided by Heron/XanEdu.

Licensing material from an Elsevier book: A hyper-text link must be included to the Elsevier homepage at http://www.elsevier.com . All content posted to the web site must maintain the copyright information line on the bottom of each image.

Posting licensed content on Electronic reserve: In addition to the above the following clauses are applicable: The web site must be password-protected and made available only to bona fide students registered on a relevant course. This permission is granted for 1 year only. You may obtain a new license for future website posting.

17. **For journal authors:** the following clauses are applicable in addition to the above:

Preprints:

A preprint is an author's own write-up of research results and analysis, it has not been peer-reviewed, nor has it had any other value added to it by a publisher (such as formatting, copyright, technical enhancement etc.).

Authors can share their preprints anywhere at any time. Preprints should not be added to or enhanced in any way in order to appear more like, or to substitute for, the final versions of articles however authors can update their preprints on arXiv or RePEc with their Accepted Author Manuscript (see below).

If accepted for publication, we encourage authors to link from the preprint to their formal publication via its DOI. Millions of researchers have access to the formal publications on ScienceDirect, and so links will help users to find, access, cite and use the best available version. Please note that Cell Press, The Lancet and some society-owned have different preprint policies. Information on these policies is available on the journal homepage.

Accepted Author Manuscripts: An accepted author manuscript is the manuscript of an article that has been accepted for publication and which typically includes author-incorporated changes suggested during submission, peer review and editor-author communications.

Authors can share their accepted author manuscript:

- immediately
  - via their non-commercial person homepage or blog
  - by updating a preprint in arXiv or RePEc with the accepted manuscript
  - via their research institute or institutional repository for internal institutional uses or as part of an invitation-only research collaboration work-group
  - directly by providing copies to their students or to research collaborators for their personal use
  - for private scholarly sharing as part of an invitation-only work group on commercial sites with which Elsevier has an agreement
- After the embargo period
  - via non-commercial hosting platforms such as their institutional repository
  - via commercial sites with which Elsevier has an agreement

In all cases accepted manuscripts should:

- link to the formal publication via its DOI

- bear a CC-BY-NC-ND license - this is easy to do
- if aggregated with other manuscripts, for example in a repository or other site, be shared in alignment with our hosting policy not be added to or enhanced in any way to appear more like, or to substitute for, the published journal article.

Published journal article (JPA): A published journal article (PJA) is the definitive final record of published research that appears or will appear in the journal and embodies all value-adding publishing activities including peer review co-ordination, copy-editing, formatting, (if relevant) pagination and online enrichment.

Policies for sharing publishing journal articles differ for subscription and gold open access articles:

Subscription Articles: If you are an author, please share a link to your article rather than the full-text. Millions of researchers have access to the formal publications on ScienceDirect, and so links will help your users to find, access, cite, and use the best available version.

Theses and dissertations which contain embedded PJAs as part of the formal submission can be posted publicly by the awarding institution with DOI links back to the formal publications on ScienceDirect.

If you are affiliated with a library that subscribes to ScienceDirect you have additional private sharing rights for others' research accessed under that agreement. This includes use for classroom teaching and internal training at the institution (including use in course packs and courseware programs), and inclusion of the article for grant funding purposes.

Gold Open Access Articles: May be shared according to the author-selected end-user license and should contain a CrossMark logo, the end user license, and a DOI link to the formal publication on ScienceDirect.

Please refer to Elsevier's posting policy for further information.

18. **For book authors** the following clauses are applicable in addition to the above: Authors are permitted to place a brief summary of their work online only. You are not allowed to download and post the published electronic version of your chapter, nor may you scan the printed edition to create an electronic version. **Posting to a repository:** Authors are permitted to post a summary of their chapter only in their institution's repository.

19. **Thesis/Dissertation**: If your license is for use in a thesis/dissertation your thesis may be submitted to your institution in either print or electronic form. Should your thesis be published commercially, please reapply for permission. These requirements include permission for the Library and Archives of Canada to supply single copies, on demand, of the complete thesis and include permission for Proquest/UMI to supply single copies, on demand, of the complete thesis. Should your thesis be published commercially, please reapply for permission. Theses and dissertations which contain embedded PJAs as part of the formal submission can be posted publicly by the awarding institution with DOI links back to the formal publications on ScienceDirect.

Elsevier Open Access Terms and Conditions

You can publish open access with Elsevier in hundreds of open access journals or in nearly 2000 established subscription journals that support open access publishing. Permitted third

party re-use of these open access articles is defined by the author's choice of Creative Commons user license. See our open access license policy for more information.

Terms & Conditions applicable to all Open Access articles published with Elsevier:

Any reuse of the article must not represent the author as endorsing the adaptation of the article nor should the article be modified in such a way as to damage the author's honour or reputation. If any changes have been made, such changes must be clearly indicated.

The author(s) must be appropriately credited and we ask that you include the end user license and a DOI link to the formal publication on ScienceDirect.

If any part of the material to be used (for example, figures) has appeared in our publication with credit or acknowledgement to another source it is the responsibility of the user to ensure their reuse complies with the terms and conditions determined by the rights holder.

Additional Terms & Conditions applicable to each Creative Commons user license:

CC BY: The CC-BY license allows users to copy, to create extracts, abstracts and new works from the Article, to alter and revise the Article and to make commercial use of the Article (including reuse and/or resale of the Article by commercial entities), provided the user gives appropriate credit (with a link to the formal publication through the relevant DOI), provides a link to the license, indicates if changes were made and the licensor is not represented as endorsing the use made of the work. The full details of the license are available at http://creativecommons.org/licenses/by/4.0.

CC BY NC SA: The CC BY-NC-SA license allows users to copy, to create extracts, abstracts and new works from the Article, to alter and revise the Article, provided this is not done for commercial purposes, and that the user gives appropriate credit (with a link to the formal publication through the relevant DOI), provides a link to the license, indicates if changes were made and the licensor is not represented as endorsing the use made of the work. Further, any new works must be made available on the same conditions. The full details of the license are available at http://creativecommons.org/licenses/by-nc-sa/4.0.

CC BY NC ND: The CC BY-NC-ND license allows users to copy and distribute the Article, provided this is not done for commercial purposes and further does not permit distribution of the Article if it is changed or edited in any way, and provided the user gives appropriate credit (with a link to the formal publication through the relevant DOI), provides a link to the license, and that the licensor is not represented as endorsing the use made of the work. The full details of the license are available at http://creativecommons.org/licenses/by-nc-nd/4.0. Any commercial reuse of Open Access articles published with a CC BY NC SA or CC BY NC ND license requires permission from Elsevier and will be subject to a fee.

Commercial reuse includes:

- Associating advertising with the full text of the Article
- Charging fees for document delivery or access
- Article aggregation
- Systematic distribution via e-mail lists or share buttons

Posting or linking by commercial companies for use by customers of those companies.

20. **Other Conditions**:

v1.10

Questions? customercare@copyright.com or +1-855-239-3415 (toll free in the US) or +1-978-646-2777.

Annexure III

Copyright Clearance Center | Marketplace™

Order Number: 1104620
Order Date: 16 Mar 2021

Payment Information

Chiranjib Gogoi
chiranjib2016@iitg.ac.in
Payment method: Invoice

Billing Address:
Mr. Chiranjib Gogoi
IIT Guwahati
Guwahati, 781039
India

+91 3612584334
chiranjib2016@iitg.ac.in

Customer Location:
Mr. Chiranjib Gogoi
IIT Guwahati
Guwahati, 781039
India

Order Details

1. Chemical Society reviews

Billing Status: Open

Order license ID	1104620-1
Order detail status	Completed
ISSN	1460-4744
Type of use	Republish in a thesis/dissertation
Publisher	ROYAL SOCIETY OF CHEMISTRY
Portion	Image/photo/illustration

0.00 USD
Republication Permission

LICENSED CONTENT

Publication Title	Chemical Society reviews	Country	United Kingdom of Great Britain and Northern Ireland
Author/Editor	Royal Society of Chemistry (Great Britain)	Rightsholder	Royal Society of Chemistry
Date	01/01/1972	Publication Type	e-Journal
Language	English	URL	http://www.rsc.org/csr

REQUEST DETAILS

Portion Type	Image/photo/illustration	Distribution	Worldwide
		Translation	Original language of publication
Number of images / photos / illustrations	1		
		Copies for the disabled?	No
Format (select all that apply)	Print		

Who will republish the content?	Not-for-profit entity	Minor editing privileges?	No
Duration of Use	Current edition and up to 5 years	Incidental promotional use?	No
Lifetime Unit Quantity	Up to 499	Currency	USD
Rights Requested	Main product		

NEW WORK DETAILS

Title	Synthesis and Characterization of Some Zn(II) and Zr(IV) Metal-Organic Frameworks and Their Applications in Fluorescence Sensing and Catalysis	Institution name	IIT Guwahati
		Expected presentation date	2021-07-15
Instructor name	Chiranjib Gogoi		

ADDITIONAL DETAILS

Order reference number	82	The requesting person / organization to appear on the license	Chiranjib Gogoi

REUSE CONTENT DETAILS

Title, description or numeric reference of the portion(s)	Scheme 1	Title of the article/chapter the portion is from	Tuning the structure and function of metal–organic frameworks via linker design
Editor of portion(s)	N/A	Author of portion(s)	Royal Society of Chemistry (Great Britain)
Volume of serial or monograph	43	Publication date of portion	1972-01-01
Page or page range of portion	5562		

Total Items: 1

Subtotal: 0.00 USD

Order Total: 0.00 USD

SPRINGER NATURE LICENSE
TERMS AND CONDITIONS

Mar 16, 2021

This Agreement between Mr. Chiranjib Gogoi ("You") and Springer Nature ("Springer Nature") consists of your license details and the terms and conditions provided by Springer Nature and Copyright Clearance Center.

License Number	5030811432186
License date	Mar 16, 2021
Licensed Content Publisher	Springer Nature
Licensed Content Publication	Korean Journal of Chemical Engineering
Licensed Content Title	Synthesis of metal-organic frameworks: A mini review
Licensed Content Author	Yu-Ri Lee et al
Licensed Content Date	Aug 17, 2013
Type of Use	Thesis/Dissertation
Requestor type	academic/university or research institute
Format	print and electronic
Portion	figures/tables/illustrations
Number of figures/tables/illustrations	1

Will you be translating?	no
Circulation/distribution	1 - 29
Author of this Springer Nature content	no
Title	Synthesis and Characterization of Some Zn(II) and Zr(IV) Metal-Organic Frameworks and Their Applications in Fluorescence Sensing and Catalysis
Institution name	IIT Guwahati
Expected presentation date	Jun 2021
Order reference number	107
Portions	Figure 1.11
Requestor Location	Mr. Chiranjib Gogoi IIT Guwahati Guwahati, 781039 India Attn: IIT Guwahati
Total	0.00 USD

Terms and Conditions

Springer Nature Customer Service Centre GmbH
Terms and Conditions

This agreement sets out the terms and conditions of the licence (the **Licence**) between you and **Springer Nature Customer Service Centre GmbH** (the **Licensor**). By clicking 'accept' and completing the transaction for the material (**Licensed Material**), you also confirm your acceptance of these terms and conditions.

1. Grant of License

1. 1. The Licensor grants you a personal, non-exclusive, non-transferable, world-wide licence to reproduce the Licensed Material for the purpose specified in your order only. Licences are granted for the specific use requested in the order and for no other use, subject to the conditions below.

1. 2. The Licensor warrants that it has, to the best of its knowledge, the rights to license reuse of the Licensed Material. However, you should ensure that the material you are requesting is original to the Licensor and does not carry the copyright of another entity (as credited in the published version).

1. 3. If the credit line on any part of the material you have requested indicates that it was reprinted or adapted with permission from another source, then you should also seek permission from that source to reuse the material.

2. Scope of Licence

2. 1. You may only use the Licensed Content in the manner and to the extent permitted by these Ts&Cs and any applicable laws.

2. 2. A separate licence may be required for any additional use of the Licensed Material, e.g. where a licence has been purchased for print only use, separate permission must be obtained for electronic re-use. Similarly, a licence is only valid in the language selected and does not apply for editions in other languages unless additional translation rights have been granted separately in the licence. Any content owned by third parties are expressly excluded from the licence.

2. 3. Similarly, rights for additional components such as custom editions and derivatives require additional permission and may be subject to an additional fee. Please apply to Journalpermissions@springernature.com/bookpermissions@springernature.com for these rights.

2. 4. Where permission has been granted **free of charge** for material in print, permission may also be granted for any electronic version of that work, provided that the material is incidental to your work as a whole and that the electronic version is essentially equivalent to, or substitutes for, the print version.

2. 5. An alternative scope of licence may apply to signatories of the STM Permissions Guidelines, as amended from time to time.

3. Duration of Licence

3. 1. A licence for is valid from the date of purchase ('Licence Date') at the end of the relevant period in the below table:

Scope of Licence	Duration of Licence
Post on a website	12 months
Presentations	12 months
Books and journals	Lifetime of the edition in the language purchased

4. Acknowledgement

4. 1. The Licensor's permission must be acknowledged next to the Licenced Material in print. In electronic form, this acknowledgement must be visible at the same time as the figures/tables/illustrations or abstract, and must be hyperlinked to the journal/book's homepage. Our required acknowledgement format is in the Appendix below.

5. Restrictions on use

5. 1. Use of the Licensed Material may be permitted for incidental promotional use and minor editing privileges e.g. minor adaptations of single figures, changes of format, colour and/or style where the adaptation is credited as set out in Appendix 1 below. Any other changes including but not limited to, cropping, adapting, omitting material that affect the meaning, intention or moral rights of the author are strictly prohibited.

5. 2. You must not use any Licensed Material as part of any design or trademark.

5. 3. Licensed Material may be used in Open Access Publications (OAP) before publication by Springer Nature, but any Licensed Material must be removed from OAP sites prior to final publication.

6. Ownership of Rights

6. 1. Licensed Material remains the property of either Licensor or the relevant third party and any rights not explicitly granted herein are expressly reserved.

7. Warranty

IN NO EVENT SHALL LICENSOR BE LIABLE TO YOU OR ANY OTHER PARTY OR ANY OTHER PERSON OR FOR ANY SPECIAL, CONSEQUENTIAL, INCIDENTAL OR INDIRECT DAMAGES, HOWEVER CAUSED, ARISING OUT OF OR IN CONNECTION WITH THE DOWNLOADING, VIEWING OR USE OF THE MATERIALS REGARDLESS OF THE FORM OF ACTION, WHETHER FOR BREACH OF CONTRACT, BREACH OF WARRANTY, TORT, NEGLIGENCE, INFRINGEMENT OR OTHERWISE (INCLUDING, WITHOUT LIMITATION, DAMAGES BASED ON LOSS OF PROFITS, DATA, FILES, USE, BUSINESS OPPORTUNITY OR CLAIMS OF THIRD PARTIES), AND
WHETHER OR NOT THE PARTY HAS BEEN ADVISED OF THE POSSIBILITY OF SUCH DAMAGES. THIS LIMITATION SHALL APPLY NOTWITHSTANDING ANY FAILURE OF ESSENTIAL PURPOSE OF ANY LIMITED REMEDY PROVIDED HEREIN.

8. Limitations

8. 1. ***BOOKS ONLY:*** Where **'reuse in a dissertation/thesis'** has been selected the following terms apply: Print rights of the final author's accepted manuscript (for clarity,

NOT the published version) for up to 100 copies, electronic rights for use only on a personal website or institutional repository as defined by the Sherpa guideline (www.sherpa.ac.uk/romeo/).

8. 2. For content reuse requests that qualify for permission under the STM Permissions Guidelines, which may be updated from time to time, the STM Permissions Guidelines supersede the terms and conditions contained in this licence.

9. Termination and Cancellation

9. 1. Licences will expire after the period shown in Clause 3 (above).

9. 2. Licensee reserves the right to terminate the Licence in the event that payment is not received in full or if there has been a breach of this agreement by you.

Appendix 1 — Acknowledgements:

For Journal Content:
Reprinted by permission from [**the Licensor**]: [**Journal Publisher** (e.g. Nature/Springer/Palgrave)] [**JOURNAL NAME**] [**REFERENCE CITATION** (Article name, Author(s) Name), [**COPYRIGHT**] (year of publication)

For **Advance Online Publication papers:**
Reprinted by permission from [**the Licensor**]: [**Journal Publisher** (e.g. Nature/Springer/Palgrave)] [**JOURNAL NAME**] [**REFERENCE CITATION** (Article name, Author(s) Name), [**COPYRIGHT**] (year of publication), advance online publication, day month year (doi: 10.1038/sj.[JOURNAL ACRONYM].)

For Adaptations/Translations:
Adapted/Translated by permission from [**the Licensor**]: [**Journal Publisher** (e.g. Nature/Springer/Palgrave)] [**JOURNAL NAME**] [**REFERENCE CITATION** (Article name, Author(s) Name), [**COPYRIGHT**] (year of publication)

Note: For any republication from the British Journal of Cancer, the following credit line style applies:

Reprinted/adapted/translated by permission from [**the Licensor**]: on behalf of Cancer Research UK: : [**Journal Publisher** (e.g. Nature/Springer/Palgrave)] [**JOURNAL NAME**] [**REFERENCE CITATION** (Article name, Author(s) Name), [**COPYRIGHT**] (year of publication)

For **Advance Online Publication** papers:
Reprinted by permission from The [**the Licensor**]: on behalf of Cancer Research UK: [**Journal Publisher** (e.g. Nature/Springer/Palgrave)] [**JOURNAL NAME**] [**REFERENCE CITATION** (Article name, Author(s) Name), [**COPYRIGHT**] (year of publication), advance online publication, day month year (doi: 10.1038/sj.[JOURNAL ACRONYM])

For Book content:
Reprinted/adapted by permission from [**the Licensor**]: [**Book Publisher** (e.g.

Palgrave Macmillan, Springer etc) [**Book Title**] by [**Book author**(s)]
[**COPYRIGHT**] (year of publication)

Other Conditions:

Version 1.3

Questions? customercare@copyright.com or +1-855-239-3415 (toll free in the US) or +1-978-646-2777.

Annexure V

Copyright Clearance Center | Marketplace™

Order Number: 1104633
Order Date: 16 Mar 2021

Payment Information

Chiranjib Gogoi
chiranjib2016@iitg.ac.in
Payment method: Invoice

Billing Address:
Mr. Chiranjib Gogoi
IIT Guwahati
Guwahati, 781039
India

+91 3612584334
chiranjib2016@iitg.ac.in

Customer Location:
Mr. Chiranjib Gogoi
IIT Guwahati
Guwahati, 781039
India

Order Details

1. Journal of materials chemistry. A, Materials for energy and sustainability

Billing Status: Open

Order license ID	1104633-1
Order detail status	Completed
ISSN	2050-7496
Type of use	Republish in a thesis/dissertation
Publisher	Royal Society of Chemistry
Portion	Chart/graph/table/figure

0.00 USD
Republication Permission

LICENSED CONTENT

Publication Title	Journal of materials chemistry. A, Materials for energy and sustainability	**Country**	United Kingdom of Great Britain and Northern Ireland
Author/Editor	Royal Society of Chemistry (Great Britain)	**Rightsholder**	Royal Society of Chemistry
Date	01/01/2013	**Publication Type**	e-Journal
Language	English	**URL**	http://pubs.rsc.org/en/journals/journalissues/ta

REQUEST DETAILS

Portion Type	Chart/graph/table/figure	**Distribution**	Worldwide
Number of charts / graphs / tables / figures requested	1	**Translation**	Original language of publication

Format (select all that apply)	Print	Copies for the disabled?	No
Who will republish the content?	Not-for-profit entity	Minor editing privileges?	No
Duration of Use	Current edition and up to 5 years	Incidental promotional use?	No
Lifetime Unit Quantity	Up to 499	Currency	USD
Rights Requested	Main product		

NEW WORK DETAILS

Title	Synthesis and Characterization of Some Zn(II) and Zr(IV) Metal-Organic Frameworks and Their Applications in Fluorescence Sensing and Catalysis	Institution name	IIT Guwahati
		Expected presentation date	2021-06-15
Instructor name	Chiranjib Gogoi		

ADDITIONAL DETAILS

Order reference number	113	The requesting person / organization to appear on the license	Chiranjib Gogoi

REUSE CONTENT DETAILS

Title, description or numeric reference of the portion(s)	Fig 1	Title of the article/chapter the portion is from	Electrochemical preparation of metal–organic framework films for fast detection of nitro explosives
Editor of portion(s)	N/A		
Volume of serial or monograph	2	Author of portion(s)	Royal Society of Chemistry (Great Britain)
Page or page range of portion	19474	Publication date of portion	2014-09-23

Total Items: 1

Subtotal: 0.00 USD

Order Total: 0.00 USD

Annexure VI

Sonochemical fabrication of Cu(II) and Zn(II) metal-organic framework films on metal substrates

Author: Osama Abuzalat,Danny Wong,Mohamed Elsayed,Simon Park,Seonghwan Kim

Publication: Ultrasonics Sonochemistry

Publisher: Elsevier

Date: July 2018

Annexure VII

JOHN WILEY AND SONS LICENSE
TERMS AND CONDITIONS

Mar 16, 2021

This Agreement between Mr. Chiranjib Gogoi ("You") and John Wiley and Sons ("John Wiley and Sons") consists of your license details and the terms and conditions provided by John Wiley and Sons and Copyright Clearance Center.

License Number	5030821407220
License date	Mar 16, 2021
Licensed Content Publisher	John Wiley and Sons
Licensed Content Publication	Advanced Functional Materials
Licensed Content Title	Post-Synthetic Modification of Metal–Organic Frameworks Toward Applications
Licensed Content Author	Sukhendu Mandal, Srinivasan Natarajan, Prabu Mani, et al
Licensed Content Date	Oct 8, 2020
Licensed Content Volume	31
Licensed Content Issue	4

Licensed Content Pages	22
Type of use	Dissertation/Thesis
Requestor type	University/Academic
Format	Print and electronic
Portion	Figure/table
Number of figures/tables	1
Will you be translating?	No
Title	Synthesis and Characterization of Some Zn(II) and Zr(IV) Metal-Organic Frameworks and Their Applications in Fluorescence Sensing and Catalysis
Institution name	IIT Guwahati
Expected presentation date	Jun 2021
Order reference number	123
Portions	Figure 1.14
Requestor Location	Mr. Chiranjib Gogoi IIT Guwahati Guwahati, 781039 India Attn: IIT Guwahati

Publisher Tax ID EU826007151

Total 0.00 USD

Terms and Conditions

TERMS AND CONDITIONS

This copyrighted material is owned by or exclusively licensed to John Wiley & Sons, Inc. or one of its group companies (each a"Wiley Company") or handled on behalf of a society with which a Wiley Company has exclusive publishing rights in relation to a particular work (collectively "WILEY"). By clicking "accept" in connection with completing this licensing transaction, you agree that the following terms and conditions apply to this transaction (along with the billing and payment terms and conditions established by the Copyright Clearance Center Inc., ("CCC's Billing and Payment terms and conditions"), at the time that you opened your RightsLink account (these are available at any time at http://myaccount.copyright.com).

Terms and Conditions

- The materials you have requested permission to reproduce or reuse (the "Wiley Materials") are protected by copyright.
- You are hereby granted a personal, non-exclusive, non-sub licensable (on a stand-alone basis), non-transferable, worldwide, limited license to reproduce the Wiley Materials for the purpose specified in the licensing process. This license, **and any CONTENT (PDF or image file) purchased as part of your order,** is for a one-time use only and limited to any maximum distribution number specified in the license. The first instance of republication or reuse granted by this license must be completed within two years of the date of the grant of this license (although copies prepared before the end date may be distributed thereafter). The Wiley Materials shall not be used in any other manner or for any other purpose, beyond what is granted in the license. Permission is granted subject to an appropriate acknowledgement given to the author, title of the material/book/journal and the publisher. You shall also duplicate the copyright notice that appears in the Wiley publication in your use of the Wiley Material. Permission is also granted on the understanding that nowhere in the text is a previously published source acknowledged for all or part of this Wiley Material. Any third party content is expressly excluded from this permission.
- With respect to the Wiley Materials, all rights are reserved. Except as expressly granted by the terms of the license, no part of the Wiley Materials may be copied, modified, adapted (except for minor reformatting required by the new Publication), translated, reproduced, transferred or distributed, in any form or by any means, and no derivative works may be made based on the Wiley Materials without the prior permission of the respective copyright owner.**For STM Signatory Publishers clearing permission under the terms of the STM Permissions Guidelines only, the terms of the license are extended to include subsequent editions and for editions in other languages, provided such editions are for the work as a whole in situ and does not involve the separate exploitation of the permitted figures or extracts,**

You may not alter, remove or suppress in any manner any copyright, trademark or other notices displayed by the Wiley Materials. You may not license, rent, sell, loan, lease, pledge, offer as security, transfer or assign the Wiley Materials on a stand-alone basis, or any of the rights granted to you hereunder to any other person.

- The Wiley Materials and all of the intellectual property rights therein shall at all times remain the exclusive property of John Wiley & Sons Inc, the Wiley Companies, or their respective licensors, and your interest therein is only that of having possession of and the right to reproduce the Wiley Materials pursuant to Section 2 herein during the continuance of this Agreement. You agree that you own no right, title or interest in or to the Wiley Materials or any of the intellectual property rights therein. You shall have no rights hereunder other than the license as provided for above in Section 2. No right, license or interest to any trademark, trade name, service mark or other branding ("Marks") of WILEY or its licensors is granted hereunder, and you agree that you shall not assert any such right, license or interest with respect thereto

- NEITHER WILEY NOR ITS LICENSORS MAKES ANY WARRANTY OR REPRESENTATION OF ANY KIND TO YOU OR ANY THIRD PARTY, EXPRESS, IMPLIED OR STATUTORY, WITH RESPECT TO THE MATERIALS OR THE ACCURACY OF ANY INFORMATION CONTAINED IN THE MATERIALS, INCLUDING, WITHOUT LIMITATION, ANY IMPLIED WARRANTY OF MERCHANTABILITY, ACCURACY, SATISFACTORY QUALITY, FITNESS FOR A PARTICULAR PURPOSE, USABILITY, INTEGRATION OR NON-INFRINGEMENT AND ALL SUCH WARRANTIES ARE HEREBY EXCLUDED BY WILEY AND ITS LICENSORS AND WAIVED BY YOU.

- WILEY shall have the right to terminate this Agreement immediately upon breach of this Agreement by you.

- You shall indemnify, defend and hold harmless WILEY, its Licensors and their respective directors, officers, agents and employees, from and against any actual or threatened claims, demands, causes of action or proceedings arising from any breach of this Agreement by you.

- IN NO EVENT SHALL WILEY OR ITS LICENSORS BE LIABLE TO YOU OR ANY OTHER PARTY OR ANY OTHER PERSON OR ENTITY FOR ANY SPECIAL, CONSEQUENTIAL, INCIDENTAL, INDIRECT, EXEMPLARY OR PUNITIVE DAMAGES, HOWEVER CAUSED, ARISING OUT OF OR IN CONNECTION WITH THE DOWNLOADING, PROVISIONING, VIEWING OR USE OF THE MATERIALS REGARDLESS OF THE FORM OF ACTION, WHETHER FOR BREACH OF CONTRACT, BREACH OF WARRANTY, TORT, NEGLIGENCE, INFRINGEMENT OR OTHERWISE (INCLUDING, WITHOUT LIMITATION, DAMAGES BASED ON LOSS OF PROFITS, DATA, FILES, USE, BUSINESS OPPORTUNITY OR CLAIMS OF THIRD PARTIES), AND WHETHER OR NOT THE PARTY HAS BEEN ADVISED OF THE POSSIBILITY OF SUCH DAMAGES. THIS LIMITATION SHALL APPLY NOTWITHSTANDING ANY FAILURE OF ESSENTIAL PURPOSE OF ANY LIMITED REMEDY PROVIDED HEREIN.

- Should any provision of this Agreement be held by a court of competent jurisdiction to be illegal, invalid, or unenforceable, that provision shall be deemed amended to achieve as nearly as possible the same economic effect as the original provision, and the legality, validity and enforceability of the remaining provisions of this Agreement

shall not be affected or impaired thereby.

- The failure of either party to enforce any term or condition of this Agreement shall not constitute a waiver of either party's right to enforce each and every term and condition of this Agreement. No breach under this agreement shall be deemed waived or excused by either party unless such waiver or consent is in writing signed by the party granting such waiver or consent. The waiver by or consent of a party to a breach of any provision of this Agreement shall not operate or be construed as a waiver of or consent to any other or subsequent breach by such other party.

- This Agreement may not be assigned (including by operation of law or otherwise) by you without WILEY's prior written consent.

- Any fee required for this permission shall be non-refundable after thirty (30) days from receipt by the CCC.

- These terms and conditions together with CCC's Billing and Payment terms and conditions (which are incorporated herein) form the entire agreement between you and WILEY concerning this licensing transaction and (in the absence of fraud) supersedes all prior agreements and representations of the parties, oral or written. This Agreement may not be amended except in writing signed by both parties. This Agreement shall be binding upon and inure to the benefit of the parties' successors, legal representatives, and authorized assigns.

- In the event of any conflict between your obligations established by these terms and conditions and those established by CCC's Billing and Payment terms and conditions, these terms and conditions shall prevail.

- WILEY expressly reserves all rights not specifically granted in the combination of (i) the license details provided by you and accepted in the course of this licensing transaction, (ii) these terms and conditions and (iii) CCC's Billing and Payment terms and conditions.

- This Agreement will be void if the Type of Use, Format, Circulation, or Requestor Type was misrepresented during the licensing process.

- This Agreement shall be governed by and construed in accordance with the laws of the State of New York, USA, without regards to such state's conflict of law rules. Any legal action, suit or proceeding arising out of or relating to these Terms and Conditions or the breach thereof shall be instituted in a court of competent jurisdiction in New York County in the State of New York in the United States of America and each party hereby consents and submits to the personal jurisdiction of such court, waives any objection to venue in such court and consents to service of process by registered or certified mail, return receipt requested, at the last known address of such party.

WILEY OPEN ACCESS TERMS AND CONDITIONS

Wiley Publishes Open Access Articles in fully Open Access Journals and in Subscription journals offering Online Open. Although most of the fully Open Access journals publish open access articles under the terms of the Creative Commons Attribution (CC BY) License only, the subscription journals and a few of the Open Access Journals offer a choice of Creative Commons Licenses. The license type is clearly identified on the article.

The Creative Commons Attribution License

The Creative Commons Attribution License (CC-BY) allows users to copy, distribute and transmit an article, adapt the article and make commercial use of the article. The CC-BY license permits commercial and non-

Creative Commons Attribution Non-Commercial License

The Creative Commons Attribution Non-Commercial (CC-BY-NC)License permits use, distribution and reproduction in any medium, provided the original work is properly cited and is not used for commercial purposes.(see below)

Creative Commons Attribution-Non-Commercial-NoDerivs License

The Creative Commons Attribution Non-Commercial-NoDerivs License (CC-BY-NC-ND) permits use, distribution and reproduction in any medium, provided the original work is properly cited, is not used for commercial purposes and no modifications or adaptations are made. (see below)

Use by commercial "for-profit" organizations

Use of Wiley Open Access articles for commercial, promotional, or marketing purposes requires further explicit permission from Wiley and will be subject to a fee.

Further details can be found on Wiley Online Library
http://olabout.wiley.com/WileyCDA/Section/id-410895.html

Other Terms and Conditions:

v1.10 Last updated September 2015

Questions? customercare@copyright.com or +1-855-239-3415 (toll free in the US) or +1-978-646-2777.

Annexure VIII

ELSEVIER LICENSE
TERMS AND CONDITIONS

Mar 16, 2021

This Agreement between Mr. Chiranjib Gogoi ("You") and Elsevier ("Elsevier") consists of your license details and the terms and conditions provided by Elsevier and Copyright Clearance Center.

License Number	5030830190496
License date	Mar 16, 2021
Licensed Content Publisher	Elsevier
Licensed Content Publication	Journal of Solid State Chemistry
Licensed Content Title	Highly sensitive and selective detection of mercury (II) based on a zirconium metal-organic framework in aqueous media
Licensed Content Author	Xin Zhang,Tifeng Xia,Ke Jiang,Yuanjing Cui,Yu Yang,Guodong Qian
Licensed Content Date	Sep 1, 2017
Licensed Content Volume	253
Licensed Content Issue	n/a
Licensed Content Pages	5
Start Page	277
End Page	281

Annexure VIII

Type of Use	reuse in a thesis/dissertation
Portion	figures/tables/illustrations
Number of figures/tables/illustrations	1
Format	both print and electronic
Are you the author of this Elsevier article?	No
Will you be translating?	No
Title	Synthesis and Characterization of Some Zn(II) and Zr(IV) Metal-Organic Frameworks and Their Applications in Fluorescence Sensing and Catalysis
Institution name	IIT Guwahati
Expected presentation date	Jun 2021
Order reference number	125
Portions	Figure 1.15
Requestor Location	Mr. Chiranjib Gogoi IIT Guwahati Guwahati, 781039 India Attn: IIT Guwahati
Publisher Tax ID	GB 494 6272 12
Total	0.00 USD

Terms and Conditions

INTRODUCTION

1. The publisher for this copyrighted material is Elsevier. By clicking "accept" in connection with completing this licensing transaction, you agree that the following terms and conditions apply to this transaction (along with the Billing and Payment terms and conditions established by Copyright Clearance Center, Inc. ("CCC"), at the time that you opened your Rightslink account and that are available at any time at http://myaccount.copyright.com).

GENERAL TERMS

2. Elsevier hereby grants you permission to reproduce the aforementioned material subject to the terms and conditions indicated.

3. Acknowledgement: If any part of the material to be used (for example, figures) has appeared in our publication with credit or acknowledgement to another source, permission must also be sought from that source. If such permission is not obtained then that material may not be included in your publication/copies. Suitable acknowledgement to the source must be made, either as a footnote or in a reference list at the end of your publication, as follows:

"Reprinted from Publication title, Vol /edition number, Author(s), Title of article / title of chapter, Pages No., Copyright (Year), with permission from Elsevier [OR APPLICABLE SOCIETY COPYRIGHT OWNER]." Also Lancet special credit - "Reprinted from The Lancet, Vol. number, Author(s), Title of article, Pages No., Copyright (Year), with permission from Elsevier."

4. Reproduction of this material is confined to the purpose and/or media for which permission is hereby given.

5. Altering/Modifying Material: Not Permitted. However figures and illustrations may be altered/adapted minimally to serve your work. Any other abbreviations, additions, deletions and/or any other alterations shall be made only with prior written authorization of Elsevier Ltd. (Please contact Elsevier's permissions helpdesk here). No modifications can be made to any Lancet figures/tables and they must be reproduced in full.

6. If the permission fee for the requested use of our material is waived in this instance, please be advised that your future requests for Elsevier materials may attract a fee.

7. Reservation of Rights: Publisher reserves all rights not specifically granted in the combination of (i) the license details provided by you and accepted in the course of this licensing transaction, (ii) these terms and conditions and (iii) CCC's Billing and Payment terms and conditions.

8. License Contingent Upon Payment: While you may exercise the rights licensed immediately upon issuance of the license at the end of the licensing process for the transaction, provided that you have disclosed complete and accurate details of your proposed use, no license is finally effective unless and until full payment is received from you (either by publisher or by CCC) as provided in CCC's Billing and Payment terms and conditions. If full payment is not received on a timely basis, then any license preliminarily granted shall be deemed automatically revoked and shall be void as if never granted. Further, in the event that you breach any of these terms and conditions or any of CCC's Billing and Payment terms and conditions, the license is automatically revoked and shall be void as if never

granted. Use of materials as described in a revoked license, as well as any use of the materials beyond the scope of an unrevoked license, may constitute copyright infringement and publisher reserves the right to take any and all action to protect its copyright in the materials.

9. Warranties: Publisher makes no representations or warranties with respect to the licensed material.

10. Indemnity: You hereby indemnify and agree to hold harmless publisher and CCC, and their respective officers, directors, employees and agents, from and against any and all claims arising out of your use of the licensed material other than as specifically authorized pursuant to this license.

11. No Transfer of License: This license is personal to you and may not be sublicensed, assigned, or transferred by you to any other person without publisher's written permission.

12. No Amendment Except in Writing: This license may not be amended except in a writing signed by both parties (or, in the case of publisher, by CCC on publisher's behalf).

13. Objection to Contrary Terms: Publisher hereby objects to any terms contained in any purchase order, acknowledgment, check endorsement or other writing prepared by you, which terms are inconsistent with these terms and conditions or CCC's Billing and Payment terms and conditions. These terms and conditions, together with CCC's Billing and Payment terms and conditions (which are incorporated herein), comprise the entire agreement between you and publisher (and CCC) concerning this licensing transaction. In the event of any conflict between your obligations established by these terms and conditions and those established by CCC's Billing and Payment terms and conditions, these terms and conditions shall control.

14. Revocation: Elsevier or Copyright Clearance Center may deny the permissions described in this License at their sole discretion, for any reason or no reason, with a full refund payable to you. Notice of such denial will be made using the contact information provided by you. Failure to receive such notice will not alter or invalidate the denial. In no event will Elsevier or Copyright Clearance Center be responsible or liable for any costs, expenses or damage incurred by you as a result of a denial of your permission request, other than a refund of the amount(s) paid by you to Elsevier and/or Copyright Clearance Center for denied permissions.

LIMITED LICENSE

The following terms and conditions apply only to specific license types:

15. **Translation**: This permission is granted for non-exclusive world **English** rights only unless your license was granted for translation rights. If you licensed translation rights you may only translate this content into the languages you requested. A professional translator must perform all translations and reproduce the content word for word preserving the integrity of the article.

16. **Posting licensed content on any Website**: The following terms and conditions apply as follows: Licensing material from an Elsevier journal: All content posted to the web site must maintain the copyright information line on the bottom of each image; A hyper-text must be included to the Homepage of the journal from which you are licensing at http://www.sciencedirect.com/science/journal/xxxxx or the Elsevier homepage for books at http://www.elsevier.com; Central Storage: This license does not include permission for a

scanned version of the material to be stored in a central repository such as that provided by Heron/XanEdu.

Licensing material from an Elsevier book: A hyper-text link must be included to the Elsevier homepage at http://www.elsevier.com . All content posted to the web site must maintain the copyright information line on the bottom of each image.

Posting licensed content on Electronic reserve: In addition to the above the following clauses are applicable: The web site must be password-protected and made available only to bona fide students registered on a relevant course. This permission is granted for 1 year only. You may obtain a new license for future website posting.

17. **For journal authors:** the following clauses are applicable in addition to the above:

Preprints:

A preprint is an author's own write-up of research results and analysis, it has not been peer-reviewed, nor has it had any other value added to it by a publisher (such as formatting, copyright, technical enhancement etc.).

Authors can share their preprints anywhere at any time. Preprints should not be added to or enhanced in any way in order to appear more like, or to substitute for, the final versions of articles however authors can update their preprints on arXiv or RePEc with their Accepted Author Manuscript (see below).

If accepted for publication, we encourage authors to link from the preprint to their formal publication via its DOI. Millions of researchers have access to the formal publications on ScienceDirect, and so links will help users to find, access, cite and use the best available version. Please note that Cell Press, The Lancet and some society-owned have different preprint policies. Information on these policies is available on the journal homepage.

Accepted Author Manuscripts: An accepted author manuscript is the manuscript of an article that has been accepted for publication and which typically includes author-incorporated changes suggested during submission, peer review and editor-author communications.

Authors can share their accepted author manuscript:

- immediately
  - via their non-commercial person homepage or blog
  - by updating a preprint in arXiv or RePEc with the accepted manuscript
  - via their research institute or institutional repository for internal institutional uses or as part of an invitation-only research collaboration work-group
  - directly by providing copies to their students or to research collaborators for their personal use
  - for private scholarly sharing as part of an invitation-only work group on commercial sites with which Elsevier has an agreement
- After the embargo period
  - via non-commercial hosting platforms such as their institutional repository
  - via commercial sites with which Elsevier has an agreement

In all cases accepted manuscripts should:

- link to the formal publication via its DOI

- bear a CC-BY-NC-ND license - this is easy to do
- if aggregated with other manuscripts, for example in a repository or other site, be shared in alignment with our hosting policy not be added to or enhanced in any way to appear more like, or to substitute for, the published journal article.

Published journal article (JPA): A published journal article (PJA) is the definitive final record of published research that appears or will appear in the journal and embodies all value-adding publishing activities including peer review co-ordination, copy-editing, formatting, (if relevant) pagination and online enrichment.

Policies for sharing publishing journal articles differ for subscription and gold open access articles:

Subscription Articles: If you are an author, please share a link to your article rather than the full-text. Millions of researchers have access to the formal publications on ScienceDirect, and so links will help your users to find, access, cite, and use the best available version.

Theses and dissertations which contain embedded PJAs as part of the formal submission can be posted publicly by the awarding institution with DOI links back to the formal publications on ScienceDirect.

If you are affiliated with a library that subscribes to ScienceDirect you have additional private sharing rights for others' research accessed under that agreement. This includes use for classroom teaching and internal training at the institution (including use in course packs and courseware programs), and inclusion of the article for grant funding purposes.

Gold Open Access Articles: May be shared according to the author-selected end-user license and should contain a CrossMark logo, the end user license, and a DOI link to the formal publication on ScienceDirect.

Please refer to Elsevier's posting policy for further information.

18. **For book authors** the following clauses are applicable in addition to the above: Authors are permitted to place a brief summary of their work online only. You are not allowed to download and post the published electronic version of your chapter, nor may you scan the printed edition to create an electronic version. **Posting to a repository:** Authors are permitted to post a summary of their chapter only in their institution's repository.

19. **Thesis/Dissertation**: If your license is for use in a thesis/dissertation your thesis may be submitted to your institution in either print or electronic form. Should your thesis be published commercially, please reapply for permission. These requirements include permission for the Library and Archives of Canada to supply single copies, on demand, of the complete thesis and include permission for Proquest/UMI to supply single copies, on demand, of the complete thesis. Should your thesis be published commercially, please reapply for permission. Theses and dissertations which contain embedded PJAs as part of the formal submission can be posted publicly by the awarding institution with DOI links back to the formal publications on ScienceDirect.

Elsevier Open Access Terms and Conditions

You can publish open access with Elsevier in hundreds of open access journals or in nearly 2000 established subscription journals that support open access publishing. Permitted third

party re-use of these open access articles is defined by the author's choice of Creative Commons user license. See our open access license policy for more information.

Terms & Conditions applicable to all Open Access articles published with Elsevier:

Any reuse of the article must not represent the author as endorsing the adaptation of the article nor should the article be modified in such a way as to damage the author's honour or reputation. If any changes have been made, such changes must be clearly indicated.

The author(s) must be appropriately credited and we ask that you include the end user license and a DOI link to the formal publication on ScienceDirect.

If any part of the material to be used (for example, figures) has appeared in our publication with credit or acknowledgement to another source it is the responsibility of the user to ensure their reuse complies with the terms and conditions determined by the rights holder.

Additional Terms & Conditions applicable to each Creative Commons user license:

CC BY: The CC-BY license allows users to copy, to create extracts, abstracts and new works from the Article, to alter and revise the Article and to make commercial use of the Article (including reuse and/or resale of the Article by commercial entities), provided the user gives appropriate credit (with a link to the formal publication through the relevant DOI), provides a link to the license, indicates if changes were made and the licensor is not represented as endorsing the use made of the work. The full details of the license are available at http://creativecommons.org/licenses/by/4.0.

CC BY NC SA: The CC BY-NC-SA license allows users to copy, to create extracts, abstracts and new works from the Article, to alter and revise the Article, provided this is not done for commercial purposes, and that the user gives appropriate credit (with a link to the formal publication through the relevant DOI), provides a link to the license, indicates if changes were made and the licensor is not represented as endorsing the use made of the work. Further, any new works must be made available on the same conditions. The full details of the license are available at http://creativecommons.org/licenses/by-nc-sa/4.0.

CC BY NC ND: The CC BY-NC-ND license allows users to copy and distribute the Article, provided this is not done for commercial purposes and further does not permit distribution of the Article if it is changed or edited in any way, and provided the user gives appropriate credit (with a link to the formal publication through the relevant DOI), provides a link to the license, and that the licensor is not represented as endorsing the use made of the work. The full details of the license are available at http://creativecommons.org/licenses/by-nc-nd/4.0. Any commercial reuse of Open Access articles published with a CC BY NC SA or CC BY NC ND license requires permission from Elsevier and will be subject to a fee.

Commercial reuse includes:

- Associating advertising with the full text of the Article
- Charging fees for document delivery or access
- Article aggregation
- Systematic distribution via e-mail lists or share buttons

Posting or linking by commercial companies for use by customers of those companies.

20. **Other Conditions**:

v1.10

Questions? customercare@copyright.com or +1-855-239-3415 (toll free in the US) or +1-978-646-2777.

Annexure IX

JOHN WILEY AND SONS LICENSE
TERMS AND CONDITIONS

Mar 16, 2021

This Agreement between Mr. Chiranjib Gogoi ("You") and John Wiley and Sons ("John Wiley and Sons") consists of your license details and the terms and conditions provided by John Wiley and Sons and Copyright Clearance Center.

License Number	5030830440459
License date	Mar 16, 2021
Licensed Content Publisher	John Wiley and Sons
Licensed Content Publication	Advanced Materials
Licensed Content Title	Stable Metal–Organic Frameworks: Design, Synthesis, and Applications
Licensed Content Author	Hong-Cai Zhou, Jialuo Li, Yu Fang, et al
Licensed Content Date	Feb 12, 2018
Licensed Content Volume	30
Licensed Content Issue	37

Licensed Content Pages	35
Type of use	Dissertation/Thesis
Requestor type	University/Academic
Format	Print and electronic
Portion	Figure/table
Number of figures/tables	1
Will you be translating?	No
Title	Synthesis and Characterization of Some Zn(II) and Zr(IV) Metal-Organic Frameworks and Their Applications in Fluorescence Sensing and Catalysis
Institution name	IIT Guwahati
Expected presentation date	Jun 2021
Order reference number	84
Portions	Figure 1.16
Requestor Location	Mr. Chiranjib Gogoi IIT Guwahati Guwahati, 781039 India Attn: IIT Guwahati

Publisher Tax ID EU826007151

Total 0.00 USD

Terms and Conditions

TERMS AND CONDITIONS

This copyrighted material is owned by or exclusively licensed to John Wiley & Sons, Inc. or one of its group companies (each a"Wiley Company") or handled on behalf of a society with which a Wiley Company has exclusive publishing rights in relation to a particular work (collectively "WILEY"). By clicking "accept" in connection with completing this licensing transaction, you agree that the following terms and conditions apply to this transaction (along with the billing and payment terms and conditions established by the Copyright Clearance Center Inc., ("CCC's Billing and Payment terms and conditions"), at the time that you opened your RightsLink account (these are available at any time at http://myaccount.copyright.com).

Terms and Conditions

- The materials you have requested permission to reproduce or reuse (the "Wiley Materials") are protected by copyright.
- You are hereby granted a personal, non-exclusive, non-sub licensable (on a stand-alone basis), non-transferable, worldwide, limited license to reproduce the Wiley Materials for the purpose specified in the licensing process. This license, **and any CONTENT (PDF or image file) purchased as part of your order,** is for a one-time use only and limited to any maximum distribution number specified in the license. The first instance of republication or reuse granted by this license must be completed within two years of the date of the grant of this license (although copies prepared before the end date may be distributed thereafter). The Wiley Materials shall not be used in any other manner or for any other purpose, beyond what is granted in the license. Permission is granted subject to an appropriate acknowledgement given to the author, title of the material/book/journal and the publisher. You shall also duplicate the copyright notice that appears in the Wiley publication in your use of the Wiley Material. Permission is also granted on the understanding that nowhere in the text is a previously published source acknowledged for all or part of this Wiley Material. Any third party content is expressly excluded from this permission.
- With respect to the Wiley Materials, all rights are reserved. Except as expressly granted by the terms of the license, no part of the Wiley Materials may be copied, modified, adapted (except for minor reformatting required by the new Publication), translated, reproduced, transferred or distributed, in any form or by any means, and no derivative works may be made based on the Wiley Materials without the prior permission of the respective copyright owner.**For STM Signatory Publishers clearing permission under the terms of the STM Permissions Guidelines only, the terms of the license are extended to include subsequent editions and for editions in other languages, provided such editions are for the work as a whole in situ and does not involve the separate exploitation of the permitted figures or extracts,**

You may not alter, remove or suppress in any manner any copyright, trademark or other notices displayed by the Wiley Materials. You may not license, rent, sell, loan, lease, pledge, offer as security, transfer or assign the Wiley Materials on a stand-alone basis, or any of the rights granted to you hereunder to any other person.

- The Wiley Materials and all of the intellectual property rights therein shall at all times remain the exclusive property of John Wiley & Sons Inc, the Wiley Companies, or their respective licensors, and your interest therein is only that of having possession of and the right to reproduce the Wiley Materials pursuant to Section 2 herein during the continuance of this Agreement. You agree that you own no right, title or interest in or to the Wiley Materials or any of the intellectual property rights therein. You shall have no rights hereunder other than the license as provided for above in Section 2. No right, license or interest to any trademark, trade name, service mark or other branding ("Marks") of WILEY or its licensors is granted hereunder, and you agree that you shall not assert any such right, license or interest with respect thereto

- NEITHER WILEY NOR ITS LICENSORS MAKES ANY WARRANTY OR REPRESENTATION OF ANY KIND TO YOU OR ANY THIRD PARTY, EXPRESS, IMPLIED OR STATUTORY, WITH RESPECT TO THE MATERIALS OR THE ACCURACY OF ANY INFORMATION CONTAINED IN THE MATERIALS, INCLUDING, WITHOUT LIMITATION, ANY IMPLIED WARRANTY OF MERCHANTABILITY, ACCURACY, SATISFACTORY QUALITY, FITNESS FOR A PARTICULAR PURPOSE, USABILITY, INTEGRATION OR NON-INFRINGEMENT AND ALL SUCH WARRANTIES ARE HEREBY EXCLUDED BY WILEY AND ITS LICENSORS AND WAIVED BY YOU.

- WILEY shall have the right to terminate this Agreement immediately upon breach of this Agreement by you.

- You shall indemnify, defend and hold harmless WILEY, its Licensors and their respective directors, officers, agents and employees, from and against any actual or threatened claims, demands, causes of action or proceedings arising from any breach of this Agreement by you.

- IN NO EVENT SHALL WILEY OR ITS LICENSORS BE LIABLE TO YOU OR ANY OTHER PARTY OR ANY OTHER PERSON OR ENTITY FOR ANY SPECIAL, CONSEQUENTIAL, INCIDENTAL, INDIRECT, EXEMPLARY OR PUNITIVE DAMAGES, HOWEVER CAUSED, ARISING OUT OF OR IN CONNECTION WITH THE DOWNLOADING, PROVISIONING, VIEWING OR USE OF THE MATERIALS REGARDLESS OF THE FORM OF ACTION, WHETHER FOR BREACH OF CONTRACT, BREACH OF WARRANTY, TORT, NEGLIGENCE, INFRINGEMENT OR OTHERWISE (INCLUDING, WITHOUT LIMITATION, DAMAGES BASED ON LOSS OF PROFITS, DATA, FILES, USE, BUSINESS OPPORTUNITY OR CLAIMS OF THIRD PARTIES), AND WHETHER OR NOT THE PARTY HAS BEEN ADVISED OF THE POSSIBILITY OF SUCH DAMAGES. THIS LIMITATION SHALL APPLY NOTWITHSTANDING ANY FAILURE OF ESSENTIAL PURPOSE OF ANY LIMITED REMEDY PROVIDED HEREIN.

- Should any provision of this Agreement be held by a court of competent jurisdiction to be illegal, invalid, or unenforceable, that provision shall be deemed amended to achieve as nearly as possible the same economic effect as the original provision, and the legality, validity and enforceability of the remaining provisions of this Agreement

shall not be affected or impaired thereby.

- The failure of either party to enforce any term or condition of this Agreement shall not constitute a waiver of either party's right to enforce each and every term and condition of this Agreement. No breach under this agreement shall be deemed waived or excused by either party unless such waiver or consent is in writing signed by the party granting such waiver or consent. The waiver by or consent of a party to a breach of any provision of this Agreement shall not operate or be construed as a waiver of or consent to any other or subsequent breach by such other party.

- This Agreement may not be assigned (including by operation of law or otherwise) by you without WILEY's prior written consent.

- Any fee required for this permission shall be non-refundable after thirty (30) days from receipt by the CCC.

- These terms and conditions together with CCC's Billing and Payment terms and conditions (which are incorporated herein) form the entire agreement between you and WILEY concerning this licensing transaction and (in the absence of fraud) supersedes all prior agreements and representations of the parties, oral or written. This Agreement may not be amended except in writing signed by both parties. This Agreement shall be binding upon and inure to the benefit of the parties' successors, legal representatives, and authorized assigns.

- In the event of any conflict between your obligations established by these terms and conditions and those established by CCC's Billing and Payment terms and conditions, these terms and conditions shall prevail.

- WILEY expressly reserves all rights not specifically granted in the combination of (i) the license details provided by you and accepted in the course of this licensing transaction, (ii) these terms and conditions and (iii) CCC's Billing and Payment terms and conditions.

- This Agreement will be void if the Type of Use, Format, Circulation, or Requestor Type was misrepresented during the licensing process.

- This Agreement shall be governed by and construed in accordance with the laws of the State of New York, USA, without regards to such state's conflict of law rules. Any legal action, suit or proceeding arising out of or relating to these Terms and Conditions or the breach thereof shall be instituted in a court of competent jurisdiction in New York County in the State of New York in the United States of America and each party hereby consents and submits to the personal jurisdiction of such court, waives any objection to venue in such court and consents to service of process by registered or certified mail, return receipt requested, at the last known address of such party.

WILEY OPEN ACCESS TERMS AND CONDITIONS

Wiley Publishes Open Access Articles in fully Open Access Journals and in Subscription journals offering Online Open. Although most of the fully Open Access journals publish open access articles under the terms of the Creative Commons Attribution (CC BY) License only, the subscription journals and a few of the Open Access Journals offer a choice of Creative Commons Licenses. The license type is clearly identified on the article.

The Creative Commons Attribution License

The Creative Commons Attribution License (CC-BY) allows users to copy, distribute and transmit an article, adapt the article and make commercial use of the article. The CC-BY license permits commercial and non-

Creative Commons Attribution Non-Commercial License

The Creative Commons Attribution Non-Commercial (CC-BY-NC)License permits use, distribution and reproduction in any medium, provided the original work is properly cited and is not used for commercial purposes.(see below)

Creative Commons Attribution-Non-Commercial-NoDerivs License

The Creative Commons Attribution Non-Commercial-NoDerivs License (CC-BY-NC-ND) permits use, distribution and reproduction in any medium, provided the original work is properly cited, is not used for commercial purposes and no modifications or adaptations are made. (see below)

Use by commercial "for-profit" organizations

Use of Wiley Open Access articles for commercial, promotional, or marketing purposes requires further explicit permission from Wiley and will be subject to a fee.

Further details can be found on Wiley Online Library
http://olabout.wiley.com/WileyCDA/Section/id-410895.html

Other Terms and Conditions:

v1.10 Last updated September 2015

Questions? customercare@copyright.com or +1-855-239-3415 (toll free in the US) or +1-978-646-2777.

Annexure X

Copyright Clearance Center | Marketplace™

Order Number: 1104646
Order Date: 16 Mar 2021

Payment Information

Chiranjib Gogoi
chiranjib2016@iitg.ac.in
Payment method: Invoice

Billing Address:
Mr. Chiranjib Gogoi
IIT Guwahati
Guwahati, 781039
India

+91 3612584334
chiranjib2016@iitg.ac.in

Customer Location:
Mr. Chiranjib Gogoi
IIT Guwahati
Guwahati, 781039
India

Order Details

1. Chemical Society reviews

Billing Status: Open

Order license ID	1104646-1
Order detail status	Completed
ISSN	1460-4744
Type of use	Republish in a thesis/dissertation
Publisher	ROYAL SOCIETY OF CHEMISTRY
Portion	Chart/graph/table/figure

0.00 USD
Republication Permission

LICENSED CONTENT

Publication Title	Chemical Society reviews	**Country**	United Kingdom of Great Britain and Northern Ireland
Author/Editor	Royal Society of Chemistry (Great Britain)	**Rightsholder**	Royal Society of Chemistry
Date	01/01/1972	**Publication Type**	e-Journal
Language	English	**URL**	http://www.rsc.org/csr

REQUEST DETAILS

Portion Type	Chart/graph/table/figure	**Distribution**	Worldwide
		Translation	Original language of publication
Number of charts / graphs / tables / figures requested	1	**Copies for the disabled?**	No

Format (select all that apply)	Print,Electronic	Minor editing privileges?	No
Who will republish the content?	Not-for-profit entity	Incidental promotional use?	No
Duration of Use	Current edition and up to 5 years	Currency	USD
Lifetime Unit Quantity	Up to 499		
Rights Requested	Main product		

NEW WORK DETAILS

Title	Synthesis and Characterization of Some Zn(II) and Zr(IV) Metal-Organic Frameworks and Their Applications in Fluorescence Sensing and Catalysis	Institution name	IIT Guwahati
		Expected presentation date	2021-06-15
Instructor name	Chiranjib Gogoi		

ADDITIONAL DETAILS

Order reference number	37	The requesting person / organization to appear on the license	Chiranjib Gogoi

REUSE CONTENT DETAILS

Title, description or numeric reference of the portion(s)	Fig. 3	Title of the article/chapter the portion is from	Metal–organic frameworks: functional luminescent and photonic materials for sensing applications
Editor of portion(s)	N/A	Author of portion(s)	Royal Society of Chemistry (Great Britain)
Volume of serial or monograph	46	Publication date of portion	2017-05-02
Page or page range of portion	3250		

Total Items: 1

Subtotal: 0.00 USD

Order Total: 0.00 USD

Annexure XI

SPRINGER NATURE LICENSE
TERMS AND CONDITIONS

Mar 16, 2021

This Agreement between Mr. Chiranjib Gogoi ("You") and Springer Nature ("Springer Nature") consists of your license details and the terms and conditions provided by Springer Nature and Copyright Clearance Center.

License Number	5030831401138
License date	Mar 16, 2021
Licensed Content Publisher	Springer Nature
Licensed Content Publication	Microchimica Acta
Licensed Content Title	Detection of cyanide via extended π-conjugation-induced fluorescence enhancement of a metal organic framework composed of terbium(III), bipyridyl and adenosine diphosphate
Licensed Content Author	Lude Wang et al
Licensed Content Date	Sep 15, 2017
Type of Use	Thesis/Dissertation
Requestor type	academic/university or research institute
Format	print and electronic
Portion	figures/tables/illustrations
Number of	1

figures/tables/illustrations	
Will you be translating?	no
Circulation/distribution	1 - 29
Author of this Springer Nature content	no
Title	Synthesis and Characterization of Some Zn(II) and Zr(IV) Metal-Organic Frameworks and Their Applications in Fluorescence Sensing and Catalysis
Institution name	IIT Guwahati
Expected presentation date	Jun 2021
Order reference number	197
Portions	Figure 1.19
Requestor Location	Mr. Chiranjib Gogoi IIT Guwahati Guwahati, 781039 India Attn: IIT Guwahati
Total	0.00 USD

Terms and Conditions

Springer Nature Customer Service Centre GmbH
Terms and Conditions

This agreement sets out the terms and conditions of the licence (the **Licence**) between you and **Springer Nature Customer Service Centre GmbH** (the **Licensor**). By clicking 'accept' and completing the transaction for the material (**Licensed Material**), you also confirm your acceptance of these terms and conditions.

1. Grant of License

1. 1. The Licensor grants you a personal, non-exclusive, non-transferable, world-wide licence to reproduce the Licensed Material for the purpose specified in your order only. Licences are granted for the specific use requested in the order and for no other use, subject to the conditions below.

1. 2. The Licensor warrants that it has, to the best of its knowledge, the rights to license reuse of the Licensed Material. However, you should ensure that the material you are requesting is original to the Licensor and does not carry the copyright of another entity (as credited in the published version).

1. 3. If the credit line on any part of the material you have requested indicates that it was reprinted or adapted with permission from another source, then you should also seek permission from that source to reuse the material.

2. Scope of Licence

2. 1. You may only use the Licensed Content in the manner and to the extent permitted by these Ts&Cs and any applicable laws.

2. 2. A separate licence may be required for any additional use of the Licensed Material, e.g. where a licence has been purchased for print only use, separate permission must be obtained for electronic re-use. Similarly, a licence is only valid in the language selected and does not apply for editions in other languages unless additional translation rights have been granted separately in the licence. Any content owned by third parties are expressly excluded from the licence.

2. 3. Similarly, rights for additional components such as custom editions and derivatives require additional permission and may be subject to an additional fee. Please apply to Journalpermissions@springernature.com/bookpermissions@springernature.com for these rights.

2. 4. Where permission has been granted **free of charge** for material in print, permission may also be granted for any electronic version of that work, provided that the material is incidental to your work as a whole and that the electronic version is essentially equivalent to, or substitutes for, the print version.

2. 5. An alternative scope of licence may apply to signatories of the STM Permissions Guidelines, as amended from time to time.

3. Duration of Licence

3. 1. A licence for is valid from the date of purchase ('Licence Date') at the end of the relevant period in the below table:

Scope of Licence	Duration of Licence
Post on a website	12 months
Presentations	12 months
Books and journals	Lifetime of the edition in the language purchased

4. Acknowledgement

4. 1. The Licensor's permission must be acknowledged next to the Licenced Material in print. In electronic form, this acknowledgement must be visible at the same time as the figures/tables/illustrations or abstract, and must be hyperlinked to the journal/book's homepage. Our required acknowledgement format is in the Appendix below.

5. Restrictions on use

5. 1. Use of the Licensed Material may be permitted for incidental promotional use and minor editing privileges e.g. minor adaptations of single figures, changes of format, colour and/or style where the adaptation is credited as set out in Appendix 1 below. Any other changes including but not limited to, cropping, adapting, omitting material that affect the meaning, intention or moral rights of the author are strictly prohibited.

5. 2. You must not use any Licensed Material as part of any design or trademark.

5. 3. Licensed Material may be used in Open Access Publications (OAP) before publication by Springer Nature, but any Licensed Material must be removed from OAP sites prior to final publication.

6. Ownership of Rights

6. 1. Licensed Material remains the property of either Licensor or the relevant third party and any rights not explicitly granted herein are expressly reserved.

7. Warranty

IN NO EVENT SHALL LICENSOR BE LIABLE TO YOU OR ANY OTHER PARTY OR ANY OTHER PERSON OR FOR ANY SPECIAL, CONSEQUENTIAL, INCIDENTAL OR INDIRECT DAMAGES, HOWEVER CAUSED, ARISING OUT OF OR IN CONNECTION WITH THE DOWNLOADING, VIEWING OR USE OF THE MATERIALS REGARDLESS OF THE FORM OF ACTION, WHETHER FOR BREACH OF CONTRACT, BREACH OF WARRANTY, TORT, NEGLIGENCE, INFRINGEMENT OR OTHERWISE (INCLUDING, WITHOUT LIMITATION, DAMAGES BASED ON LOSS OF PROFITS, DATA, FILES, USE, BUSINESS OPPORTUNITY OR CLAIMS OF THIRD PARTIES), AND
WHETHER OR NOT THE PARTY HAS BEEN ADVISED OF THE POSSIBILITY OF SUCH DAMAGES. THIS LIMITATION SHALL APPLY NOTWITHSTANDING ANY FAILURE OF ESSENTIAL PURPOSE OF ANY LIMITED REMEDY PROVIDED HEREIN.

8. Limitations

8. 1. ***BOOKS ONLY:*** Where **'reuse in a dissertation/thesis'** has been selected the following terms apply: Print rights of the final author's accepted manuscript (for clarity,

NOT the published version) for up to 100 copies, electronic rights for use only on a personal website or institutional repository as defined by the Sherpa guideline (www.sherpa.ac.uk/romeo/).

8. 2. For content reuse requests that qualify for permission under the STM Permissions Guidelines, which may be updated from time to time, the STM Permissions Guidelines supersede the terms and conditions contained in this licence.

9. Termination and Cancellation

9. 1. Licences will expire after the period shown in Clause 3 (above).

9. 2. Licensee reserves the right to terminate the Licence in the event that payment is not received in full or if there has been a breach of this agreement by you.

Appendix 1 — Acknowledgements:

For Journal Content:
Reprinted by permission from [**the Licensor**]: [**Journal Publisher** (e.g. Nature/Springer/Palgrave)] [**JOURNAL NAME**] [**REFERENCE CITATION** (Article name, Author(s) Name), [**COPYRIGHT**] (year of publication)

For **Advance Online Publication papers:**
Reprinted by permission from [**the Licensor**]: [**Journal Publisher** (e.g. Nature/Springer/Palgrave)] [**JOURNAL NAME**] [**REFERENCE CITATION** (Article name, Author(s) Name), [**COPYRIGHT**] (year of publication), advance online publication, day month year (doi: 10.1038/sj.[JOURNAL ACRONYM].)

For Adaptations/Translations:
Adapted/Translated by permission from [**the Licensor**]: [**Journal Publisher** (e.g. Nature/Springer/Palgrave)] [**JOURNAL NAME**] [**REFERENCE CITATION** (Article name, Author(s) Name), [**COPYRIGHT**] (year of publication)

Note: For any republication from the British Journal of Cancer, the following credit line style applies:

Reprinted/adapted/translated by permission from [**the Licensor**]: on behalf of Cancer Research UK: : [**Journal Publisher** (e.g. Nature/Springer/Palgrave)] [**JOURNAL NAME**] [**REFERENCE CITATION** (Article name, Author(s) Name), [**COPYRIGHT**] (year of publication)

For **Advance Online Publication** papers:
Reprinted by permission from The [**the Licensor**]: on behalf of Cancer Research UK: [**Journal Publisher** (e.g. Nature/Springer/Palgrave)] [**JOURNAL NAME**] [**REFERENCE CITATION** (Article name, Author(s) Name), [**COPYRIGHT**] (year of publication), advance online publication, day month year (doi: 10.1038/sj.[JOURNAL ACRONYM])

For Book content:
Reprinted/adapted by permission from [**the Licensor**]: [**Book Publisher** (e.g.

Palgrave Macmillan, Springer etc) [**Book Title**] by [**Book author**(s)]
[**COPYRIGHT**] (year of publication)

Other Conditions:

Version 1.3

Questions? customercare@copyright.com or +1-855-239-3415 (toll free in the US) or +1-978-646-2777.

Annexure XII

ELSEVIER LICENSE
TERMS AND CONDITIONS

Mar 16, 2021

This Agreement between Mr. Chiranjib Gogoi ("You") and Elsevier ("Elsevier") consists of your license details and the terms and conditions provided by Elsevier and Copyright Clearance Center.

License Number	5030840162055
License date	Mar 16, 2021
Licensed Content Publisher	Elsevier
Licensed Content Publication	Applied Surface Science
Licensed Content Title	Postsynthetic modification of metal–organic framework for hydrogen sulfide detection
Licensed Content Author	Xin Zhang,Jianmin Zhang,Quan Hu,Yuanjing Cui,Yu Yang,Guodong Qian
Licensed Content Date	Nov 15, 2015
Licensed Content Volume	355
Licensed Content Issue	n/a
Licensed Content Pages	6
Start Page	814
End Page	819

Annexure XII

Type of Use	reuse in a thesis/dissertation
Portion	figures/tables/illustrations
Number of figures/tables/illustrations	1
Format	both print and electronic
Are you the author of this Elsevier article?	No
Will you be translating?	No
Title	Synthesis and Characterization of Some Zn(II) and Zr(IV) Metal-Organic Frameworks and Their Applications in Fluorescence Sensing and Catalysis
Institution name	IIT Guwahati
Expected presentation date	Jun 2021
Order reference number	122
Portions	Figure 1.20
Requestor Location	Mr. Chiranjib Gogoi IIT Guwahati Guwahati, 781039 India Attn: IIT Guwahati
Publisher Tax ID	GB 494 6272 12
Total	0.00 USD

Terms and Conditions

INTRODUCTION

1. The publisher for this copyrighted material is Elsevier. By clicking "accept" in connection with completing this licensing transaction, you agree that the following terms and conditions apply to this transaction (along with the Billing and Payment terms and conditions established by Copyright Clearance Center, Inc. ("CCC"), at the time that you opened your Rightslink account and that are available at any time at http://myaccount.copyright.com).

GENERAL TERMS

2. Elsevier hereby grants you permission to reproduce the aforementioned material subject to the terms and conditions indicated.

3. Acknowledgement: If any part of the material to be used (for example, figures) has appeared in our publication with credit or acknowledgement to another source, permission must also be sought from that source. If such permission is not obtained then that material may not be included in your publication/copies. Suitable acknowledgement to the source must be made, either as a footnote or in a reference list at the end of your publication, as follows:

"Reprinted from Publication title, Vol /edition number, Author(s), Title of article / title of chapter, Pages No., Copyright (Year), with permission from Elsevier [OR APPLICABLE SOCIETY COPYRIGHT OWNER]." Also Lancet special credit - "Reprinted from The Lancet, Vol. number, Author(s), Title of article, Pages No., Copyright (Year), with permission from Elsevier."

4. Reproduction of this material is confined to the purpose and/or media for which permission is hereby given.

5. Altering/Modifying Material: Not Permitted. However figures and illustrations may be altered/adapted minimally to serve your work. Any other abbreviations, additions, deletions and/or any other alterations shall be made only with prior written authorization of Elsevier Ltd. (Please contact Elsevier's permissions helpdesk here). No modifications can be made to any Lancet figures/tables and they must be reproduced in full.

6. If the permission fee for the requested use of our material is waived in this instance, please be advised that your future requests for Elsevier materials may attract a fee.

7. Reservation of Rights: Publisher reserves all rights not specifically granted in the combination of (i) the license details provided by you and accepted in the course of this licensing transaction, (ii) these terms and conditions and (iii) CCC's Billing and Payment terms and conditions.

8. License Contingent Upon Payment: While you may exercise the rights licensed immediately upon issuance of the license at the end of the licensing process for the transaction, provided that you have disclosed complete and accurate details of your proposed use, no license is finally effective unless and until full payment is received from you (either by publisher or by CCC) as provided in CCC's Billing and Payment terms and conditions. If full payment is not received on a timely basis, then any license preliminarily granted shall be deemed automatically revoked and shall be void as if never granted. Further, in the event that you breach any of these terms and conditions or any of CCC's Billing and Payment terms and conditions, the license is automatically revoked and shall be void as if never

granted. Use of materials as described in a revoked license, as well as any use of the materials beyond the scope of an unrevoked license, may constitute copyright infringement and publisher reserves the right to take any and all action to protect its copyright in the materials.

9. Warranties: Publisher makes no representations or warranties with respect to the licensed material.

10. Indemnity: You hereby indemnify and agree to hold harmless publisher and CCC, and their respective officers, directors, employees and agents, from and against any and all claims arising out of your use of the licensed material other than as specifically authorized pursuant to this license.

11. No Transfer of License: This license is personal to you and may not be sublicensed, assigned, or transferred by you to any other person without publisher's written permission.

12. No Amendment Except in Writing: This license may not be amended except in a writing signed by both parties (or, in the case of publisher, by CCC on publisher's behalf).

13. Objection to Contrary Terms: Publisher hereby objects to any terms contained in any purchase order, acknowledgment, check endorsement or other writing prepared by you, which terms are inconsistent with these terms and conditions or CCC's Billing and Payment terms and conditions. These terms and conditions, together with CCC's Billing and Payment terms and conditions (which are incorporated herein), comprise the entire agreement between you and publisher (and CCC) concerning this licensing transaction. In the event of any conflict between your obligations established by these terms and conditions and those established by CCC's Billing and Payment terms and conditions, these terms and conditions shall control.

14. Revocation: Elsevier or Copyright Clearance Center may deny the permissions described in this License at their sole discretion, for any reason or no reason, with a full refund payable to you. Notice of such denial will be made using the contact information provided by you. Failure to receive such notice will not alter or invalidate the denial. In no event will Elsevier or Copyright Clearance Center be responsible or liable for any costs, expenses or damage incurred by you as a result of a denial of your permission request, other than a refund of the amount(s) paid by you to Elsevier and/or Copyright Clearance Center for denied permissions.

LIMITED LICENSE

The following terms and conditions apply only to specific license types:

15. **Translation**: This permission is granted for non-exclusive world **English** rights only unless your license was granted for translation rights. If you licensed translation rights you may only translate this content into the languages you requested. A professional translator must perform all translations and reproduce the content word for word preserving the integrity of the article.

16. **Posting licensed content on any Website**: The following terms and conditions apply as follows: Licensing material from an Elsevier journal: All content posted to the web site must maintain the copyright information line on the bottom of each image; A hyper-text must be included to the Homepage of the journal from which you are licensing at http://www.sciencedirect.com/science/journal/xxxxx or the Elsevier homepage for books at http://www.elsevier.com; Central Storage: This license does not include permission for a

scanned version of the material to be stored in a central repository such as that provided by Heron/XanEdu.

Licensing material from an Elsevier book: A hyper-text link must be included to the Elsevier homepage at http://www.elsevier.com . All content posted to the web site must maintain the copyright information line on the bottom of each image.

Posting licensed content on Electronic reserve: In addition to the above the following clauses are applicable: The web site must be password-protected and made available only to bona fide students registered on a relevant course. This permission is granted for 1 year only. You may obtain a new license for future website posting.

17. **For journal authors:** the following clauses are applicable in addition to the above:

Preprints:

A preprint is an author's own write-up of research results and analysis, it has not been peer-reviewed, nor has it had any other value added to it by a publisher (such as formatting, copyright, technical enhancement etc.).

Authors can share their preprints anywhere at any time. Preprints should not be added to or enhanced in any way in order to appear more like, or to substitute for, the final versions of articles however authors can update their preprints on arXiv or RePEc with their Accepted Author Manuscript (see below).

If accepted for publication, we encourage authors to link from the preprint to their formal publication via its DOI. Millions of researchers have access to the formal publications on ScienceDirect, and so links will help users to find, access, cite and use the best available version. Please note that Cell Press, The Lancet and some society-owned have different preprint policies. Information on these policies is available on the journal homepage.

Accepted Author Manuscripts: An accepted author manuscript is the manuscript of an article that has been accepted for publication and which typically includes author-incorporated changes suggested during submission, peer review and editor-author communications.

Authors can share their accepted author manuscript:

- immediately
  - via their non-commercial person homepage or blog
  - by updating a preprint in arXiv or RePEc with the accepted manuscript
  - via their research institute or institutional repository for internal institutional uses or as part of an invitation-only research collaboration work-group
  - directly by providing copies to their students or to research collaborators for their personal use
  - for private scholarly sharing as part of an invitation-only work group on commercial sites with which Elsevier has an agreement
- After the embargo period
  - via non-commercial hosting platforms such as their institutional repository
  - via commercial sites with which Elsevier has an agreement

In all cases accepted manuscripts should:

- link to the formal publication via its DOI

- bear a CC-BY-NC-ND license - this is easy to do
- if aggregated with other manuscripts, for example in a repository or other site, be shared in alignment with our hosting policy not be added to or enhanced in any way to appear more like, or to substitute for, the published journal article.

Published journal article (JPA): A published journal article (PJA) is the definitive final record of published research that appears or will appear in the journal and embodies all value-adding publishing activities including peer review co-ordination, copy-editing, formatting, (if relevant) pagination and online enrichment.

Policies for sharing publishing journal articles differ for subscription and gold open access articles:

Subscription Articles: If you are an author, please share a link to your article rather than the full-text. Millions of researchers have access to the formal publications on ScienceDirect, and so links will help your users to find, access, cite, and use the best available version.

Theses and dissertations which contain embedded PJAs as part of the formal submission can be posted publicly by the awarding institution with DOI links back to the formal publications on ScienceDirect.

If you are affiliated with a library that subscribes to ScienceDirect you have additional private sharing rights for others' research accessed under that agreement. This includes use for classroom teaching and internal training at the institution (including use in course packs and courseware programs), and inclusion of the article for grant funding purposes.

Gold Open Access Articles: May be shared according to the author-selected end-user license and should contain a CrossMark logo, the end user license, and a DOI link to the formal publication on ScienceDirect.

Please refer to Elsevier's posting policy for further information.

18. **For book authors** the following clauses are applicable in addition to the above: Authors are permitted to place a brief summary of their work online only. You are not allowed to download and post the published electronic version of your chapter, nor may you scan the printed edition to create an electronic version. **Posting to a repository:** Authors are permitted to post a summary of their chapter only in their institution's repository.

19. **Thesis/Dissertation**: If your license is for use in a thesis/dissertation your thesis may be submitted to your institution in either print or electronic form. Should your thesis be published commercially, please reapply for permission. These requirements include permission for the Library and Archives of Canada to supply single copies, on demand, of the complete thesis and include permission for Proquest/UMI to supply single copies, on demand, of the complete thesis. Should your thesis be published commercially, please reapply for permission. Theses and dissertations which contain embedded PJAs as part of the formal submission can be posted publicly by the awarding institution with DOI links back to the formal publications on ScienceDirect.

Elsevier Open Access Terms and Conditions

You can publish open access with Elsevier in hundreds of open access journals or in nearly 2000 established subscription journals that support open access publishing. Permitted third

party re-use of these open access articles is defined by the author's choice of Creative Commons user license. See our open access license policy for more information.

Terms & Conditions applicable to all Open Access articles published with Elsevier:

Any reuse of the article must not represent the author as endorsing the adaptation of the article nor should the article be modified in such a way as to damage the author's honour or reputation. If any changes have been made, such changes must be clearly indicated.

The author(s) must be appropriately credited and we ask that you include the end user license and a DOI link to the formal publication on ScienceDirect.

If any part of the material to be used (for example, figures) has appeared in our publication with credit or acknowledgement to another source it is the responsibility of the user to ensure their reuse complies with the terms and conditions determined by the rights holder.

Additional Terms & Conditions applicable to each Creative Commons user license:

CC BY: The CC-BY license allows users to copy, to create extracts, abstracts and new works from the Article, to alter and revise the Article and to make commercial use of the Article (including reuse and/or resale of the Article by commercial entities), provided the user gives appropriate credit (with a link to the formal publication through the relevant DOI), provides a link to the license, indicates if changes were made and the licensor is not represented as endorsing the use made of the work. The full details of the license are available at http://creativecommons.org/licenses/by/4.0.

CC BY NC SA: The CC BY-NC-SA license allows users to copy, to create extracts, abstracts and new works from the Article, to alter and revise the Article, provided this is not done for commercial purposes, and that the user gives appropriate credit (with a link to the formal publication through the relevant DOI), provides a link to the license, indicates if changes were made and the licensor is not represented as endorsing the use made of the work. Further, any new works must be made available on the same conditions. The full details of the license are available at http://creativecommons.org/licenses/by-nc-sa/4.0.

CC BY NC ND: The CC BY-NC-ND license allows users to copy and distribute the Article, provided this is not done for commercial purposes and further does not permit distribution of the Article if it is changed or edited in any way, and provided the user gives appropriate credit (with a link to the formal publication through the relevant DOI), provides a link to the license, and that the licensor is not represented as endorsing the use made of the work. The full details of the license are available at http://creativecommons.org/licenses/by-nc-nd/4.0. Any commercial reuse of Open Access articles published with a CC BY NC SA or CC BY NC ND license requires permission from Elsevier and will be subject to a fee.

Commercial reuse includes:

- Associating advertising with the full text of the Article
- Charging fees for document delivery or access
- Article aggregation
- Systematic distribution via e-mail lists or share buttons

Posting or linking by commercial companies for use by customers of those companies.

20. **Other Conditions**:

v1.10

Questions? customercare@copyright.com or +1-855-239-3415 (toll free in the US) or +1-978-646-2777.

Annexure XIII

ELSEVIER LICENSE
TERMS AND CONDITIONS

Mar 16, 2021

This Agreement between Mr. Chiranjib Gogoi ("You") and Elsevier ("Elsevier") consists of your license details and the terms and conditions provided by Elsevier and Copyright Clearance Center.

License Number	5030840879438
License date	Mar 16, 2021
Licensed Content Publisher	Elsevier
Licensed Content Publication	Applied Catalysis A: General
Licensed Content Title	Metal–organic frameworks: A tunable platform to access single-site heterogeneous catalysts
Licensed Content Author	Megan C. Wasson,Cassandra T. Buru,Zhijie Chen,Timur Islamoglu,Omar K. Farha
Licensed Content Date	Sep 25, 2019
Licensed Content Volume	586
Licensed Content Issue	n/a
Licensed Content Pages	1
Start Page	117214
End Page	0

Annexure XIII

Type of Use	reuse in a thesis/dissertation
Portion	figures/tables/illustrations
Number of figures/tables/illustrations	1
Format	both print and electronic
Are you the author of this Elsevier article?	No
Will you be translating?	No
Title	Synthesis and Characterization of Some Zn(II) and Zr(IV) Metal-Organic Frameworks and Their Applications in Fluorescence Sensing and Catalysis
Institution name	IIT Guwahati
Expected presentation date	Jun 2021
Order reference number	226
Portions	Figure 1.21
Requestor Location	Mr. Chiranjib Gogoi IIT Guwahati Guwahati, 781039 India Attn: IIT Guwahati
Publisher Tax ID	GB 494 6272 12
Total	0.00 USD

Terms and Conditions

INTRODUCTION

1. The publisher for this copyrighted material is Elsevier. By clicking "accept" in connection with completing this licensing transaction, you agree that the following terms and conditions apply to this transaction (along with the Billing and Payment terms and conditions established by Copyright Clearance Center, Inc. ("CCC"), at the time that you opened your Rightslink account and that are available at any time at http://myaccount.copyright.com).

GENERAL TERMS

2. Elsevier hereby grants you permission to reproduce the aforementioned material subject to the terms and conditions indicated.

3. Acknowledgement: If any part of the material to be used (for example, figures) has appeared in our publication with credit or acknowledgement to another source, permission must also be sought from that source. If such permission is not obtained then that material may not be included in your publication/copies. Suitable acknowledgement to the source must be made, either as a footnote or in a reference list at the end of your publication, as follows:

"Reprinted from Publication title, Vol /edition number, Author(s), Title of article / title of chapter, Pages No., Copyright (Year), with permission from Elsevier [OR APPLICABLE SOCIETY COPYRIGHT OWNER]." Also Lancet special credit - "Reprinted from The Lancet, Vol. number, Author(s), Title of article, Pages No., Copyright (Year), with permission from Elsevier."

4. Reproduction of this material is confined to the purpose and/or media for which permission is hereby given.

5. Altering/Modifying Material: Not Permitted. However figures and illustrations may be altered/adapted minimally to serve your work. Any other abbreviations, additions, deletions and/or any other alterations shall be made only with prior written authorization of Elsevier Ltd. (Please contact Elsevier's permissions helpdesk here). No modifications can be made to any Lancet figures/tables and they must be reproduced in full.

6. If the permission fee for the requested use of our material is waived in this instance, please be advised that your future requests for Elsevier materials may attract a fee.

7. Reservation of Rights: Publisher reserves all rights not specifically granted in the combination of (i) the license details provided by you and accepted in the course of this licensing transaction, (ii) these terms and conditions and (iii) CCC's Billing and Payment terms and conditions.

8. License Contingent Upon Payment: While you may exercise the rights licensed immediately upon issuance of the license at the end of the licensing process for the transaction, provided that you have disclosed complete and accurate details of your proposed use, no license is finally effective unless and until full payment is received from you (either by publisher or by CCC) as provided in CCC's Billing and Payment terms and conditions. If full payment is not received on a timely basis, then any license preliminarily granted shall be deemed automatically revoked and shall be void as if never granted. Further, in the event that you breach any of these terms and conditions or any of CCC's Billing and Payment terms and conditions, the license is automatically revoked and shall be void as if never

granted. Use of materials as described in a revoked license, as well as any use of the materials beyond the scope of an unrevoked license, may constitute copyright infringement and publisher reserves the right to take any and all action to protect its copyright in the materials.

9. Warranties: Publisher makes no representations or warranties with respect to the licensed material.

10. Indemnity: You hereby indemnify and agree to hold harmless publisher and CCC, and their respective officers, directors, employees and agents, from and against any and all claims arising out of your use of the licensed material other than as specifically authorized pursuant to this license.

11. No Transfer of License: This license is personal to you and may not be sublicensed, assigned, or transferred by you to any other person without publisher's written permission.

12. No Amendment Except in Writing: This license may not be amended except in a writing signed by both parties (or, in the case of publisher, by CCC on publisher's behalf).

13. Objection to Contrary Terms: Publisher hereby objects to any terms contained in any purchase order, acknowledgment, check endorsement or other writing prepared by you, which terms are inconsistent with these terms and conditions or CCC's Billing and Payment terms and conditions. These terms and conditions, together with CCC's Billing and Payment terms and conditions (which are incorporated herein), comprise the entire agreement between you and publisher (and CCC) concerning this licensing transaction. In the event of any conflict between your obligations established by these terms and conditions and those established by CCC's Billing and Payment terms and conditions, these terms and conditions shall control.

14. Revocation: Elsevier or Copyright Clearance Center may deny the permissions described in this License at their sole discretion, for any reason or no reason, with a full refund payable to you. Notice of such denial will be made using the contact information provided by you. Failure to receive such notice will not alter or invalidate the denial. In no event will Elsevier or Copyright Clearance Center be responsible or liable for any costs, expenses or damage incurred by you as a result of a denial of your permission request, other than a refund of the amount(s) paid by you to Elsevier and/or Copyright Clearance Center for denied permissions.

LIMITED LICENSE

The following terms and conditions apply only to specific license types:

15. **Translation**: This permission is granted for non-exclusive world **English** rights only unless your license was granted for translation rights. If you licensed translation rights you may only translate this content into the languages you requested. A professional translator must perform all translations and reproduce the content word for word preserving the integrity of the article.

16. **Posting licensed content on any Website**: The following terms and conditions apply as follows: Licensing material from an Elsevier journal: All content posted to the web site must maintain the copyright information line on the bottom of each image; A hyper-text must be included to the Homepage of the journal from which you are licensing at http://www.sciencedirect.com/science/journal/xxxxx or the Elsevier homepage for books at http://www.elsevier.com; Central Storage: This license does not include permission for a

scanned version of the material to be stored in a central repository such as that provided by Heron/XanEdu.

Licensing material from an Elsevier book: A hyper-text link must be included to the Elsevier homepage at http://www.elsevier.com . All content posted to the web site must maintain the copyright information line on the bottom of each image.

Posting licensed content on Electronic reserve: In addition to the above the following clauses are applicable: The web site must be password-protected and made available only to bona fide students registered on a relevant course. This permission is granted for 1 year only. You may obtain a new license for future website posting.

17. **For journal authors:** the following clauses are applicable in addition to the above:

Preprints:

A preprint is an author's own write-up of research results and analysis, it has not been peer-reviewed, nor has it had any other value added to it by a publisher (such as formatting, copyright, technical enhancement etc.).

Authors can share their preprints anywhere at any time. Preprints should not be added to or enhanced in any way in order to appear more like, or to substitute for, the final versions of articles however authors can update their preprints on arXiv or RePEc with their Accepted Author Manuscript (see below).

If accepted for publication, we encourage authors to link from the preprint to their formal publication via its DOI. Millions of researchers have access to the formal publications on ScienceDirect, and so links will help users to find, access, cite and use the best available version. Please note that Cell Press, The Lancet and some society-owned have different preprint policies. Information on these policies is available on the journal homepage.

Accepted Author Manuscripts: An accepted author manuscript is the manuscript of an article that has been accepted for publication and which typically includes author-incorporated changes suggested during submission, peer review and editor-author communications.

Authors can share their accepted author manuscript:

- immediately
  - via their non-commercial person homepage or blog
  - by updating a preprint in arXiv or RePEc with the accepted manuscript
  - via their research institute or institutional repository for internal institutional uses or as part of an invitation-only research collaboration work-group
  - directly by providing copies to their students or to research collaborators for their personal use
  - for private scholarly sharing as part of an invitation-only work group on commercial sites with which Elsevier has an agreement
- After the embargo period
  - via non-commercial hosting platforms such as their institutional repository
  - via commercial sites with which Elsevier has an agreement

In all cases accepted manuscripts should:

- link to the formal publication via its DOI

- bear a CC-BY-NC-ND license - this is easy to do
- if aggregated with other manuscripts, for example in a repository or other site, be shared in alignment with our hosting policy not be added to or enhanced in any way to appear more like, or to substitute for, the published journal article.

Published journal article (JPA): A published journal article (PJA) is the definitive final record of published research that appears or will appear in the journal and embodies all value-adding publishing activities including peer review co-ordination, copy-editing, formatting, (if relevant) pagination and online enrichment.

Policies for sharing publishing journal articles differ for subscription and gold open access articles:

Subscription Articles: If you are an author, please share a link to your article rather than the full-text. Millions of researchers have access to the formal publications on ScienceDirect, and so links will help your users to find, access, cite, and use the best available version.

Theses and dissertations which contain embedded PJAs as part of the formal submission can be posted publicly by the awarding institution with DOI links back to the formal publications on ScienceDirect.

If you are affiliated with a library that subscribes to ScienceDirect you have additional private sharing rights for others' research accessed under that agreement. This includes use for classroom teaching and internal training at the institution (including use in course packs and courseware programs), and inclusion of the article for grant funding purposes.

Gold Open Access Articles: May be shared according to the author-selected end-user license and should contain a CrossMark logo, the end user license, and a DOI link to the formal publication on ScienceDirect.

Please refer to Elsevier's posting policy for further information.

18. **For book authors** the following clauses are applicable in addition to the above: Authors are permitted to place a brief summary of their work online only. You are not allowed to download and post the published electronic version of your chapter, nor may you scan the printed edition to create an electronic version. **Posting to a repository:** Authors are permitted to post a summary of their chapter only in their institution's repository.

19. **Thesis/Dissertation**: If your license is for use in a thesis/dissertation your thesis may be submitted to your institution in either print or electronic form. Should your thesis be published commercially, please reapply for permission. These requirements include permission for the Library and Archives of Canada to supply single copies, on demand, of the complete thesis and include permission for Proquest/UMI to supply single copies, on demand, of the complete thesis. Should your thesis be published commercially, please reapply for permission. Theses and dissertations which contain embedded PJAs as part of the formal submission can be posted publicly by the awarding institution with DOI links back to the formal publications on ScienceDirect.

Elsevier Open Access Terms and Conditions

You can publish open access with Elsevier in hundreds of open access journals or in nearly 2000 established subscription journals that support open access publishing. Permitted third

party re-use of these open access articles is defined by the author's choice of Creative Commons user license. See our open access license policy for more information.

Terms & Conditions applicable to all Open Access articles published with Elsevier:

Any reuse of the article must not represent the author as endorsing the adaptation of the article nor should the article be modified in such a way as to damage the author's honour or reputation. If any changes have been made, such changes must be clearly indicated.

The author(s) must be appropriately credited and we ask that you include the end user license and a DOI link to the formal publication on ScienceDirect.

If any part of the material to be used (for example, figures) has appeared in our publication with credit or acknowledgement to another source it is the responsibility of the user to ensure their reuse complies with the terms and conditions determined by the rights holder.

Additional Terms & Conditions applicable to each Creative Commons user license:

CC BY: The CC-BY license allows users to copy, to create extracts, abstracts and new works from the Article, to alter and revise the Article and to make commercial use of the Article (including reuse and/or resale of the Article by commercial entities), provided the user gives appropriate credit (with a link to the formal publication through the relevant DOI), provides a link to the license, indicates if changes were made and the licensor is not represented as endorsing the use made of the work. The full details of the license are available at http://creativecommons.org/licenses/by/4.0.

CC BY NC SA: The CC BY-NC-SA license allows users to copy, to create extracts, abstracts and new works from the Article, to alter and revise the Article, provided this is not done for commercial purposes, and that the user gives appropriate credit (with a link to the formal publication through the relevant DOI), provides a link to the license, indicates if changes were made and the licensor is not represented as endorsing the use made of the work. Further, any new works must be made available on the same conditions. The full details of the license are available at http://creativecommons.org/licenses/by-nc-sa/4.0.

CC BY NC ND: The CC BY-NC-ND license allows users to copy and distribute the Article, provided this is not done for commercial purposes and further does not permit distribution of the Article if it is changed or edited in any way, and provided the user gives appropriate credit (with a link to the formal publication through the relevant DOI), provides a link to the license, and that the licensor is not represented as endorsing the use made of the work. The full details of the license are available at http://creativecommons.org/licenses/by-nc-nd/4.0. Any commercial reuse of Open Access articles published with a CC BY NC SA or CC BY NC ND license requires permission from Elsevier and will be subject to a fee.

Commercial reuse includes:

- Associating advertising with the full text of the Article
- Charging fees for document delivery or access
- Article aggregation
- Systematic distribution via e-mail lists or share buttons

Posting or linking by commercial companies for use by customers of those companies.

20. **Other Conditions**:

v1.10

Questions? customercare@copyright.com or +1-855-239-3415 (toll free in the US) or +1-978-646-2777.

Publications & Conferences

Journal Articles:

1. A Zr-based metal-organic framework with DUT-52 topology and containing a trifluoroacetamido functionalized linker for aqueous phase fluorescence sensing of cyanide ion and aerobic oxidation of cyclohexane.

   C. Gogoi, N. Nagarjun, S. Roy, M. SK, D. Volkmer, A. Dhakshinamoorthy, S. Biswas. *Inorg. Chem.* 2021, **60**, 4539-4550.

2. Specific fluorescence sensing of hydrogen sulphide by an azide functionalized Zr(IV) MOF with DUT-52 topology.

   C. Gogoi, A. Kumar, M. SK, S. Biswas. *Microporous and mesoporous mater.*, 2021, **311**, 110725-110732.

3. Metal-Organic Framework (MOF) Derived Recyclable, Superhydrophobic Composite of Cotton Fabrics for the Facile Removal of Oil Spills.

   R. Dalapati, S. Nandi, **C. Gogoi**, A. Shome and S. Biswas. *ACS Appl. Mater. Interfaces*. 2021, **13**, 8563-8573.

4. Aqueous-phase nanomolar detection of dichromate by a recyclable Cd(II) metal-organic framework.

   C. Gogoi, S. Biswas. *Cryst. Growth Des*. 2021, **21**, 2680-2689.

5. Diffusion driven nanostructuring of metal-organic frameworks (MOFs) for graphene hydrogel based tunable heterostructures: Highly active electrocatalyst for efficient water oxidation.

   U. Maiti, A. Sikdar, A. Majumdar, A. Gogoi, P. Dutta, M. Borah, S. Maiti, **C. Gogoi**, K. A. Reddy, Y. Oh. *J. Mater. Chem. A.*, 2021, **9**, 7640-7649.

6. Rational design of a functionalized aluminum metal-organic framework as a turn-Off fluorescence sensor for α-ketoglutaric acid.

   A. Das, M. Alam, **C. Gogoi**, R. Dalapati, and S. Biswas. *Dalton Trans.* 2020, **49**, 16928-16934.

7. A pyrazine core based luminescent Zr(IV) organic framework for specific sensing of Fe^{3+}, picric acid and $Cr_2O_7^{2-}$.

   C. Gogoi, H. Reinsch and S. Biswas, *CrystEngComm*, 2019, **21**, 6252-6260.

8. A new 3D luminescent Zn(II)–organic framework containing a quinoline-2,6-dicarboxylate linker for the highly selective sensing of Fe(III) ions.
   C. Gogoi, M. Yousufuddin and S. Biswas, *Dalton Trans.* 2019, ***48***, 1766-1773.
9. A new quinoline based luminescent Zr(IV) metal–organic framework for the ultrasensitive recognition of 4-nitrophenol and Fe(III) ions.
   C. Gogoi, S. Biswas, *Dalton Trans.* 2018, ***48***, 14696-14705.

Conferences Attended:

1. Chemconvene –2017, IIT Guwahati, Assam, India.
2. Frontiers in Chemical Sciences (FICS) –2018, IIT Guwahati, Assam, India.
3. International Conference on Emerging Trends in Chemical Sciences (ETCS) - 2018, Dibrugrah University, Assam, India.
4. International Conference on Synthetic Potent Molecule and its Application (ICSPMIA) -2018, Sikkim Manipal Institute of Technology, Sikkim, India.
5. Research Conclave 2019, IIT Guwahati, Assam, India.
6. Modern Trends in Inorganic Chemistry (MTIC XVIII) - 2019, IIT Guwahati, Assam, India.
7. 4th International Conference on Recent Advances in Material Chemistry (ICRAMC) -2020, SRM Institute of Science and Technology. Kattankulathur, Tamil Nadu, India.

The End